

1262
513
0

BIBLIOTHEEK TU Delft
P 1262 5130



C

356796

629.11:012.3:

629.11.073.243.

THE WHEEL SHIMMY PHENOMENON
A THEORETICAL AND EXPERIMENTAL INVESTIGATION
WITH PARTICULAR REFERENCE TO THE
NON-LINEAR PROBLEM

BIBLIOTHEEK
TECHNISCHE UNIVERSITEIT
DELFT

THE WHEEL SHIMMY PHENOMENON

A THEORETICAL AND EXPERIMENTAL INVESTIGATION
WITH PARTICULAR REFERENCE TO THE
NON-LINEAR PROBLEM

PROEFSCHRIFT

TER VERKRIJGING VAN DE GRAAD VAN
DOCTOR IN DE TECHNISCHE WETENSCHAPPEN
AAN DE TECHNISCHE HOGESCHOOL
TE DELFT OP GEZAG VAN DE RECTOR MAGNIFICUS
IR. H. J. DE WIJS, HOGLERAAR
IN DE AFDELING DER MIJNBOUWKUNDE,
VOOR EEN COMMISSIE UIT DE SENAAAT TE
VERDEDIGEN OP WOENSDAG 14 DECEMBER 1966
DES NAMIDDAGS TE 4 UUR

DOOR

1262 5130

HANS BASTIAAN PACEJKA

WERKTUIGKUNDIG INGENIEUR
GEBOREN TE ROTTERDAM



Druk. V. R. B. Kleine der A 3-4 Groningen

Dit proefschrift is goedgekeurd door de promotoren
Prof. Dr. Ir. A. D. de Pater
Prof. Ir. H. C. A. van Eldik Thieme

*Aan mijn ouders
Aan mijn vrouw*

CONTENTS

	page
Chapter I INTRODUCTION	1
1 Preliminary remarks	1
2 Outline of literature	1
3 Outline of thesis	3
Chapter II THEORY OF TYRE BEHAVIOUR	5
1 Survey of literature	6
2 Differential equations and boundary conditions	11
3 Stationary behaviour for any slip value	22
4 Non-stationary behaviour for vanishing slip	38
5 Approximate non-stationary behaviour for finite slip	50
6 Influence of gyroscopic couple due to tyre deformation	54
Chapter III MATHEMATICAL DESCRIPTION OF THE VEHICLE	61
1 Physical description of the model considered	62
2 Geometrical considerations	64
3 Kinematical considerations	70
4 Virtual displacements	72
5 Dynamical considerations	73
6 Equations of motion	74
7 Non-dimensional quantities	78

Chapter IV	ANALYTICAL INVESTIGATION OF AUTONOMOUS SYSTEMS	83
1	Determination of the stability of linear systems	84
1.1	The Hurwitz criterium for stability	84
1.2	The third-order system	87
1.3	The fifth-order system	90
1.4	The seventh-order system	96
2	Investigation of non-linear systems with the aid of equivalent linear equations	98
2.1	Determination of "limit-amplitudes"	98
2.2	Stability of limit-cycles	102
2.3	The third-order system	106
2.4	The fifth-order system	123
2.5	The seventh-order system	125
3	Application of the theory for piece-wise linear systems	128
3.1	Stability of the stationary motion	129
3.2	The small limit-cycle	133
3.3	Stability of the small limit-cycle	135
Chapter V	INVESTIGATIONS WITH THE AID OF AN ELECTRONICAL ANALOGUE COMPUTER	139
1	The third-order system	139
1.1	Circuit diagrams	139
1.2	Stability of the linear system	143
1.3	The phase space of the non-linear system	144
1.4	The self-excitation area	148
1.5	The response to unbalance torque	150
2	The tenth- and twelfth-order system	154
2.1	Mathematical description	154
2.2	Simulation of test vehicle	155
2.3	Influence of changing parameter values	158
Chapter VI	EXPERIMENTAL INVESTIGATIONS	163
1	Full-scale experiments with test vehicle on the road	163
2	Tyre frequency response tests on rotating drum	169
3	Experiments with mechanical model	175

Chapter VII	CONCLUDING REMARKS	177
	NOTATIONS	180
	REFERENCES	185
	SUMMARY	189
	SAMENVATTING	191

At the top of each page the current chapter number (Roman figure) has been indicated. Cross-references have been made as follows:

Sec.X,x means section x of chapter X,

Sec.x means section x of current chapter,

Eq.X.(x) means equation x of chapter X,

Eq.(x) means equation (x) of current chapter.

References to figures and tables have been made in an analogous way.

CHAPTER I

INTRODUCTION

1. *Preliminary remarks*

Since the introduction of pneumatic tyres, automobiles and aircraft have suffered from unstable oscillatory swivel motions. These oscillations exhibited by the steerable wheels, popularly known as "shimmy", may sometimes assume grave proportions and cause failure of mechanical components or result in loss of control of the vehicle.

Pneumatic tyres are used primarily for obtaining better roadholding and comfort. The vertical and lateral elasticity of the tyre introduce additional degrees of freedom of motion, which are coupled with the angular motions of the wheel about the swivel axis. Such a coupling may lead to the occurrence of an oscillatory instability of the stationary rectilinear motion.

Hitherto, many investigators have tried to analyze the shimmy phenomenon. Their analyses were, however, strictly linear. The non-linearities occurring in the system, such as tyre characteristics, dry friction and clearance, are important factors, which have considerable influence upon the manner in which shimmy manifests itself. The linear theories may in most cases indicate the cause of instability, but they fail to give a correct description of the real phenomenon.

2. *Outline of literature*

Fromm [1] (1931) was one of the first investigators who developed a theory for the shimmy motion of automobiles. Besides his advanced theoretical work, as a result of which the gyroscopic coupling between the angular motions about a longitudinal axis and the swivel axis was believed to be the main factor causing shimmy [1, p.10], he has carried out and described, together with his co-authors Becker and Maruhn, some tests on a system with rigid front axle. Also Den Hartog [2] and Rocard [3] have treated this

"gyroscopic shimmy" for systems with live axles. The phenomenon was furthermore examined experimentally by Olley [4].

Another sort of shimmy, occurring both with aircraft and automobiles equipped with independent front wheel suspensions, is closely related to the deformability of the tyre. We should distinguish in this respect the static lateral stiffness and the so-called cornering stiffness of the tyre. For shimmy, both these above properties are important. It may be noted that with the self-sustained hunting movements of railway vehicles, originally investigated among others by Carter [5] (1915-16), the influence of the static lateral stiffness of the steel tyre can be neglected when compared to the influence of the lateral slip. This means that the slip phenomenon can be treated as stationary. This will in general be permitted when stationary or relatively slowly varying motions of vehicles are investigated.

Up to now the latter sort of shimmy, to which we refer here as "tyre shimmy", has been investigated exclusively in connection with aircraft. An outline of literature on tyre theories is given in Sec. II. 1. The stability of simple systems, such as a wheel equipped with an elastic tyre capable of swivelling about a king-pin that moves along a straight line, has been theoretically investigated among others by Kantrowitz [28] (1937, U.S.A.), Von Schlippe and Dietrich [34] (1941, Germany), Greidanus [30] (1942, Holland) and later by Smiley [40]. The experiments carried out by Von Schlippe and Dietrich [34] and Schrode [43] substantiate the theories for the stability of simple systems as described in references [34,40] in qualitative respect. Marstrand [42] has carried out tests with a "twin contact" tyre. By introducing a tread pattern consisting of two longitudinal ribs he could prevent shimmy. Schrode obtained the same tendency by making the tread surface flatter and wider. In both cases the increase in damping through longitudinal tread deformations may be responsible for the stabilizing effect.

De Pater [7] and Van Bommel [8] have recently developed theories for the non-linear problem of the hunting phenomenon occurring with railway vehicles. The harmonic balance method employed by them for solving the non-linear differential equations approximately is essentially the same as the one used here in the non-linear shimmy analysis to be treated in chapter IV.

3. *Outline of thesis*

The thesis is mainly concerned with shimmy due to tyre lateral flexibility, occurring with automobiles. A theory is developed for the stationary and non-stationary behaviour of tyres, assuming a finite contact area between tyre and road. The influences of the elasticity of tread rubber and of the gyroscopic effect of the tyre are considered. The tyre is fitted to a wheel, which rotates about a stub axle; the latter can swivel about a king-pin which is attached to a system of which the complexity is gradually increased during the course of the investigation. The influence of suspension elasticity, chassis elasticity and of the steering system are studied. Up to three non-linearities are introduced, viz., degressive tyre characteristics, dry friction in the king-pin bearings and rotational clearance in the wheel bearings. The first non-linearity causes limitation of the shimmy amplitude. The second non-linearity stabilizes the stationary motion of the vehicle and shimmy may only occur when sufficient wheel unbalance or other external disturbance is present. The third non-linear element has a destabilizing effect and shimmy may arise even without any unbalance or external disturbance being present.

In order to substantiate theoretical findings, experiments have been carried out with a test vehicle and a simple scale model. Full scale tyre tests showed that the tyre theory developed is essentially correct. The shimmy behaviour of the test vehicle and of the mechanical model could be explained with the non-linear theory developed.

Some of the most important results of this investigation have been published already in condensed form [9,10].

CHAPTER II

THEORY OF TYRE BEHAVIOUR

The contact problem of tyre and road may be considered as a special case of the general problem of two elastic bodies of revolution pressed to each other with a given force. The road will be assumed to be a smooth level boundary surface of an undeformable half space, while the tyre may be represented by some elastic model. When the tyre moves over the road, apart from the deformations due to the vertical force in the static situation, in general, additional horizontal deformations will occur. When the wheel moves in such a way that the contact points of an imaginary tyre, which differs from the real tyre only in that respect that it does not show horizontal deformations, do not move with respect to the road, we speak of pure rolling. When all the contact points of that imaginary tyre show mutually the same relative velocity with respect to the road, we speak of longitudinal (fore and aft-) slip when this velocity and the rolling velocity have the same direction; we speak of lateral (side-) slip when the relative velocity is directed perpendicularly to the rolling velocity. The angle between wheel centre plane (direction of rolling) and the vector of the velocity of the wheel centre is called slip angle. When the wheel rotates about a vertical axis through the wheel centre without showing longitudinal or lateral slip, we speak of pure spin. A real tyre will show additional horizontal deformations. In case of dry-frictional contact, the additional horizontal deformations may cause regions of adhesion besides regions of sliding. In the following, the terms slip and sliding will always be used in the sense as expressed above. In the literature on this subject we find some difference in nomenclature; Kalker [16] for instance uses the terms slip and overall slip in cases where we use sliding and slip respectively; other authors sometimes use the word creep or drift for what we call slip.

1. *Survey of literature*

In the whole complex of theoretical studies on the tangential contact between tyre and road, one may distinguish two main groups. The first group deals with investigations of the steady state behaviour of the rolling body. In that case the body moves in such a way that a constant slip velocity in the rolling direction and perpendicular to it occurs, while in some cases also a constant turning velocity (spin) is considered. The second group is concerned with the study of the non-stationary behaviour of the tyre. Here, the lateral slip and angular motions have a character varying with time; in most cases sinusoidal variations are considered.

We notice a fundamental difference in structure of the mathematical tyre model in the two groups mentioned. In all theories on the stationary (steady state) motion, a model consisting of an elastic structure (the carcass) provided with a great number of elastic blocks (rubber profile elements) is employed. The profile elements contact the road surface in the area of contact where a region of sliding may occur when locally the adhesion limit is exceeded. In the non-stationary investigations, until now, profile elements have always been omitted and in addition adhesion has always been considered in the entire contact area. Instead of speaking of a contact area entirely being in adhesion, we may prefer to speak of a contact area where vanishing regions of sliding occur.

In the first group in principle always an elastically supported beam is introduced for the representation of the carcass of the tyre. In the non-stationary investigations, two different trends exist: sometimes a beam model is used, but we also encounter the employment of the elastically supported stretched string model. With the exception of one case, the non-stationary tyre investigations have been restricted to models showing point or line contact.

A historical outline of literature on rolling behaviour, as will be given below, should also mention something of the work that has been done on the problem of the stationary rolling and slipping motion of two elastic homogeneous bodies pressed to each other. In most of these theories equal elastic constants of the two co-operating bodies are assumed (steel-on-steel problem).

The two-dimensional problem of two parallel cylinders slipping only in the direction of rolling was treated by Carter [11] in 1926 and by Fromm [12] in 1927, the latter also for unequal elastic constants. Much later (in 1958)

Johnson (see i. a. [16] for references) developed an approximate three-dimensional theory for rolling balls with an elliptical contact area in which a similar area of adhesion is assumed which touches the leading edge of the contact area for the case of slipping in and perpendicular to the direction of rolling. The case of infinitesimal slip and spin where the sliding region vanishes, has been treated in a later paper by Johnson [13] and more recently by De Pater [14] and by Kalker [15]. The case of very large slip and spin in which no adhesion occurs, is investigated by Lutz and Wernitz (cf. [16]). In 1967 Kalker finally published a numerical method [16] with which the transmitted force and couple from one body to the other for any slip and spin can be calculated together with the stress distribution and the shape of adhesion and sliding regions in the contact area.

Concerning the investigation of stationary tyre motion, we must in the first place mention Brouhiet [18] (1925) and Fromm (1930) (cf. [19]) who were probably the first to recognize the important role that lateral slip of tyres plays in automobile motions. Fromm [19] developed a theory for the variation of lateral force with lateral slip in which he neglected the influence of the lateral flexibility of the carcass of the tyre; however, he did take into account the elasticity of the profile elements and the possibility of sliding.

Fiala [20] and later Freudenstein [21] developed theories in which, as an extension of Fromm's theory, the carcass is represented by an elastically supported beam of infinite length. The deflection of the beam was found by assuming the lateral load acting on the beam in a manner, symmetric with respect to the vertical plane through the wheel axis. Freudenstein also studied the behaviour for pure spin, i. e. turning without lateral slip. He found that at high values of spin (circular path with small radius) front sliding also occurs.

Recently Frank [22] presented an analogue computer method with which he determined the tyre deflection and force distribution for constant slip angles, i. e. lateral slip values. The carcass is represented by a stretched beam and a comparison is made between the string and beam model. It appeared from an analysis of Fourier extensions that the deflection of the string model came closer to that of a conventional tyre and the deflection of a beam model more to that of a radial ply tyre.

The combination of lateral and longitudinal slip was treated by Pacejka [23] for the simple model exhibiting a

rigid carcass provided with flexible profile elements. In [24] he introduced the carcass flexibility in an approximate form. The characteristics obtained for the lateral force and the aligning torque (i. e. the torque about the vertical axis) for a given slip angle as a function of longitudinal driving or braking force were similar to those, obtained experimentally by Nordeen and Cortese [26]. Bergman [25] also gave a theory based on different considerations. His results appear to fit very well for the case of driving forces.

Recently Savkoor [27] investigated the influence of non-linear friction coefficients depending on sliding velocity, temperature and contact pressure. The history of motion also appears to be a factor influencing the frictional behaviour. He could indicate the effect of road surface textures, tread profile shapes and rubber properties. He studied moreover the correspondence of tyre models with real tyres. As a result he could indicate that both the string and beam model are fair approximations of the real tyre.

In the theories describing the non-stationary behaviour of tyres one can indicate two trends. One group of authors assumed a bending stiffness of the carcass and the other based its theory on the string concept. As said before, no profile elements and no sliding were considered.

Probable the first investigators who tried to describe the tyre behaviour mathematically in behalf of the study of shimmy are Kantrowitz [28] and Wiley [29]. In spite of their rough and theoretically unsatisfactory assumptions, their theories, which are similar to each other, resulted in a fair correspondence with measured values of divergence of subsequent wheel deflections and frequency of the shimmy motion. Kantrowitz introduced the term kinematic shimmy, which is obtained when all inertia effects of the system are omitted. This sort of shimmy will occur at very low velocities of travel, where the frequency tends to zero but where the wavelength remains finite. In this case the non-castered tyre, i. e. with a vertical swivel axis, shows a symmetrical or more precisely a nearly symmetrical lateral deformation. Furthermore, Kantrowitz studied the damping effect of the gyroscopic couple due to lateral distortion of the rotating tyre. This effect has not been taken into account by any other author treating this subject. Smiley [40] predicts that tyre inertia effects will come into play at a velocity of the order of magnitude of $270 \sqrt{R}$ mph, where R denotes the tyre radius, expressed in feet.

Another theory, apparently inspired by Kantrowitz' work, was developed in 1942 by Greidanus [30]. Where Kantrowitz'

work shows features of both the beam and the string, Greidanus is consistent in applying the bending principle in his important study. Besides the slope also the curvature of the peripheral line just in front of the contact point is important for the further development of the motion. Also in Greidanus' model a vanishing area of contact was considered as may be deduced from his way of treatment. A new aspect introduced by Greidanus is the influence of camber, i.e. of tilting the wheel plane, on the lateral deflection of the peripheral line. The influence of camber considered, however, is not justifiable in our opinion. This opinion is based on the fact that the points on the peripheral line of a cambered tyre move parallel to the wheel centre plane, so that the vertical projection of that line on the road surface just in front of the region of contact does not represent the increment in path of the contact points. Another effect of wheel camber, viz. the accompanying lateral tyre force (camber thrust), is not taken into account by Greidanus. We notice furthermore that his theory takes into account the lateral shift of the point in which the resultant vertical load is acting, due to lateral tyre distortion. This effect results in an additional moment about the swivel axis when this axis is inclined over the caster angle ϵ with respect to the vertical. It can be shown, however, that this additional moment amounts to the order of ϵ multiplied by the aligning torque. For small caster angles this effect may very well be neglected.

In a discussion on Saito's paper [31] Pacejka has given the differential equations which govern the kinematical variations in lateral tyre distortion for the beam type model with finite contact length. These equations appear to be identical to those given by Greidanus when the influence of camber is not considered and the contact length is taken equal to zero.

In 1962 Saito [31] presented a theory using a tyre model consisting of an elastic beam of which a finite length makes contact with the road. The theory is based on an approximative treatment of the kinematic behaviour of the contact line. Frequency response curves are given for the force and moment with respect to lateral and angular motions of the wheel plane. In order to obtain better agreement with results obtained experimentally, Saito introduced theoretically unjustifiable empirical corrections.

Besides this group of investigators which were inspired by the work of Kantrowitz, another group exists which has studied the problem with the aid of tyre models more or less based on the string concept.

In 1941 Fromm [32] gave a simple theory where this model (although not mentioned by name) is investigated for the case of point contact. A similar theory was developed by Bourcier de Carbon [33] in 1948 together with an extension, not being very clear, which increases the order of the system by one.

In 1941 Von Schlippe [34] presented his well-known theory of the kinematics of a rolling tyre. He introduced the concept of the stretched string model. For the first time a finite contact length was considered. In the same paper Dietrich applied this theory on the shimmy problem. Mathematical difficulties arose in the form of transcendental equations due to the retardational effect of the assumption of a finite contact length. Later on, two papers of Von Schlippe and Dietrich [35, 36] were published in which also the effect of the width of the contact area is considered. Two rigidly connected co-axial wheels both fitted with a one-dimensional string type model are considered. The strings and their elastic supports are supposed to be elastic also in circumferential direction. In [35] this theory is applied correctly for the case of constant path curvature. In [36] the influence of tread width is studied for the shimmy motion. In equation (6) of this article the substitution of d^2y/ds^2 for $1/R$ is doubtful. A correct substitution would be the spin $d\phi/ds$ (Von Schlippe notation). The corrective factor ρ appearing in the expression of the aligning torque [36, Eq. (77)] with which the influence of roundness of the tyre is meant to be expressed, is erroneous. According to our view this influence is completely cancelled by the torque exerted by the radial reactive forces due to tension in the string which is stretched around an imaginary cylinder. Smiley [40] and Hadekel [37] adopted the same erroneous corrective factor. In the early forties also Temple developed a tyre theory similar to that of Von Schlippe. The work is partly published by Hadekel [37].

Segel [38] derived the correct frequency response functions for the one-dimensional string type model and it appeared that similar response curves arise as those obtained with Saito's approximate theory for the beam model (see also [31, discussion]).

A simple, completely different theory is proposed by Moreland [39]. Moreland introduced a time lag term which illustrates that he failed to recognize that tyre behaviour is essentially path dependent. For this reason it can be expected that his theory may be correct for only one value of forward speed.

Smiley [40] gave a summary theory resembling the one-

dimensional theory of Von Schlippe [34]. He has correlated various known theories with several systematic approximations to his summary theory.

In principle, the string theory is simpler than the beam theory, as with the string model only the deflection of the foremost point determines the path of the tread for certain wheel movements, whereas with the beam model also the slope in the foremost point has to be taken into account as an additional variable. The latter leads to an increase in order of the system by one. No or little difference in linear response appears to occur between string and beam models when the parameter values are chosen properly.

The tyre theory which will be presented in the subsequent sections, can be seen as an extension of the theories based on the string type model. In principle, the tyre model to be investigated is considered massless and has a contact area of a finite width and length; a new aspect in investigations of non-stationary tyre behaviour is that the carcass is provided with a great number of elastic profile elements. A correction is made to account for the gyroscopic couple due to variation of lateral tyre deformation. Subsequently to the treatment of the stationary tyre behaviour considering partial sliding, a linear non-stationary theory will be presented. The frequency response curves will be given and several approximations discussed. Finally, an approximative method will be described with which partial sliding in the contact area in the case of non-stationary motion is introduced.

2. Differential equations and boundary conditions

Consider an elastic rotationally symmetric body representing a wheel with tyre rolling over a smooth horizontal surface representing the road. Fixed to the road a co-ordinate system $(0, x, y, z)$ is assumed of which the x - and y -axes lie in the road surface and the z -axis points downwards (cf. Fig. 1). Another co-ordinate system (C, ξ, η, ζ) is introduced of which the axes ξ and η lie in the $(x, 0, y)$ plane and ζ points downwards. The system moves with respect to the fixed system in such a way that the ξ -axis lies in the wheel centre plane and the η -axis forms the projection of the wheel axis. The body is deformed vertically so that a finite contact area is present. The centre C travels with a constant speed V over the $(x, 0, y)$ plane. The travelled distance s equals:

$$s = V t, \quad (1)$$

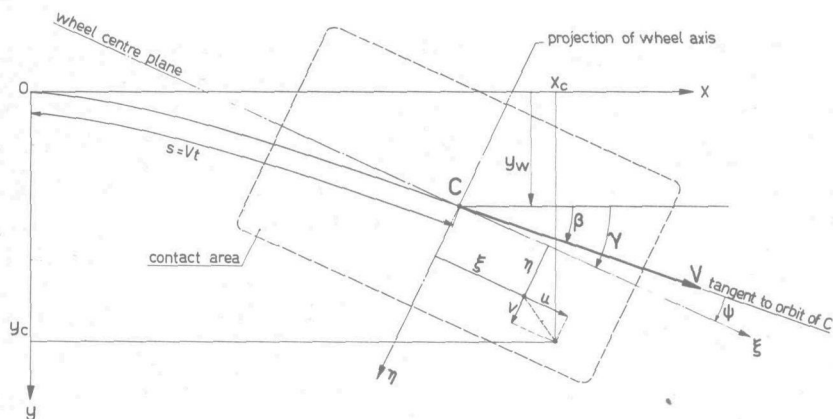


Fig. 1. Top view of contact area, showing position with respect to co-ordinate system fixed in space.

where t denotes the time. The tangent to the orbit of C makes an angle β with the fixed x -axis. With respect to this tangent the ξ -axis is rotated with an angle ψ . The angular deviation of the wheel plane with respect to the x -axis is denoted by:

$$\gamma = \beta + \psi . \quad (2)$$

For small values of β the following relation with y_w , the lateral co-ordinate of C , holds:

$$\beta = \frac{dy_w}{ds} . \quad (3)$$

The horizontal displacements of a contact point with respect to its position in the horizontally undeformed situation with co-ordinates (ξ, η) are indicated by u and v in ξ - and η -direction respectively. The displacements are functions of ξ, η and the independent variable s or t .

The components in ξ - and η -direction of the sliding velocity (W) of a point of a rolling body in the contact area with respect to the road read in general:

$$\left. \begin{aligned} W_{\xi} &= W_{0\xi} - \eta\omega\zeta - V_{0\xi} \frac{\partial u}{\partial \xi} - V_{0\eta} \frac{\partial u}{\partial \eta} + \frac{\partial u}{\partial t} , \\ W_{\eta} &= W_{0\eta} + \xi\omega\zeta - V_{0\xi} \frac{\partial v}{\partial \xi} - V_{0\eta} \frac{\partial v}{\partial \eta} + \frac{\partial v}{\partial t} , \end{aligned} \right\} \quad (4)$$

where $(W_{0\xi}, W_{0\eta})$ denotes the vector of the sliding velocity

of the point C' of the tyre, which coincides with the centre C at the instant considered, in case that horizontal deformations would not occur; $(V_{0\xi}, V_{0\eta})$ is the vector of the rolling velocity with which point C moves relatively to C' under the same circumstances. Moreover, ω_ζ denotes the angular velocity of the system (C, ξ, η, ζ) about the ζ -axis (yawing velocity):

$$\omega_\zeta = \dot{\gamma} = \dot{\beta} + \dot{\psi} . \quad (5)$$

We will restrict ourselves to small values of lateral slip, and assume $|\psi| \ll 1$. For the system under consideration, i.e. the tyre, where only rolling in ξ -direction occurs, the following relations hold:

$$V_{0\xi} = V \quad \text{and} \quad V_{0\eta} = 0 . \quad (6)$$

We will restrict ourselves furthermore to cases where the longitudinal slip velocity $W_{0\xi} = 0$, which is approximately the case in reality when no driving or braking couples are applied. For the lateral slip velocity we obtain:

$$W_{0\eta} = -V\psi . \quad (7)$$

We introduce the variable φ denoting the spin:

$$\varphi = \frac{\omega_\zeta}{V} = \frac{d\gamma}{ds} . \quad (8)$$

The latter part of this relation holds owing to Eqs. (1) and (5). We finally obtain the following expressions for the sliding velocities of a point with co-ordinates (ξ, η) :

$$\left. \begin{aligned} W_\xi / V &= -\eta\varphi - \frac{\partial u}{\partial \xi} + \frac{\partial u}{\partial s} , \\ W_\eta / V &= -\psi + \xi\varphi - \frac{\partial v}{\partial \xi} + \frac{\partial v}{\partial s} . \end{aligned} \right\} \quad (9)$$

When the vector of the pressure exerted by the tyre upon the road is denoted by (p_ξ, p_η, p_ζ) , we obtain the following relations for the case with finite friction coefficient μ . In an adhesion region, defined as the area where no sliding occurs ($W_\xi = W_\eta = 0$), the relations

$$\left. \begin{aligned} \frac{\partial u}{\partial \xi} - \frac{\partial u}{\partial s} &= -\eta\varphi, \quad \frac{\partial v}{\partial \xi} - \frac{\partial v}{\partial s} = -\psi + \xi\varphi, \\ \sqrt{p_\xi^2 + p_\eta^2} &< \mu p_\zeta \end{aligned} \right\} \quad (10)$$

hold, and in a sliding region the relations (9). For the pressure we obtain in vectorial form:

$$(p_{\xi}, p_{\eta}) = \frac{\mu p_{\zeta}}{W} (W_{\xi}, W_{\eta}), \quad (11)$$

where

$$W = \sqrt{W_{\xi}^2 + W_{\eta}^2}, \quad (12)$$

the velocity components W_{ξ} , W_{η} being determined by (9).

For the case that only lateral slip occurs ($\varphi=0$) and in addition $p_{\xi} = W_{\xi} = 0$ throughout the contact area, which may occur with simplified systems to be treated, the relations (9), (10) and (11) reduce to:

$$\left. \begin{aligned} \frac{\partial v}{\partial \xi} - \frac{\partial v}{\partial s} &= -\psi, \\ |p_{\eta}| &< \mu p_{\zeta} \end{aligned} \right\} \text{in an adhesion region,} \quad (13)$$

$$\left. \begin{aligned} \frac{\partial v}{\partial \xi} - \frac{\partial v}{\partial s} &= -\psi - \frac{W_{\eta}}{V}, \\ p_{\eta} &= \mu p_{\zeta} \operatorname{sgn} W_{\eta} \end{aligned} \right\} \text{in a sliding region.} \quad (14)$$

The equations above apply in general. Their solutions contain constants of integration which depend on the construction of the tyre, of which an approximate physical description will be given now.

The massless "running band" model of the pneumatic tyre to be investigated is shown in figure 2. The carcass is

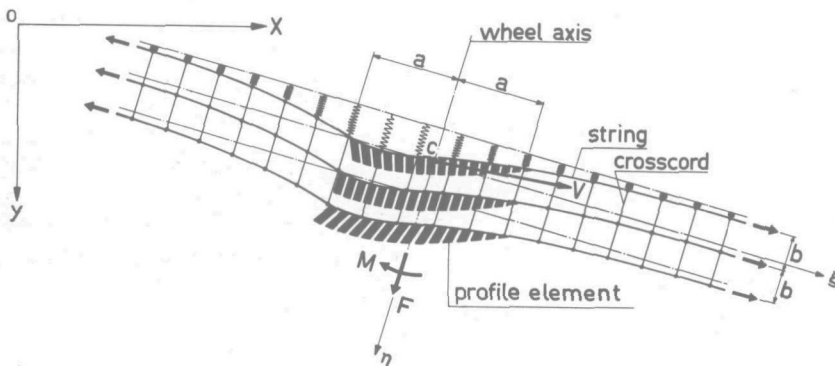


Fig. 2. Top view of tyre model.

represented by a number of elastically supported parallel strings under tension, which are connected by cross cords. The points of connection can move only laterally and their mutual distance remains the same. When the strings are deformed laterally the rubber in between will be sheared. Through the continuous elastic support axial forces distributed over the length of the band can be transmitted to the wheel plane. To this band under tension several rows of an infinite number of elastic blocks representing profile elements, are attached. In the contact area of length $2a$ and width $2b$ the ends of these elements have contact with the road surface.

The longitudinal deformation u is assumed to be proportional to the longitudinal component of the contact pressure. The following relation holds:

$$p_{\xi} = -c^*u, \quad (15)$$

where p_{ξ} is the force and c^* the longitudinal stiffness of the profile elements, both per unit area.

The lateral deflection v is composed by the lateral deflection of the string v_s , and the lateral deflection of the profile rubber v_p :

$$v = v_s + v_p. \quad (16)$$

We will consider only the case where v_p is constant along the width of the contact area, as will occur in cases to be investigated. We assume v_p to vary proportionally with p_{η} as expressed by:

$$p_{\eta} = -c_p v_p, \quad (17)$$

where p_{η} denotes the force and c_p the lateral stiffness of the profile elements, both per unit length.

For obtaining an expression for the deflection of the strings we must consider the equilibrium of an element of the tyre model as shown in figure 3, where the longitudinal displacements u , resulting in a second-order effect, are not considered. In lateral direction the equilibrium of forces acting on the element with length $d\xi$ and full tread width $2b$, results in the following equation:

$$\begin{aligned} -p_{\eta} d\xi - c_s v_s d\xi + D - D - \frac{\partial D}{\partial \xi} d\xi - S_1 \frac{\partial v_s}{\partial \xi} + \\ + S_1 \left(\frac{\partial v_s}{\partial \xi} + \frac{\partial^2 v_s}{\partial \xi^2} d\xi \right) = 0, \end{aligned} \quad (18)$$

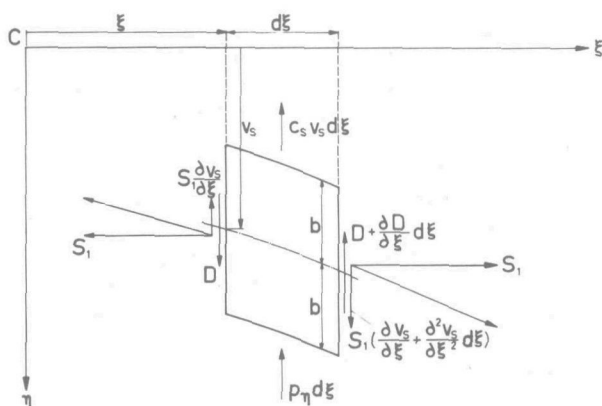


Fig.3. Equilibrium of deflected tyre element.

where c_s denotes the carcass stiffness ("pneumatic stiffness") per unit length, S_1 the longitudinal component of the total tension force in the strings and D the shear force in the cross section of the band. The shear force is assumed to be a linear function of the shear angle, according to the formula:

$$D = -S_2 \frac{\partial v_s}{\partial \xi} . \quad (19)$$

With the introduction of the constant $S = S_1 + S_2$ we deduce from Eq. (18):

$$p_\eta = S \frac{\partial^2 v_s}{\partial \xi^2} - c_s v_s . \quad (20)$$

In the part of the tyre not making contact with the road the contact pressure vanishes so that:

$$S \frac{\partial^2 v_s}{\partial \xi^2} - c_s v_s = 0 \quad \text{for } |\xi| > a . \quad (21)$$

For the part making contact we obtain with Eqs. (20), (17) and (16):

$$S \frac{\partial^2 v_s}{\partial \xi^2} - c_s v_s = -c_p (v - v_s) \quad \text{for } |\xi| < a . \quad (22)$$

We introduce the tyre constants:

$$\sigma = \sqrt{\frac{S}{c_s}}, \quad \sigma_c = \sqrt{\frac{S}{c_s + c_p}} \quad \text{and} \quad \epsilon = \frac{\sigma_c}{\sigma} = \sqrt{\frac{1}{1 + c_p/c_s}}. \quad (23)$$

With increasing profile rubber stiffness the value of the parameter ϵ decreases until it vanishes when $c_p \rightarrow \infty$ which represents the case that no profile elements are introduced.

$$\sigma^2 \frac{\partial^2 v_s}{\partial \xi^2} - v_s = p_\eta / c_s, \quad (24)$$

$$\sigma^2 \frac{\partial^2 v_s}{\partial \xi^2} - v_s = 0 \quad \text{for } |\xi| > a, \quad (25)$$

$$\sigma_c^2 \frac{\partial^2 v_s}{\partial \xi^2} - v_s = -(1 - \epsilon^2) v \quad \text{for } |\xi| < a. \quad (26)$$

For large values of $|\xi|$ the deflection v_s tends to zero. Therefore the solution (25) reads:

$$\left. \begin{aligned} v_s &= C_1 e^{-\xi/\sigma} & \text{for } \xi > a, \\ v_s &= C_2 e^{\xi/\sigma} & \text{for } \xi < -a. \end{aligned} \right\} \quad (27)$$

At the boundaries $\xi = \pm a$ we obtain consequently:

$$\left. \begin{aligned} v_s &= -\sigma \lim_{\xi \downarrow a} \frac{\partial v}{\partial \xi} & \text{for } \xi = a, \\ v_s &= \sigma \lim_{\xi \uparrow -a} \frac{\partial v}{\partial \xi} & \text{for } \xi = -a. \end{aligned} \right\} \quad (28)$$

Since for $\xi = \pm a$ the deflection v_s and its derivative $\partial v_s / \partial \xi$ vary continuously with ξ , the latter due to the fact that no finite concentrated forces can act on the strings with finite deflection v_p and finite stiffness c_p (cf. also Eqs. (17) and (20)), in the expressions (28) the limit signs may be omitted, after which they can be used as boundary conditions for the solution of equation (26). For the determination of the integration constants occurring in the solutions of the first-order partial differential equations (9) the additional conditions that the deflections v and u vary continuously

at the leading edge, where $\xi = a$, are still needed. That this continuity does take place can be proved in the following way.

For the case which may occur in reality, where μ is finite and the vertical pressure gradually tends to zero at the leading and trailing edges of the contact area, it will be obvious that the profile elements show no deflection just after entering the contact area or just before leaving this area. The deflections consequently vary continuously in the neighbourhood of both edges in this case.

For the extreme case where finite shear stresses are available at the leading and trailing edge of the contact area ($\mu \rightarrow \infty$) a finite deflection may occur at these edges. Figure 4a shows the deflected centre peripheral line for the case of a very large but finite value of μ . Small vanishing regions of sliding are considered at the edges with deflections (u, v_p) tending to zero for $\xi \rightarrow \pm a$. Sliding occurs in the regions $a - \epsilon_1 < \xi < a$ and $-a < \xi < -a + \epsilon_2$ where ϵ_1 and ϵ_2 are vanishing quantities. At the boundaries of the adhesion zone the deflection of the profile rubber is denoted by (u_1, v_{p1}) at the leading edge and by (u_2, v_{p2}) at the trailing edge.

In figure 4b an arbitrary course of the deflection in the front region of sliding is assumed. It is easy to recognize that at least in one point in that region the slope $\partial u / \partial \xi$ obtains the value:

$$\frac{\partial u}{\partial \xi} = - \frac{u_1}{\epsilon_1} . \quad (29)$$

At this point all the terms in the right-hand member of the first equation of (9), except $\partial u / \partial \xi$, will be negligible with respect to $\partial u / \partial \xi$ when u_1 is finite and $\epsilon_1 \rightarrow 0$. For the sliding velocity in longitudinal direction in the point considered we may write consequently according to the equations (9):

$$W_{\xi 1} = V \frac{u_1}{\epsilon_1} . \quad (30a)$$

In an analogous way we obtain for the other component and for the sliding velocities occurring in certain points at the rear:

$$W_{\eta 1} = V \frac{v_{p1}}{\epsilon_1} , \quad (30b)$$

$$W_{\xi 2} = -V \frac{u_2}{\epsilon_2}, \quad (30c)$$

$$W_{\eta 2} = -V \frac{v_{p2}}{\epsilon_2}. \quad (30d)$$

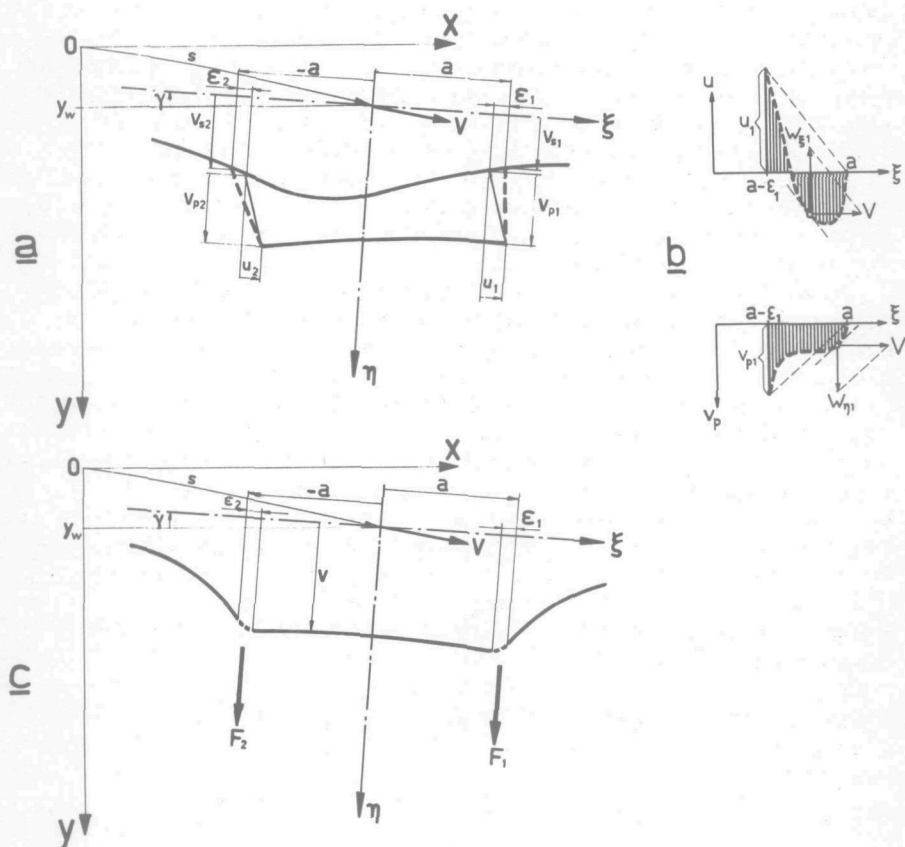


Fig. 4. Probable tyre deformations at vanishing sliding.
 a: With profile rubber, b: In vanishing region of sliding ($\epsilon_1 \rightarrow 0$), c: Without profile rubber.

In the parts of the front- and rear sliding regions where the deflections u have the same sign as u_1 and u_2 respectively, points can always be indicated (cf. Fig. 4b) where the longitudinal components of the sliding velocity have the same

sign as the longitudinal velocity components expressed by (30a) and (30c) respectively. The horizontal shear force acting from the road upon a profile element is always directed opposite to the sense of the sliding velocity of that element with respect to the road. Consequently there are points in the front sliding region where the longitudinal component of the shear force is directed opposite to the sense of the longitudinal deflections while in the rear sliding region points occur where the longitudinal components of forces and deflections are equally directed. The first finding is incompatible and the latter is compatible with the fact that the force must be in equilibrium with the internal reactive force due to elastic deformation. Similar findings are obtained for the lateral deflections and forces. It can be concluded that the leading edge cannot show a finite deflection in contrast to the trailing edge, where the sliding velocities can be compatible with the reactive forces throughout the sliding region.

Until now we have considered the case of finite profile stiffness. We will now turn to the extreme case showing an infinitely stiff profile rubber which in fact represents the tyre without profile elements. It should be investigated now whether the slope $\partial v_s / \partial \xi$ ($= \partial v / \partial \xi$) varies continuously at $\xi = \pm a$. In the case of finite friction coefficient and vertical pressure it is clear that no kink can exist, because then no concentrated force can be transmitted. The case of $\mu \rightarrow \infty$ may be investigated by assuming small vanishing regions of sliding which means that μ is taken large but finite. This principle has been suggested by Kalker [17].

Consider a sliding region $a - \epsilon_1 < \xi < a$ where $\epsilon_1 \rightarrow 0$ when $\mu \rightarrow \infty$ (see Fig. 4c). The sliding velocities are according to equation (4):

$$\text{for } \xi = a - \epsilon_1: W_{\eta} / V = -\psi + a \varphi - \left(\frac{\partial v}{\partial \xi} - \frac{\partial v}{\partial s} \right)_{\xi=a-\epsilon_1} = 0, \quad (31)$$

$$\text{for } \xi = a: W_{\eta} / V = -\psi + a \varphi - \left(\frac{\partial v}{\partial \xi} - \frac{\partial v}{\partial s} \right)_{\xi=a}. \quad (32)$$

Because of the fact that the deflection v varies continuously, we may write:

$$(v)_{\xi=a-\epsilon_1} = (v)_{\xi=a} + \epsilon_1 \cdot w \quad (33)$$

where w is of the order of $\partial v / \partial \xi$ and is a function of ϵ_1 and s . We obtain for the sliding velocity at the leading edge ($\xi = a$):

$$\begin{aligned}
 W_{\eta} &= V \left\{ \left(\frac{\partial v}{\partial \xi} - \frac{\partial v}{\partial s} \right)_{\xi=a-\epsilon_1} - \left(\frac{\partial v}{\partial \xi} - \frac{\partial v}{\partial s} \right)_{\xi=a} \right\} = \\
 &= V \left\{ \left(\frac{\partial v}{\partial \xi} \right)_{\xi=a-\epsilon_1} - \left(\frac{\partial v}{\partial \xi} \right)_{\xi=a} \right\} - \epsilon_1 V \frac{dw}{ds} \quad (34)
 \end{aligned}$$

of which the last term vanishes for $\epsilon_1 \rightarrow 0$.

The lateral force acting on the string over the length $a - \epsilon_1 < \xi < a$ would be:

$$F_1 = S \left\{ \left(\frac{\partial v}{\partial \xi} \right)_{\xi=a-\epsilon_1} - \left(\frac{\partial v}{\partial \xi} \right)_{\xi=a} \right\} + \epsilon_1 c_s \cdot (v)_{\xi=a} \quad (35)$$

of which the last term tends to zero for $\epsilon_1 \rightarrow 0$. The force appears to have the same sign as the sliding velocity and thus is not compatible with this velocity. But the corresponding force and velocity at the trailing edge appear to be opposite in sign so that they are compatible with each other. Consequently, a kink may only appear at the trailing edge. It is shown that the sliding velocity at the trailing edge does not vanish for $\mu \rightarrow \infty$, in contrast to the sliding velocity at the leading edge, which is a result that corresponds to findings of De Pater [14, Fig.7] and Kalker [15, p.148] for the steel-on-steel problem.

Also at the transition between adhesion and sliding regions, v_s and $\partial v_s / \partial \xi$ as well as v vary continuously when a continuous pressure distribution is considered. Complete sets of boundary conditions will be given with the treatment of the specific problems in the subsequent sections.

The forces and the moment acting on the tyre may be computed by integration over the contact area A . The forces in longitudinal and lateral directions become respectively:

$$T = - \int_A p_{\xi} dA \quad , \quad F = - \int_A p_{\eta} dA \quad (36)$$

The moment about the vertical axis reads:

$$M = \int_A (p_{\xi} \eta - p_{\eta} \xi) dA \quad (37)$$

Here p_{ξ} and p_{η} are both forces per unit area. The longitudinal force will become zero in the cases to be treated in the subsequent sections. In general this force is negligible for a freely rolling tyre (no braking or driving torque applied). The vertical load of the tyre will be denoted by N .

In the case of purely lateral slip the tyre models con-

sidered do not show longitudinal deformations so that $p_{\xi}=0$; the lateral force and the moment read then:

$$F = - \int_{-a}^a p_{\eta} d\xi \quad , \quad M = - \int_{-a}^a p_{\eta} \xi d\xi \quad , \quad (38)$$

where p_{η} denotes a force per unit length.

The group of investigators concerned with the steel-on-steel problem mostly use notations which differ here and there from those employed above. For the sake of convenience we have listed some important relations below; the symbols shown in each left-hand member correspond to notations of de Pater [14], Kalker [16] and others:

$$v_y = -\psi; \quad T_x (=F_x) = -T; \quad T_y (=F_y) = -F; \quad M_z = -M. \quad (38a)$$

3. Stationary behaviour for any slip value

This section deals with the derivation of mathematical expressions for the deflections of the strings and profile elements and in addition for the cornering force F and the aligning torque M as a function of the slip angle ψ for stationary rectilinear motions ($\varphi=0$).

The vertical force distribution per unit length is assumed to be parabolic along the ξ -axis, which is a fair approximation of distributions met in reality (see for instance Martin [45]). We obtain for the lateral force distribution in regions of sliding:

$$p_{\eta} = \mu p_{\zeta} \operatorname{sgn} W_{\eta} \quad (39)$$

where

$$p_{\zeta} = p_{\zeta_0} \{1 - (\xi/a)^2\} \quad (40)$$

with $p_{\zeta_0} = \frac{3N}{8ab}$ denoting the maximum value of p_{ζ} at $\xi = 0$.

It is convenient to introduce non-dimensional quantities shown in table 1. For simplicity we shall henceforth omit the underlinings indicating the quantities to be non-dimensional.

We shall first investigate the tyre at high slip values (slip angles), so that no regions of adhesion occur. Next the slip value will be reduced until adhesion starts in a certain point. The point where this occurs will be determined for

Table 1. Non-dimensional quantities.

$$\begin{array}{l}
 \tau_o = \frac{\mu p \zeta_o}{c_s a}, \quad \underline{\psi} = \frac{\psi}{\tau_o}, \quad \underline{v} = \frac{v}{\tau_o a}, \quad \underline{\xi} = \frac{\xi}{a}, \quad \underline{\sigma} = \frac{\sigma}{a}, \quad \underline{\sigma}_c = \frac{\sigma_c}{a}, \\
 \underline{e}' = \frac{e'}{a}, \quad \underline{C} = \frac{C}{c_s a^2}, \quad \underline{C}_M = \frac{C_M}{c_s a^3}, \quad \underline{p}_\eta = \frac{p_\eta}{\tau_o c_s a} = \frac{p_\eta}{\mu p \zeta_o}, \\
 \underline{F} = \frac{F}{\tau_o c_s a^2} = \frac{F}{\mu p \zeta_o a}, \quad \underline{M} = \frac{M}{\tau_o c_s a^3} = \frac{M}{\mu p \zeta_o a^2}, \quad \underline{N} = \frac{N}{\mu p \zeta_o a}.
 \end{array}$$

several configurations. After that we will examine the tyre moving at even smaller slip values and finally at vanishing slip.

3A. Total sliding

When total sliding occurs, expression (14) is applicable over the whole contact length. We shall assume positive values of the slip angle ψ so that positive deflections and negative sliding velocities occur.

The lateral force distribution will be now, according to (39) and table 1:

$$p_\eta = -(1 - \xi^2). \quad (41)$$

Equation (24) governing the deflection of the string becomes consequently in non-dimensional form in the stationary case:

$$\sigma^2 \frac{d^2 v_s}{d\xi^2} - v_s = -1 + \xi^2; \quad (42)$$

owing to the boundary conditions (28) the solution becomes:

$$v_s = \sigma(\sigma + 1) \left(e^{-\frac{1+\xi}{\sigma}} + e^{-\frac{1-\xi}{\sigma}} \right) + 1 - 2\sigma^2 - \xi^2. \quad (43)$$

The deflection of the profile rubber becomes with (17), (23) and (41):

$$v_p = \frac{\epsilon^2}{1 - \epsilon^2} (1 - \xi^2). \quad (44)$$

Hence the total deflection reads according to (16):

$$v = \sigma(\sigma + 1) \left(e^{-\frac{1+\xi}{\sigma}} + e^{-\frac{1-\xi}{\sigma}} \right) - 2\sigma^2 + \frac{1 - \xi^2}{1 - \epsilon^2}. \quad (47)$$

The sliding velocity for stationary motions becomes according to equations (9):

$$W_\eta/V = -\psi - \frac{dv}{d\xi}. \quad (46)$$

When the slip angle ψ is gradually reduced, the sliding velocity will become zero for the first time in the point where the slope $-\partial v/\partial \xi$ is maximal, i.e. where $\partial^2 v/\partial \xi^2$ vanishes or at the leading edge.

The first derivative of v with respect to ξ becomes:

$$\frac{dv}{d\xi} = -(\sigma + 1) \left(e^{-\frac{1+\xi}{\sigma}} - e^{-\frac{1-\xi}{\sigma}} \right) - 2 \frac{\xi}{1 - \epsilon^2}. \quad (47)$$

The second derivative becomes:

$$\begin{aligned} \frac{d^2v}{d\xi^2} &= \frac{\sigma + 1}{\sigma} \left(e^{-\frac{1+\xi}{\sigma}} + e^{-\frac{1-\xi}{\sigma}} \right) - \frac{2}{1 - \epsilon^2} = \\ &= \frac{v_s}{\sigma^2} - \frac{1 - \xi^2}{\sigma^2} - 2 \frac{\epsilon^2}{1 - \epsilon^2}. \end{aligned} \quad (48)$$

The point of inflexion appears to have the same ξ co-ordinate as the point of intersection of the deflection curve $\eta = v_s$ and the parabola $\eta = 1 - \xi^2 + 2\sigma^2\epsilon^2/(1 - \epsilon^2)$. Figure 5a shows the deflection curves of the string for several values of σ and the parabolas for various ϵ . The points of inflexion of these curves are shown as well as the points indicating the ξ -values where the contact lines have their maximum slope $-\partial v/\partial \xi$ and where consequently for the first time adhesion occurs. Only in the case that no points of inflexion are present, first adhesion will occur at the leading edge. The parabola for $\epsilon = 0$ coincides with the deflection curve of the string for $\sigma = 0$.

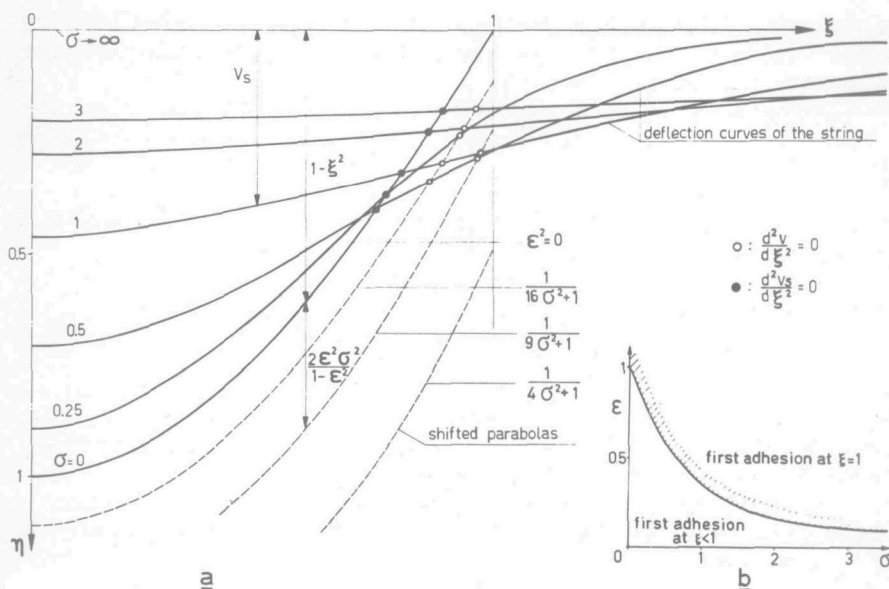


Fig. 5a. Graphical method for determining the points of inflexion of the contact line of the tyre under total sliding conditions.

b. Relation between σ and ϵ according to Eq. (48a).

It appears that the point of first adhesion is situated somewhat behind the leading edge, when the quantity ϵ is smaller than a certain value depending on σ , i.e. when the stiffness of the profile rubber is greater than a certain value. This means that when reducing the slip angle further, two sliding regions will occur: a small region before and a much larger one behind the adhesion region. The limit value of ϵ above which first adhesion occurs at the leading edge, can be calculated by means of the following formula:

$$\epsilon^2 = \frac{1 - \sigma \operatorname{th} \sigma^{-1}}{1 + \sigma} \quad (48a)$$

This relation between ϵ and σ , plotted in figure 5b has been derived from (43) and (48) by putting $\xi = 1$ and $d^2v/d\xi^2 = 0$.

3B. Partial sliding

We shall first examine the case of relatively large ϵ such that no sliding region at the leading edge can arise. Afterwards the case of $\epsilon = 0$ will be considered (no profile

The direction of sliding will be assumed to be negative in the entire sliding region as a logical consequence of the behaviour with total sliding. The sliding direction may afterwards be checked by means of equation (51).

There are five constants of integration and one unknown a_2 . We therefore need six boundary conditions in order to compute these. The conditions read:

$$\left. \begin{aligned} \xi = 1 & : v_s = v (=v_1), \quad \frac{dv_s}{d\xi} = -\frac{v_s}{\sigma}, \\ \xi = a_2 & : \lim_{\xi \uparrow a_2} \left(\frac{dv_s}{d\xi}, v_s, v \right) = \lim_{\xi \downarrow a_2} \left(\frac{dv_s}{d\xi}, v_s, v \right), \\ \xi = -1 & : \frac{dv_s}{d\xi} = \frac{v_s}{\sigma}. \end{aligned} \right\} \quad (54)$$

Integration of equation (49) yields, when the deflection at $\xi = 1$ is denoted by v_1 :

$$v = v_1 + (1 - \xi)\psi \quad \text{for} \quad a_2 < \xi < 1. \quad (55)$$

Using the boundary conditions for $\xi = 1$, we may solve v_s from equations (50). Expressed in terms of v_1 and ψ we obtain for $a_2 < \xi < 1$:

$$\begin{aligned} v_s = & \left[\frac{1}{2} \epsilon \left\{ (1 + \epsilon) e^{\frac{1-\xi}{\sigma_c}} - (1 - \epsilon) e^{-\frac{1-\xi}{\sigma_c}} \right\} + (1 - \epsilon^2) \right] v_1 + \\ & - (1 - \epsilon^2) \left[\frac{1}{2} \sigma_c \left(e^{\frac{1-\xi}{\sigma_c}} - e^{-\frac{1-\xi}{\sigma_c}} \right) - 1 + \xi \right] \psi. \end{aligned} \quad (56)$$

The solution of equation (53) for the sliding region contains two integration constants, of which one can be computed with the use of the boundary condition for $\xi = -1$. We obtain then for $-1 < \xi < a_2$:

$$v_s = \sigma(\sigma + 1) e^{-\frac{1+\xi}{\sigma}} + C_2 e^{\xi/\sigma} + 1 - 2\sigma^2 - \xi^2. \quad (57)$$

For the solution of the three unknowns v_1 , a_2 (or ψ) and C_2 we have the three remaining conditions in the point $\xi = a_2$

at our disposal. Finally we obtain ψ as a function of a_2 :

$$\psi = 2 \frac{\left[\frac{1 - a_2^2}{1 - \epsilon^2} + 2\sigma \left\{ a_2 - \sigma + (\sigma + 1) e^{-\frac{1+a_2}{\sigma}} \right\} \right] \cdot B + \epsilon \frac{1 - a_2^2}{1 - \epsilon^2} \cdot A}{A \cdot D + C \cdot B} \quad (58)$$

where

$$A = 2 + (1 + \epsilon) e^{\frac{1-a_2}{\sigma c}} + (1 - \epsilon) e^{-\frac{1-a_2}{\sigma c}},$$

$$B = -2\epsilon + (1 + \epsilon) e^{\frac{1-a_2}{\sigma c}} - (1 - \epsilon) e^{-\frac{1-a_2}{\sigma c}},$$

$$C = 2(1 - a_2) + \sigma(1 - \epsilon^2) \left(2 - e^{\frac{1-a_2}{\sigma c}} - e^{-\frac{1-a_2}{\sigma c}} \right),$$

$$D = 2\epsilon(1 - a_2) + \sigma(1 - \epsilon^2) \left(e^{\frac{1-a_2}{\sigma c}} - e^{-\frac{1-a_2}{\sigma c}} \right).$$

Once the value of ψ is known, v_1 can be calculated:

$$v_1 = \frac{-2\epsilon \frac{1 - a_2^2}{1 - \epsilon^2} + D \cdot \psi}{B} \quad (59)$$

The constant C_2 becomes:

$$C_2 = \left\{ v_1 + (1 - a_2)\psi - \sigma(\sigma + 1) e^{-\frac{1+a_2}{\sigma}} + 2\sigma^2 - \frac{1 - a_2^2}{1 - \epsilon^2} \right\} e^{-\frac{a_2}{\sigma}} \quad (60)$$

Insertion of ψ , v_1 and C_2 for given a_2 in equations (56) and (57) results in the co-ordinates of the string, after which the shape of the contact line can be calculated with the use of equations (55) and (52).

For the special case of $\epsilon = 1/7.5$ and $\sigma = 3.7411$, this has been carried out for a number of values of a_2 . Figure 7 shows the shape of the string and the contact line for several slip angles ψ . The obliquely shaded area indicates the sliding regions, growing with increasing slip angle until the whole

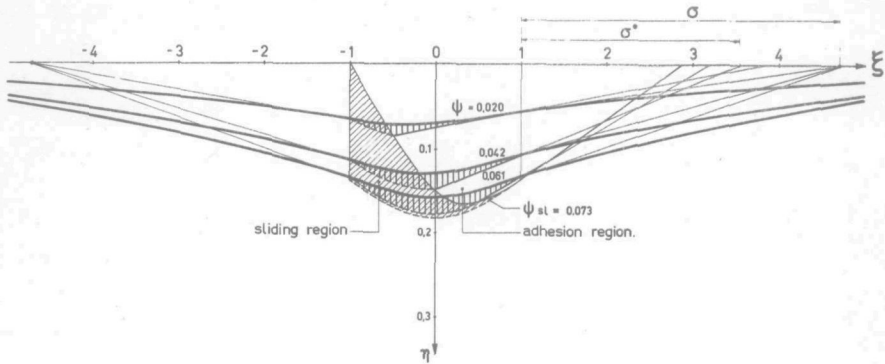


Fig. 7. The deflected tyre model provided with profile rubber ($\sigma^*=3$, $\epsilon=1/7.5$) for various slip angles. The shaded area indicates the regions where sliding occurs.

contact line slides. Larger slip angles will not alter the shape anymore.

A check has revealed that the deflection of the profile rubber in the straight portion of the contact line remains in the case considered below the maximum possible values, so that no front sliding will occur, which is in agreement with findings shown in figure 5b. Also the slope of the contact line in the sliding region remains smaller than ψ so that the direction of sliding assumed is correct.

We define the relaxation length σ^* as the distance between the leading edge of the contact area and the point of intersection of the elongation of the straight portion of the contact line with the ξ -axis. The values of σ and ϵ mentioned above were chosen in such a way that σ^* tends to the value 3 for $\psi \rightarrow 0$ (cf. Sec. 3C, Eq. (77), Table 2). We observe, that the relaxation length decreases from the value 3 when the sliding region vanishes until a value somewhat less than 2 when total sliding occurs.

Once the deflection of the tyre model is known, the force and moment can be calculated. Integration over the contact length with the use of the expressions (14) and (17) as indicated by equations (38) yields:

$$\begin{aligned}
 F = F_{\text{slip}} + F_{\text{adhesion}} &= \frac{1}{3}(2+3a_2 - a_2^3) + (v_1 + \psi)(1-a_2) - \frac{1}{2}(1-a_2^2)\psi + \\
 &+ \frac{1}{2} \sigma \left[\left\{ (1 + \epsilon)v_1 - (1 - \epsilon^2)\sigma\psi \right\} \left(1 - e^{-\frac{1-a_2}{\sigma c}} \right) + \right. \\
 &\quad \left. + \left\{ (1 - \epsilon)v_1 - (1 - \epsilon^2)\sigma\psi \right\} \left(1 - e^{-\frac{1-a_2}{\sigma c}} \right) \right]. \quad (61)
 \end{aligned}$$

$$\begin{aligned}
 M = M_{\text{slip}} + M_{\text{adhesion}} = & -\frac{1}{4}(1-2a_2^2+a_2^4) + \frac{1}{2}(v_1+\psi)(1-a_2^2) - \frac{1}{3}(1-a_2^3)\psi + \\
 & + \frac{1}{2}\sigma \left[\left\{ (1+\epsilon)v_1 - (1-\epsilon^2)\sigma\psi \right\} \left\{ 1+\sigma_c - (a_2+\sigma_c)e^{-\frac{1-a_2}{\sigma_c}} \right\} + \right. \\
 & \left. + \left\{ (1-\epsilon)v_1 - (1-\epsilon^2)\sigma\psi \right\} \left\{ 1-\sigma_c - (a_2-\sigma_c)e^{-\frac{1-a_2}{\sigma_c}} \right\} \right]. \quad (62)
 \end{aligned}$$

Figure 8 shows the characteristics calculated for the

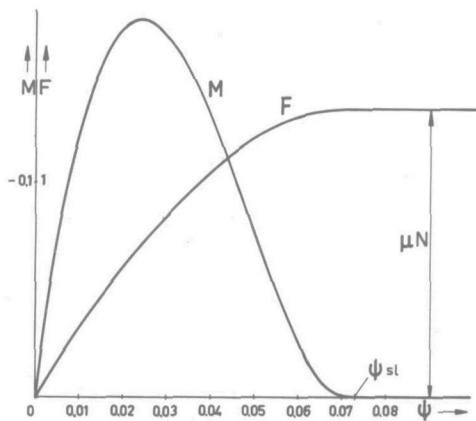


Fig.8. Tyre cornering characteristics for the tyre model with profile rubber ($\sigma^*=3$, $\epsilon=1/7.5$).

cornering force F and the aligning torque M as a function of the slip angle ψ . The slope of the curves become zero at the slip angle $\psi=\psi_{sl}$ where total sliding starts. The shape is similar to those obtained from experiments or from calculations in which alternative models are used as those of Fiala [20], Freudenstein [21] or Pacejka [23].

The phenomenon that in practice the aligning torque obtains a positive value for large slip angles, cannot be explained with our model. It is probably caused among other things by the longitudinal forces due to rolling resistance of which the resultant acts out of the wheel plane due to the lateral deformation of the tyre and thus forms a couple about the vertical axis opposed to the aligning torque. Another important factor helping the moment to become positive is the fact that the coefficient of friction is not a constant but depends on the sliding velocity (cf. Savkoor [27]).

As mentioned before the general case of relatively large

stiffness of the profile elements, showing an additional sliding region at the leading edge, will not be studied because of the great complexity involved. We will treat only the case of infinite stiffness of the profile rubber ($\epsilon=0$, $\sigma^*=\sigma$, $v_p=0$, $v=v_s$). Figure 9 shows the simple string model

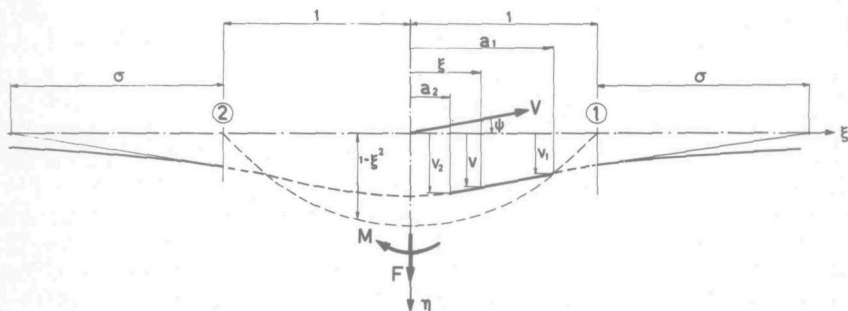


Fig.9. The deflected tyre model without profile rubber showing two sliding regions.

in deflected situation. Two regions of sliding are expected, one at the front ($a_1 < \xi < 1$) and the other at the rear ($-1 < \xi < a_2$).

In the region of adhesion equation (13) holds. In the stationary case we obtain:

$$\frac{dv}{d\xi} = -\psi \quad \text{for} \quad a_2 < \xi < a_1. \quad (63)$$

For the sliding regions the following equations apply according to equations (14), (24) and (41):

$$\left. \begin{aligned} \frac{dv}{d\xi} &= -\psi - \frac{W_\eta}{V} \end{aligned} \right\} \begin{aligned} &\text{for } a_1 < \xi < 1 \\ &\text{and } -1 < \xi < a_2. \end{aligned} \quad (64)$$

$$\left. \begin{aligned} \sigma^2 \frac{d^2v}{d\xi^2} - v &= (1 - \xi^2) \operatorname{sgn} W_\eta \end{aligned} \right\} \quad (65)$$

Equation (63) indicates again that the contact line is straight in the region of adhesion ($d^2v/d\xi^2 = 0$). In this region the following inequality holds according to equations (24), (13), (39) and table 1:

$$v < 1 - \xi^2 \quad \text{for} \quad a_2 < \xi < a_1, \quad (66)$$

which means that the straight portion of the contact line lies inside the parabola $v = 1 - \xi^2$. The points of inflection of the contact line are located on this parabola when $W_\eta < 0$ in these points. Near the two edges $\xi = \pm 1$ the available lateral force tends to zero. Since a finite deflection $v > 0$ is present in these places, the curvature of the string will be concave ($d^2v/d\xi^2 > 0$) according to (65).

After these general observations, we shall examine the shape of the contact line starting from the trailing edge. In the rear portion of the contact line $dv/d\xi > 0$, so that according to (64) $W_\eta < 0$. Until the contact line intersects the parabola, the shape remains concave. Inside the parabola, however, the curve becomes convex. At $\xi = a_2$ the adhesion region is entered. At $\xi = a_1$ the front sliding region is entered. When this latter point of transition lies inside the parabola, according to (65) the curve must be convex just in front of that point when the sliding velocity is negative. This shape, however, leads to an increase in slope, so that according to (64) the sliding direction becomes positive in that case, which is in contradiction with the assumption. In the same way a concave shape can be shown to be impossible. The conclusion is that this point of transition must lie on the parabola. The curve in the front sliding region can only be concave, so that $W_\eta < 0$. Its curvature tends to zero when the parabola is approached. We may conclude that throughout the contact area $W_\eta \leq 0$ and that no more than one adhesion region can arise.

For the front sliding region the following boundary conditions apply:

$$\left. \begin{aligned} \xi = 1 : \quad \frac{dv}{d\xi} &= -\frac{v}{\sigma}, \\ \xi = a_1 : \quad \frac{dv}{d\xi} &= -\psi, \quad \frac{d^2v}{d\xi^2} = 0, \quad (v = 1 - a_1^2). \end{aligned} \right\} \quad (67)$$

These conditions suffice to find the solution for the contact line of the front sliding region and with it the value a_1 . It appears that the front part is not affected by the rear portion. For the adhesion region the condition within brackets may be employed.

For the rear sliding region in which the deflection does depend on what happens in the front, the following conditions apply:

$$\left. \begin{aligned} \xi = a_2 : \quad v &= v_1 + (a_1 - a_2)\psi, \quad \frac{dv}{d\xi} = -\psi, \\ \xi = -1 : \quad \frac{dv}{d\xi} &= \frac{v}{\sigma}, \end{aligned} \right\} \quad (68)$$

where v_1 denotes again the deflection of the foremost point in the adhesion region. The conditions (68) are needed to determine the constants of integration and the unknown a_2 for the solution in the rear sliding region. Altogether we have five constants of integration and two unknown lengths a_1 and a_2 , which may be determined with the aid of the 4 + 3 conditions (67) and (68).

The solution for the front sliding region reads:

$$v = \sigma \left\{ \psi + (\sigma + 1) e^{\frac{a_1 - 1}{\sigma}} - 2a_1 \right\} e^{\frac{a_1 - \xi}{\sigma}} + (\sigma + 1) \sigma e^{\frac{\xi - 1}{\sigma}} + 1 - 2\sigma^2 - \xi^2; \quad (69)$$

together with the condition $v_1 = 1 - a_1^2$ we obtain:

$$\psi = 2 \left\{ a_1 + \sigma - (\sigma + 1) e^{\frac{a_1 - 1}{\sigma}} \right\}. \quad (70)$$

With the numerical method of Newton-Raphson a_1 can be solved as a function of ψ , after which v can be calculated as a function of ξ for $a_1 < \xi < 1$. The deflection in the adhesion region becomes:

$$v = v_1 + (a_1 - \xi)\psi = 1 - a_1^2 + (a_1 - \xi)\psi. \quad (71)$$

The solution for the rear sliding region reads:

$$v = \sigma \left\{ -\psi + (\sigma + 1) e^{-\frac{a_2 + 1}{\sigma}} + 2a_2 \right\} e^{\frac{\xi - a_2}{\sigma}} + (\sigma + 1) \sigma e^{-\frac{\xi + 1}{\sigma}} + 1 - 2\sigma^2 - \xi^2. \quad (72)$$

The unknown a_2 can be solved with the aid of the condition $v_2 = v_1 + (a_1 - a_2)\psi$. This condition reads with the use of expression (72):

$$2\sigma(\sigma + 1) e^{-\frac{a_2 + 1}{\sigma}} - (\sigma - a_2)^2 = 2\sigma(\sigma + 1) e^{\frac{a_1 - 1}{\sigma}} - (\sigma + a_1)^2 + (a_1 - a_2 + 2\sigma)\psi. \quad (73)$$

The solution of a_2 for certain ψ may again be carried out by means of the Newton-Raphson method. Equation (72)

gives then the deflection v as a function of ξ for $-1 < \xi < a_2$.

For the value of the relaxation length $\sigma=3$ the contact line has been calculated. Figure 10 shows the results. The

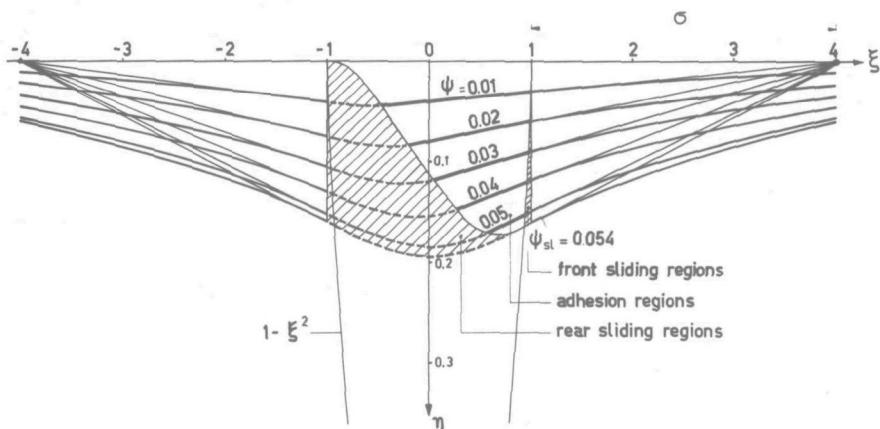


Fig.10. The deflected tyre model without profile rubber ($\sigma=3$, $\epsilon=0$) for various slip angles. The shaded areas indicate the regions where sliding occurs.

shaded areas indicate the regions of the contact line where sliding occurs. A part of the parabola shown forms the boundary between adherence and front sliding regions. Another curve forms the rear boundary of the adherence regions. These two curves intersect when total sliding starts at a slip angle $\psi_{sl} = 0.054$.

When no front sliding would be taken into account, a solution very close to the real solution will be obtained because of the fact that the sliding portion of the contact line at the leading edge is practically straight and short with respect to the contact length. Another consequence is that the variation in relaxation length with slip angle will be very small.

The cornering force and the aligning torque are found by integrating along the contact line. We obtain:

$$\begin{aligned}
 F &= \int_{-1}^{a_2} (1 - \xi^2) d\xi + \int_{a_2}^{a_1} v d\xi + \int_{a_1}^1 (1 - \xi^2) d\xi = \\
 &= \frac{4}{3} + a_2 - a_1 + \frac{1}{3} (a_1^3 - a_2^3) + \frac{1}{2} (a_1 - a_2) (v_1 + v_2), \quad (74)
 \end{aligned}$$

$$\begin{aligned}
 M &= \int_{-1}^{a_2} (1 - \xi^2) \xi \, d\xi + \int_{a_2}^{a_1} v \xi \, d\xi + \int_{a_1}^1 (1 - \xi^2) \xi \, d\xi = \\
 &= -\frac{1}{2} (a_1^2 - a_2^2) + \frac{1}{4} (a_1^4 - a_2^4) + \frac{1}{2} (a_1 + a_2)(a_1 v_2 - a_2 v_1) + \\
 &\quad + \frac{1}{3} (a_1^2 + a_1 a_2 + a_2^2) (v_1 - v_2). \tag{75}
 \end{aligned}$$

The results of the computations carried out with the aid of a digital computer are shown in figure 11. In contrast

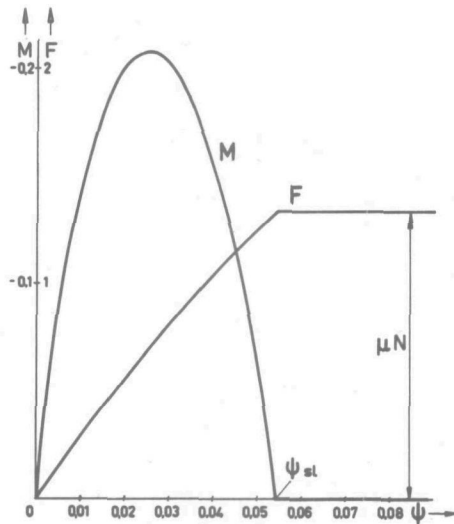


Fig. 11. Tyre cornering characteristics for the tyre model without profile elements ($\sigma=3$, $\varepsilon=0$).

to the characteristics of the more elaborate model shown in figure 8, the curves show a discontinuity at a slip angle where total sliding starts. The model behaves, as far as the force is concerned, more or less, like a spring in series with a Coulomb frictional element.

The fact, that both front and rear sliding regions exist in the case treated above, may lead to the conclusion that at each edge a concentrated force will act in case of vanishing sliding. This conclusion is not correct, since large forces per unit length can be transmitted only in a portion where a convex deflection of the string occurs. The latter is the case at the rear, inside of the parabola, only

so that for $\psi \rightarrow 0$ a concentrated force will occur at the rear only. We may remark, that according to calculations not being reproduced here, in the case of a rectangular pressure distribution no front sliding will occur for the model considered.

3C. Vanishing sliding

The stationary behaviour in case of vanishing sliding regions, so for friction coefficients tending to infinity or slip angles tending to zero (see Figs.12a, b), is the next problem to be investigated.

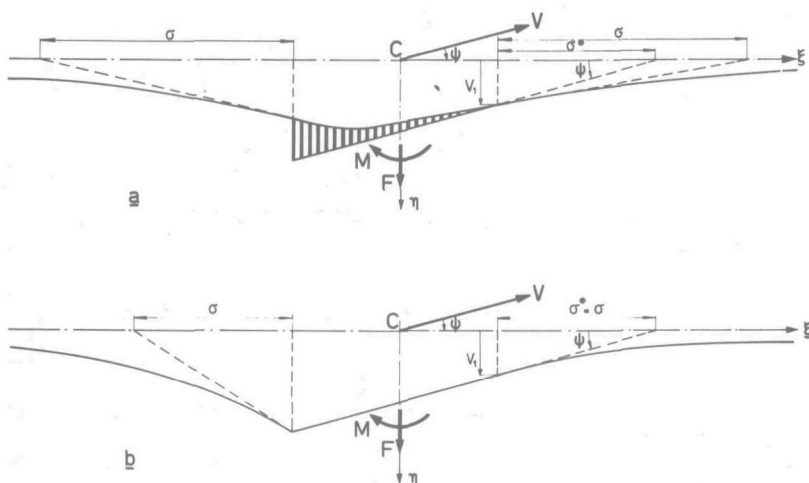


Fig.12. The deflected tyre model at vanishing sliding.
a: With profile rubber, b: Without profile rubber.

Along the whole contact line adhesion occurs. Equations (13) and (26) apply thus for $-1 < \xi < 1$. For $\xi = -1$ the solution of equation (26) given by expression (56) has as boundary condition the last relation of (54). With the aid of this condition the deflection v_1 can be calculated. Omitting the detailed calculations, we obtain:

$$v_1 = \sigma^* \psi, \quad (76)$$

where

$$\sigma^* = \frac{\sigma \left\{ (1 + \epsilon) e^{2/\sigma_c} + (1 - \epsilon) e^{-2/\sigma_c} - 2 \right\} - 4}{\frac{1 + \epsilon}{1 - \epsilon} e^{2/\sigma_c} + \frac{1 - \epsilon}{1 + \epsilon} e^{-2/\sigma_c} + 2}, \quad (77)$$

which is the expression for the relaxation length as defined before (see Fig.12a). The relaxation length tends to the value σ when the profile stiffness becomes infinite (see Fig.12b).

By using equations (56), (55) and (16) the deflection of the profile elements can be calculated, after which expressions for the force and moment can be obtained with (17) and (38). We define:

$$F = C \psi \quad \text{and} \quad M = -C_M \psi \quad (78)$$

with C and C_M denoting the non-dimensional cornering stiffnesses (see for definition Table 1). These coefficients turn out to obtain the following values:

$$\begin{aligned} C &= 2(1-\epsilon^2) \left[\sigma^* + 1 - \frac{1}{4} \sigma \sigma^* \left\{ (1+\epsilon) e^{2/\sigma_c} + (1-\epsilon) e^{-2/\sigma_c} - 2 \right\} + \right. \\ &\quad \left. + \frac{1}{4} \sigma^2 (1-\epsilon^2) (e^{2/\sigma_c} + e^{-2/\sigma_c} - 2) \right], \\ C_M &= 2(1-\epsilon^2) \left[\frac{1}{3} - \frac{1}{4} \sigma \left\{ \sigma^* (1+\epsilon) - \sigma (1-\epsilon^2) \right\} \left\{ 1 + e^{2/\sigma_c} + \sigma_c (1 - e^{2/\sigma_c}) \right\} \right. \\ &\quad \left. - \frac{1}{4} \sigma \left\{ \sigma^* (1-\epsilon) - \sigma (1-\epsilon^2) \right\} \left\{ 1 + e^{-2/\sigma_c} - \sigma_c (1 - e^{-2/\sigma_c}) \right\} \right]. \end{aligned} \quad (79)$$

When the profile elements are omitted ($\epsilon \rightarrow 0$), these equations reduce to:

$$C = 2(\sigma+1)^2 \quad \text{and} \quad C_M = 2 \left\{ \sigma(\sigma+1) + \frac{1}{3} \right\}, \quad (80)$$

or in dimensional form:

$$C = 2 c_s (\sigma+a)^2 \quad \text{and} \quad C_M = 2 c_s a \left\{ \sigma(\sigma+a) + \frac{1}{3} a^2 \right\}. \quad (81)$$

The ratio of C_M and C will be defined as the pneumatic trail e' , which indicates the point in rear of the contact centre where the resulting lateral force is acting. For a number of values for σ and ϵ , the resulting relaxation length σ^* and pneumatic trail e' are listed in table 2. It is remarkable that the employment of profile rubber of a relatively very high stiffness ($c_p/c_s = 55$) does reduce σ^* and e' that much. The model with profile rubber may give results close to those obtained experimentally (cf.

Fonda and Radt [41, Figs. 25, 34]).

Table 2. Influence of model parameters.

tyre model	tyre data			relaxation length σ^*	pneumatic trail e'
	σ	e	c_p/c_s		
stretched string (Von Schlippe)	3.7411	0	∞	3.7411	0.803
	3	0	∞	3	0.772
stretched string + profile rubber	3.7411	$\frac{1}{7.5}$	55	3	0.49
profile rubber only (rigid carcass)	∞	1	0	0	1/3

4. Non-stationary behaviour for vanishing slip

In this section we will investigate the non-stationary behaviour of a tyre. We will restrict ourselves to linearised systems where sliding in the contact area does not occur ($\mu \rightarrow \infty$ or $\psi \rightarrow 0$ and $\varphi \rightarrow 0$). The response of the force F and the moment M with respect to arbitrary variations in ψ and φ will be determined for the model with profile rubber and for some approximative concepts. We will return to quantities with dimension.

4A. Exact theory

The contact equations (9) apply when W_ξ and W_η are taken equal to zero. They read then:

$$\left. \begin{aligned} \frac{\partial u}{\partial \xi} - \frac{\partial u}{\partial s} &= -\eta \varphi, \\ \frac{\partial v}{\partial \xi} - \frac{\partial v}{\partial s} &= -\psi + \xi \varphi. \end{aligned} \right\} \quad (82)$$

These partial differential equations will be solved by using Laplace transformation. The Laplace transforms are written in capitals. We will not transform with respect to time, as is done usually, but with respect to the travelled distance $s = Vt$, where V is a constant. The Laplace transform

of a variable quantity, generally indicated by q , is defined through:

$$\mathcal{L}\{q(s)\} = Q(p_s) = \int_0^{\infty} e^{-p_s s} q(s) ds. \quad (83)$$

With the initial condition $u(\xi, 0) = v(\xi, 0) = 0$ at $s = 0$ we obtain:

$$\frac{dU}{d\xi} - p_s U = -\eta \Phi, \quad (84a)$$

$$\frac{dV}{d\xi} - p_s V = -\Psi + \xi \Phi. \quad (84b)$$

The solutions of these ordinary first-order differential equations read:

$$U = C_u e^{p_s \xi} + \frac{1}{p_s} \eta \Phi, \quad (85a)$$

$$V = C_v e^{p_s \xi} + \frac{1}{p_s} \Psi - \frac{1}{p_s} \left(\frac{1}{p_s} + \xi \right) \Phi. \quad (85b)$$

The terms $C_u e^{p_s \xi}$ and $C_v e^{p_s \xi}$ point to a retardational behaviour. These terms appear to represent the Laplace transforms of the co-ordinates of a contact point with respect to a co-ordinate system fixed in space, with axes nearly parallel to the ξ - and η -axes ($\gamma \ll 1$, i.e. powers of γ negligible, cf. Fig.1). For these co-ordinates x_c and y_c evidently the following property holds:

$$x_c(\xi, s) = x_c(r, s + \xi - r), \quad y_c(\xi, s) = y_c(r, s + \xi - r), \quad (86)$$

where r is some arbitrary value ranging from $-a$ to $+a$. It indicates the non-sliding condition of the contact points.

The coefficients C_u and C_v are constants of integration. They are functions of p_s and depend on the tyre construction, expressed i. a. by equation (26) and the boundary conditions (Eqs. (28) and further). The condition at the leading edge:

$$\xi = a: \quad u = 0 \quad \text{or} \quad U = 0 \quad (87)$$

leads to the following expression for C_u :

$$C_u = -\frac{1}{p_s} \eta \Phi e^{-p_s a}. \quad (88)$$

For the determination of C_v we turn to equation (26) which reads in transformed way:

$$\sigma_c^2 \frac{d^2 V_s}{d\xi^2} - V_s = -(1 - \epsilon^2) V \quad (89)$$

With equation (85b) we obtain the differential equation:

$$\sigma_c^2 \frac{d^2 V_s}{d\xi^2} - V_s = -(1 - \epsilon^2) \left\{ C_v e^{p_s \xi} + \frac{1}{p_s} \Psi - \frac{1}{p_s} \left(\frac{1}{p_s} + \xi \right) \Phi \right\}. \quad (90)$$

the solution of which reads:

$$V_s = C_+ e^{\xi/\sigma_c} + C_- e^{-\xi/\sigma_c} + (1 - \epsilon^2) \left\{ \frac{C_v e^{p_s \xi}}{1 - \sigma_c^2 p_s^2} + \frac{1}{p_s} \Psi - \frac{1}{p_s} \left(\frac{1}{p_s} + \xi \right) \Phi \right\}. \quad (91)$$

The three constants of integration C_v , C_+ and C_- may be solved with the aid of the three boundary conditions:

$$\left. \begin{aligned} \xi = a: \quad v_s = v, \quad \frac{\partial v_s}{\partial \xi} = -\frac{v_s}{\sigma} \quad \text{or } V_s = V, \quad \frac{dV}{d\xi} = -\frac{V}{\sigma}, \\ \xi = -a: \quad \frac{\partial v_s}{\partial \xi} = \frac{v_s}{\sigma} \quad \text{or } \frac{dV}{d\xi} = \frac{V}{\sigma}. \end{aligned} \right\} \quad (92)$$

For the constants C_+ and C_- we obtain in terms of Ψ, Φ and C_v :

$$C_{\mp} = \frac{1}{2} (1 \pm \epsilon) \left[\left\{ 1 - \frac{1 \mp \epsilon}{1 \pm \sigma_c p_s} \right\} C_v e^{p_s a} \pm \frac{\epsilon}{p_s} \Psi + \mp \frac{\epsilon}{p_s} \left\{ \frac{1}{p_s} + a + \sigma (1 \mp \epsilon) \right\} \Phi \right] e^{\pm \frac{a}{\sigma_c}} \quad (93)$$

and finally for the constant C_v :

$$C_v = C_{\psi} \Psi + C_{\phi} \Phi \quad (94)$$

where

$$C_{\psi} = -(2 + A_+ + A_-) / (p_s A),$$

$$C_{\varphi} = \left[(2 + A_+ + A_-) / p_s + a (-2 + A_+ + A_-) + \right. \\ \left. + \sigma \{ -2 + (1 - \epsilon) A_+ + (1 + \epsilon) A_- \} \right] / (p_s A)$$

with

$$A = (1 + \sigma p_s) \left(\frac{A_+}{1 + \sigma_c p_s} + \frac{A_-}{1 - \sigma_c p_s} \right) e^{p_s a} + 2 \frac{1 - \sigma p_s}{1 - \sigma_c^2 p_s^2} e^{-p_s a}, \\ A_{\pm} = \frac{1 \pm \epsilon}{1 \mp \epsilon} e^{\pm \frac{a}{\sigma_c}}.$$

With the aid of equations (15), (16), (17) and (36), (37) the forces and the moment can be calculated. In (36) and (37) instead of $p_{\eta} dA$, where p_{η} is a force per unit area, we may as well write $p_{\eta} d\xi$ with p_{η} denoting a force per unit length, because of the fact that p_{η} does not vary in axial direction, as η does not appear in the expressions for the lateral deflections.

Because of the anti-symmetry of the longitudinal deflections u (cf. Eqs. (85a, 88)) we obtain for the Laplace transform of the longitudinal force and thus also for the longitudinal force itself:

$$\mathcal{L}\{T\} = 0, \quad T = 0. \quad (95)$$

The Laplace transform of the moment M^* due to longitudinal deflections becomes:

$$\mathcal{L}\{M^*\} = -c^* \int_A U \eta dA = -\frac{1}{p_s} c^* \Phi \int_{\eta=-b}^b \eta^2 d\eta \int_{\xi=-a}^a (1 - e^{p_s(\xi-a)}) d\xi = \\ = M_{\psi}^* \Psi + M_{\varphi}^* \Phi, \quad (96)$$

with the transfer functions:

$$\left. \begin{aligned} M_{\psi}^* &= 0, \\ M_{\varphi}^* &= -\frac{\kappa}{ap_s} \left\{ 1 - \frac{1}{2ap_s} (1 - e^{-2p_s a}) \right\} \end{aligned} \right\} \quad (97)$$

where the quantity

$$\kappa = \frac{4}{3} a^2 b^3 c^* \quad (98)$$

is introduced. It may be noted that $\frac{2}{3} b^3 c^*$ represents the torsional stiffness per unit length of a small tread element of full width.

In the expressions for the force F and the moment M' due to lateral deformations, formed below, we have introduced the overall stiffness per unit length:

$$c = 1/(1/c_p + 1/c_s) = \epsilon^2 c_p = (1-\epsilon^2) c_s. \quad (99)$$

For the sake of abbreviation we shall moreover use the following constants:

$$\left. \begin{aligned} B_{\psi_{\pm}} &= -\frac{1}{2} \sigma (1 \pm \epsilon) \left[\frac{1 + \sigma p_s}{1 \pm \sigma_c p_s} e^{p_s a} C_{\psi} - \frac{1}{p_s} \right], \\ B_{\varphi_{\pm}} &= -\frac{1}{2} \sigma (1 \pm \epsilon) \left[\frac{1 + \sigma p_s}{1 \pm \sigma_c p_s} e^{p_s a} C_{\varphi} - \frac{1}{p_s^2} - \frac{1}{p_s} \left\{ a + \sigma (1 \mp \epsilon) \right\} \right]. \end{aligned} \right\} \quad (100)$$

The Laplace transforms of the force and moment are:

$$\mathcal{L} \{F\} = F_{\psi} \Psi + F_{\varphi} \Phi, \quad (101)$$

$$\mathcal{L} \{M'\} = M'_{\psi} \Psi + M'_{\varphi} \Phi. \quad (102)$$

The transfer functions used in these expressions read:

$$\begin{aligned} (F_{\psi}, F_{\varphi}) &= c \left\{ 2 \frac{a}{p_s} \left(1, -\frac{1}{p_s} \right) + \frac{1 - \sigma^2 p_s^2}{1 - \sigma_c^2 p_s^2} \frac{e^{p_s a} - e^{-p_s a}}{p_s} (C_{\psi}, C_{\varphi}) + \right. \\ &\quad \left. - \left(1 - e^{2a/\sigma_c} \right) (B_{\psi+}, B_{\varphi+}) - \left(1 - e^{-2a/\sigma_c} \right) (B_{\psi-}, B_{\varphi-}) \right\}, \quad (103) \end{aligned}$$

$$\begin{aligned} (M'_{\psi}, M'_{\varphi}) &= c \left[-\frac{2}{3} \frac{a^2}{p_s} (0, 1) + \frac{1 - \sigma^2 p_s^2}{1 - \sigma_c^2 p_s^2} \left(a \frac{e^{p_s a} + e^{-p_s a}}{p_s} - \frac{e^{p_s a} - e^{-p_s a}}{p_s^2} \right) \right. \\ &\quad \left. + (C_{\psi}, C_{\varphi}) - \left\{ a \left(1 + e^{2a/\sigma_c} \right) + \sigma_c \left(1 - e^{2a/\sigma_c} \right) \right\} (B_{\psi+}, B_{\varphi+}) + \right. \\ &\quad \left. - \left\{ a \left(1 + e^{-2a/\sigma_c} \right) - \sigma_c \left(1 - e^{-2a/\sigma_c} \right) \right\} (B_{\psi-}, B_{\varphi-}) \right]. \quad (104) \end{aligned}$$

The total moment about the ξ -axis is obtained by adding up the expressions (96) and (102):

$$M = M^* + M' . \quad (105)$$

The total transfer function becomes:

$$M_\psi = M'_\psi , \quad M_\varphi = M^*_\varphi + M'_\varphi . \quad (106)$$

By transforming back the expressions above, we should be able to find the deflection, the force and the moment as a function of s .

As far as the shimmy motion is concerned, we are interested in the response to sinusoidal motions. The frequency response functions can easily be found from the transfer functions by replacing the operator p_s by $i\omega_s$ (see among others Effertz und Kolberg [46, p.70]). The reduced frequency ω_s has the dimension $1/L$ and equals $2\pi/\lambda$, where λ denotes the wavelength of the motion. With constant velocity V , ω_s is proportional to the frequency $\omega = V\omega_s$. The variables ψ and φ have the advantage, that the treatment is completely general and is not restricted to motions in the neighbourhood of the x -axis. When, however, we are dealing with sinusoidal motions with the wheelplane only slightly deviated from the (x, z) plane, it is convenient to replace ψ and φ by the variables γ and y_w or $\beta (= dy_w/ds$ for $\beta \ll 1$) (see Fig.1). In the actual shimmy analysis γ and y_w will be used. The following relations are applicable (cf. Eqs. (2, 3, 8)):

$$\frac{d\gamma}{ds} = \varphi , \quad \beta (= \frac{dy_w}{ds}) = \gamma - \psi , \quad (107a)$$

or transformed:

$$\Gamma = \frac{1}{p_s} \Phi , \quad B (= p_s Y_w) = \frac{1}{p_s} \Phi - \Psi . \quad (107b)$$

The Laplace transform of the force and moments may be written now as follows:

$$\left. \begin{aligned} \mathcal{L} \{F\} &= F_\gamma \Gamma + F_\beta B , \\ \mathcal{L} \{M^*\} &= M_\gamma^* \Gamma + M_\beta^* B , \\ \mathcal{L} \{M'\} &= M'_\gamma \Gamma + M'_\beta B \end{aligned} \right\} \quad (108)$$

The transfer functions with respect to γ and β written in terms of the transfer functions with respect to ψ and φ become:

$$\left. \begin{aligned} F_\gamma &= F_\psi + p_s F_\varphi, & F_\beta & (= \frac{1}{p_s} F_{y_w}) = -F_\psi, \\ M_\gamma^* &= p_s M_\varphi^*, & M_\beta^* & (= \frac{1}{p_s} M_{y_w}^*) = 0, \\ M_\gamma' &= M_\psi' + p_s M_\varphi', & M_\beta' & (= \frac{1}{p_s} M_{y_w}') = -M_\psi'. \end{aligned} \right\} \quad (109)$$

The frequency response functions, $F_\gamma(i\omega_s)$ etc., are the complex ratios between output, F etc., and the input, γ etc. For the tyre model treated here ($\sigma^* = 3a$, $\epsilon = 1/7.5$) their absolute and phase relationship have been calculated.

In figures 13a, b, c, d the various responses as a ratio to their steady state values are shown as a function of the non-dimensional quantity $\omega_s a$. Figure 13e shows the response M_γ^* divided by the constant κ/a , with respect to the value of which M_γ^* approaches when $\omega_s \rightarrow \infty$. Also the approximate responses treated below are shown in these figures.

The phase angles φ are taken positive when the output lags behind the input, which appears to be the case with the force and moment due to lateral deformations. The moment due to longitudinal deformations M^* , however, appears to lead in phase. The phase lead of M^* causes a reduction in phase lag of the total moment M with respect to γ , as has been illustrated in the diagram of figure 14.

In the complex plane shown in this figure the response curves are drawn for the moment M' which applies for an infinitely thin tyre and for the moment $M = M' + M^*$ for a tyre of finite width with $\kappa = C_M a$. The moments are made non-dimensional by division by the steady-state value M_0 . The curve for a tyre with $\kappa = C_M a$ is obtained by vectorial addition of M' and M^* . Curves for other values of κ may be obtained by multiplying the vector of M^* by the factor $\kappa/C_M a$. The calculated behaviour of the linear tyre model has unmistakeable points of agreement with courses found experimentally at low values of the swivel frequency (see Sec. VI. 2, p.171). At higher values of the frequency, the influence of the gyroscopic couple due to tyre deformation, dealt with in Sec. 6, is no longer negligible.

The couple M^* with mainly a damping effect may suppress the shimmy, as will be seen later. We may further remark that above a certain value of κ the curve for the total

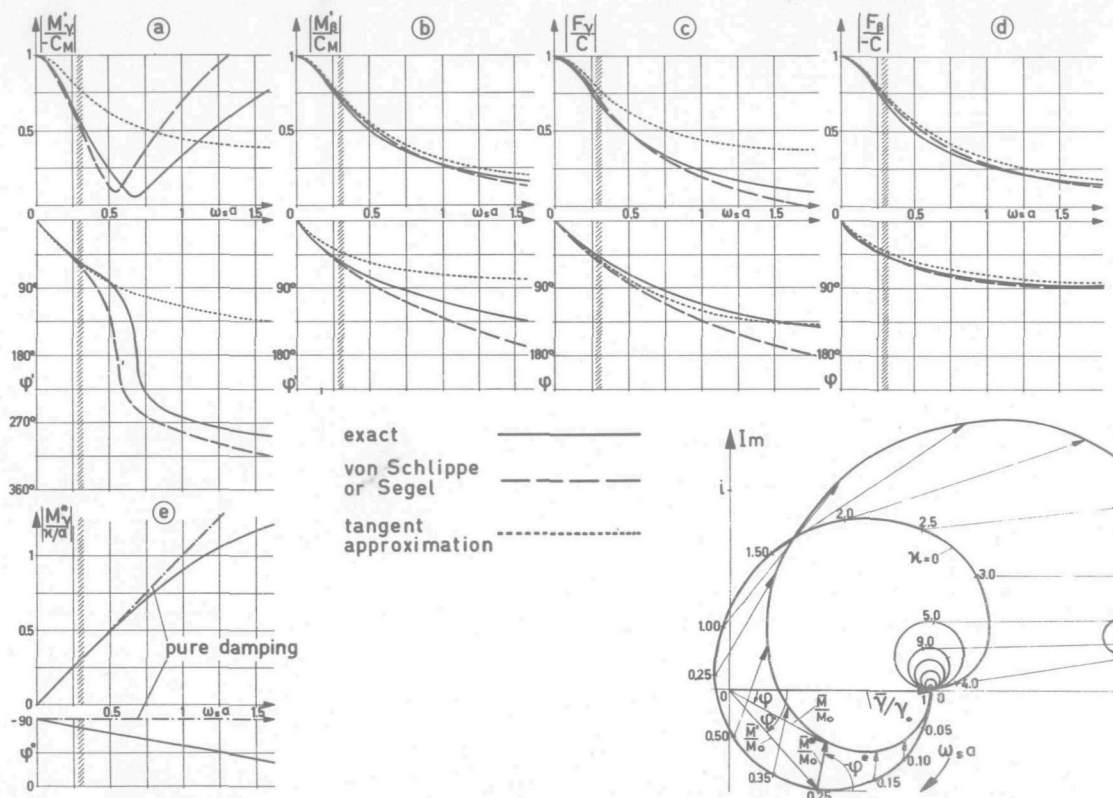


Fig.13. Exact and approximate response characteristics of force and moment with respect to γ and β ($\sigma^*=3a, \epsilon=1/7.5$).

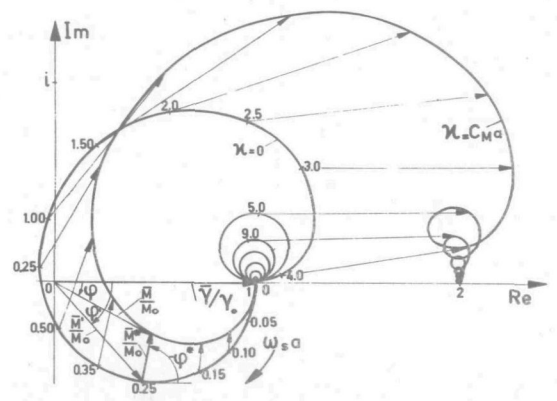


Fig.14. Response curve in the complex plane for the moment with respect to γ ($\sigma^*=3a, \epsilon=1/7.5$).

couple M/M_0 will not encircle the origin but will remain at the right-hand side of this point. This appears to be a typical property of curves obtained experimentally, which has not been explained, before. The point of intersection of the curve for M and the real axis (Fig. 14) represents the point of "kinematic" shimmy (cf. Kantrowitz [28] and Saito [31]). This sort of shimmy may occur at very low values of speed of travel, where the frequency and consequently the moments due to viscous damping and inertia acting about the king-pin axis become very small.

It may be noted that, taking strictly, we could confine ourselves to the determination of the stationary response and the non-stationary response to the angular motion γ . The angular motion of the wheel plane about the vertical axis through the wheel centre can be composed by two motions: an angular motion, in magnitude equal to γ , about a vertical axis through the point ($\xi = \sigma^* + a$, $\eta = 0$) (see also Fig. 12) and a lateral translation $y_w = (\sigma^* + a)\gamma$. The response with respect to the angular motion about the axis through the wheel centre will consequently be equal to the sum of the responses with respect to the latter two motions. The first motion always immediately yields stationary response because of the fact that the elongation of the stationary contactline intersects the wheel plane in the point of rotation. With the use of the quantities C and C_M indicating the stationary cornering stiffnesses, we obtain:

$$\left. \begin{aligned} F_\gamma \cdot \gamma &= C \cdot \gamma + F_{y_w} \cdot y_w, \\ M'_\gamma \cdot \gamma &= -C_M \cdot \gamma + M'_{y_w} \cdot y_w, \end{aligned} \right\} \quad (110)$$

from which the equations

$$\left. \begin{aligned} F_{y_w} &= p_s F_\beta = \frac{1}{\sigma^* + a} (F_\gamma - C), \\ M'_{y_w} &= p_s M'_\beta = \frac{1}{\sigma^* + a} (M'_\gamma + C_M), \end{aligned} \right\} \quad (111)$$

can be derived. They show that the calculations of the stationary and non-stationary responses to the angular motion γ would suffice.

4B. Approximations

In behalf of the investigation of the shimmy motion where mostly wavelengths occur relatively large with respect to

the contact length (of the order of 10 times) it is sufficient to employ approximations which correspond in response fairly well with the exact response for values of ω_s at the left-hand side of the hatched band shown in figure 13.

In order to obtain an impression of the usefulness of the approximations, to be treated below, we shall equalize the terms containing ω_s in the zeroth and first degree in the expanded frequency response functions with respect to γ and y_w to each other. This can be realized by considering same values for the cornering stiffnesses and for the relaxation lengths in the successive approximations.

The moment M^* due to longitudinal deformations may be approximated by a pure damping couple of which the characteristics are shown in figure 13e. In the shimmy analysis we shall make use of the formula:

$$M^* = -\kappa\varphi = -\kappa \frac{d\gamma}{ds}, \quad (112)$$

where κ , as defined by (98), is the coefficient of damping due to longitudinal tread deformations and where furthermore use has been made of relation (8).

In the development of approximations for the response functions of force and moment due to lateral tread deformations we shall as a first step investigate a simplified model without profile rubber and of vanishing width. The non-stationary response of this model has already been examined by Segel [38].

The simplified system may be regarded as an extreme case of the complete model as treated above. For $c_p \rightarrow \infty$ we obtain for the string deflection in the region of contact according to (85b) and (94):

$$V = V_s = \frac{1}{p_s} \left[\frac{-\Psi + (\sigma + a + 1/p_s)\Phi}{1 + \sigma p_s} e^{p_s(\xi-a)} + \Psi - \left(\xi + \frac{1}{p_s}\right)\Phi \right]. \quad (113)$$

At the leading edge the deflection becomes:

$$V_1 = \frac{\sigma}{1 + \sigma p_s} (\Psi - a\Phi), \quad (114)$$

or transformed back:

$$\frac{dv_1}{ds} + \frac{v_1}{\sigma} = \psi - a\varphi = \gamma - \frac{dy_w}{ds} - a \frac{d\gamma}{ds}, \quad (115)$$

where use has been made of the relations (2), (3) and (8).

This first-order differential equation may be found immediately from the original partial differential equation (10), when the condition that for $\xi = a$ the slope becomes $\frac{\partial v}{\partial \xi} = -\frac{v_1}{\sigma}$ is taken into account.

The force and moment response may be found either directly from the formulae (103) and (104) or by starting anew from the deflection as given by expression (113). We obtain the following transfer functions:

$$\begin{aligned} (F_{\psi}, F_{\varphi}) = \frac{c}{p_s} & \left[2(\sigma+a) \left(1, -\frac{1}{p_s} \right) + \frac{1}{p_s} \left(1 + \frac{\sigma p_s^{-1}}{\sigma p_s + 1} e^{-2p_s a} \right) \right. \\ & \left. \cdot \left(-1, \sigma+a + \frac{1}{p_s} \right) \right], \end{aligned} \quad (116)$$

$$\begin{aligned} (M_{\psi}^I, M_{\varphi}^I) = \frac{c}{p_s} & \left[2a \left\{ \sigma(\sigma+a) + \frac{1}{3} a^2 \right\} (0, -1) + \right. \\ & \left. + \frac{a(1+e^{-2p_s a}) + p_s \left\{ \sigma(\sigma+1) - 1/p_s^2 \right\} (1-e^{-2p_s a})}{(\sigma p_s + 1) p_s} \right. \\ & \left. \cdot \left(-1, \sigma+a + \frac{1}{p_s} \right) \right], \end{aligned} \quad (117)$$

from which the transfer functions with respect to γ and β may be obtained by using the relations (109). The response formulae in the latter form, but in which p_s is replaced by $i\omega_s$ so that frequency response functions are obtained, are already given by Segel [38]. Figure 13 also shows the response curves of the simplified model considered (Segel) for $\sigma^* = \sigma = 3a$. Qualitative differences do not appear. Quantitatively, the deviation from the response of the model with profile rubber becomes larger for shorter wavelengths (larger ω_s). In the region important for shimmy analysis at the left-hand side of the hatched band, very good correspondence exists. The simplified concept, however, is still too complicated to be used in the actual shimmy analysis. We shall therefore consider two approximations of the response of the simplified model.

A first approximate description of the behaviour of this simplified model, originates from Von Schlippe [34]. We shall refer to this approach as approximation I. The contact line is considered to be a straight line connecting the

two endpoints of the real contact line (see Fig.15). Only the deflections v_1 and v_2 of these points are of importance now. For the force and moment transformed we obtain with the aid of expressions (81) and (99):

$$\left. \begin{aligned} \mathcal{L} \{F\} &= c (\sigma + a) (V_1 + V_2) = C \frac{V_1 + V_2}{2(\sigma + a)}, \\ \mathcal{L} \{M'\} &= c \left\{ \sigma(\sigma + a) + \frac{1}{3} a^2 \right\} (V_1 - V_2) = C_M \frac{V_1 - V_2}{2a}. \end{aligned} \right\} \quad (118)$$

With the aid of (113) the transfer functions become:

$$(F_\psi, F_\phi) = (\sigma + a) \frac{c}{p_s} \left\{ 2 \left(1, -\frac{1}{p_s} \right) + \frac{1 + e^{-2p_s a}}{\sigma p_s + 1} (-1, \sigma + a + 1/p_s) \right\}, \quad (119)$$

$$(M'_\psi, M'_\phi) = \left\{ \sigma(\sigma + a) + \frac{1}{3} a^2 \right\} \frac{c}{p_s} \left\{ 2a(0, -1) + \frac{1 - e^{-2p_s a}}{\sigma p_s + 1} (-1, \sigma + a + 1/p_s) \right\}. \quad (120)$$

The responses with respect to γ and β obtained with the aid of formulae (109) appear to coincide practically with those obtained from formulae (116) and (117) in the investigated range of wavelengths (see curves "von Schlippe or Segel" in Figs.13).

Simulation of the Von Schlippe representation by means of an analogue computer appeared feasible although complicated. In this simulation use has been made of equation (115) for obtaining v_1 and of the retardational behaviour as expressed by (86) in order to generate v_2 .

A second approximation (referred to as approximation II) of the simple string model assumes a straight contact line which touches the real contact line in the leading point. The deflection of the string according to the tangent concept is shown in figure 15.

The deflection v_1 given by equation (114) is the only variable upon which the whole lateral deflection and thus F and M' depend. The following expressions apply:

$$\left. \begin{aligned} \mathcal{L} \{F\} &= 2 c (\sigma + a)^2 V_1 / \sigma = C V_1 / \sigma, \\ \mathcal{L} \{M'\} &= -2 c a \left\{ \sigma(\sigma + a) + \frac{1}{3} a^2 \right\} V_1 / \sigma = -C_M V_1 / \sigma, \end{aligned} \right\} \quad (121)$$

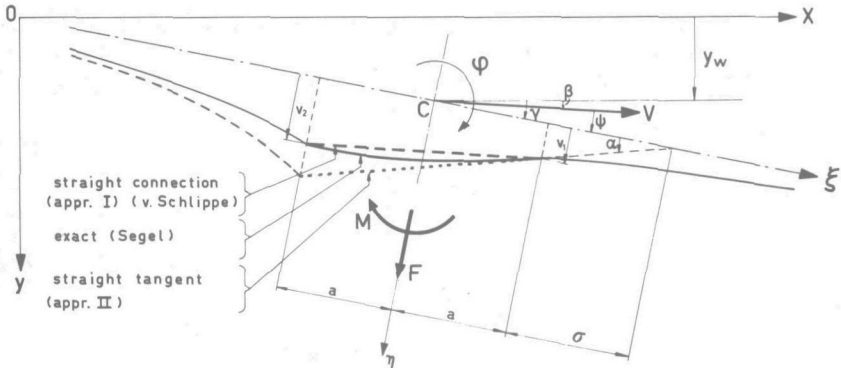


Fig. 15. The simplified model together with two approximate concepts.

which yields with the use of expression (114):

$$(F_{\psi}, F_{\varphi}) = \frac{2c(\sigma+a)^2}{\sigma p_s + 1} (1, -a), \quad (122)$$

$$(M'_{\psi}, M'_{\varphi}) = - \frac{2ca \left\{ \sigma(\sigma+a) + \frac{1}{3}a^2 \right\}}{\sigma p_s + 1} (1, -a). \quad (123)$$

The characteristics of the response to γ and β obtained with the formulae (109) are shown in the figures 13. The curves do not show such a good correspondence to the original characteristics as the preceding approximations do. The relaxation property, however, is fairly well represented in case of large wavelengths. The simulation by means of an analogue computer, using equation (115), is simple and may be checked by the better representation of Von Schlippe. In the linear analytical treatment of the shimmy phenomenon the simplest approximation II will be used only. In the non-linear treatment the approximations will be employed in adapted form as will be discussed in the next section.

5. Approximate non-stationary behaviour for finite slip

The very complicated treatment of the complete general behaviour of the rolling tyre of which the wheel axle exerts lateral and angular motions, will not be developed here. It does not appear to be necessary because of the fact that we are dealing with oscillatory motions with wavelengths many times

larger than the contact length of the tyre. This implies that the shape of the deflection of the tyre approaches the stationary shape, i.e. shows an almost straight contact line in case of complete adhesion.

We will consider the special case of the tyre model without profile rubber. Sliding at the leading edge will not be considered, which is very well permissible as we have seen in Sec. 3B. The part of the model in front of the rear sliding region will behave then completely according to the linear theory. The deflection v_1 will depend, also for larger amplitudes, on the axle motions according to equation (115). This will thus only be the case at angles $\alpha = v_1/\sigma$ (slope at leading edge, cf. Fig.15) not surpassing the slip angle ψ_{sl} where total sliding starts. We shall not exceed this value in the shimmy analysis.

As pointed out above we can very well suffice with the simple string model in the shimmy range of wavelengths. With increasing slip angles the relaxation length tends to decrease as appeared from the investigation of the stationary behaviour of the model with profile rubber. In equation (115) we could possibly introduce a relaxation length σ depending on the deflection v_1 . In further analysis, however, we will take σ as a constant because these variations will not influence the phenomenon essentially. Moreover, it would cause almost unsurmountable difficulties in the simulation.

The application of approximation II, i.e. the concept of the straight contact line touching the real contact line at the leading edge, suggests the assumption that the force and moment depend on v_1/σ according to the stationary tyre characteristics. This assumption will be applied in the majority of the non-linear shimmy investigation.

If we want a verification of this simple approximation with the Von Schlippe theory (approximation I), we have to adapt also the latter theory to the non-linear circumstances. In the linear case the force and moment depend on the front and rear deflections v_1 and v_2 only. We can imagine two axial springs mounted at the ends of the contact region (see Fig.16). The ends of the springs making contact with

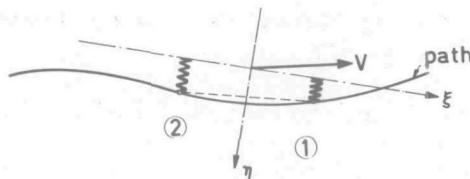


Fig.16. The two-spring tyre model.

the road follow the path of the contact line as dictated by the Von Schlippe theory. These two springs with equal stiffnesses can fully accomplish the force and moment response according to Von Schlippe.

We shall consider now the non-linear system where the ends of the springs will slide in lateral direction when a certain limit of contact force is exceeded. In this way we can also tackle the non-linear problem at least until total sliding arises.

The stationary characteristics of the system considered are shown in figure 17. Three cases are to be distinguished:

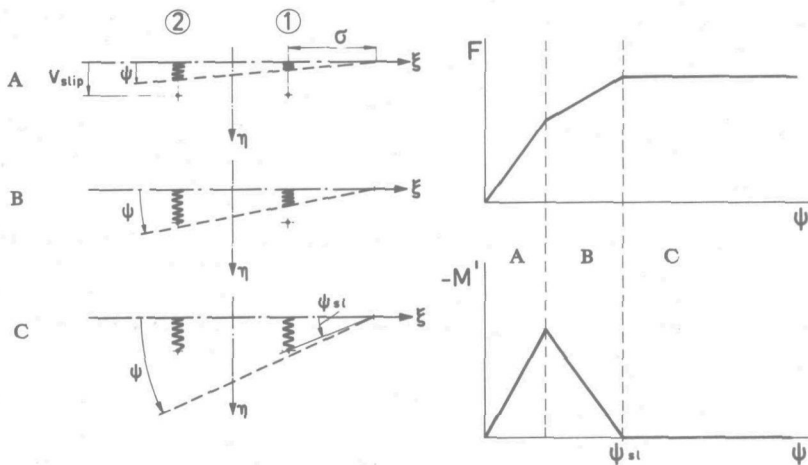


Fig.17. Stages through which the two-spring tyre model with dry-frictional road contact passes at increasing slip angle.

(A) adhesion in the points 1 and 2; (B) only adhesion in 1; (C) sliding in 1 and 2. These steady state characteristics, already resembling the real curves to an astonishing degree, may be improved by giving the two springs such characteristics that the cornering characteristics of the "two-spring" model, of which the spring ends do not slide now, equal the curves desired.

We call the spring forces F_1 and F_2 respectively. The following relations apply:

$$F = F_1 + F_2 \text{ and } M_1' = a (F_1 - F_2) \quad (124)$$

or inversely:

$$F_1 = \frac{1}{2}(F + M'/a) \text{ and } F_2 = \frac{1}{2}(F - M'/a). \quad (125)$$

Figure 18 gives an example of the determination of the functions $F_1(v_1)$ and $F_2(v_2)$ (in non-dimensional form)

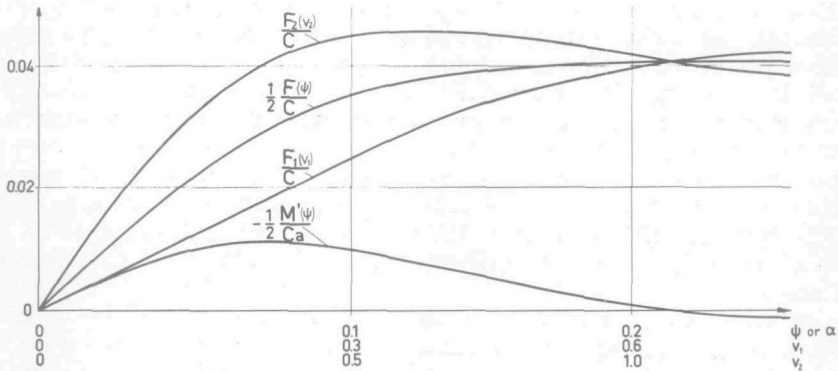


Fig. 18. Method for determining the spring characteristics of the two-spring model from original cornering characteristics.

where it must be kept in mind that the following relation exists in the stationary case:

$$\psi = \alpha = \frac{v_1}{\sigma} = \frac{v_2}{\sigma + 2a}. \quad (126)$$

The described method has been applied in the investigation treated in Sec. V.1.2, where use has been made of the analogue computer and the influence of the retardation term has been examined.

The additional moment M^* due to longitudinal deformations will be influenced by partial sliding too. Short wavelengths and large amplitudes will effect longitudinal sliding at the rear of the contact area. Taken strictly, longitudinal and lateral slip can no longer be considered independently from each other; the one influences the other. The two moments M^* and M' , however, will not obtain their maximum at the same time. A phase difference from $\frac{1}{4}\pi$ to about $\frac{1}{2}\pi$ radians will occur in the range of wavelengths considered.

It was decided not to consider the sliding in longitudinal direction because of the nearly unsurmountable difficulties which the mathematical treatment of the non-stationary case would give. Thus for simplification the degressive course of M^* with the amplitude of the motion will not be taken

into account either, again because it will not touch the essence of the shimmy phenomenon.

A component of the motion of the wheel plane not yet considered is the change in camber angle φ_w , denoting the deviation of the wheel plane from its vertical position. This angular motion of the wheel about the line of intersection of wheel centre plane and road surface gives rise to an additional variation in F and also to a much smaller extent in M .

The main effect is that the radial force, which is a function of the tyre deflection, obtains a lateral component, being the camber force. While oscillating about the line of intersection mentioned, there is no need for the string of a thin tyre model to come out of the wheel plane as long as no sliding occurs, since all motions take place in that wheel plane.

In the case of a tyre with finite width there will be a difference in rolling radius between both sides of the tyre in cambered position, which causes the tyre to produce a small couple about the vertical ζ -axis acting on the wheel in positive sense and thus trying to turn the wheel to the inside.

The force and moment due to camber will be relatively small. We confine ourselves only to the linear contribution to F which assumedly does not influence other forces and moments:

$$F_c = C_c \varphi_w, \quad (127)$$

where $C_c \approx N$, denoting the vertical tyre load. For the total lateral force we obtain:

$$F_{\text{tot}} = F + F_c. \quad (128)$$

6. Influence of gyroscopic couple due to tyre deformation

Tyre tests which were carried out in order to measure the response of tyre force and moment to oscillatory motions of the wheel axle, have indicated that a certain time effect exists and that consequently tyre behaviour is not purely path dependent. The results of the experiments concerning the response of M , described in Sec. VI.2 (p.169) cannot be explained fully unless a gyroscopic effect is introduced. We will do this in an approximative manner.

Figure 19 gives a diagrammatic view of the deflected

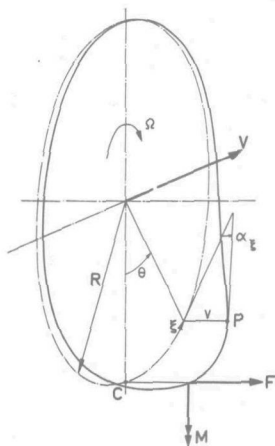


Fig.19. The deflected tyre peripheral line.

peripheral line of the tyre. The deflection v is a function of the co-ordinate ξ and the time t . For a certain point P on the peripheral line with lateral deflection v , the relative lateral substantial velocity, i.e. the velocity with respect to the wheel centre plane of a material point fixed to the tyre, reads:

$$\frac{dv}{dt} = \frac{\partial v}{\partial t} + \frac{\partial v}{\partial \xi} \frac{d\xi}{dt} . \quad (129)$$

The relative lateral acceleration of P becomes:

$$\frac{d^2 v}{dt^2} = \frac{\partial^2 v}{\partial t^2} + \frac{\partial^2 v}{\partial t \partial \xi} \frac{d\xi}{dt} + \left(\frac{\partial^2 v}{\partial \xi^2} \frac{d\xi}{dt} + \frac{\partial^2 v}{\partial \xi \partial t} \right) \frac{d\xi}{dt} . \quad (130)$$

Introducing the slope α_ξ , the tyre radius R and the angular velocity Ω , satisfying the relations

$$\alpha_\xi = -\frac{\partial v}{\partial \xi} , \quad \dot{\alpha}_\xi = -\frac{\partial^2 v}{\partial \xi \partial t} \quad \text{and} \quad R \Omega = -\frac{d\xi}{dt} \quad (131)$$

we obtain:

$$\frac{d^2 v}{dt^2} = \frac{\partial^2 v}{\partial t^2} + 2\dot{\alpha}_\xi R \Omega - \frac{\partial \alpha_\xi}{\partial \xi} R^2 \Omega^2 . \quad (132)$$

In order to estimate the order of magnitude of the influence of the first term in (132) we shall compare the elastic force per unit length of the tyre circumference with the corresponding force due to the acceleration $\partial^2 v / \partial t^2$. The lateral elastic force per unit length f_{el} becomes for a simple string model:

$$f_{el} = c v . \quad (133)$$

The acceleration force per unit length due to tyre inertia f_{in} becomes for a sinusoidal motion with frequency ω :

$$f_{in} = - \frac{m'_t}{2\pi R} \omega^2 v . \quad (134)$$

The stiffness $c (= c_s)$ follows from relation (81). The effective mass m' amounts to about 70% of the total tyre mass m_t . With a relaxation length $\sigma^* = \sigma = 1.8a$ and additional tyre data given in tables 3A, B (p. 59) we obtain for the ratio f_{in}/f_{el} for a frequency $\omega = 42.6$ rad/s ($n = 6.8$ c/s):

$$\left| \frac{f_{in}}{f_{el}} \right| = \frac{m'_t \omega^2}{2\pi R c} \approx 6\% . \quad (135)$$

In view of this relatively low percentage we will neglect for simplicity the first term of expression (132).

The laterally deviated tyre element is subjected to both the lateral acceleration and the centripetal acceleration. The couple due to tyre inertia, acting about the vertical axis through the wheel centre, is obtained by integrating the contributions of the tyre elements along the circumference. When taking into account the moment due to the last two terms of (132) together with the moment due to the centripetal acceleration we find:

$$M_{in} = - \int 2 \alpha \xi R^2 \Omega \sin \theta d m'_t + R \Omega^2 \int (R^2 \frac{d\alpha \xi}{d\xi} - v) \sin \theta d m'_t , \quad (136)$$

where $\theta = \xi/R$ and $dm'_t = m'_t d\theta/2\pi$. It appears that the last integral vanishes for deflections v given by the expressions (113) and (27) which hold for the simple massless string model in case of non-stationary motions.

The remaining term represents the gyroscopic couple. This couple, denoted by M_{gyr} , can be written as follows:

$$M_{\text{gyr}} = - \frac{m_t' R^2 \Omega}{\pi} \int_0^{2\pi} \alpha_\xi \sin \theta d\theta = - I_t' \Omega \frac{d}{dt} \left\{ \frac{1}{\pi} \int_0^{2\pi} \alpha_\xi \sin \theta d\theta \right\} \quad (137)$$

where I_t' denotes the effective fraction of the tyre polar moment of inertia. The part in between $\{ \}$ indicates the coefficient A_1 of the first odd harmonic $A_1 \sin \theta$ of the Fourier expansion of $\alpha_\xi(\theta)$. An imaginary peripheral line having a deflection $\alpha_\xi(\theta)$ exactly equal to $A_1 \sin \theta$ would lie in a plane passing through the longitudinal centre wheel axis. We obtain for the gyroscopic couple:

$$M_{\text{gyr}} = - I_t' \Omega A_1, \quad (138)$$

which is in agreement with well-known expressions for rotating discs. The value $A_1 R$ will be approximately proportional to the maximum lateral tyre deflection or to the lateral force F divided through the static lateral stiffness of the non-rolling tyre C_y . The value I_t' is proportional to $m_t R^2$ and Ω equals V/R . Consequently we may transform the relation (138) into:

$$M_{\text{gyr}} = -c_{\text{gyr}} \cdot m_t R^2 \cdot \frac{V}{R} \cdot \frac{F}{C_y R} = -C_{\text{gyr}} V \dot{F}, \quad (139)$$

where the non-dimensional constant c_{gyr} is the product of the two proportionality factors involved and the constant C_{gyr} is related to c_{gyr} as follows:

$$C_{\text{gyr}} = c_{\text{gyr}} \frac{m_t}{C_y}. \quad (140)$$

With the relations

$$V = \frac{\omega}{\omega_s} \quad \text{and} \quad \dot{F} = i\omega F, \quad (141)$$

the first relation already being introduced in Sec. 4A (p. 43), and with F_0 and M_0 denoting the stationary cornering force and moment and $e' = -M_0/F_0 = C_M/C$ denoting the pneumatic trail, we obtain for (139):

$$\frac{M_{\text{gyr}}}{M_0} = \frac{i\omega^2}{\omega_s} \frac{C_{\text{gyr}}}{e' F_0} F. \quad (142)$$

The gyroscopic couple considered will not be influenced by

lateral and angular motions of the wheel plane itself as long as this plane remains vertical.

For the case $\omega^2 C_{\text{gyr}} a/e' = 0.1$ the influence of the gyroscopic couple on the response curve for $\kappa = C_M a$ of figure 14 is shown in figure 20. The vectors of M_{gyr} are

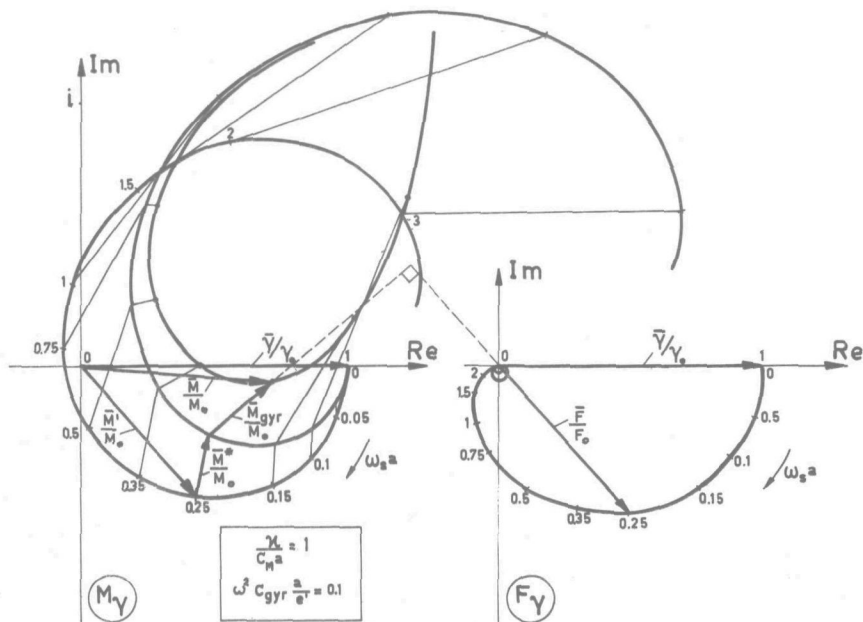


Fig. 20. The influence of the gyroscopic couple upon the response curve for M with respect to γ ($\sigma^* = 3a$, $\epsilon = 1/7.5$).

directed perpendicularly to the corresponding vectors of F . The absolute values are proportional to $|\bar{F}|/(F_0 \omega_s a)$ and will consequently tend to infinity for $\omega_s a \rightarrow 0$ or $V \rightarrow \infty$ at a given frequency ω . The vectors \bar{M}' , \bar{M}^* and \bar{M}_{gyr} should be added in order to find the resulting moment:

$$\bar{M} = \bar{M}' + \bar{M}^* + \bar{M}_{\text{gyr}}. \quad (143)$$

For a given wavelength, thus for a given value of $\omega_s a$, according to expression (142) the gyroscopic couple increases quadratically with the frequency of the swivel motion. A time influence, approximately similar to what is shown here, has been observed indeed in practice on the drum test stand (cf. Sec. VI. 2, p. 173).

For the system treated in Sec. V. 2. 2 (p. 155) which represents

the test vehicle, the following tyre data apply:

Table 3A. Data of test vehicle tyre.

C	$= 70000 \text{ N/rad,}$	a	$= 0.138 \text{ m,}$
C_M	$= 3900 \text{ Nm/rad,}$	e'	$= 0.62 a = 0.086 \text{ m,}$
C_y	$= 180000 \text{ N/m,}$	σ^*	$= 1.5 a = 0.21 \text{ m,}$
ϵ'	$= 1/7.5 \text{ (estimated),}$	R	$= 0.5 \text{ m.}$

In order to account for the reduction in relaxation length with increasing slip angle (cf. Sec. 3B, p.29) σ^* is taken somewhat lower than the value $1.8 a$, obtained from the formula:

$$\sigma^* = \frac{C}{C_y} \cdot a, \quad (144)$$

which represents the relaxation length at zero slip angle. The formula (144) can be derived from figure 12a with the use of the first formula (78) and the fact that $F = C_y \times$ average lateral tyre deflection (cf. Fonda and Radt [41]). The reduction ratio $1.5/1.8$ is an estimation based on experimentally obtained response curves for $\gamma_0 = 0.75^\circ$ and 6° (cf. Sec. VI.2).

The quantities c_{gyr} and κ are derived from drum test results (Sec. VI.2). We have made use of formula (98), which says that the coefficient κ depends quadratically on the contact length. The remaining data read:

Table 3B. Data of test vehicle tyre.

κ	$= \left(\frac{0.138}{0.115} \right)^2 \cdot 112 = 163 = 0.122 Ca^2 = 0.2 C_M a \text{ Nm}^2,$
m_t	$= 35 \text{ kg,}$
c_{gyr}	$= 0.12,$
C_{gyr}	$= c_{\text{gyr}} m_t / C_y = 2.3 \times 10^{-5} \text{ kgm/N}$

In figure 21 the response of M with respect to γ is shown in the exact manner for the frequency $n = 6.8 \text{ c/s}$ ($\omega = 43 \text{ rad/s}$). Together with the exact representation, an approximate response curve is shown which is obtained with the aid of approximation II (tangent concept) with $\sigma = 1.5 a$ and the linear damping concept according to equation (112) but with a much larger value for κ , viz. $\kappa = 0.6 Ca^2$. A fair ap-

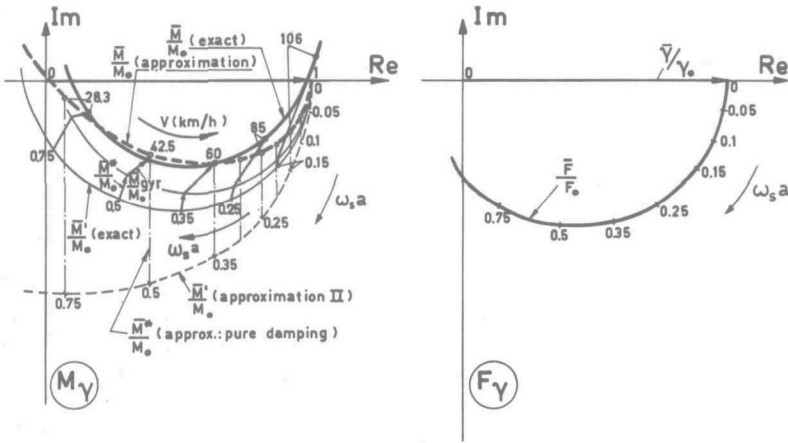


Fig. 21. Exact and approximate theoretical response curves for tyre of test vehicle.

proximation is obtained in the velocity range 35-85 km/h as appears from the figure. Inside this range the simulated vehicle appears to exhibit shimmy. The shimmy frequency, moreover, remains near the considered value $n = 6.8$ c/s.

In the case considered (cf. Sec. VI.1), the amplitude γ_0 is about 4-5 times larger than the amplitude β_0 so that a correction of the response with respect to β , in order to account for the gyroscopic effect, does not seem necessary.

These considerations and in addition the fact that M_{gyr} and M^* do not vary with amplitude in such a strongly depressive way as M' , do contribute to the opinion that the approximate representation of the tyre behaviour as described in the preceding sections is satisfactory in a certain speed range when κ is given an adequate value. A much more difficult and complicated simulation of the tyre does not seem necessary in most cases. The application of the approximate simulation gave excellent results compared with full scale vehicle tests (cf. Sec. V.2.2).

At velocities higher than ca. 85 km/h the effective damping will become considerably larger than as predicted through the approximation. In the case that for a given wavelength the frequency is appreciably lower than the considered one (6.8 c/s), the gyroscopic couple is smaller, and consequently the total effective damping will be a little lower than according to the approximation. This fact may only be important in the study of subcritical shimmy of the system with released steering-wheel, treated in Sec. V.2.2.

CHAPTER III

MATHEMATICAL DESCRIPTION OF THE VEHICLE

This chapter deals with the derivation of the equations of motion of a model which is expected to behave, at least as far as the shimmy motion is concerned, approximately as the real automobile.

Due to the limited capacity of the analogue computer which was used, the model employed is largely simplified compared to the more elaborate one developed by Pacejka in [47]. The latter model represents a four-wheeled vehicle moving over a smooth horizontal surface; it is equipped with four independent wheel suspensions, arbitrarily situated king-pins and wheel planes, an elastic chassis and a steering-wheel system.

In the theory to be developed here, we confine ourselves to the description of the motion of only the front part of the vehicle restricted to small deviations from a rectilinear path. Due to the assumed symmetry of the vehicle and anti-symmetry of the motion, this part of the vehicle can approximately be considered as a one-wheel-system when suitable parameter values are chosen.

In order to derive the equations of motion we need an exact description of the model considered. Since we will apply the method of Lagrange we have to determine the kinetic and potential energy of the system as well as the generalized forces acting upon it. For this, the geometry, kinetics and virtual displacements of several system elements have to be known.

In the ensuing theory any form of slip property, discussed in chapter II, is admitted as well as any function for the king-pin friction in which a form of clearance in the wheel bearings may be considered. For the rest, only linear terms are admitted in the equations of motion which means that only terms of up to the second degree in the displacement quantities will have to be taken into account in the potential and kinetic energy as well as in the power of the generalized forces. We will investigate the system in the most suitable order beginning with a physical description.

1. Physical description of the model considered

A diagram of the model in rear, side and top-view is shown in figure 1. With respect to the co-ordinate system $(0, x, y, z)$ which is fixed with respect to space and of which the $(x, 0, y)$ plane represents the road surface, a parallel co-ordinate system $(\bar{0}, \bar{x}, \bar{y}, \bar{z})$ moves along the x -axis with a velocity V , representing the speed of travel of the automobile.

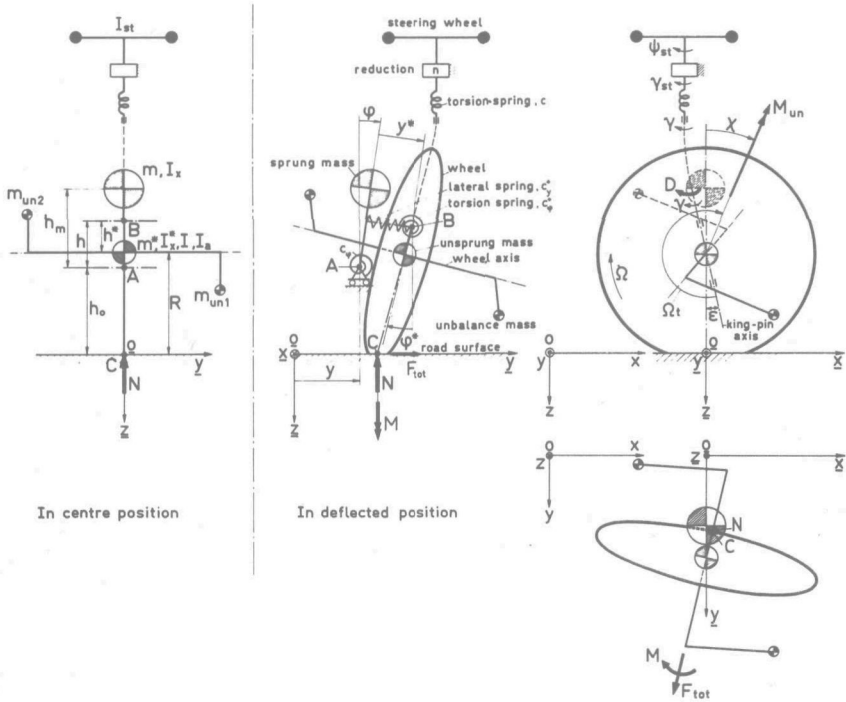


Fig.1. Rear, side and top view of the vehicle model considered.

In the $(y, 0, z)$ plane the mass centre of the part, representing half the front part of the sprung mass of the vehicle, is located. It has a mass m and a moment of inertia I_x about a longitudinal axis through the mass centre. The sprung part can move laterally and it may show a torsion angle about the longitudinal axis (A) situated parallel to the x -axis; the restoring torque equals the torsion angle multiplied by the torsional chassis stiffness c_φ .

The unsprung part has a mass m^* of which the centre is located in the wheel centre plane and on the wheel axis.

The non-swivelling part has a moment of inertia I_x^* about the longitudinal axis through the mass centre. The unsprung part is attached to the chassis in a flexible way through two springs, one with lateral stiffness c_y^* and the other with torsional stiffness c_ϕ^* . The unsprung part may rotate about a longitudinal axis $\phi(B)$; this centre of torsion can deflect laterally with respect to the chassis. During the motion the points A and B and the mass centres remain in the $(y, 0, z)$ plane.

The wheel, which is a part of the unsprung mass, rotates with an angular velocity Ω about its axle, which in turn is capable of swivelling about the king-pin. The king-pin axis lies in the wheel plane and intersects the wheel axis. It is inclined with respect to the vertical by an angle ϵ . The total swivelling part has a moment of inertia about the king-pin axis denoted by I . The moment of inertia of the wheel about the wheel axis is denoted by I_a .

The steering system is attached to the axle in some mechanical way (dotted line in Fig. 1). The steering system consists of a steering-wheel with a moment of inertia I_{st} about its axis of rotation, a reduction which reduces the steering-wheel angle by a factor n , and an elastic element with torsional stiffness c . For simplicity, damping in the steering system, except king-pin damping, is not considered.

The geometry of the system in the centre position is shown at the left-hand side of the figure. The co-ordinates $y, \phi, y^*, \phi^*, \gamma$ and ψ_{st} ($= n \cdot \gamma_{st}$) which are necessary to describe the geometry of the system in some deviated position, are shown at the right-hand side. Two additional co-ordinates ρ and χ which are constrained to the six co-ordinates mentioned, denote the change in tyre radius and the angle of rotation of the wheel about its axle respectively.

It will be clear that, with this one-wheel system, for the values of the masses, etc. and the stiffnesses of the chassis and the steering system half the values of the magnitudes applicable for a two-wheeled model should be taken.

The forces and moments acting on this system are the internal couple D , acting about the king-pin and originating from friction in the bearings, and the external forces and moments acting in the contact area between tyre and road. The lateral force F_{tot} , acts in C, which is the point of intersection of the $(x, 0, y)$ plane, the vertical plane through the wheel axis and the wheel centre plane. The vector of F_{tot} lies in the horizontal plane $(x, 0, y)$ and in the vertical plane through the wheel axis. The moment M acts about a vertical axis. The force N , which represents the static tyre vertical load, is supposed to act in C. For the determination of F_{tot} and M we refer to chapter II.

A longitudinal tyre force and a moment about the lateral axis, both resulting from rolling resistance, as well as a couple about a longitudinal axis through C, are disregarded in this simplified model, as they are very small with respect to other tyre forces and moments.

The couple M_{un} due to unbalance acts on the wheel about an axis fixed to the wheel, lying in the wheel plane and passing through the wheel axis (see Fig.1). The axis about which M_{un} acts rotates together with the wheel about the wheel axis and shows an angle χ ($=\Omega t + \text{constant}$) with respect to the vertical. The horizontal component of the unbalance couple is $M_{un} \sin \chi$. The component acting along the king-pin axis becomes herewith $-M_{un} \cos(\chi + \epsilon)$. The amplitude M_{un} varies quadratically with the forward speed V and is proportional to the magnitude of the unbalance masses $m_{un1,2}$. The unbalance couple will be introduced in the mathematical description via the kinetic energy of the masses $m_{un1,2}$.

2. Geometrical considerations

In behalf of further analysis the positions of several points of the model will be determined with respect to the moving co-ordinate system $(\underline{Q}, \underline{x}, \underline{y}, \underline{z})$. The positions will be denoted

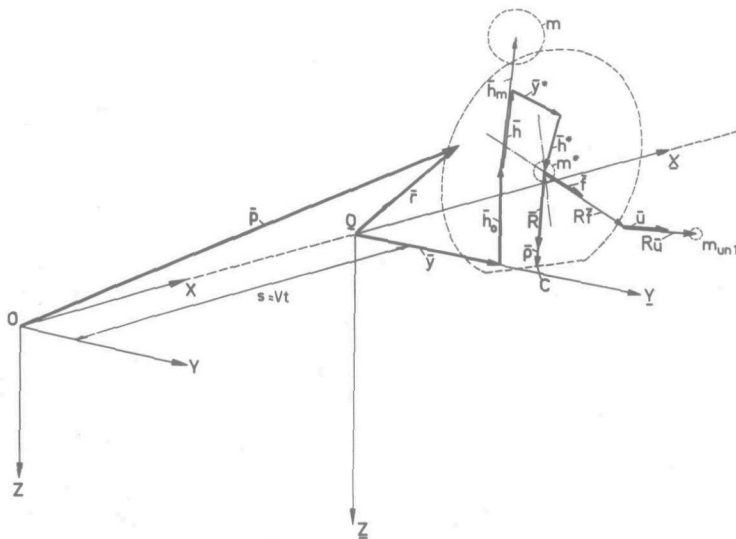


Fig.2. Vectors indicating the positions of important points of the system.

by means of vectors symbolized by \bar{r} in general. With respect to the fixed co-ordinate system (0, x, y, z) the position reads:

$$\bar{p} = \begin{pmatrix} Vt \\ 0 \\ 0 \end{pmatrix} + \bar{r}. \quad (1)$$

Figure 2 shows the vectors defining the positions of several points of interest. In the centre position (cf. Fig. 1) the position vectors for the centres of the masses m , m^* , $m_{un1,2}$ and for point C are defined as:

$$\begin{aligned} \bar{r}_0 &= \begin{pmatrix} 0 \\ 0 \\ -h_0 - h_m \end{pmatrix}, \quad \bar{r}_0^* = \begin{pmatrix} 0 \\ 0 \\ -R \end{pmatrix}, \quad \bar{r}_{un10} = R \begin{pmatrix} \cos \chi \\ 1 \\ \sin \chi - 1 \end{pmatrix}, \\ \bar{r}_{un20} &= R \begin{pmatrix} -\cos \chi \\ 1 \\ -\sin \chi - 1 \end{pmatrix}, \quad \bar{r}_{w0} = \begin{pmatrix} 0 \\ 0 \\ 0 \end{pmatrix}. \end{aligned} \quad (2)$$

The position of the unbalance masses with respect to the wheel centre can in principle be chosen arbitrarily; the location indicated by (2) appears to be convenient for further treatment. In a deviated situation the positions of the centres of m and m^* become:

$$\begin{aligned} \bar{r} &= \begin{pmatrix} r_x \\ r_y \\ r_z \end{pmatrix} = \begin{pmatrix} 0 \\ y \\ 0 \end{pmatrix} + \begin{pmatrix} 0 \\ 0 \\ -h_0 \end{pmatrix} + \begin{pmatrix} 0 \\ h_m \sin \varphi \\ -h_m \cos \varphi \end{pmatrix} \approx \\ &\approx \begin{pmatrix} 0 \\ y + h_m \varphi \\ -h_0 - h_m (1 - \frac{1}{2} \varphi^2) \end{pmatrix}, \end{aligned} \quad (3)$$

$$\begin{aligned} \bar{r}^* &= \begin{pmatrix} r_x^* \\ r_y^* \\ r_z^* \end{pmatrix} = \begin{pmatrix} 0 \\ y \\ 0 \end{pmatrix} + \begin{pmatrix} 0 \\ 0 \\ -h_0 \end{pmatrix} + \begin{pmatrix} 0 \\ h \sin \varphi \\ -h \cos \varphi \end{pmatrix} + \begin{pmatrix} 0 \\ y^* \cos \varphi \\ y^* \sin \varphi \end{pmatrix} + \\ &+ \begin{pmatrix} 0 \\ -h^* \sin \varphi^* \\ h^* \cos \varphi^* \end{pmatrix} \approx \begin{pmatrix} 0 \\ y + h \varphi + y^* - h^* \varphi^* \\ -h_0 - h (1 - \frac{1}{2} \varphi^2) + y^* \varphi + h^* (1 - \frac{1}{2} \varphi^{*2}) \end{pmatrix} \end{aligned} \quad (4)$$

where only the terms of up to the second degree are regarded.

The determination of the position of the wheel plane and the location of point C needs deeper consideration. The position of an arbitrary point of the axle in deflected situation

is denoted by a vector \bar{f} with co-ordinates with respect to the system $(0^*, x^*, y^*, z^*)$ having axes parallel to the axes of the fixed system $(0, x, y, z)$ and origin 0^* coinciding with the masscentre of m^* . In the centre position $\bar{f} = \bar{f}_0$. When the unsprung mass is rotated over the torsion angle φ^* (the other displacements remaining equal to zero), the vector can be represented by:

$$\bar{f} = \bar{A}_{\varphi}^* \cdot \bar{f}_0, \quad (5)$$

where the transformation matrix \bar{A}_{φ}^* reads:

$$\bar{A}_{\varphi}^* = \begin{pmatrix} 1 & 0 & 0 \\ 0 & \cos \varphi^* & -\sin \varphi^* \\ 0 & \sin \varphi^* & \cos \varphi^* \end{pmatrix}. \quad (6)$$

The vector \bar{f}_0 has co-ordinates with respect to the system $(0^*, x_{\varphi}^*, y_{\varphi}^*, z_{\varphi}^*)$ which in the centre position coincides with $(0^*, x^*, y^*, z^*)$ and which is fixed to the steering head, the non-swivelling part of the unsprung mass. By multiplication with the transformation matrix (6) we obtain co-ordinates with respect to the system $(0^*, x^*, y^*, z^*)$. The determination of the vector after a deflection γ about the king-pin will be done in stages.

With respect to the system $(0^*, x_{\epsilon}, y_{\epsilon}, z_{\epsilon})$ of which the y_{ϵ} -axis coincides with the y_{φ}^* -axis but of which the z_{ϵ} -axis and x_{ϵ} -axis are turned about the y_{φ}^* -axis over an angle ϵ so that the z_{ϵ} -axis coincides with the king-pin axis, the vector reads:

$$\bar{f}_{\epsilon,0} = \bar{A}_{\epsilon}^{-1} \cdot \bar{f}_0, \quad (7)$$

where

$$\bar{A}_{\epsilon} = \begin{pmatrix} \cos \epsilon & 0 & \sin \epsilon \\ 0 & 1 & 0 \\ -\sin \epsilon & 0 & \cos \epsilon \end{pmatrix}. \quad (8)$$

The inversed matrix \bar{A}_{ϵ}^{-1} may be obtained simply by substituting in \bar{A}_{ϵ} for ϵ its opposite value. When the axle and with it the system $(0^*, x_{\gamma}, y_{\gamma}, z_{\gamma})$ originally coinciding with $(0^*, x_{\epsilon}, y_{\epsilon}, z_{\epsilon})$ is rotated about the king-pin axis over an angle γ , the vector \bar{f} reads with respect to the system $(0^*, x_{\epsilon}, y_{\epsilon}, z_{\epsilon})$:

$$\bar{f}_{\epsilon,\gamma} = \bar{A}_{\gamma} \cdot \bar{f}_{\epsilon,0}, \quad (9)$$

where

$$\bar{A}_\gamma = \begin{pmatrix} \cos \gamma & -\sin \gamma & 0 \\ \sin \gamma & \cos \gamma & 0 \\ 0 & 0 & 1 \end{pmatrix}. \quad (10)$$

Transformed back to the system $(0^*, x_\varphi^*, y_\varphi^*, z_\varphi^*)$ the vector reads:

$$\bar{f}_\varphi^* = \bar{A}_\epsilon \cdot \bar{f}_{\epsilon, \gamma}. \quad (11)$$

Finally we obtain for the vector \bar{f} with respect to $(0^*, x^*, y^*, z^*)$ instead of (5):

$$\bar{f} = \bar{A}_\varphi^* \cdot \bar{f}_\varphi^* = \bar{A}_\varphi^* \cdot \bar{A}_\epsilon \cdot \bar{A}_\gamma \cdot \bar{A}_\epsilon^{-1} \cdot \bar{f}_0 = \bar{A} \cdot \bar{f}_0, \quad (12)$$

where

$$\bar{A} = \bar{A}_\varphi^* \cdot \bar{A}_\epsilon \cdot \bar{A}_\gamma \cdot \bar{A}_\epsilon^{-1}. \quad (13)$$

The transformation matrix \bar{A} reads, when terms are neglected which are of the third or higher degree in the variables and when furthermore the powers of the constant quantity ϵ higher than of the first degree are disregarded, the latter being permissible since only small values of ϵ will be considered (cf. [48] where ϵ^2 has been taken into account):

$$\bar{A} = \begin{pmatrix} 1 - \frac{1}{2} \gamma^2 & -\gamma & \frac{1}{2} \epsilon \gamma^2 \\ \gamma & \frac{1}{\varphi^*} + \epsilon \gamma & -\epsilon \gamma - \varphi^* \\ \gamma \varphi^* + \frac{1}{2} \epsilon \gamma^2 & 1 - \frac{1}{2} \gamma^2 & 1 - \frac{1}{2} \varphi^{*2} - \epsilon \varphi^* \gamma \end{pmatrix}. \quad (14)$$

Now suppose that \bar{f} is a unit vector and is directed along the wheel axis so that in the centre position, its co-ordinates are given by:

$$\bar{f}_0 = \begin{pmatrix} 0 \\ 1 \\ 0 \end{pmatrix}. \quad (15)$$

In the disturbed case we obtain:

$$\bar{f} = \begin{pmatrix} f_x \\ f_y \\ f_z \end{pmatrix} = \bar{A} \cdot \bar{f}_0 = \begin{pmatrix} -\gamma \\ 1 - \frac{1}{2} \gamma^2 & -\frac{1}{2} \varphi^{*2} & -\epsilon \varphi^* \gamma \\ \frac{1}{\varphi^*} + \epsilon \gamma \end{pmatrix}. \quad (16)$$

The angles defining the position of the wheel plane are ψ_w which denotes the deviation of the line of intersection of the wheel plane and the road from the x-direction, and

φ_w which indicates the angular displacement of the wheel plane about this line of intersection with respect to its vertical position. We obtain (see Fig. 3):

$$\sin \varphi_w = f_z \text{ and } \sin \psi_w = - \frac{f_x}{\cos \varphi_w} . \quad (17)$$

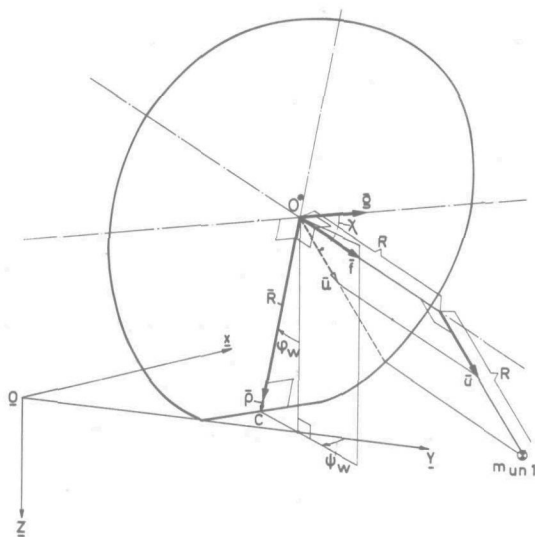


Fig. 3. Angles indicating the positions of the wheel centre plane and of the unbalance mass.

When applying the aforementioned neglects we obtain:

$$\varphi_w = \varphi^* + \epsilon\gamma \text{ and } \psi_w = \gamma . \quad (18)$$

The location of point C with respect to $(\underline{0}, \underline{x}, \underline{y}, \underline{z})$ denoted by the vector \bar{r}_w becomes:

$$\bar{r}_w = \bar{r}^* + \bar{R} + \bar{\rho} . \quad (19)$$

The vector $\bar{R} + \bar{\rho}$ reads (see Fig. 3):

$$\begin{aligned} \bar{R} + \bar{\rho} &= (R + \rho) \begin{pmatrix} \sin \varphi_w \sin \psi_w \\ -\sin \varphi_w \cos \psi_w \\ \cos \varphi_w \end{pmatrix} \approx \\ &\approx R \begin{pmatrix} (\varphi^* + \epsilon\gamma)\gamma \\ -\varphi^* - \epsilon\gamma \\ 1 - \frac{1}{2}\varphi^{*2} - \epsilon\gamma\varphi^* \end{pmatrix} + \rho \begin{pmatrix} 0 \\ -\varphi^* \\ 1 \end{pmatrix} + \epsilon\gamma \end{pmatrix} . \quad (20)$$

For the vectors \bar{R} and $\bar{\rho}$ with absolute values R and ρ respectively we obtain:

$$\bar{R} = R \begin{pmatrix} (\varphi^* + \epsilon\gamma)\gamma \\ -\varphi^* - \epsilon\gamma \\ 1 - \frac{1}{2}\varphi^{*2} - \epsilon\gamma\varphi^* \end{pmatrix}. \quad (21a)$$

and

$$\bar{\rho} = \rho \begin{pmatrix} 0 \\ -\varphi^* - \epsilon\gamma \\ 1 \end{pmatrix}. \quad (21b)$$

With (4) we obtain for (19):

$$\bar{r}_w = \begin{pmatrix} x_w \\ y_w \\ z_w \end{pmatrix} = \begin{pmatrix} R(\varphi^* + \epsilon\gamma)\gamma \\ y + h\varphi + y^* - h^*\varphi^* - (R + \rho)(\varphi^* + \epsilon\gamma) \\ \frac{1}{2}h\varphi^2 + y^*\varphi - \frac{1}{2}h^*\varphi^{*2} - R(\frac{1}{2}\varphi^{*2} + \epsilon\gamma\varphi^*) + \rho \end{pmatrix}. \quad (22)$$

The condition of constraint saying that the endpoint of \bar{r}_w lies on road level, which implies that $z_w = 0$, yields the expression for the change in tyre radius:

$$\rho = -\frac{1}{2}h\varphi^2 - y^*\varphi + \frac{1}{2}h^*\varphi^{*2} + R(\frac{1}{2}\varphi^{*2} + \epsilon\gamma\varphi^*) \quad (23)$$

which contains only terms of the second degree in magnitude, because of the anti-symmetry of the motion.

The location of the centres of the unbalance masses $m_{un 1,2}$ is represented by the vectors:

$$\bar{r}_{un 1} = \bar{r}^* + R(\bar{f} + \bar{u}), \quad \bar{r}_{un 2} = \bar{r}^* - R(\bar{f} + \bar{u}), \quad (24)$$

where \bar{f} and \bar{u} are considered as unit vectors. We introduce the horizontal unit vector \bar{g} lying in the wheel plane and pointed forwards (see Fig. 3):

$$\bar{g} = \begin{pmatrix} \cos \psi_w \\ \sin \psi_w \\ 0 \end{pmatrix} \approx \begin{pmatrix} 1 - \frac{1}{2}\gamma^2 \\ \gamma \\ 0 \end{pmatrix}. \quad (25)$$

The vector \bar{u} becomes expressed in terms of the vectors \bar{R} and \bar{g} :

$$\bar{u} = \frac{1}{R} \bar{R} \sin \chi + \bar{g} \cos \chi. \quad (26)$$

Due to the fact that $m_{un 1}$ and $m_{un 2}$ are situated anti-symmetrically, zeroth order terms containing the factor

m_{un} are expected in the final equations of motion, where:

$$m_{un} = m_{un1} + m_{un2}. \quad (27)$$

Other terms containing this small factor m_{un} will not be taken into account in these equations. Therefore we will neglect in the expressions for $\bar{r}_{un1,2}$ displacement terms of the order higher than one. We obtain for \bar{r}_{un1} :

$$\bar{r}_{un1} = R \begin{pmatrix} -\gamma + \cos \chi \\ (y + h\varphi + y^* - h^*\dot{\varphi}^*)/R + 1 - (\dot{\varphi}^* + \epsilon\gamma) \sin \chi + \gamma \cos \chi \\ -1 + \dot{\varphi}^* + \epsilon\gamma + \sin \chi \end{pmatrix} \quad (28a)$$

and for \bar{r}_{un2} :

$$\bar{r}_{un2} = R \begin{pmatrix} \gamma - \cos \chi \\ (y + h\varphi + y^* - h^*\dot{\varphi}^*)/R - 1 + (\dot{\varphi}^* + \epsilon\gamma) \sin \chi - \gamma \cos \chi \\ -1 - \dot{\varphi}^* - \epsilon\gamma - \sin \chi \end{pmatrix} \quad (28b)$$

3. Kinematical considerations

The velocity vectors of the mass centres are determined by differentiating the position vectors (3) and (4) with respect to time. We obtain for the velocity vectors with respect to the fixed system with (1):

$$\dot{\vec{p}} = \begin{pmatrix} V \\ 0 \\ 0 \end{pmatrix} + \dot{\vec{r}} = \begin{pmatrix} V \\ \dot{y} + h_m \dot{\varphi} \\ h_m \dot{\varphi} \end{pmatrix}, \quad (29)$$

$$\dot{\vec{p}}^* = \begin{pmatrix} V \\ 0 \\ 0 \end{pmatrix} + \dot{\vec{r}}^* = \begin{pmatrix} V \\ \dot{y} + h\dot{\varphi} + \dot{y}^* - h^*\dot{\varphi}^* \\ h\dot{\varphi}\dot{\varphi} + y^*\dot{\varphi} + \dot{y}^*\dot{\varphi} - h^*\dot{\varphi}^*\dot{\varphi}^* \end{pmatrix}. \quad (30)$$

The angular velocity vector for the sprung mass reads:

$$\vec{\omega} = \begin{pmatrix} \omega_x \\ \omega_y \\ \omega_z \end{pmatrix} = \begin{pmatrix} \dot{\varphi} \\ 0 \\ 0 \end{pmatrix}. \quad (31)$$

For the non-swivelling part of the unsprung mass the vector becomes:

$$\vec{\omega}^* = \begin{pmatrix} \omega_x^* \\ \omega_y^* \\ \omega_z^* \end{pmatrix} = \begin{pmatrix} \dot{\varphi}^* \\ 0 \\ 0 \end{pmatrix}. \quad (32)$$

For simplicity the swivelling part is assumed to be rotationally symmetric about the wheel axis. Therefore we need to know only the absolute value ω_w of the angular velocity vector $\bar{\omega}_w$ of the non-rotating part, which lies in the wheel plane, and the angular velocity ω_a of the rotating part, i.e. the wheel, about the wheel axis. We obtain the following:

$$\omega_w = |\dot{\bar{f}}| = \sqrt{\dot{\gamma}^2 + \dot{\varphi}^{*2} + 2\epsilon \dot{\varphi}^* \dot{\gamma}}, \quad (33)$$

and with the condition of no slip in longitudinal direction:

$$\omega_a = (\bar{f} \times \bar{u}) \dot{\bar{u}} = -\Omega + \dot{\psi}_w \sin \varphi_w \approx -\Omega + \dot{\gamma}(\varphi^* + \epsilon\gamma) \quad (34)$$

in which Ω denotes the rolling velocity, being the time derivative of the angle χ :

$$\Omega = \dot{\chi}. \quad (35)$$

The rolling velocity equals the stationary value plus terms of the second or higher order of magnitude. This is correct in the considered symmetric one-wheel system where driving or braking forces are not applied. The non-holonomic equation of constraint reads:

$$\dot{\chi} = \frac{V}{R} + \text{order}(2). \quad (36)$$

Since in equations of constraint second-order terms can be omitted in our first-order theory when the constrained variable (χ) is not earlier eliminated than in the equations of motion, which is necessary in the case of non-holonomic constraints, we may consider $\Omega = \dot{\chi}$ as a constant and therefore the system as holonomic. For the four-wheel system treated in [47] the non-holonomic equation of constraint contains first-order terms in the variables which makes the system non-holonomic.

Apart from the second-order terms we obtain for the integral of (35):

$$\Omega t - \pi - \epsilon = \chi, \quad (37)$$

through which the relation between χ and t is defined in a convenient way (cf. Fig.1).

The velocity vectors for the centres of the unbalance masses with respect to the fixed co-ordinate system become by differentiating (28a, b) with respect to time and by making use of relations (35) and (1):

by differentiating (28a, b) with respect to time and by making use of relations (35) and (1):

$$\begin{aligned} \dot{\bar{p}}_{un1} &= R \left(\begin{array}{l} V/R - \dot{\gamma} - \Omega \sin \chi \\ (\dot{y} + h \dot{\phi} + \dot{y}^* - h^* \dot{\phi}^*) / R - (\dot{\phi}^* + \epsilon \dot{\gamma} + \gamma \Omega) \sin \chi + \\ \dot{\phi}^* + \epsilon \dot{\gamma} + \Omega \cos \chi \end{array} \right) - \{ (\dot{\phi}^* + \epsilon \gamma) \Omega - \dot{\gamma} \} \cos \chi \\ \dot{\bar{p}}_{un2} &= R \left(\begin{array}{l} V/R + \dot{\gamma} + \Omega \sin \chi \\ (\dot{y} + h \dot{\phi} + \dot{y}^* - h^* \dot{\phi}^*) / R + (\dot{\phi}^* + \epsilon \dot{\gamma} + \gamma \Omega) \sin \chi + \\ - \dot{\phi}^* - \epsilon \dot{\gamma} - \Omega \cos \chi \end{array} \right) + \{ (\dot{\phi}^* + \epsilon \gamma) \Omega - \dot{\gamma} \} \cos \chi \end{aligned} \quad (38b)$$

The steering-wheel has an angular velocity about its axis of rotation equal to the time derivative of the angular displacement:

$$\omega_{st} = \dot{\psi}_{st} \quad (39)$$

4. Virtual displacements

In behalf of the determination of the generalized forces the virtual displacements of the line of intersection of wheel centre plane and road surface will be determined.

When the position of the system is varied by a small amount, the location of point C is changed in a manner as indicated by the vector $\delta \bar{r}_w$, obtained by varying \bar{r}_w (22), where only terms of the first degree are needed since in the centre position no constant horizontal forces are acting in C upon the wheel. This is correct in the case where only first-order terms will be taken into account in the final equations of motion.

$$\delta \bar{r}_w = \begin{pmatrix} \delta x_w \\ \delta y_w \\ \delta z_w \end{pmatrix} = \begin{pmatrix} 0 \\ \delta y + h \delta \phi + \delta y^* - h^* \delta \phi^* - R(\delta \phi^* + \epsilon \delta \gamma) \\ 0 \end{pmatrix} \quad (40)$$

Actually, we need the co-ordinates of the displacement vector with respect to the co-ordinate system (C, x_w, y_w, z_w) of which the x_w -axis coincides with the line of intersection and the z_w -axis is directed vertically. In linear respect, however, no changes in the co-ordinates occur.

The amount with which the line of intersection is rotated about the vertical axis, reads (cf. Eq. (18)):

$$\delta\psi_w = \delta\gamma, \quad (41)$$

which denotes the virtual displacement of the wheel plane about the king-pin axis.

5. Dynamical considerations

The kinetic energy is composed by the energies of the sprung mass, the non-swivelling unsprung mass, the swivelling part, the unbalance mass and the steering-wheel. For twice the kinetic energy we obtain:

$$2T = m \left| \dot{\vec{p}} \right|^2 + I_x \omega_x^2 + m^* \left| \dot{\vec{p}}^* \right|^2 + I_x^* \omega_x^{*2} + I \omega_w^2 + \\ + I_a \omega_a^2 + I_{st} \omega_{st}^2 + m_{un1} \left| \dot{\vec{p}}_{un1} \right|^2 + m_{un2} \left| \dot{\vec{p}}_{un2} \right|^2. \quad (42)$$

While restricting ourselves to terms of up to the second degree in the variables and the small factor m_{un} (27) and furthermore neglecting powers of ϵ higher than of the first degree, we obtain with the aid of the expressions of section 3:

$$2T = m \left\{ V^2 + (\dot{y} + h_m \dot{\varphi})^2 \right\} + I_x \dot{\varphi}^2 + \\ + m^* \left\{ V^2 + (\dot{y} + h \dot{\varphi} + \dot{y}^* - h^* \dot{\varphi}^*)^2 \right\} + I_x^* \dot{\varphi}^{*2} + \\ + I (\dot{\gamma}^2 + \dot{\varphi}^{*2} + 2 \epsilon \dot{\varphi}^* \dot{\gamma}) + I_a \left\{ \Omega^2 - 2 \Omega \dot{\gamma} (\varphi^* + \epsilon \gamma) \right\} + I_{st} \dot{\psi}_{st}^2 + \\ + m_{un} R^2 \left\{ V^2/R^2 + \Omega^2 + 2 \Omega \dot{\gamma} \sin \chi + 2 \Omega (\dot{\varphi}^* + \epsilon \dot{\gamma}) \cos \chi \right\}. \quad (43)$$

The change in potential energy of the system, due to deflections of the springs and variations in height of the mass centres, is expressed by

$$2U = -2 m g r_z + c_\varphi \varphi^2 - 2 m^* g r_z^* + c_y^* y^{*2} + c_\varphi^* (\varphi^* - \varphi)^2 + \\ + c_b \rho^2 - 2 N \rho + c \left(\gamma - \frac{1}{n} \psi_{st} \right)^2 + \text{constant} \quad (44)$$

where N denotes the static vertical load.

Substitution of the expressions for r_z (3), r_z^* (4) and ρ (23) from section 2 yields, when only terms of the second degree are regarded:

$$2U = -mgh_m \varphi^2 + c_\varphi \varphi^2 - m^* g \left\{ h \varphi^2 + 2 y^* \varphi - h^* \varphi^{*2} \right\} + \\ + c_y^* y^{*2} + c_\varphi^* (\varphi^* - \varphi)^2 - N \left\{ -h \varphi^2 - 2 y^* \varphi + h^* \varphi^{*2} + \right. \\ \left. + R (\varphi^{*2} + 2 \epsilon \gamma \varphi^*) \right\} + c \left(\gamma - \frac{1}{n} \psi_{st} \right)^2. \quad (45)$$

The virtual work done by the external tyre forces and moments and by the frictional moment D acting about the king-pin reads:

$$\delta W = F_{\text{tot}} \delta y_w + M \delta \psi_w + D \delta \gamma, \quad (46)$$

which with the aid of the expressions found in section 4 becomes:

$$\delta W = F_{\text{tot}} \left\{ \delta y + h \delta \varphi + \delta y^* - h^* \delta \varphi^* - R (\delta \varphi^* + \epsilon \delta \gamma) \right\} + M \delta \gamma + D \delta \gamma. \quad (47)$$

The way in which tyre force F_{tot} and moment M , appearing in this equation, depend on the variables, has been treated in chapter II. These relations will be presented again in the next section where also the moment D will be defined.

6. Equations of motion

For each of the six independent co-ordinates, determining the shape and position of the system, i.e.:

$$y, \varphi, y^*, \varphi^*, \gamma \text{ and } \psi_{st} \quad (48)$$

we may determine the equations of motion with the aid of the Lagrangian method. The equations read for each of the six variables q_i :

$$\frac{d}{dt} \frac{\partial T}{\partial \dot{q}_i} - \frac{\partial T}{\partial q_i} + \frac{\partial U}{\partial q_i} = Q_i \quad (i = 1, 2, \dots, 6) \quad (49)$$

where Q_i denotes the generalized force determined by the equation:

$$\delta W = \sum_{i=1}^6 Q_i \delta q_i. \quad (50)$$

Besides the six second-order differential equations of motion (49) an additional equation is needed which governs the lateral deflection of the tyre. In approximate form this latter equation may be a linear differential equation of the first order. The total order of the system seems to be then of the thirteenth order. However, the variable y is cyclic,

which means that only the first or higher derivatives with respect to time of that variable occur in the equations, so that in total the order of the system reduces to the twelfth order.

The six equations of motion read after some manipulations, through which the first equation (51) is obtained by subtracting the original first and third equation from each other and furthermore the second equation (52) is obtained by subtracting the original second and fourth equation from each other:

for the lateral displacement y :

$$m (\ddot{y} + h_m \ddot{\varphi}) - c_y \dot{y} - (N - m^*g) \varphi = 0 ; \quad (51)$$

for the angular displacement φ :

$$\begin{aligned} & (mh_m + m^*h) \ddot{y} + (I_x + mh_m^2 + m^*h^2) \ddot{\varphi} + m^*h (\dot{y} - h^* \dot{\varphi}) + \\ & + \left\{ c_\varphi + c_\dot{\varphi} + (N - m^*g) h - mgh_m \right\} \varphi + (N - m^*g) y + \\ & - c_\dot{\varphi} \dot{\varphi} = h F_{\text{tot}} ; \end{aligned} \quad (52)$$

for the lateral deflection y^* :

$$m^* (\ddot{y} + h \ddot{\varphi} + \dot{y} - h^* \dot{\varphi}) + (N - m^*g) \varphi + c_y \dot{y} = F_{\text{tot}} ; \quad (53)$$

for the angular displacements φ^* :

$$\begin{aligned} & - m^*h^* \ddot{y} - m^*h^*h \ddot{\varphi} - m^*h^* \dot{y} + (I + I_x^* + m^*h^{*2}) \ddot{\varphi} + I \epsilon \ddot{\gamma} + \\ & + I_a \Omega \dot{\gamma} - c_\dot{\varphi} \dot{\varphi} + \left\{ c_\varphi^* - N (h^* + R) + m^*gh^* \right\} \varphi + NR \epsilon \gamma = \\ & = - (h^* + R) F_{\text{tot}} + m_{\text{un}} R^2 \Omega^2 \sin \chi ; \end{aligned} \quad (54)$$

for the wheel deflection γ :

$$\begin{aligned} & I (\ddot{\gamma} + \epsilon \ddot{\varphi}^*) - I_a \Omega \dot{\varphi}^* - NR \epsilon \dot{\varphi}^* + c (\gamma - \frac{1}{n} \psi_{\text{st}}) = \\ & = - R \epsilon F_{\text{tot}} + M + D - m_{\text{un}} R^2 \Omega^2 \cos (\chi + \epsilon) ; \end{aligned} \quad (55)$$

for the steering-wheel deflection ψ_{st} :

$$I_{\text{st}} \ddot{\psi}_{\text{st}} + \frac{1}{n} c \left(\frac{1}{n} \psi_{\text{st}} - \gamma \right) = 0 ; \quad (56)$$

for the lateral deflection of the foremost contact point v_1 according to equation II.(115):

$$\frac{dv_1}{ds} + \frac{v_1}{\sigma} = \gamma - \frac{dy_w}{ds} - a \frac{d\gamma}{ds} \quad (57a)$$

or with the time as independent variable:

$$\dot{v}_1 + V \frac{v_1}{\sigma} = V \gamma - \dot{y}_w - a \dot{\gamma}, \quad (57b)$$

The position of the wheel plane is defined by φ_w (18), ψ_w (18) and y_w (22):

$$\varphi_w = \varphi^* + \epsilon \gamma, \quad (58)$$

$$\psi_w = \gamma, \quad (59)$$

$$y_w = y + h \varphi + y^* - h^* \varphi^* - R(\varphi^* + \epsilon \gamma). \quad (60)$$

A specification of D , F_{tot} and M will follow now. For the damping couple D we restrict ourselves to certain cases, in general indicated by the function:

$$D = -g(\dot{\gamma}, \gamma). \quad (61)$$

The case of dry-frictional damping in the king-pin bearing and a type of clearance as shown in figure 4 which may

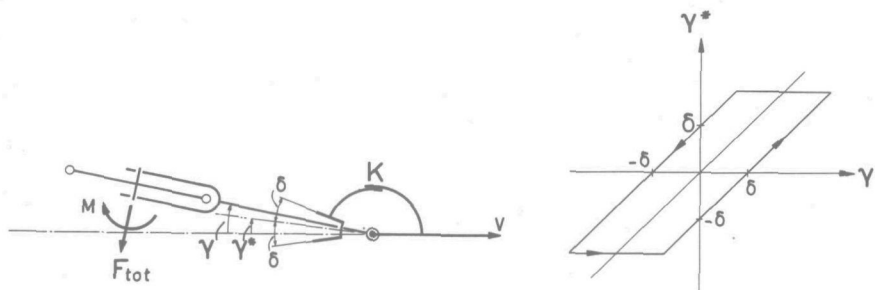


Fig. 4. The case of dry friction K and clearance δ applied to a simplified model.

represent rotational clearance in the wheel bearings, is described by the following equations:

$$D = -K \operatorname{sgn} \dot{\gamma}^* \quad (62a)$$

with a new variable γ^* varying in the range:

$$\gamma - \delta \leq \gamma^* \leq \gamma + \delta \quad (63a)$$

with δ denoting half the clearance angle and where applies:

$$\left. \begin{array}{l} \text{if } |\gamma^* - \gamma| < \delta \quad \text{then } \dot{\gamma}^* = 0, \\ \text{if } |\gamma^* - \gamma| = \delta \quad \text{then } \dot{\gamma}^* = \dot{\gamma}, \\ \text{with the additional condition:} \\ \text{if } \operatorname{sgn} \dot{\gamma} = -\operatorname{sgn} (\gamma - \gamma^*) \text{ then } \dot{\gamma}^* = 0. \end{array} \right\} \quad (63b)$$

The case of dry friction without clearance is described by:

$$D = -K \operatorname{sgn} \dot{\gamma}, \quad (62b)$$

while the linear representation is given by:

$$D = -k \dot{\gamma}. \quad (62c)$$

For the tyre lateral force F and couple M' we will apply two approximations described in chapter II. One is based on the Von Schlippe theory and the other on the straight tangent concept, both in modified form when non-linear cases are considered. For M^* we will make use of the approximation according to Eq. II. (112). We obtain according to Eqs. II. (127, 128, 105, 112):

$$F_{\text{tot}} = F + F_c, \quad (64)$$

$$M = M' + \bar{M}^*, \quad (65)$$

$$F_c = N \varphi_w, \quad (66)$$

$$M^* = -\kappa d\gamma/ds = -\frac{\kappa}{V} \dot{\gamma}. \quad (67)$$

APPROXIMATION I:

The y co-ordinate of the foremost contact point reads according to figure II. 15:

$$y_{c1} = y_w + a\gamma + v_1. \quad (68)$$

According to the second relation II.(86) we obtain for the last contact point:

$$y_{c2}(s) = y_c(-a, s) = y_c(a, s-2a) = y_{c1}(s-2a), \quad (69)$$

The deflection v_2 at the trailing edge becomes then:

$$v_2 = y_{c2} - y_w + a\gamma. \quad (70)$$

The force and moment are functions of v_1 and v_2 (see Fig.II.18). They read according to the relations II.(124):

$$F = F_1(v_1) + F_2(v_2) \quad (71a), \quad M' = a \left\{ F_1(v_1) - F_2(v_2) \right\} \quad (72a)$$

or in linear form according to the expressions II.(118):

$$F = \frac{1}{2} C \frac{v_1 + v_2}{\sigma + a} \quad (71b), \quad M' = \frac{1}{2} C_M \frac{v_1 - v_2}{a}. \quad (72b)$$

APPROXIMATION II:

The force and moment are functions of α according to the stationary tyre characteristics (see Fig.II.18):

$$F = F(\alpha) \quad (73a), \quad M' = M'(\alpha) \quad (74a)$$

or in linear form

$$F = C \alpha \quad (73b), \quad M' = -C_M \alpha \quad (74b)$$

where α denotes the slope at the foremost contact point (see Fig.II.15):

$$\alpha = v_1 / \sigma. \quad (75)$$

7. Non-dimensional quantities

In order to reduce the number of parameters, which is especially important for the approximative systems of low order, and furthermore to obtain coefficients in general being of the order of magnitude of 1, which among other things is important for the analogue computations, we will introduce non-dimensional quantities as listed in table 1. The quantity C denotes the cornering stiffness at zero slip angle except in Sec.IV.2, where C obtains a more general

Table 1. Non dimensional quantities.

\underline{t}	$= t \sqrt{Ca/I}$	β	$= I_a a/(IR)$
\underline{V}	$= V \sqrt{I/Ca^3}$	β_{st}	$= n^2 I_{st}/I$
$\underline{\Omega}$	$= \Omega \sqrt{I/Ca}$	$\beta_{\dot{\varphi}}$	$= (I + I_x^* + m^* h^{*2})/I = I_{\dot{\varphi}}^*/I$
$\underline{\omega}$	$= \omega \sqrt{I/Ca}$	β_{φ}	$= (I_x + m h_m^2 + m^* h^{*2})/I = I_{\varphi}/I$
$\underline{\omega}_s$	$= \omega_s a = \omega a/V = 2 \pi a/\lambda$	μ^*	$= m^* a^2/I$
$\underline{\omega}_{un}$	$= \omega_{un} a = a/R$	μ	$= m a^2/I$
$\underline{\lambda}$	$= \lambda/a$	μ_{un}	$= m_{un} a^2/I$
$\underline{\lambda}_{un}$	$= \lambda_{un}/a$	\underline{D}	$= D/(Ca)$
\underline{k}	$= k/\sqrt{ICa}$	$\underline{g}(\dot{\gamma}, \gamma)$	$= g(\dot{\gamma}, \gamma)/(Ca)$
\underline{x}	$= x/(Ca^2)$	\underline{F}	$= F/C$
\underline{K}	$= K/(Ca)$	\underline{M}	$= M/(Ca)$
\underline{C}	$= C/C_0$	\underline{N}	$= N/C$
\underline{C}_M	$= C_M/C_0$	\underline{N}^*	$= (N - m^* g)/C$
\underline{c}	$= c/(Ca)$	\underline{f}^*	$= -(M^* - eF)/(C_0 a)$
$\underline{c}_{\dot{\varphi}}$	$= c_{\dot{\varphi}}^*/(Ca)$	γ_{st}	$= \psi_{st}/n$
\underline{c}_y^*	$= c_y^* a/C$	\underline{e}^*	$= e^*/a = C_M/(Ca)$
\underline{c}_{φ}	$= (c_{\varphi} - mgh_m)/(Ca)$	\underline{s}	$= s/a$
			} analogous for subscripted quantities
			} analogous for $y, R, e, \text{etc.}$

meaning. In that section we shall replace C in the denominator of the non-dimensional quantities by the symbol C_0 denoting the cornering stiffness at zero slip angle. The quantity β is the coefficient determining the gyroscopic coupling between the variables γ and φ^* .

The equations of motion as stated in the preceding section read in non-dimensional form after omitting the underlinings, making use of (37) and writing V/R for the rolling speed Ω :

$$\mu (\ddot{y} + h_m \ddot{\varphi}) - c_y^* y^* - N' \varphi = 0, \quad (76)$$

$$(\mu h_m + \mu^* h) \ddot{y} + \beta_{\varphi} \ddot{\varphi} + \mu^* h (\ddot{y}^* - h^* \ddot{\varphi}^*) + (c_{\varphi} + c_{\varphi}^* + N'h) \varphi + N'y^* - c_{\varphi}^* \varphi^* = h F_{tot}, \quad (77)$$

$$\mu^* (\ddot{y} + h \ddot{\varphi} + \ddot{y}^* - h^* \ddot{\varphi}^*) + N' \varphi + c_y^* y^* = F_{tot}, \quad (78)$$

$$- \mu^* h^* (\ddot{y} + h \ddot{\varphi} + \ddot{y}^*) + \beta_{\varphi}^* \ddot{\varphi}^* + \epsilon \dot{\gamma} + \beta V \dot{\gamma} - c_{\varphi}^* \varphi + (c_{\varphi}^* - N'h - NR) \varphi^* +$$

$$- NR \epsilon \gamma = - (h^* + R) F_{tot} - \mu_{un} V^2 \sin (Vt/R - \epsilon), \quad (79)$$

$$\begin{aligned} \ddot{\gamma} + \epsilon \ddot{\varphi}^* - \beta V \dot{\varphi}^* - NR \epsilon \varphi^* + c(\gamma - \gamma_{st}) = \\ = -R \epsilon F_{tot} + M + D + \mu_{un} V^2 \cos Vt/R, \end{aligned} \quad (80)$$

$$\beta_{st} \ddot{\gamma}_{st} + c(\gamma_{st} - \gamma) = 0, \quad (81)$$

$$\frac{dv_1}{ds} + \frac{v_1}{\sigma} = \gamma - \frac{dy_w}{ds} - \frac{d\gamma}{ds} \quad \text{or} \quad (82a)$$

$$\dot{v}_1 + V \frac{v_1}{\sigma} = V \gamma - \dot{y}_w - \dot{\gamma}, \quad (82b)$$

$$\varphi_w = \varphi^* + \epsilon \gamma, \quad (83)$$

$$y_w = y + h \varphi + y^* - h^* \varphi^* - R(\varphi^* + \epsilon \gamma). \quad (84)$$

Specification of D , F_{tot} and M :

$D(= -g(\dot{\gamma}, \gamma)) = -K \operatorname{sgn} \dot{\gamma}^*$ (85a) or $D = -K \operatorname{sgn} \dot{\gamma}$ (85b) or $D = -k\dot{\gamma}$ (85c)

$$\left. \begin{aligned} \gamma - \delta \leq \gamma^* \leq \gamma + \delta \\ \text{if } |\gamma^* - \gamma| < \delta \text{ then } \dot{\gamma}^* = 0, \text{ if } |\gamma^* - \gamma| = \delta \text{ then } \dot{\gamma}^* = \dot{\gamma} \\ \text{if } \operatorname{sgn} \dot{\gamma} = -\operatorname{sgn}(\gamma - \gamma^*) \text{ then } \dot{\gamma}^* = 0. \end{aligned} \right\} \quad (86)$$

$$F_{tot} = F + F_c, \quad (87)$$

$$M = M' + M^*, \quad (88)$$

$$F_c = N \varphi_w, \quad (89)$$

$$M^* = -\kappa d\gamma/ds = -\frac{\kappa}{V} \dot{\gamma}, \quad (90)$$

APPROXIMATION I:

$$y_{c1} = y_w + \gamma + v_1, \quad (91)$$

$$y_{c2}(s) = y_{c1}(s-2), \quad (92)$$

$$v_2 = y_{c2} - y_w + \gamma, \quad (93)$$

$$F = F_1(v_1) + F_2(v_2) \text{ (non-lin.)}, \quad (94a)$$

$$F = \frac{1}{2} \frac{v_1 + v_2}{\sigma + 1} \text{ (linear)}, \quad (94b)$$

$$M' = F_1 (v_1) - F_2 (v_2) \text{ (non-lin.)}, \quad (95a)$$

$$M' = \frac{1}{2} e' (v_1 - v_2) \text{ (linear)}. \quad (95b)$$

APPROXIMATION II :

$$\alpha = v_1 / \sigma, \quad (96)$$

$$F = F' (\alpha) \text{ (non-lin.)}, \quad (97a)$$

$$F = \alpha \text{ (linear)}, \quad (97b)$$

$$M' = M' (\alpha) \text{ (non-lin.)}, \quad (98a)$$

$$M' = - e' \alpha \text{ (linear)}. \quad (98b)$$

In the subsequent sections the product $R\epsilon$ will be replaced by the symbol e denoting the caster length.

$$e = R \epsilon. \quad (99)$$

For the sake of simplicity we will omit the underlinings, indicating the quantities being non-dimensional, in the sequel too, when confusion is out of the question.

CHAPTER IV

ANALYTICAL INVESTIGATION OF AUTONOMOUS SYSTEMS

More or less drastic simplifications of the system as described in Secs. III. 6, 7 are necessary before the system can be investigated analytically. Because of this, we have restricted ourselves in this chapter to the investigation of systems of up to the seventh order, both linear and non-linear. The investigation starts with the third-order system: a wheel with elastic tyre capable of swivelling about a fixed king-pin. This system is extended to the fifth-order system showing lateral or torsional elasticity of the suspension. Finally the steering-wheel is introduced resulting in a seventh-order system.

The analytical study has been split up into three parts: the investigation of the system treated as a linear system, as a weakly non-linear system and finally as a piece-wise linear system.

The fact that shimmy can occur at all because of self-excitation, can be explained sufficiently by means of the linear theory to be treated in Sec. 2. Analytical methods originating from Hurwitz or others enable us to determine stability boundaries in the parameter space of the approximate linear system.

In reality, however, the automobile is a non-linear system. For a complete description of its behaviour the system has to be treated as such. At least the most important non-linear elements directly influencing the shimmy have to be taken into account. In contrast to problems such as flutter, it is not possible to restrict oneself to a linear treatment, as the real system may have both a stable centre position and a stable limit-cycle; the latter situation being attainable only through some external disturbance.

The non-linear element, mainly responsible for the behaviour near the centre position of the moving vehicle, is the dry friction in the king-pin bearings. The behaviour may be changed completely when a clearance in the wheel bearings is introduced. A third non-linearity to be considered is that caused by the tyre characteristics; this non-linearity is responsible for limiting the amplitude of the motion.

The autonomous non-linear problem could be treated with the aid of known analytical approximative methods. The non-autonomous system, however, was too complicated to solve analytically, so that we have proceeded to use an analogue computer. Chapter V deals with this latter investigation.

The analytical approximative method here employed and described in Sec. 2.1 is based on the method of the harmonic balance of Krylov and Bogoljubov. In this method the non-linear equations are reduced to equivalent linear equations with coefficients depending on the amplitude and frequency of the motion. With this approximative method the amplitudes of the limit-cycles and their stability can be determined. The application of a digital computer has increased the usefulness of this method.

Another analytical method is based on the fact that with small amplitudes the system can be considered to be piecewise linear. In our case this method is useful in particular for the study of motions near the centre position. In contrast to the methods mentioned above, this method enables us to examine the stability of the centre position of the moving automobile. In Sec. 3 a single case without clearance is treated with the use of this method.

For the sake of completeness we refer to [49] where two graphical methods are given; one for a simplified second-order system (isocline method) and the other for the third-order system. With these methods the complete trajectories towards a stable situation can be constructed in the phase plane and phase space respectively. The shape and the magnitude of the limit-cycles can be determined. These graphical methods, especially the second one, turned out to take up too much time to compete with the analogue computer.

1. *Determination of the stability of linear systems*

1.1. The Hurwitz criterium for stability

A set of linear differential equations has an asymptotically stable solution when all the roots of the characteristic equation of this set have negative real parts, i.e. when they are located in the left half of the complex plane. The characteristic equation has the following general form:

$$a_0 p^n + a_1 p^{n-1} + \dots + a_{n-1} p + a_n = 0, \quad (1)$$

when we assume a solution of the differential equations of the form Ce^{pt} . A necessary and sufficient condition for "monotonous" stability, that is when all real roots are negative, is that all coefficients a_i ($i=0, 1, \dots, n$) are positive:

$$a_i > 0 \quad (i=0, 1, \dots, n). \tag{2}$$

The system is not necessarily asymptotically stable in this case since occurring complex roots are not yet regarded. In order to cover the case of "oscillatory" stability too, that is the case when the real parts of the complex roots are negative and where the real roots are left out of consideration, it is necessary to satisfy the classical stability criterium of Hurwitz [50]. The criterium reads:

$$H_j > 0 \quad (j=1, 2, \dots, n). \tag{3}$$

where H_j is one of the so-called Hurwitz determinants. The j -th determinant has the following general form:

$$H_j = \begin{vmatrix} a_1 & a_0 & 0 & 0 & \dots & 0 \\ a_3 & a_2 & a_1 & a_0 & \dots & 0 \\ a_5 & a_4 & a_3 & a_2 & \dots & 0 \\ \vdots & \vdots & \vdots & \vdots & \ddots & \vdots \\ a_{2j-1} & a_{2j-2} & a_{2j-3} & a_{2j-4} & \dots & a_j \end{vmatrix} \quad (j=1, 2, \dots, n) \tag{4}$$

where a_i is a_i of (1) when $0 < i < n$ and $a_i = 0$ when $i > n$ or $i < 0$. In addition to the determinants (4) we shall also need H_0 and H_{-1} which are defined as:

$$H_0 = 1, \quad H_{-1} = 1/a_0. \tag{5}$$

The inequalities (3) are necessary and sufficient conditions for asymptotic stability of the n -th order system. Cremer [51] has shown that when the conditions (2) are satisfied, not all the conditions (3) are necessary for asymptotic stability, but that some are redundant. It is sufficient to satisfy the conditions (cf. Klotter [52, p.191]):

$$\left. \begin{aligned} a_i > 0 \quad (i=0, 1, \dots, n) . \\ H_{n-1-2j} > 0 \quad (j=0, 1, \dots, \frac{1}{2}(n-3)) . \end{aligned} \right\} \tag{6}$$

where the last condition $H_2 > 0$ is redundant when n is even. The $2m$ complex roots of the characteristic equation (1)

may in general be written as:

$$\left. \begin{aligned} p_k &= r_k + i\omega_k \\ p_{m+k} &= r_k - i\omega_k \end{aligned} \right\} (k = 1, 2, \dots, m) \quad (7)$$

and the real roots as:

$$p_{2m+l} = q_l \quad (l=1, 2, \dots, n-2m). \quad (8)$$

It can be shown that (cf. Orlando [53]):

$$a_n \sim \prod_{l=1}^{n-2m} q_l \quad (9)$$

and

$$H_{n-1} \sim \prod_{k=1}^m r_k, \quad (10)$$

which indicates that a_n and H_{n-1} change their signs each time when an additional monotonous and oscillatory instability respectively occurs. The coefficient a_n , consequently, will be the first to change its sign from positive to negative when due to a change of some parameter value a domain of monotonous instability is entered from an asymptotically stable area. The determinant H_{n-1} will be the first to become negative when a domain of oscillatory instability is entered from an asymptotically stable region. The boundary of the domain where oscillatory instability occurs, is formed by the part of $H_{n-1} = 0$ where the remainder of the conditions (6) are fulfilled. For this part Bautin (cf. Magnus [54]) has introduced the notation:

$$(H_{n-1}) = 0. \quad (11)$$

Accordingly we may introduce:

$$(a_n) = 0 \quad (12)$$

as the boundary between asymptotically stable and monotonously unstable regions, which is represented by that part of $a_n = 0$ where the remainder of (6) is satisfied.

The natural frequency occurring at the boundary of oscillatory instability can be calculated with the aid of the

formula (cf. Cremer [55]):

$$\omega^2 = \frac{a_n H_{n-3}}{H_{n-2}} \quad (13)$$

1.2. The third-order system

The simplest system which is capable of showing an unstable oscillatory motion is of the third order. In order to obtain the equation of such a simplified system in which γ and v_1 are the only variables, the remaining variables: y , φ , y^* , φ^* and γ_{st} must be taken equal to zero. The equations III.(80) and III.(82a) are the essential differential equations of motion for this system. For simplicity, the rotational stiffness c shall be taken equal to zero in the case to be considered. Only autonomous systems are considered, so that $\mu_{un} = 0$.

The essential variable γ denotes the angle of rotation of the wheel plane about the king-pin, which moves along a rectilinear path with velocity V . The axis of the king-pin lying in the wheel plane intersects the road surface at a distance e in front of the wheel axis. According to III.(99) this caster length e replaces the value $R\epsilon$, indicating the caster of a wheel with an inclined king-pin axis, passing through the wheel axis.

Figure 1 shows an equivalent system diagrammatically.

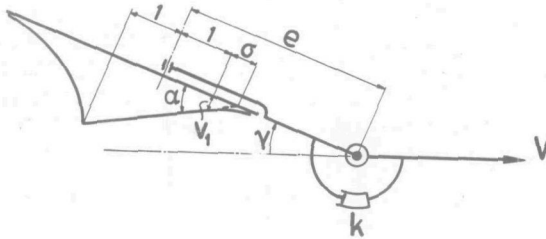


Fig.1. Model of the third-order system.

Here a vertical king-pin axis is considered, a configuration which does not change the differential equations for the third-order system within the degree of approximation considered (ϵ^2 neglected).

Neglecting the remaining variables of the system described in chapter III distorts the behaviour of the system more or less. The studies of more elaborate systems, described in

Sec. 1.3. and for non-linear systems in Secs. 2.5 and V.2., have revealed, however, that the principal features remain unchanged. The fact that the sprung mass and the lateral stiffness of the suspension are relatively large, makes this understandable.

The tyre will be described with the aid of approximation II based on the straight tangent conception and governed by the equations III. (96, 97b, 98b). For the damping couple D only the linear representation according to equation III. (85c) is relevant. With $y = \varphi = y^* = \varphi^* = \gamma_{st} = c = \mu_{un} = 0$ and the equations III. (83, 84, 85c, 87, 88, 89, 90, 96, 97b, 98b, 99) we obtain for the quantities occurring in equation III. (80):

$$R \epsilon = e, F_{tot} = \alpha, M = -e'\alpha - \frac{\kappa}{V} \dot{\gamma}, D = -k\dot{\gamma}$$

and for the quantities occurring in equation III. (82a):

$$v_1 = \sigma\alpha, y_w = -e\gamma.$$

The equations of motion in non-dimensional form III. (80, 82a) reduce to:

$$V^2 \frac{d^2\gamma}{ds^2} + (kV + \kappa) \frac{d\gamma}{ds} = -(e + e')\alpha, \quad (14)$$

$$\sigma \frac{d\alpha}{ds} + \alpha = -(1-e) \frac{d\gamma}{ds} + \gamma. \quad (15)$$

As independent variable we have introduced here for both equations: the non-dimensional travelled distance $s = Vt$. When we assume the set (14), (15) to have a solution of the form $Ce^{p_s s}$ the characteristic equation of the third degree becomes:

$$V^2 \sigma p_s^3 + \left\{ V^2 + (kV + \kappa)\sigma \right\} p_s^2 + \left\{ (e-1)(e+e') + kV + \kappa \right\} p_s + e + e' = 0 \quad (16)$$

The stability criterium reads according to the conditions (6):

$$\left. \begin{aligned} a_0 > 0, a_1 > 0, a_2 > 0, a_3 > 0, \\ H_2 = \begin{vmatrix} a_1 & a_0 \\ a_3 & a_2 \end{vmatrix} > 0, \end{aligned} \right\} \quad (17)$$

where the determinant is obtained by putting $j = 2$ and $n = 3$

in expression (4). The following conditions appear to be sufficient in the case considered:

$$\left\{ V^2 + (kV + \kappa)\sigma \right\} \left\{ (e-1)(e+e') + kV + \kappa \right\} > V^2 \sigma (e+e'), \quad (18a)$$

$$e + e' > 0. \quad (18b)$$

The stability boundaries can be found by making equations of the above inequalities. The first equation indicates the boundary for oscillatory instability and the second one for monotonous instability. Figure 2 shows the boundaries in

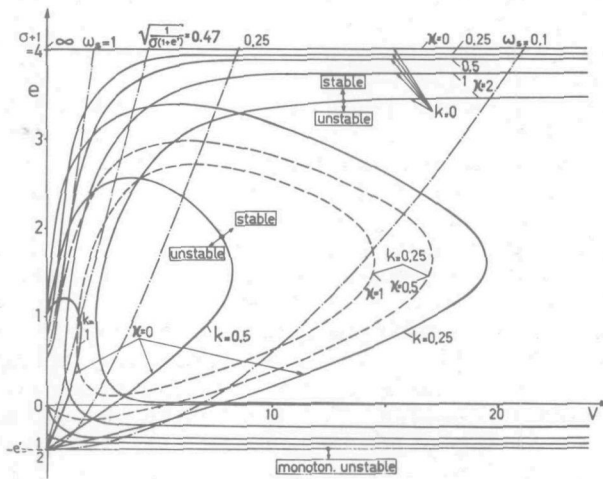


Fig.2. Unstable areas for the third-order system ($e'=0.5, \sigma=3$).

the (V, e) plane for a number of combinations of the two damping parameters. For the rest of the parameters the values $\sigma = 3$ and $e' = 0.5$, normally encountered in practice, are taken.

The frequency of the vibration on the boundary can be determined from equation (16), when the quantity p_s is replaced by $i\omega_s$. The symbol ω_s represents the so-called reduced frequency or path frequency

$$\omega_s = \frac{2\pi}{\lambda} = \frac{\omega}{V} \quad (19)$$

where λ denotes the non-dimensional wavelength of the motion and ω the non-dimensional frequency related to

time. From the two resulting equations $kV + \kappa$ can be eliminated. From the final equation the course of curves for constant ω_s can be derived. A few curves are shown in figure 2.

An increase in damping reduces the unstable area until it vanishes at certain combinations of k and κ . For the case that the damping due to tyre deformations vanishes ($\kappa = 0$) the well-known areas of instability (cf. Smiley [40]) are obtained. It appears that a tyre with a κ sufficiently large ($\kappa > \frac{1}{4}(e'+1)^2$) causes the area to detach itself from the e -axis. For $k > 0$, closed curves arise in the (V, e) plane ($V > 0$).

Placing a rotational spring about the king-pin results in a smaller unstable area within the boundary of the system without this spring. This can be verified rather simply (cf. Pacejka [48]).

Also when the more exact tyre theory of Von Schlippe is used the curves can become closed in themselves even for $\kappa = 0$, as has been found with the aid of a special electronical analogue computer circuit treated in chapter V. For an analytical treatment we refer to the work of Von Schlippe and Dietrich [34].

As a conclusion we may already draw at this stage of the investigation that, basically, an increase in value of the original tyre parameters with dimension: σ , a and e' , i.e. the relaxation length, half the contact length and the pneumatic trail, stimulate shimmy. The sum of these quantities in fact represents the distance between the upper and lower stability boundaries in figure 2 for the case of zero damping. The sum $\sigma + a$ is the coefficient of $i\omega_s$ in the second term of the expanded frequency response functions of F and M' with respect to γ (cf. II.(122, 123, 109)), which indicates its main responsibility for the phase lag of M' and F with respect to γ . This phase lag may lead to self-excitation. It may be noted that the sum of relaxation length and half the contact length $\sigma + a$ in fact equals the quotient of cornering stiffness C and lateral stiffness of the standing tyre C_y (cf. Eq. II.(144)).

An increase in e will in the first place enlarge the self-exciting couple about the king-pin but will in the second place increase the component of F and M' due to purely lateral motions (y_w) in which latter case phase lead occurs. The increase in damping due to this effect will suppress shimmy at large values of e .

1.3. The fifth-order system

Two different kinds of extensions of the third-order system

are treated in this section. The intention is to show the influence of the torsional stiffness c_{φ}^* and of the lateral stiffness c_y^* of the wheel suspension. Compared to the system of the preceding section the number of variables is increased by one, representing either the torsion angle φ^* of the king-pin about a longitudinal axis, or the lateral motion y^* of the king-pin.

The following set of equations, corresponding to equations III. (79, 80 and 82b) describe the system with torsion. They are obtained in a manner analogous to the way as described for the third-order system.

$$\left. \begin{aligned} \beta^* \ddot{\varphi}^* + \{c_{\varphi}^* + (N-N') h^*\} \dot{\varphi}^* + \beta V \dot{\gamma} &= - (R+h^*) \alpha, \\ \ddot{\gamma} + (k + \kappa/V) \dot{\gamma} - \beta V \dot{\varphi}^* &= - (e+e') \alpha, \\ \sigma \dot{\alpha} + V \alpha &= (R+h^*) \dot{\varphi}^* - (1-e) \dot{\gamma} + V \gamma. \end{aligned} \right\} \quad (20)$$

Terms containing ϵ , which are small with respect to neighbouring terms, are neglected. This approximation is correct for small ϵ , the assumption having been considered from the outset of the investigation. The system governed by the above equations is shown diagrammatically in figure 3.

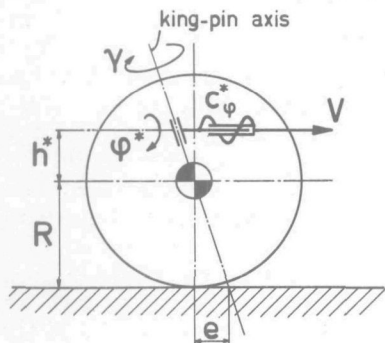


Fig. 3. Model of the fifth-order system with torsional flexibility.

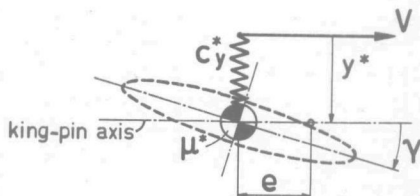


Fig. 4. Model of the fifth-order system with lateral flexibility.

For a system with lateral flexibility instead of torsional flexibility of the wheel suspension the equations of motion become according to equations III. (78, 80 and 82b) with the same approximations introduced as in the previous case:

$$\left. \begin{aligned} \mu^* \ddot{y}^* + c_y^* \dot{y}^* &= \alpha \\ \ddot{\gamma} + (k + \kappa/V) \dot{\gamma} &= - (e + e') \alpha \\ \sigma \dot{\alpha} + V \alpha &= - \dot{y}^* - (1 - e) \dot{\gamma} + V \gamma \end{aligned} \right\} \quad (21)$$

The system described through the equations (21) is shown diagrammatically in figure 4.

The systems (20) and (21) may be described by the same set of equations:

$$\left. \begin{aligned} \mu_{\eta} \ddot{\eta} + c_{\eta} \dot{\eta} - \beta_{\eta} V \dot{\gamma} &= \alpha \\ \dot{\gamma} + (k + \kappa/V) \gamma + \beta_{\eta} V \dot{\eta} &= - (e + e') \alpha \\ \sigma \dot{\alpha} + V \alpha &= - \dot{\eta} - (1-e) \dot{\gamma} + V \gamma \end{aligned} \right\} \quad (22)$$

in which the new quantities have been introduced as listed in the table below.

Table 1. Introduction of new quantities for the systems showing torsional and lateral flexibility respectively.

	torsional	lateral
$\eta =$	$-(R + h^*) \varphi^*$	y^*
$\beta_{\eta} =$	$\beta / (R + h^*)$	0
$\mu_{\eta} =$	$\beta_{\varphi}^* / (R + h^*)^2$	μ^*
$c_{\eta} =$	$\{c_{\varphi}^* + (N - N') h^*\} / (R + h^*)^2$	c_y^*

The stiffness c_{η} in fact denotes the non-dimensional lateral stiffness of the suspension at road level and μ_{η} the non-dimensional unsprung mass reduced to a point at road level, in both cases. The system appears to be determined by eight parameters. One parameter $(R+h^*)$ has been eliminated through the manipulations above. The characteristic equation of (22) becomes:

$$\sum_{i=0}^5 a_i p^{5-i} = 0. \quad (23)$$

After multiplication with V the coefficients read:

$$\left. \begin{aligned} a_0 &= \mu_{\eta} \sigma, \\ a_1 &= \mu_{\eta} \{V + (k + \kappa/V) \sigma\}, \\ a_2 &= (c_{\eta} \sigma + 1) + \mu_{\eta} V (k + \kappa/V) - \mu_{\eta} (e + e') (1 - e) + \beta_{\eta}^2 V^2 \sigma, \\ a_3 &= c_{\eta} V + (k + \kappa/V) (c_{\eta} \sigma + 1) + \beta_{\eta}^2 V^3 - \beta_{\eta} V (1 + e') + \mu_{\eta} V (e + e'), \\ a_4 &= c_{\eta} V (k + \kappa/V) + \beta_{\eta} V^2 - c_{\eta} (e + e') (1 - e), \\ a_5 &= c_{\eta} V (e + e'). \end{aligned} \right\} \quad (24)$$

As pointed out in Sec. 1.1. the system governed by equation (22) is stable when all coefficients a_i and moreover the Hurwitz determinants H_2 and H_4 are positive. The determinants read according to (4):

$$H_2 = \begin{vmatrix} a_1 & a_0 \\ a_3 & a_2 \end{vmatrix}, \quad H_4 = \begin{vmatrix} a_1 & a_0 & 0 & 0 \\ a_3 & a_2 & a_1 & a_0 \\ a_5 & a_4 & a_3 & a_2 \\ 0 & 0 & a_5 & a_4 \end{vmatrix}. \quad (25)$$

In the (V, e) plane the stability boundaries have been determined for several cases. On these boundaries H_4 equals zero. Throughout the part of the (V, e) plane considered the coefficients and the determinant H_2 appear to remain positive in these cases. The calculations are carried out for several values of the stiffness c_η for the cases $\beta_\eta = 0$ (lateral flexibility, see Fig. 5) and $\beta_\eta = 0.1$ (torsional flexibility,

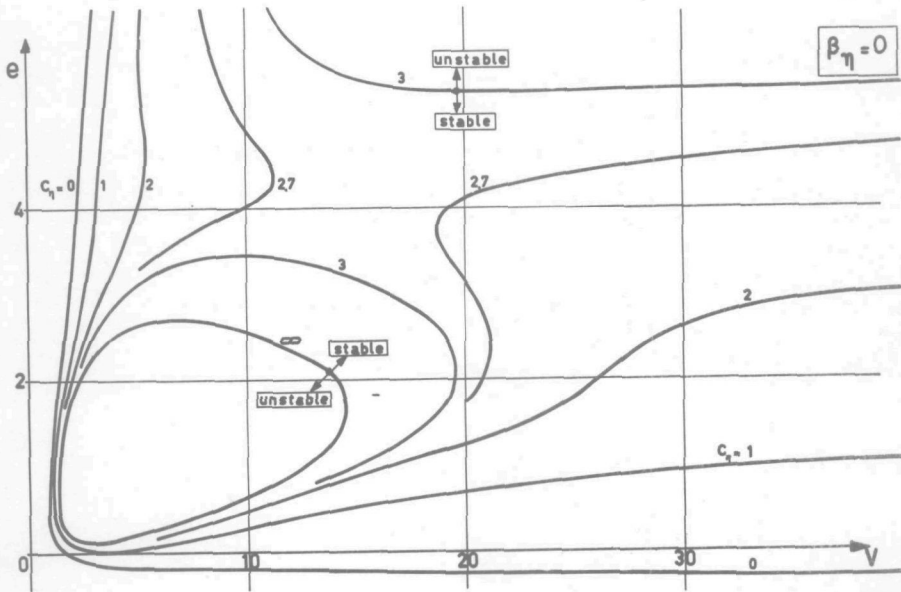


Fig. 5. Influence of lateral stiffness on the stability areas ($e^*=0.5, \sigma=3, \kappa=1, k=0.25, \mu_\eta=0.5$).

see Fig. 6). The influence of variation in gyroscopic coupling represented by β_η is shown in figure 7 for $c_\eta = 1$. The rest of the parameter values are:

$$e' = 0.5, \sigma = 3, \kappa = 1, k = 0.25, \mu_{\eta} = 0.5. \quad (26)$$

The calculations have been carried out with the aid of a digital computer.

Because of the restriction that in the fifth-order system

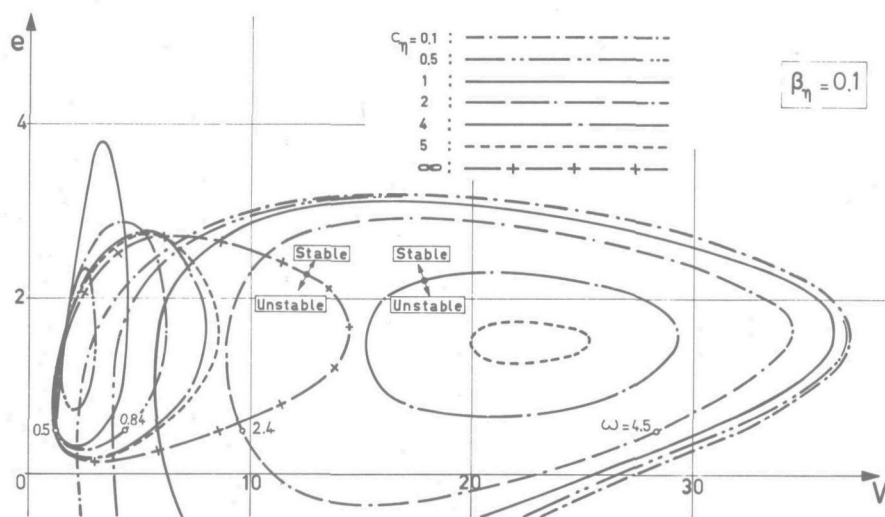


Fig. 6. Influence of torsional stiffness on the stability areas ($e' = 0.5, \sigma = 3, \kappa = 1, k = 0.25, \mu_{\eta} = 0.5$).

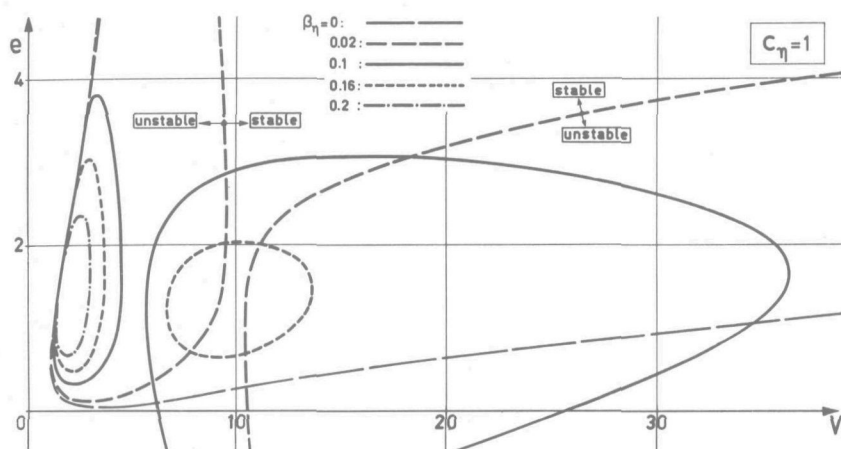


Fig. 7. Influence of gyroscopic coupling on the stability areas ($e' = 0.5, \sigma = 3, \kappa = 1, k = 0.25, \mu_{\eta} = 0.5$).

considered the mass centre must lie on the king-pin axis, large values of e are only of academic interest. The system would then represent the case where the king-pin remains vertical but is shifted over a caster length e , while the mass centre of the swivelling part remains on the king-pin axis. For automobiles, practical values encountered remain below the value $e = 0.5$.

Figure 5 shows that the unstable area increases with decreasing lateral stiffness of the suspension. Especially at great values of e and V the situation becomes more dangerous.

It has been found that the much less realistic system of the fourth order, fitted with a tyre without relaxation property ($\sigma=a=0$) but with lateral slip possibility (C finite) only shows open curves like those in figure 5 for the cases $c_\eta = 0$ and $c_\eta = 3$ (upper branch). It may be concluded that the lateral elasticity of the suspension causes instability in the higher V and e ranges while the lateral tyre elasticity results in an instability region closer to the origin of the (V, e) plane.

Introduction of a torsional elasticity in the suspension instead of the purely lateral elasticity results in a considerable change in the qualitative behaviour of the system. Referring to figure 6 we note that an entirely new unstable area may arise below a certain value of torsional stiffness at relatively high speeds due to the gyroscopic coupling. With decreasing stiffness c_η this new area grows especially towards smaller values of the speed V , while the original unstable area situated closer to the origin becomes smaller until it vanishes.

It appears that the oscillation at the boundary of the new area, referred to as the area of "gyroscopic shimmy" or "wobble", has a frequency greater than the natural frequency of the torsional motion $\omega_{\eta_0} = \sqrt{c_\eta/\mu_\eta}$. The frequency on the boundary of the original area, where an oscillation occurs sometimes referred to as "tyre shimmy", is lower than the natural frequency mentioned. Figure 6 shows the instantaneous frequency ω in a few points; the natural frequency ω_{η_0} in these points equals $\omega_{\eta_0} = 2$. An analysis of a simplified second-order system treated in [9] makes it understandable that gyroscopic shimmy may occur at low values of the natural frequency ω_{η_0} .

The fact that the gyroscopic shimmy occurs with a low torsional stiffness of the suspension suggests that this is the type of shimmy which occurs with live axles when pneumatic tyres are fitted. This shimmy has especially been observed with wheels oscillating in vertical direction so violently that the road contact is lost periodically (see

Olley [4]). The latter phenomenon may be a condition for this kind of shimmy to take place, because in that case the average stiffness of the suspension about a longitudinal axis reduces, which results in a shift towards lower speed values of the left-hand boundary of the unstable area.

Figure 7 shows that large values of the moment of inertia I_a of the wheel about its axle, which finds expression in large β_η 's, may stabilize the system again.

1.4. The seventh-order system

A more realistic model provided with a steering system may be described by equation III. (81) in addition to the set (22) describing the fifth-order system. In the second equation of (22) an additional term will appear according to III. (80). We obtain:

$$\left. \begin{aligned} \mu_\eta \ddot{\eta} + c_\eta \dot{\eta} - \beta_\eta V \dot{\gamma} &= \alpha, \\ \dot{\gamma} + \beta_{st} \ddot{\gamma}_{st} + (k + \kappa/V) \dot{\gamma} + \beta_\eta V \dot{\eta} &= - (e + e') \alpha, \\ \sigma \dot{\alpha} + V \alpha &= - \dot{\eta} - (1 - e) \dot{\gamma} + V \gamma, \\ \beta_{st} \ddot{\gamma}_{st} + c(\gamma_{st} - \gamma) &= 0. \end{aligned} \right\} \quad (27)$$

With the aid of the last equation the variable γ_{st} can be written in terms of γ for the case of sinusoidal motions with frequency ω :

$$\gamma_{st} = \frac{1}{1 - \frac{\beta_{st}}{c} \omega^2} \gamma. \quad (28)$$

This expression substituted in the second equation of (27) suggests the introduction of an equivalent moment of inertia about the king-pin axis:

$$I_{eq} = I \left(1 + \frac{\beta_{st}}{1 - \lambda} \right) \quad (29)$$

in which the quantity λ is defined by:

$$\lambda = \left(\frac{\omega}{\omega_{sto}} \right)^2 \quad (30)$$

where

$$\omega_{sto} = \sqrt{\frac{c}{\beta_{st}}} \quad (31)$$

denotes the natural frequency of the steering system.

Now the set of equations (22) also appear to apply for the extended system when the non-dimensional parameters β_η , μ_η , k and V , all of them depending on I (cf. Table III.1 (p.79) and Table 1 (p.92)) are replaced by the parameters $\beta_{\eta eq}$, $\mu_{\eta eq}$, k_{eq} and V_{eq} respectively, the new quantities depending in the same way upon I_{eq} . The following relations hold:

$$\beta_{\eta eq} = \frac{\beta_\eta}{1 + \frac{\beta_{st}}{1-\lambda}}, \mu_{\eta eq} = \frac{\mu_\eta}{1 + \frac{\beta_{st}}{1-\lambda}}, k_{eq} = \frac{k}{\sqrt{1 + \frac{\beta_{st}}{1-\lambda}}}, V_{eq} = V \sqrt{1 + \frac{\beta_{st}}{1-\lambda}}. \quad (32)$$

For each assumed value of λ the stability boundaries and the frequencies occurring on the boundary can be calculated in the same way as has been done for the real fifth-order system. The frequency ω_{eq} obtained is related to the actual frequency ω as follows:

$$\omega_{eq}^2 = \omega^2 \left(1 + \frac{\beta_{st}}{1-\lambda} \right) \quad (33)$$

from which expression the actual frequency can be calculated. The quantity ω^2 has to be compared with the assumed value $\lambda \omega_{sto}^2$. The point on the boundary where the two values are equal is a point of the boundary of the system with steering-wheel. By repeating the calculation for a great number of values of λ the boundary for the system with steering-wheel may be determined.

In figure 8 the stability boundaries for the super and subcritical case of steering oscillations ($\lambda > 1$ and $\lambda < 1$ respectively) are shown for a certain configuration. The unstable area for $c_\eta = 4$ shown at the left-hand side of figure 6 appears to be replaced by a larger area where $\lambda < 1$ and inside of it a smaller area where two pairs of roots of the characteristic equation of the seventh-order system give rise to instability and consequently a vibration occurs composed by a subcritical ($\lambda < 1$) and a supercritical ($\lambda > 1$) unstable motion. This result should be clear because of the fact that the effective rotational stiffness about the king-pin is positive for $\lambda > 1$ and negative for $\lambda < 1$, which makes the area smaller and larger respectively (cf. Sec. 1.2). The

area of gyroscopic shimmy at the right-hand side of figure 8 is only slightly reduced compared to the corresponding area in figure 6.

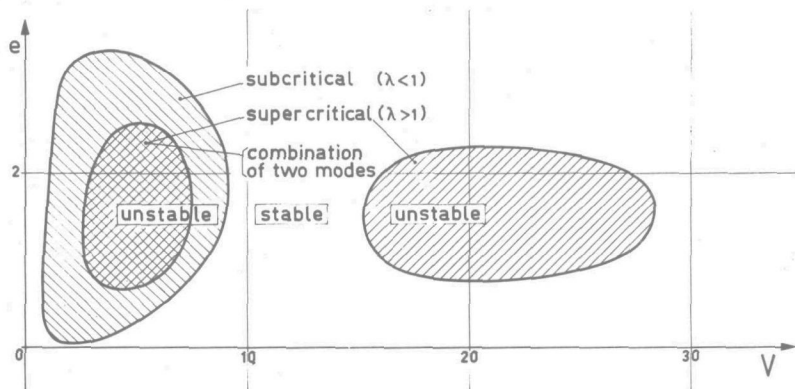


Fig. 8. The unstable areas of the fifth-order system extended with a steering-wheel (total 7th-order) ($\beta_{\eta}=0.1, c_{\eta}=4, \mu_{\eta}=0.5, \beta_{st}=0.7, c=0.4, \sigma=3, e'=0.5, k=0.25, \kappa=1$).

2. Investigation of non-linear systems with the aid of equivalent linear equations

2.1. Determination of "limit-amplitudes"

In this section the method given by Magnus [54, 46] for the investigation of motions near a limit-cycle is followed in principle. The largest value obtained by some representative system variable during the motion on a limit-cycle, a closed curve in the phase space which is followed when the motion has a periodic nature, will be designated by the term "limit-amplitude". Magnus' method permits a relatively simple analytical treatment of the non-linear problem. It is based on the theory of the harmonic balance of Krylov and Bogoljubov.

The accuracy of the approximate solution of the non-linear differential equations cannot be judged in an analytical manner. It is known, however, that the approximation is good when the oscillations, performed by the non-linear system, have one predominant harmonic. This is the case when the non-linearities are not too strong and when the stationary solution of the equivalent linear system represents a motion of only one frequency. Experiments with a shimmying automobile showed that the system vibrates with one predominant

frequency. It seems permissible therefore to apply the principle of the harmonic balance to this non-linear system. The results obtained by means of this analytical method may be compared with analogue computer solutions.

For the general description of the method an n -th order non-linear system is considered, which is described by a set of differential equations containing non-linear terms. The restriction has been made here that each non-linear term is governed by only one variable and its time derivative.

The n first-order differential equations can be written in the form:

$$\dot{x}_i = \sum_{j=1}^n \left\{ a_{ij} x_j + b_{ij} \dot{x}_j + f_{ij}(x_j, \dot{x}_j) \right\} \quad (i = 1, 2, \dots, n) \quad (34)$$

where x_i is one of the co-ordinates of the n -th order system, denoting either the displacement or the velocity of a part of the system. The sum $\sum f_{ij}$ represents the non-linear part of the i -th equation. In cases normally encountered f_{ij} vanishes when x_j denotes a velocity and consequently \dot{x}_j an acceleration. There are several possibilities for writing the equations in the form (34). In general it will be tried through transformations to obtain as few terms f_{ij} as possible.

The equations (34) are replaced by the linear system:

$$\dot{x}_i = \sum_{j=1}^n (a_{ij}^* x_j + b_{ij}^* \dot{x}_j) \quad (i = 1, 2, \dots, n) \quad (35)$$

with coefficients a_{ij}^* and b_{ij}^* which in general are functions of the amplitude of a variable and the frequency of the motion. These functions are chosen in such a way that, when x_j is varied sinusoidally, the first harmonic of the part of equation (34) governed by x_j (and \dot{x}_j) equals the corresponding part in equation (35).

Say x_j is thought to vary like

$$x_j = A_j \sin \theta_j, \quad \text{where } \theta_j = \omega t + \varphi_j, \quad (36)$$

so that

$$\dot{x}_j = A_j \omega \cos \theta_j. \quad (37)$$

The coefficients a_{ij}^* and b_{ij}^* of the equation (35) are made equal now to the Fourier coefficients of the first harmonic of the part between { } on the right-hand side of equation

(34) in which (36) and (37) are thought to be filled in:

$$\begin{aligned} a_{ij}^* &= \frac{1}{\pi A_j} \int_0^{2\pi} \left\{ a_{ij} x_j + b_{ij} \dot{x}_j + f_{ij}(x_j, \dot{x}_j) \right\} \sin \theta_j d\theta_j = \\ &= a_{ij} + \frac{1}{\pi A_j} \int_0^{2\pi} f_{ij} \sin \theta_j d\theta_j, \end{aligned} \quad (38)$$

$$\begin{aligned} b_{ij}^* &= \frac{1}{\pi \omega A_j} \int_0^{2\pi} \left\{ a_{ij} x_j + b_{ij} \dot{x}_j + f_{ij}(x_j, \dot{x}_j) \right\} \cos \theta_j d\theta_j = \\ &= b_{ij} + \frac{1}{\pi \omega A_j} \int_0^{2\pi} f_{ij} \cos \theta_j d\theta_j. \end{aligned} \quad (39)$$

In general the integrals are functions of the amplitude A_j and of the frequency ω .

For stationary oscillatory motions the ratio of the amplitude A_j and some reference amplitude A of reference co-ordinate x can be found in principle as a function of the frequency. The coefficients a_{ij}^* and b_{ij}^* can thus be expressed as functions of only A and ω . We assume that these relations approximately hold for almost stationary oscillatory motions too.

The characteristic equation of the equivalent linear set of equations (35) reads:

$$\sum_{k=0}^n a_k p^{n-k} = 0. \quad (40)$$

For the system to vibrate in a limit-cycle a solution of (35) in the form

$$x_j = A_j \sin(\omega t + \varphi_j) \quad (41)$$

must exist. The system has such a solution when the characteristic equation (40) has one pair of imaginary roots and for the rest roots with a negative real part, which causes the rest of the solutions to die out. The condition for this to occur is expressed by the formula (11) which reads:

$$(H_{n-1}) = 0 \quad (11)$$

indicating that part of $H_{n-1} = 0$ where the rest of the conditions (6) are fulfilled. The absolute values of the two imaginary roots which represent the frequency of the motion on the limit-cycle, can be calculated with the aid of the formula (13):

$$\omega^2 = \frac{a_n H_{n-3}}{H_{n-2}} \quad (13)$$

Consider the case that m equivalent coefficients $a_{ij}^*(A, \omega)$ and $b_{ij}^*(A, \omega)$ occur in the system (35). In the coefficient space an m -dimensional surface can be constructed on which (H_{n-1}) vanishes. For each of the points on this surface the frequency ω can be calculated with formula (13). With the aid of the formulae (38) and (39) for $a_{ij}^*(A, \omega)$ and $b_{ij}^*(A, \omega)$ the m values of the amplitude A belonging to each of the m coefficient values a_{ij}^* and b_{ij}^* can be calculated. We can calculate A for each of the points of the m -dimensional surface mentioned. The m amplitude surfaces of the m -th dimension which arise in this way, may be plotted in the coefficient space with one of the coefficient axes also acting as amplitude axis. The m amplitude surfaces may have a few discrete points in common. These points represent the amplitudes of the limit-cycles.

The procedure may be simplified when $m-1$ equivalent coefficients contain a parameter which can be considered as an unknown quantity. For each point on the surface where $(H_{n-1}) = 0$, the amplitude of the limit-cycle can now be calculated with the aid of the remaining coefficient. The

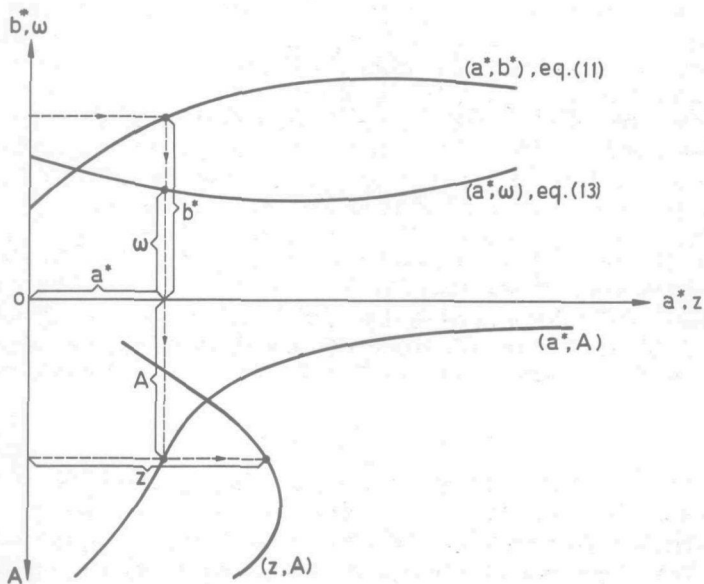


Fig. 9. Determination of the limit-amplitude A for a certain value of coefficient b^* .

values of the unknown parameters in the other $m-1$ coefficients, necessary to obtain the limit-cycle, may be computed afterwards. As an illustration a two-dimensional case with two equivalent coefficients, say a^* and b^* (subscripts omitted) is shown in figure 9. Coefficient a^* is a function of A, ω and an unknown parameter z , while b^* is only a function of A and ω . In figure 9 a certain value of b^* is chosen and the corresponding value of a^* required on a limit-cycle is determined with the aid of formule (11). With formula (13) the frequency ω is calculated after which the amplitude A can be calculated from $b^* = b^*(A, \omega)$ (Eq.(39)). Once A is known the value of z can be computed from $a^* = a^*(A, \omega, z)$ (Eq.(38)). By repeating the procedure for several values of b^* the amplitudes of the limit-cycle and the frequency are known as a function of z (see curve (z, A) in Fig. 9).

2.2. Stability of limit-cycles

When the coefficients a_{ij}^* and b_{ij}^* do not depend upon the frequency or when the frequency remains constant with varying amplitude, it is possible to construct a curve in the coefficient space according to which the coefficients change with varying amplitude A . In the general case where the coefficients depend on both amplitude and frequency, not being a constant, it is not easy to determine the curve which is followed in the coefficient space, even in the neighbourhood of the limit-amplitude.

The points of intersection between this curve and the surface where $(H_{n-1})=0$ indicate the amplitudes of the limit-cycles. As for $(H_{n-1}) < 0$ the amplitude tends to increase, it may be understood that a limit-cycle is stable when the surface is crossed by the curve with increasing amplitude from the part of the space where $(H_{n-1}) < 0$ to the part where $(H_{n-1}) > 0$ and vice versa.

The rate of change of the Hurwitz determinant with amplitude in the neighbourhood of the limit-cycle is represented by:

$$\frac{dH_{n-1}}{dA} = \frac{\partial H_{n-1}}{\partial A} + \frac{\partial H_{n-1}}{\partial \omega} \frac{d\omega}{dA}. \quad (42)$$

In [59] we have studied the stability of certain systems with the aid of a method, not being reproduced here, in which the influence of the variation of ω (last term of Eq. (42)) has been taken into account. For weakly non-linear

systems, to which the use of the method of the harmonic balance is restricted, this last term will be of the second order of magnitude in the small non-linear parameter; because second-order terms are disregarded in the harmonic balance method, calculation of this last term would not make sense. In the cases considered, however, a noticeable improvement in the results has been obtained by introducing this additional term. In Sec. 2.3C an illustration of the influence of taking into account the variation of ω , resulting from the above mentioned study, will be given.

When we restrict ourselves to first-order terms, we may adopt the simple qualitative criterium of stability postulated by Magnus [54]):

$$\left. \begin{array}{l} \text{limit-cycle stable} \quad \text{if } \partial H_{n-1} / \partial A > 0, \\ \text{limit-cycle unstable} \quad \text{if } \partial H_{n-1} / \partial A < 0. \end{array} \right\} \quad (43)$$

We shall transform this qualitative criterium into a quantitative one, from which also the degree of stability of a limit-cycle can be judged. We will not exclude the effect of the last term of (42). Consider again the polynomial (40):

$$\sum_{k=0}^n a_k p^{n-k} = 0. \quad (40)$$

In the neighbourhood of a limit-cycle this equation has no longer purely imaginary roots. The roots become then:

$$p = \delta r \pm i \omega, \quad (44)$$

where δr denotes the real part of the root and ω the frequency in the deviated situation. A new quantity p_1 is introduced now:

$$p_1 = p - \delta r. \quad (45)$$

When δa_k denotes the variation of a_k due to a deviation from the limit-cycle we obtain for (40) after substitution of $p = p_1 + \delta r$:

$$\sum_{k=0}^n \left\{ a_{k,0} + \delta a_k + (n-k+1) a_{k-1,0} \delta r \right\} p_1^{n-k} = 0 \quad (46)$$

where $a_{i,0}$ denotes the value of a_i on the limit-cycle and $a_{-1,0} = 0$. Products of variations δa_k and δr are neglected.

Equation (46) has one pair of purely imaginary roots, the absolute value of which represents the frequency ω of the deviated motion. Hence, the $(n-1)$ -th Hurwitz determinant H_{n-1}^1 of the polynomial (46) should be zero. We may write:

$$H_{n-1}^1 = H_{n-1,0} + \delta H_{n-1} + b \cdot \delta r = 0. \quad (47)$$

Since on the limit-cycle

$$H_{n-1}^1 = H_{n-1,0} = 0, \quad (48)$$

we obtain from (47):

$$\delta H_{n-1} = -b \cdot \delta r. \quad (49)$$

where b is a constant and δH_{n-1} is a linear function of $\delta a_0 \dots \delta a_n$. We obtain from (49):

$$\frac{dH_{n-1}}{dA} = -b \frac{dr}{dA}. \quad (50)$$

We have not yet succeeded in proving in general that b must be a positive quantity but this has turned out to be the case in all the special problems we have investigated. It is expected to be positive because evidently the following conditions apply:

$$\left. \begin{array}{l} \text{limit-cycle stable} \quad \text{if } S < 0, \\ \text{limit-cycle unstable} \quad \text{if } S > 0, \end{array} \right\} \quad (51)$$

in which is introduced the "stability value" S of the limit-cycle:

$$S = 2\pi \frac{A_0}{\omega_0} \frac{dr}{dA}, \quad (52)$$

where A_0 and ω_0 denote the amplitude and the frequency on the limit-cycle respectively; dr/dA is the derivative on the limit-cycle of the real part of the root of (40), the latter being purely imaginary when the motion is exactly on the limit-cycle. Instead of using the total derivative shown above, the partial derivative with respect to the amplitude A may be taken with ω kept constant; in this case the conditions (51) correspond to (43) indicated by Magnus.

In fact, the stability value S has a practical meaning. The

stability value appears to represent the rate of change of the increase in amplitude with the amplitude as illustrated in figure 10. This relation may be derived in the following

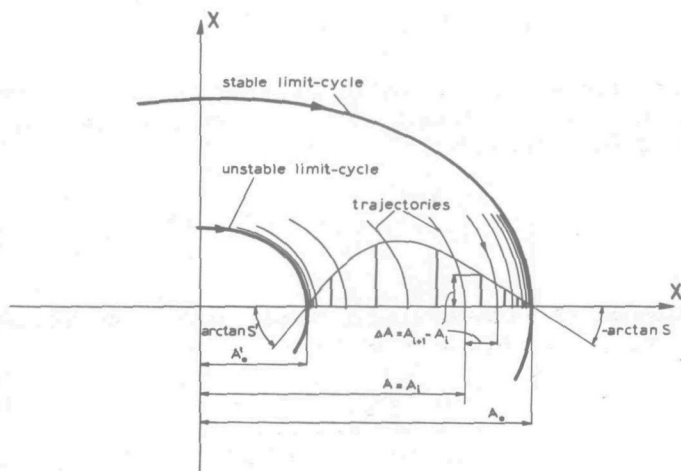


Fig. 10. Signification of the stability value S .

way. Consider the solution of co-ordinate x in the neighbourhood of a limit-cycle:

$$x = A_i e^{(\delta r t + \psi_i)} \sin(\omega t + \varphi_i). \quad (53)$$

where A_i represents the amplitude at the i -th crossing with the x -axis shown in figure 10. For $t = t_i$ we have chosen:

$$\left. \begin{aligned} \omega t_i + \varphi_i &= \frac{1}{2} \pi, \\ \delta r t_i + \psi_i &= 0, \end{aligned} \right\} \quad (54)$$

so that then

$$x = A_i.$$

A motion close to the limit-cycle is considered, so that:

$$A_i \approx A_0. \quad (55)$$

The variation of the amplitude is governed by:

$$A = A_i e^{(\delta r t + \psi_i)}. \quad (56)$$

Herewith we obtain for the amplitude at the $(i+1)$ -th crossing:

$$A_{i+1} = A_i e^{\delta r \frac{2\pi}{\omega}} \quad (57)$$

in which for δr and ω their average values in the cycle considered may be taken. Expression (57) results in the increment in amplitude:

$$\Delta A = A_{i+1} - A_i = A_i \left(e^{\delta r \frac{2\pi}{\omega}} - 1 \right) = A_o \delta r \frac{2\pi}{\omega_o} \text{ for } \delta r \rightarrow 0. \quad (58)$$

The rate of change with amplitude of this increment becomes:

$$\frac{d\Delta A}{dA} = 2\pi \frac{A_o}{\omega_o} \frac{dr}{dA} = S, \quad (59)$$

which is identical to the stability value (52).

2.3. The third-order system

The non-linear equations of the third order are obtained similarly to the way in which the linear equations (14) and (15) are derived from the original equations III. (80, 82a). Instead of applying the equations III. (85c, 97b, 98b) we will now use the equations III. (85a, 85b, 97a, 98a). The two equations of motion read in general form:

$$\left. \begin{aligned} \ddot{\gamma} + g^*(\dot{\gamma}, \gamma) &= -f^*(\alpha), \\ \sigma \dot{\alpha} + V\alpha &= -(1-e)\dot{\gamma} + V\gamma, \end{aligned} \right\} \quad (60)$$

where

$$f^*(\alpha) = -M' + eF, \quad (61)$$

$$g^*(\dot{\gamma}, \gamma) = g(\dot{\gamma}, \gamma) + \kappa\dot{\gamma}/V. \quad (62)$$

The tyre non-stationary behaviour is described again through approximation II. The term $f^*(\alpha)$ represents the total couple about the king-pin axis due to lateral tread deformations and $g^*(\dot{\gamma}, \gamma)$ the damping couple due to friction in the king-pin

bearings and to longitudinal tread deformations in the contact-area.

The linear equivalent set of equations has the following form:

$$\left. \begin{aligned} \dot{\gamma} + k^* \dot{\gamma} + c \gamma &= - C^* \alpha, \\ \sigma \dot{\alpha} + V \alpha &= - (1-e) \dot{\gamma} + V \gamma, \end{aligned} \right\} \quad (63)$$

They are obtained from (60) by replacing $g^*(\dot{\gamma}, \gamma)$ by $k^* \dot{\gamma} + c \gamma$ and $f^*(\alpha)$ by $C^* \alpha$. In the linear case, C^* would be equal to $e + e'$ (cf. Eq. (14)). The coefficients k^* , c and C^* are now not considered as constants but as functions of a reference amplitude, say of γ , and of the frequency ω of the motion.

In order to determine these functions we consider the sinusoidal variation:

$$\gamma = \gamma_0 \sin \theta, \text{ where } \theta = \omega t \quad (64)$$

so that

$$\dot{\gamma} = \gamma_0 \omega \cos \theta. \quad (65)$$

The second variable α becomes then:

$$\alpha = \alpha_0 \sin (\theta - \varphi) \quad (66)$$

or

$$\alpha = \alpha_0 \sin \tau, \text{ where } \tau = \theta - \varphi. \quad (66a)$$

The terms $k^* \dot{\gamma} + c \gamma$ and $C^* \alpha$ are to be made equal to the first harmonics of $g^*(\dot{\gamma}, \gamma)$ and $f^*(\alpha)$ respectively. This is realized with the aid of the following integrals over one period of the oscillation. The equivalent quantities become:

$$k^* = \frac{1}{\pi \omega \gamma_0} \int_0^{2\pi} g^*(\dot{\gamma}, \gamma) \cos \theta \, d\theta, \quad (67)$$

$$c = \frac{1}{\pi \gamma_0} \int_0^{2\pi} g^*(\dot{\gamma}, \gamma) \sin \theta \, d\theta, \quad (68)$$

$$C^* = \frac{1}{\pi \alpha_0} \int_0^{2\pi} f^*(\alpha) \sin \tau \, d\tau. \quad (69)$$

The equivalent cornering stiffnesses C and C_M , corresponding to the linear stiffnesses introduced in II. (78), are related to the total equivalent stiffness C^* as follows:

$$C_M + e C = C^* \quad (70)$$

and become accordingly:

$$C_M = \frac{-1}{\pi \alpha_0} \int_0^{2\pi} M'(\alpha) \sin \tau d \tau \quad \text{and} \quad C = \frac{1}{\pi \alpha_0} \int_0^{2\pi} F(\alpha) \sin \tau d \tau. \quad (71)$$

In order to investigate a practical case we shall consider dry friction in the king-pin bearings and rotational clearance in the system as shown in figure III.4 (p. 76). A clearance as considered might occur approximately when play exists in the bearings of the swivelling wheel. The dry-frictional couple is denoted by K and the total clearance angle by 2δ .

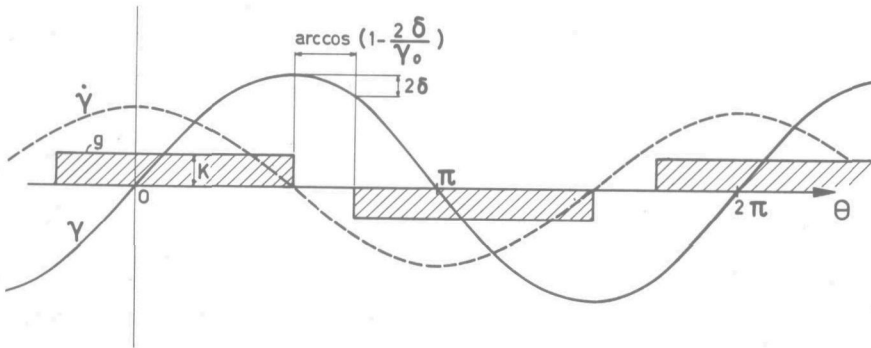


Fig. 11. Course of the function $g(\dot{\gamma}, \gamma)$ with θ .

Figure 11 shows how the couple $g(\dot{\gamma}, \gamma)$ varies with time for a sinusoidally changing γ . Expression (67) becomes with (62):

$$\begin{aligned} k^* &= \frac{1}{\pi \omega \gamma_0} \int_0^{2\pi} g^*(\dot{\gamma}, \gamma) \cos \theta d \theta = \frac{\kappa}{V} + \frac{2}{\pi \omega \gamma_0} \int_{\frac{1}{2}\pi}^{\frac{3}{2}\pi} g(\dot{\gamma}, \gamma) \cos \theta d \theta = \\ &= \frac{\kappa}{V} + \frac{2}{\pi \omega \gamma_0} \int_{\frac{1}{2}\pi + \arccos(1 - 2\delta/\gamma_0)}^{\frac{3}{2}\pi} (-K) \cos \theta d \theta = \frac{\kappa}{V} + \frac{4K}{\pi \omega \gamma_0} \left(1 - \frac{\delta}{\gamma_0}\right), \end{aligned}$$

which denotes the equivalent coefficient of damping about the

king-pin. The equivalent coefficient of damping only due to friction in the king-pin bearings becomes then:

$$k = k^* - \frac{\kappa}{V} = \frac{4K}{\pi\omega\gamma_0} \left(1 - \frac{\delta}{\gamma_0}\right). \tag{72}$$

Expression (68) for the equivalent rotational stiffness becomes:

$$\begin{aligned} c &= \frac{1}{\pi\gamma_0} \int_0^{2\pi} g^*(\dot{\gamma}, \gamma) \sin \theta \, d\theta = \frac{2}{\pi\gamma_0} \int_{\frac{1}{2}\pi}^{\frac{3}{2}\pi} g(\dot{\gamma}, \gamma) \sin \theta \, d\theta = \\ &= \frac{2}{\pi\gamma_0} \int_{\frac{1}{2}\pi + \arccos(1-2\delta/\gamma)}^{\frac{3}{2}\pi} (-K) \sin \theta \, d\theta = \frac{4K}{\pi\gamma_0} \sqrt{\frac{\delta}{\gamma_0} - \left(\frac{\delta}{\gamma_0}\right)^2} \end{aligned} \tag{73}$$

The third integral (69) for the moment about the king-pin due to tyre lateral deformations has to be determined graphically, as the tyre characteristics are given in the form of curves. The integral reads:

$$\begin{aligned} \int_0^{2\pi} f^*(\alpha_0 \sin \tau) \sin \tau \, d\tau &= 4 \int_0^{\frac{1}{2}\pi} f^*(\alpha_0 \sin \tau) \sin \tau \, d\tau = \\ &= -4 \int_{\tau=0}^{\tau=\frac{1}{2}\pi} f^*(\alpha_0 \sin \tau) \, d\cos \tau. \end{aligned} \tag{74}$$

The function $f^*(\alpha) = f^*(\alpha_0 \sin \tau)$ may be transformed into a function $\underline{f}^*(\alpha_0 \cos \tau)$ as shown in figure 12. For each

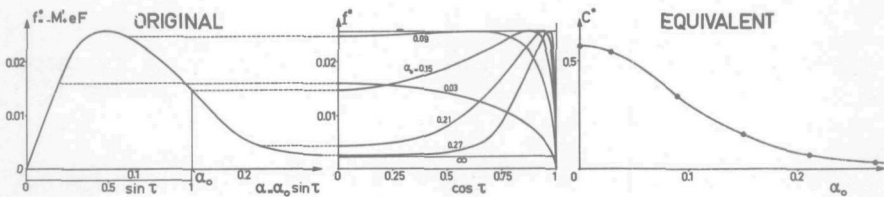


Fig. 12. Transformation of original tyre cornering characteristic to equivalent characteristic.

amplitude α_0 the variation of \underline{f}^* with $\cos \tau$ can be constructed. The integral

$$\begin{aligned}
 - \int_{\tau=0}^{\tau=\frac{1}{2}\pi} f^* (\alpha_0 \sin \tau) d \cos \tau &= - \int_{\tau=0}^{\tau=\frac{1}{2}\pi} \underline{f}^* (\alpha_0 \cos \tau) d \cos \tau = \\
 &= \int_0^1 \underline{f}^* (\alpha_0 \cos \tau) d \cos \tau \quad (75)
 \end{aligned}$$

can easily be determined for a number of values of α_0 for instance by means of a planimeter. After multiplication by the factor $4/\pi\alpha_0$ the equivalent stiffness C^* is obtained. The C^* values may be collected as a function of the amplitude α_0 in a graph, representing the equivalent tyre characteristic. In programs for digital computations the procedure is automated so that, starting from the original characteristic, the equivalent characteristic is obtained, with which further calculations are carried out.

The characteristic equation of the system (63) becomes:

$$\sigma p^3 + (V + \sigma k^*) p^2 + \left\{ k^* V + c\sigma - (1-e) C^* \right\} p + V(c + C^*) = 0 \quad (76)$$

This equation shows a pair of purely imaginary roots when the second Hurwitz determinant vanishes. This criterium leads to the following relation between the parameters k^* , c and C^* for given values of σ and V :

$$(V + \sigma k^*) \left\{ k^* V + c\sigma - (1-e) C^* \right\} = \sigma V (c + C^*) \quad (77)$$

The frequency of the periodic motion, which occurs when the relation (77) holds, can easily be found when in (76) p is replaced by $i\omega = i\omega_s V$:

$$\omega^2 = \omega_s^2 V^2 = \frac{c + C^*}{1 + \sigma k^*/V} \quad (78)$$

Moreover the ratio of the amplitudes γ_0 and α_0 as a function of the frequency is needed. From the second equation (63) we obtain for sinusoidal motions:

$$\frac{\alpha}{\gamma} = \frac{(1-e) i\omega - V}{\sigma i\omega + V} \quad (79)$$

and hence

$$\frac{\alpha_0}{\gamma_0} = \sqrt{\frac{(1-e)^2 \omega^2 + V^2}{\sigma^2 \omega^2 + V^2}} \quad (80)$$

2.3A. The limit-amplitude as a function of viscous and dry damping

First of all the system with only one non-linear element, the tyre cornering characteristic, will be discussed. Clearance is not taken into account and the damping is supposed to be linear. Consequently, the coefficient k^* is a constant now and the stiffness c equals zero. A graph can be made which gives C^* as a function of k^* according to formula (77) which gives the condition for periodic motions. For each value of k^* the value of C^* belonging to the limit-cycle can thus be found. The equivalent characteristic shown in figure 12 may then be employed in order to find the amplitude α_0 of the slip angle which produces the value of C^* needed. After the calculation of ω with (78) the corresponding value of γ_0 follows from equation (80). When a number of k^* values are taken, a graph of the amplitude of the limit-cycle γ_0 may be plotted against the applied damping k^* .

It appears to be convenient to combine the graphs in a manner as shown in figure 13. The upper right graph shows

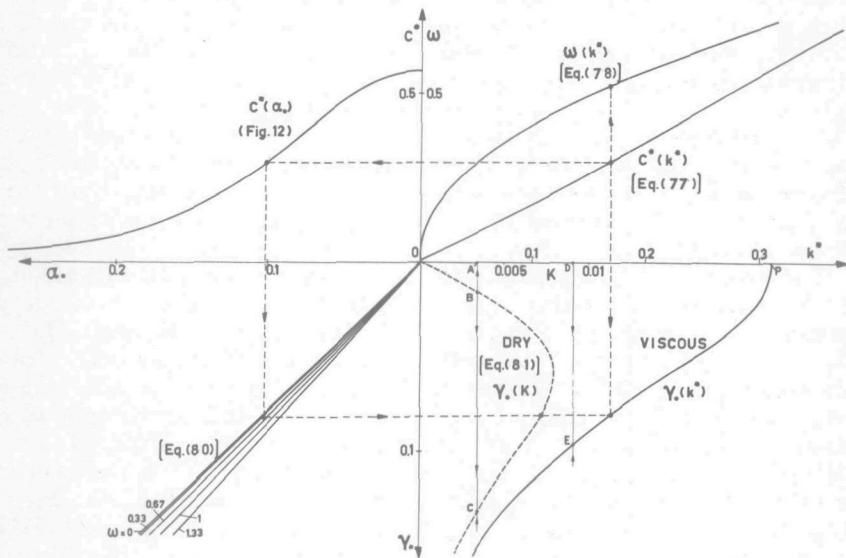


Fig. 13. Determination of the limit-amplitudes γ_0 ($V=6,66, \sigma=3, e=0, k=0, \delta=0$).

C^* and ω as a function of k^* according to the criterium where the Hurwitzian vanishes. The upper left quadrant gives the equivalent tyre characteristic and the lower left diagram

shows the frequency response of α_0 with respect to γ_0 . In the fourth quadrant the variation of the limit-amplitude γ_0 with k^* is shown as the final result. The graphs of figure 13 hold for the combination of parameter values: $V = 6.66$, $\sigma = 3$ and $e = 0$.

The step from viscous to Coulomb damping is rather a simple extension of this procedure. Equation (72) with $\delta = 0$ gives the relation between k and K . It reads:

$$k = \frac{4K}{\pi\omega\gamma_0} \text{ or } K = \frac{\pi}{4} k\omega\gamma_0. \quad (81)$$

The dry-frictional couple K giving the same amount of damping as the viscous damping with constant $k=k^*-\kappa/V$ follows from this last formula. In the fourth quadrant of figure 13 the course of γ_0 as a function of K is shown as a dotted line for the case $\kappa = 0$. The influence of κ is treated in Sec. 2. 3D.

It is noted from the fourth quadrant of figure 13 that for a given value of K , below a certain maximum, two limit-amplitudes (points B and C) occur, while with viscous damping only one limit-cycle can arise (point E). The linear theory, which holds for small amplitudes in the case of viscous damping, reveals that the system is unstable for values of k^* less than a certain critical value (point P). Above that value the system is stable. With the non-linear system of which the centre position is unstable, the deflection of the motion increases until the limit-amplitude (point E in figure 13) is reached. This final situation is expected to be stable.

The case of dry friction shows a more complex situation. It is difficult to establish the stability of the stationary motion and the two limit-cycles (points A, B and C). A rigorous treatment of the motions with small amplitudes follows in Sec. 3. The stability of the limit-cycles is examined in Sec. 2. 3C. As a logical consequence of the situation with viscous damping we may anticipate that the largest amplitude is stable again. The centre position (A) is expected to be stable too, because of the fact that the equivalent coefficient of damping tends to infinity when the amplitude becomes zero. Consequently we may expect that the small limit-cycle (B) situated in between the two stable situations is unstable.

It appears thus that the motion dies out, in the case of dry friction, when the amplitude is smaller than that of the unstable limit-cycle. On the other hand the amplitude increases with time when the amplitude of the unstable limit-

from Eqs. (77) and (78). For given κ in each point of the diagram the values of ω , c and k (72) are known. The curves for constant γ_0/δ can be found now by making use of the expression:

$$c = \frac{k\omega}{\sqrt{\gamma_0/\delta - 1}}, \quad (82)$$

which can be derived by eliminating K from the equations (72) and (73). In the case considered κ is taken equal to zero, so that $k = k^*$.

The second quadrant remains unchanged. The third quadrant shows the amplitude relations for several values of γ_0/δ . For given γ_0/δ the amplitude relation can be obtained from formula (80), after that for ω the value given along the curve for γ_0/δ considered in the first quadrant is substituted.

In the fourth quadrant the course of γ_0 for a number of values of the clearance δ is shown. It may be found in the following way (see Fig. 14). Choose a value of γ_0 and determine the ratio γ_0/δ for the δ value considered. From the point on the γ_0/δ line in the third quadrant follow a vertical line until the curve in the second quadrant is reached. Follow now a horizontal line until the curve in the first quadrant for the γ_0/δ value considered is attained. In this last point the values of c and ω can be determined. With the aid of formula (72) or (73) the value of K may then be calculated after which K can be plotted in the fourth quadrant against γ_0 .

It is noted from the fourth quadrant that in a certain range of K and for not too much clearance three limit-cycles may occur. In the figure such a case is indicated (points A, B, C and D). D indicates the presumed stable large limit-amplitude and C the consequently unstable smaller limit-amplitude. B represents the amplitude of the small stable limit-cycle, which appears to arise in the case of clearance. A is the unstable centre position of the system. Other situations with only one possible limit-cycle, either large or small, may arise when the friction is decreased or increased respectively (points E and F). For given K , the introduction of a sufficient amount of clearance causes the large shimmy amplitude to occur without the necessity of an external disturbance. Clearance obviously has a destabilizing effect, as has often been observed in practice.

Systems with and without clearance are also investigated with the aid of an analogue computer. The results are given in V.1.3. Figure V.5 shows the amplitude curves which are in very good agreement with the curves found here

through approximate analytical means.

Figure 15 gives an overall picture of the behaviour of the cases considered successively for a certain value of forward speed. Also the projection of the limit-cycles on the phase-plane ($\gamma, \dot{\gamma}$) are shown. Their shape is known from the analogue computer studies and from the graphical solutions [49].

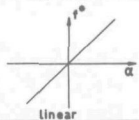
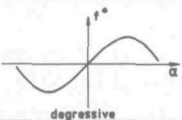
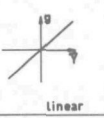
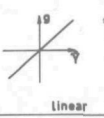
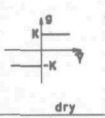
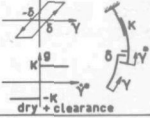
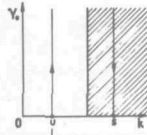
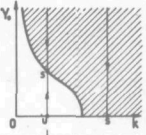
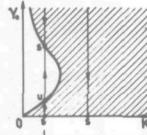
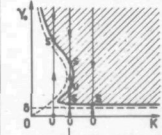
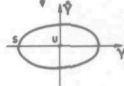
tyre characteristic	 linear	 degressive		
king-pin damping	 linear	 linear	 dry	 dry + clearance
limit-amplitudes	 0 u s k	 0 u s k	 0 s s s K	 0 u s s K
limit-cycles				
stability	S(table) or U(nstable)	S or U-S	S or S-U-S	U-S or U-S-U-S or U-S

Fig. 15. Overall picture of the behaviour of systems considered. Besides linear behaviour, new aspects due to introduction of a number of non-linear elements are shown.

Referring to this figure the following conclusions may be drawn:

1. The degressive shape of the tyre characteristic causes the amplitude to have a finite limit.
2. The introduction of dry friction results in the necessity of an external disturbance in order to initiate shimmy.
3. For both viscous and dry-frictional damping an upper limit of the damping factor exists above which no shimmy can occur.
4. Clearance has a destabilizing effect. With sufficient clearance it is possible that, in spite of the dry friction, large amplitudes may be attained without an external disturbance.

2.3C. The stability of the limit-cycles

The method described in Sec. 2.2 will be used in order to determine the stability of the limit-cycles, the amplitudes of which being found in the preceding sections.

The characteristic equation of the third-order system has the following general form:

$$a_0(\gamma_0, \omega) p^3 + a_1(\gamma_0, \omega) p^2 + a_2(\gamma_0, \omega) p + a_3(\gamma_0, \omega) = 0 \quad (83)$$

which has a pair of purely imaginary roots in case we are on the limit-cycle. In a situation slightly deviated from the limit-cycle, the polynomial with the new characteristic root $p_1 = p - \delta r$ reads after neglectation of products of increments according to (46):

$$(a_{0,0} + \delta a_0) p_1^3 + (a_{1,0} + \delta a_1 + 3a_{0,0} \delta r) p_1^2 + (a_{2,0} + \delta a_2 + 2a_{1,0} \delta r) p_1 + (a_{3,0} + \delta a_3 + a_{2,0} \delta r) = 0. \quad (84)$$

The vanishing second determinant of Hurwitz of this characteristic equation reads after neglectation of products of increments:

$$H'_2 = H_{2,0} + \delta H_2 + b \delta r = 0, \quad (85)$$

where

$$H_{2,0} = a_{1,0} a_{2,0} - a_{0,0} a_{3,0} = 0, \quad (86)$$

$$\delta H_2 = a_{2,0} \delta a_1 + a_{1,0} \delta a_2 - a_{0,0} \delta a_3 - a_{3,0} \delta a_0, \quad (87)$$

$$b = 2(a_{1,0}^2 + a_{0,0} a_{2,0}). \quad (88)$$

As expected the constant b is a positive quantity. For simplicity we will henceforth omit the additional subscript 0 denoting that the value on the limit-cycle is meant. According to (85) and (86) we obtain:

$$\frac{dr}{dA} = \frac{dr}{d\gamma_0} = - \frac{1}{b} \frac{dH_2}{d\gamma_0}. \quad (89)$$

For the stability values S (52) we obtain with (87) and (88):

$$S = 2\pi \frac{A_0}{\omega_0} \frac{dr}{dA} = - \frac{\pi \gamma_0 / \omega_0}{a_1^2 + a_0 a_2} \left(a_2 \frac{da_1}{d\gamma_0} + a_1 \frac{da_2}{d\gamma_0} - a_0 \frac{da_3}{d\gamma_0} - a_3 \frac{da_0}{d\gamma_0} \right) \quad (90)$$

in which according to (43) partial derivatives may suffice instead of total derivatives.

The coefficients of the characteristic equation become according to (76):

$$\left. \begin{aligned} a_0 &= \sigma, \\ a_1 &= V + \sigma k^*, \\ a_2 &= k^*V + c\sigma - (1-e)C^*, \\ a_3 &= V(c + C^*), \end{aligned} \right\} \quad (91)$$

where k^* , c and C^* are functions of γ_0 and ω . The partial derivatives of the coefficients a_k with respect to γ_0 read:

$$\left. \begin{aligned} \frac{\partial a_0}{\partial \gamma_0} &= 0, \\ \frac{\partial a_1}{\partial \gamma_0} &= \sigma \frac{\partial k^*}{\partial \gamma_0}, \\ \frac{\partial a_2}{\partial \gamma_0} &= V \frac{\partial k^*}{\partial \gamma_0} + \sigma \frac{\partial c}{\partial \gamma_0} - (1-e) \frac{\partial C^*}{\partial \gamma_0}, \\ \frac{\partial a_3}{\partial \gamma_0} &= V \left(\frac{\partial c}{\partial \gamma_0} + \frac{\partial C^*}{\partial \gamma_0} \right). \end{aligned} \right\} \quad (92)$$

With the aid of the expressions (72), (73) and (80) we obtain for the partial derivatives of k^* , c and C^* .

$$\left. \begin{aligned} \frac{\partial k^*}{\partial \gamma_0} &= -\frac{4K}{\pi\omega\gamma_0^2} \left(1 - 2\frac{\delta}{\gamma_0} \right), \\ \frac{\partial c}{\partial \gamma_0} &= -\frac{2K}{\pi\gamma_0^2} = \frac{3-4\delta/\gamma_0}{\sqrt{\gamma_0/\delta-1}}, \\ \frac{\partial C^*}{\partial \gamma_0} &= \frac{dC^*}{d\alpha_0} \frac{\partial \alpha_0}{\partial \gamma_0} = \frac{dC^*}{d\alpha_0} \frac{\alpha_0}{\gamma_0}. \end{aligned} \right\} \quad (93)$$

From figure 12 which shows the equivalent tyre characteristic, $dC^*/d\alpha_0$ can be determined.

For the system considered in figure 13 and 14, the stability value S has been calculated for some combinations of dry friction (K) and clearance (δ). In figure 16 the results

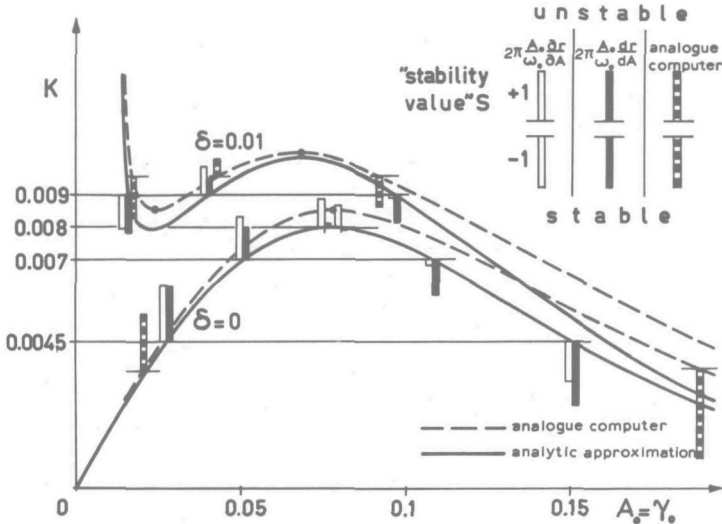


Fig. 16. Comparison of stability values obtained.

of two analytical methods, one using the partial derivative and the other the total derivative (for details see [59]), are shown together with results obtained from analogue computations using the method as indicated in figure 10. According to the total derivative method in which the influence of the frequency rate of change is taken into account, the signs of the stability values obtained are everywhere as expected. Also quantitatively the results correspond very well with the analogue computer results. The method normally used, in which the partial derivative is applied, appears to give a qualitatively correct answer in most cases. It may be noted, however, that at the top of the curve for $\delta=0$, where S should be zero, this simpler method predicts an appreciable stability value. In this respect, the more complicated total derivative method is preferable.

2.3D. The limit-amplitudes as a function of forward speed; the self-excitation area

In order to study the influence of the speed V , it is necessary to repeat the calculations dealt with in Sec. 2.3A for a number of values of V . The area in the (V, γ_0) plane in-

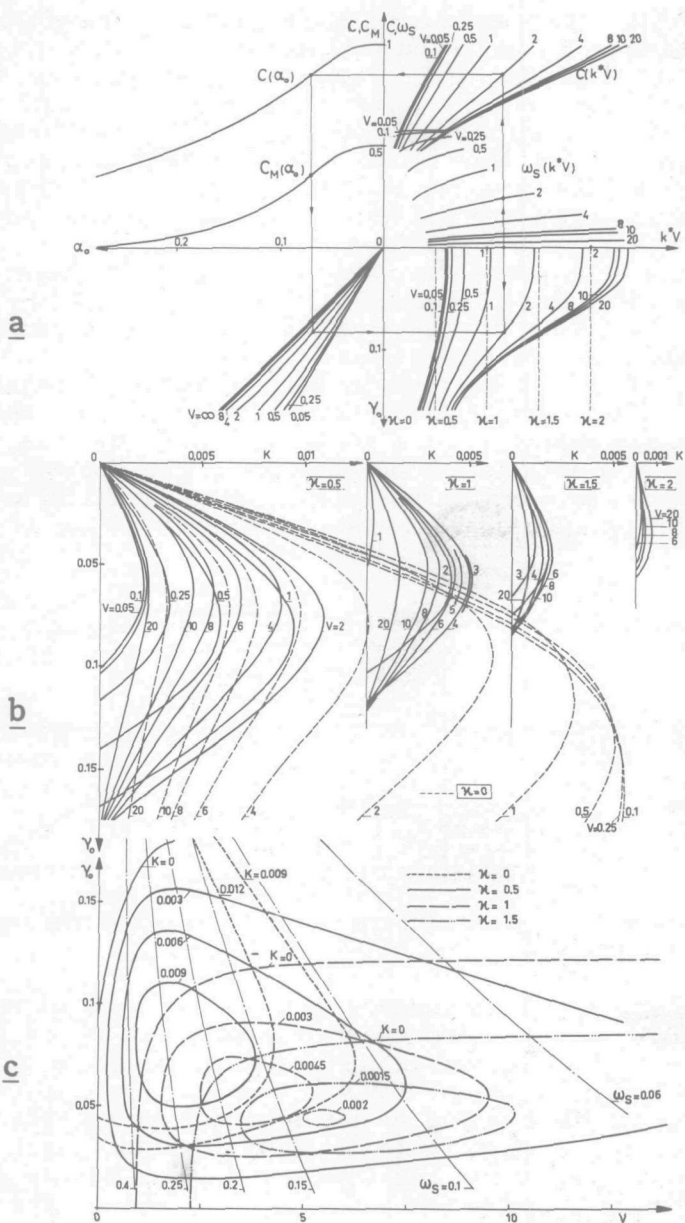


Fig. 17. Three stages for the determination of the limit-amplitudes as a function of speed V ($\sigma=3, e=0.1$).

side which self-excitation occurs, will be called self-excitation area. From now on the clearance will be disregarded, which implies that $c=0$. Parameters will be: the damping couple K due to dry friction and the damping coefficient κ due to longitudinal tread deformations. The calculations are carried out for two values of caster: $e = 0.1$ and $e = 0$. Concerning the tyre, we take again for the non-dimensional relaxation length $\sigma=3$ and for the non-dimensional pneumatic trail at zero slip angle $e' = 0.5$.

Figure 17a shows the diagram for $e=0.1$, which is analogous to figure 13 but which is extended now for several values of V . The first quadrant contains the curves for the equivalent cornering stiffness C where the Hurwitzian becomes zero and the curves for the reduced frequency ω_s belonging to them. The parameter $k*V$ has been chosen as abscissa, which appears to be advantageous when the influence of κ is going to be examined. The second quadrant shows the equivalent tyre characteristics produced in stages from the original characteristics as shown in figure 18 (cf.

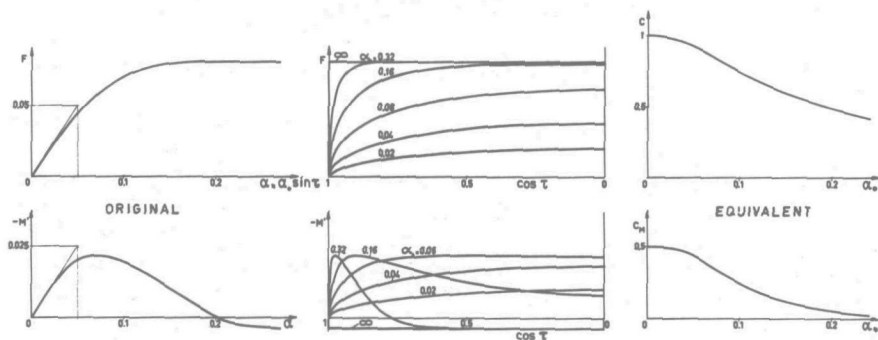


Fig. 18. Determination of equivalent tyre cornering characteristics from original characteristics.

Eqs. (71)). Via the amplitude relation for several values of V , shown in the third quadrant, the limit-amplitude γ_0 is found which is plotted in the fourth quadrant as a function of the applied value of $k*V$.

In order to investigate the influence of κ , according to Eq. (72) the γ_0 -axis may be shifted to the right over a distance $\Delta k*V = \kappa$. The figure shows the positions of the axis for the cases $\kappa = 0, 0.5, 1.0, 1.5$ and 2 . The rest of the equivalent coefficient of viscous damping at the right-hand side of the axes, $kV = k*V - \kappa$, should be realized through a dry-frictional couple K the value of which may be calculated with the aid of the second formula (81) and plot-

ted in graphs shown in figure 17b for several values of κ . From the curves of figure 17b the course of the limit-amplitudes in the (V, γ_0) plane may be derived for given values of K and κ . Figure 17c shows the areas inside which self-excitation occurs and outside which the amplitude decreases with time until a stable situation of equilibrium has been reached.

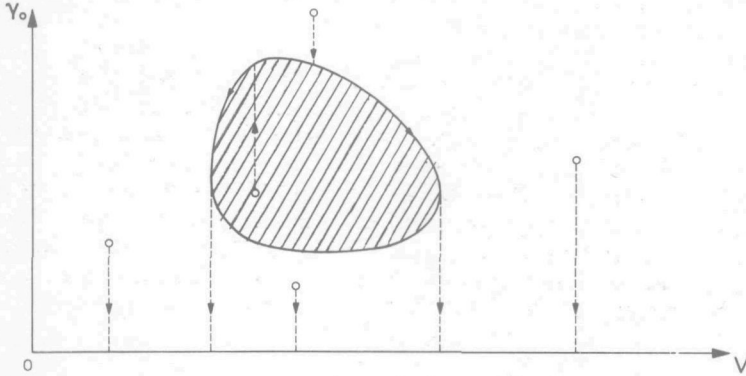


Fig. 19. An area of self-excitation and the influence of choosing the initial values of γ .

Figure 19 shows such a self-excitation area. The upper boundary represents the course of the stable shimmy amplitude, while the lower boundary indicates the unstable limit-amplitude as a function of forward speed V . The concept of self-excitation area is of great value. It gives almost immediately a nearly complete insight in the behaviour of the system. The location of the area indicates the speed range where shimmy may occur; the size gives an idea of the degree of self-excitation; the height of the lower boundary determines the amount of disturbance needed in order to start shimmy; the upper limit indicates the amplitude of the shimmy motion. This upper boundary is followed when the speed is varied. When one of the two points where the tangent becomes vertical is passed, the motion dies out.

The area becomes smaller for greater values of K and κ . For small values of κ the curves are open at the left-hand side, which means that no lower limit of the speed range exists. At low values of V , where the wavelength of the motion becomes too small relatively to the contact length (i. e. ω_s too large, see Fig. 17a) the simple tyre theory is no longer realistic.

With the aid of an analogue computer both the simple and the more elaborate tyre model have been simulated (see Sec.

V.1.4). The computer study with the simple model gave a very good correspondence with the results found here. The system provided with the more exact tyre model appeared to be more stable especially at low velocities, which resulted in a reduction in self-excitation area at the left-hand side of the figure (see Fig. V.10).

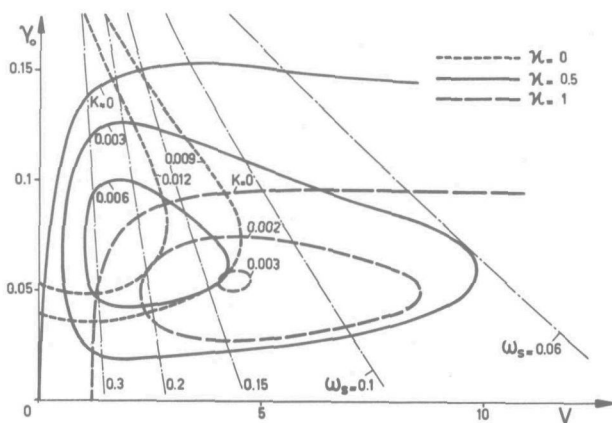


Fig. 20. Self-excitation areas ($\sigma=3$, $e=0$).

Figure 20 shows the self-excitation areas for the case that $e=0$. Compared with figure 17 this little decrease in caster causes a considerable reduction in self-excitation area for the same values of damping, which illustrates the destabilizing effect of an increase in caster as has been established already in the linear treatment.

A three-dimensional graph in the (V, e, γ_0) space would show for finite K and sufficient κ a pear-shaped body in which self-excitation occurs, floating in between the planes $\gamma_0=0$, $V=0$, $e=-e'$ and $e=1+\sigma$ (see also Fig. 2).

The influence of the moment of inertia I of the swivelling part about the king-pin axis follows clearly from the fact that in the case of dry friction I appears only in the non-dimensional expression for the speed of travel $\underline{V} = V \sqrt{I/Ca^3}$ (underlinings introduced again). The conclusion is that with dry friction the same phenomenon will take place at velocities proportional to the reciprocal value of the square root of the moment of inertia I .

The influence of the introduction of a rotational spring about the king-pin with stiffness c (cf. Eq. III. (55)) can easily be found by introducing an equivalent moment of inertia $I_{eq} = I - c/(\omega_s^2 V^2)$. In dimensional form $I_{eq} V^2 = IV^2 - c/\omega_s^2$ should be

constant for the same phenomenon to take place. This leads to the conclusion that by means of an increase in c the speed range of shimmy is raised; a similar effect thus as a decrease in I .

The influence of changing tyre parameters is basically the same in the linear case which has been discussed in Sec. 1.2.

2.4. The fifth-order system

This higher order system will also be treated with the aid of equivalent linearisation. Again the characteristic equation is needed containing the equivalent linear parameters similar to those occurring in the third-order system. The equivalent stiffnesses C and C_M will be introduced again.

The non-linear system is described by the non-dimensional set of equivalent linear equations, analogous to the equations (22) of the linear system:

$$\left. \begin{aligned} \mu_\eta \ddot{\eta} + c_\eta \dot{\eta} - \beta_\eta V \dot{\gamma} &= C \alpha, \\ \ddot{\gamma} + k^* \dot{\gamma} + \beta_\eta V \dot{\eta} &= -(C e + C_M) \alpha, \\ \sigma \dot{\alpha} + V \alpha &= -\dot{\eta} - (1-e) \dot{\gamma} + V \gamma. \end{aligned} \right\} \quad (94)$$

The coefficients of the characteristic equation

$$\sum_{i=0}^5 a_i p^{5-i} = 0, \quad (95)$$

which is analogous to equation (23), read:

$$\left. \begin{aligned} a_0 &= \mu_\eta \sigma, \\ a_1 &= \mu_\eta (V + k^* \sigma), \\ a_2 &= (c_\eta \sigma + C) + \mu_\eta V k^* - \mu_\eta (C e + C_M) (1-e) + \beta_\eta^2 V^2 \sigma, \\ a_3 &= c_\eta V + k^* (c_\eta \sigma + C) + \beta_\eta^2 V^3 - \beta_\eta V (C + C_M) + \mu_\eta V (C e + C_M), \\ a_4 &= c_\eta V k^* + \beta_\eta V^2 C - c_\eta (C e + C_M) (1-e), \\ a_5 &= c_\eta V (C e + C_M). \end{aligned} \right\} \quad (96)$$

The non-dimensional equivalent stiffnesses C and C_M are functions of the amplitude α_0 as shown in figure 18. The non-dimensional equivalent coefficient of damping $k^* = k + \kappa/V$ depends on the amplitude γ_0 and the frequency ω according to equation (72) with $\delta=0$, as no clearance will be considered in this section. The remaining parameters are given quantities.

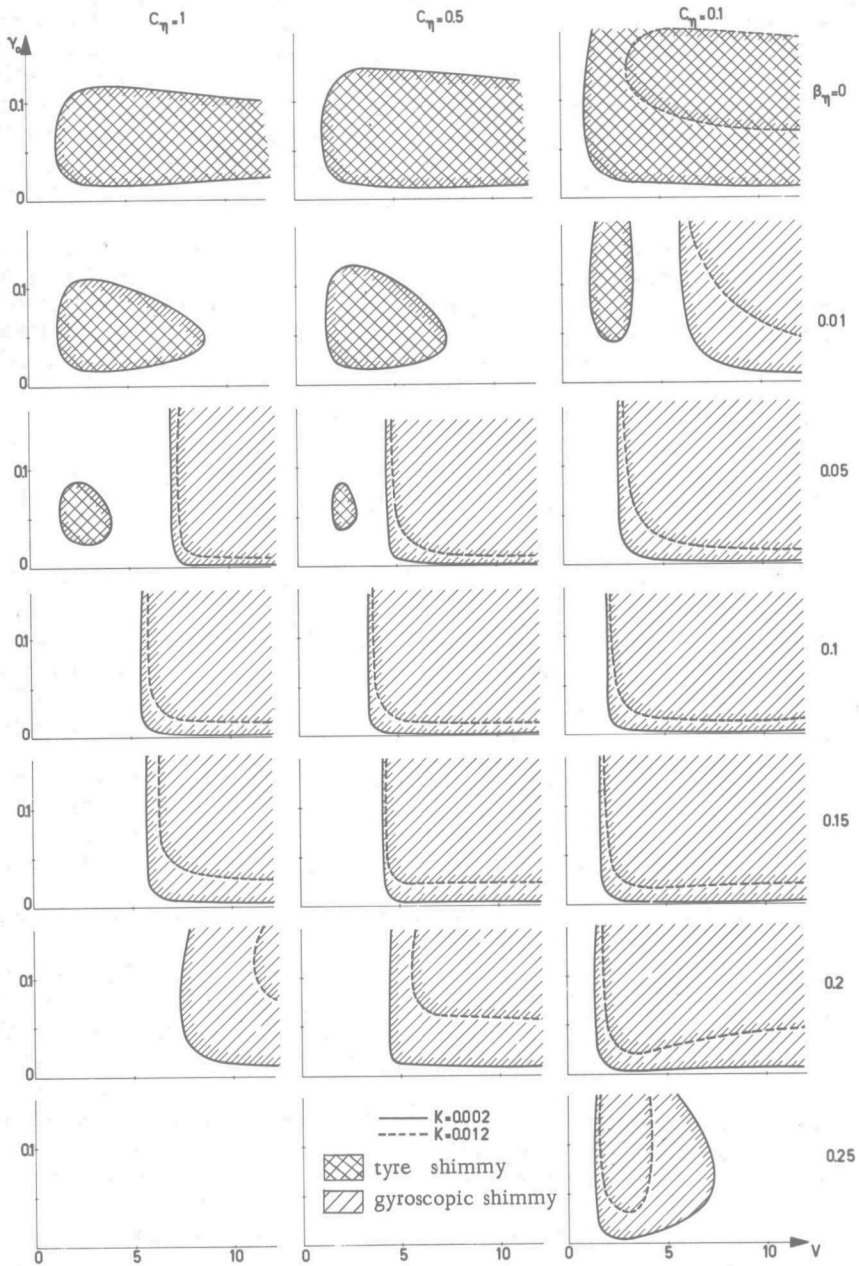


Fig. 21. Self-excitation areas as a function of lateral (torsional) stiffness c_η and gyroscopic coupling factor β_η . ($\sigma=3, e=0.1, \mu_\eta=0.5, \kappa=1$).

The method of Newton-Raphson has been used in order to find the curves, analogous to those shown in the first quadrant of figure 17a, which give k^* as a function of C for vanishing Hurwitzian H_4 . When for these combinations of k^* and C all the coefficients of (95) and the lower determinants are positive, only one pair of imaginary roots exists and for the rest roots with a negative real part. The calculations are carried out completely with the aid of a digital computer.

Since for all cases investigated the values of H_2 and H_3 and of the coefficients remain positive in the relevant part of the first quadrant, no double frequency motions are expected. With the electronical analogue computer indeed only mono-frequency oscillations were observed with the autonomous system.

Figure 21 shows the area of self-excitation for a number of combinations of the gyroscopic coupling factor β_η and the stiffness c_η . Two values of the dry-frictional couple K are considered. The rest of the parameters have the following values:

$$\sigma = 3, e = 0.1, \mu_\eta = 0.5, \kappa = 1. \quad (97)$$

For $\beta_\eta = 0$ (purely lateral stiffness, no rotation about longitudinal axis) the area becomes larger for decreasing lateral stiffness c_η . At a stiffness $c_\eta = 1$ the areas, however, are not appreciably larger than with the third-order system where $c_\eta \rightarrow \infty$.

A finite β_η may cause the appearance of a new phenomenon. A new area of self-excitation arises at the right-hand side of the shrunk original area. In the new area shimmy occurs due to gyroscopic coupling. There is no or a very high upper limit-amplitude because of the fact that in the mathematical model the rotational motion about a longitudinal axis is not restricted by stops.

At increasing values of the coupling factor β_η the area of gyroscopic shimmy extends to lower speeds V while the area of tyre shimmy reduces and finally vanishes. The lower the stiffness c_η the more effect the gyroscopic coupling has. Very high values of β_η (not shown in Fig. 21 for all cases) turned out to cause the gyroscopic shimmy to vanish too. The manner in which the area vanishes is completely different for stiff and soft systems.

2.5. The seventh-order system

For the examination of the influence of connecting a steering-

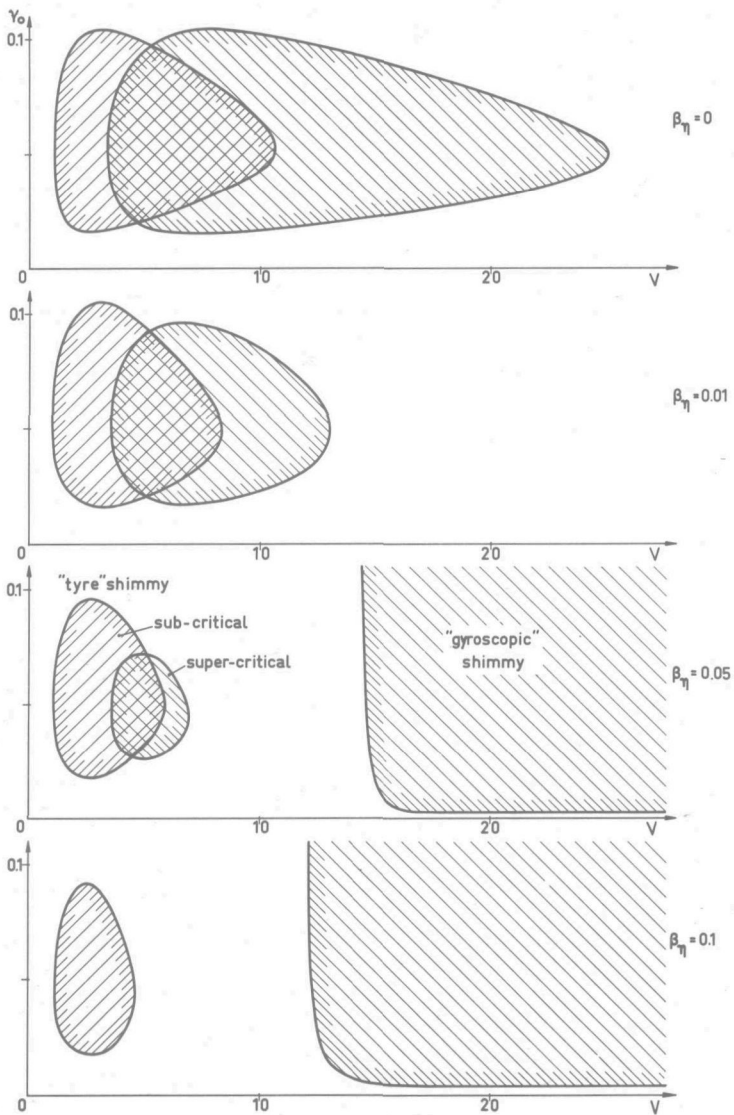


Fig. 22. Self-excitation areas for the system with steering-wheel ($\sigma=3, e=0.1, \mu_\eta=0.5, c_\eta=4, \beta_{st}=0.7, c=0.4, K=0.002, \kappa=1$).

wheel to the system, the same procedure is followed as in the linear analysis (cf. Sec. 1.4). The same linear extensions but now of the system treated in Sec. 2.4 are applied.

For a great number of λ values the areas of self-excitation are calculated for the equivalent fifth-order system and in each point the instantaneous frequency is compared to the assumed one. Through interpolation the limit-amplitudes for the system with steering-wheel are found.

Figure 22 shows areas of self-excitation for several values of β_η . The parameter values of the considered system are:

$$\left. \begin{aligned} K &= 0.002, \quad \kappa = 1, \quad \sigma = 3, \quad e = 0.1, \\ \mu_\eta &= 0.5, \quad \beta_{st} = 0.7, \quad c_\eta = 4, \quad c = 0.4. \end{aligned} \right\} \quad (98)$$

Comparison with figure 8 shows a qualitative change in behaviour with respect to the linear system. While with the linear system the supercritical tyre shimmy occurs within the subcritical speed range, here specific super and subcritical ranges occur which may overlap each other partly. The areas of high frequency supercritical tyre shimmy always occur at higher speeds than the areas of low frequency subcritical tyre shimmy.

An increase in gyroscopic coupling (β_η) results in a reduction in the tyre shimmy areas and may cause the appearance of the gyroscopic self-excitation area. In the latter area supercritical frequencies occur with respect to the natural frequencies of both the steering-wheel system (ω_{sto}) and the suspension system ($\omega_{\eta 0}$).

How the exact course of the motion will be, especially in the overlapping areas, has not been studied analytically owing to the great complexity involved. The study with the analogue computer reveals, that indeed such sort of overlapping areas exist. No combined stationary oscillations take place. Either the supercritical or the subcritical upper boundary is followed depending on initial conditions. When decreasing the velocity, the supercritical motion jumps over to the subcritical mode in the overlapping area, whereas the subcritical motion dies out when its area is exceeded through a variation in V (cf. Fig. V.16).

The low frequency subcritical shimmy may easily be suppressed by the driver. The higher frequency supercritical shimmy cannot be suppressed in most cases, even by locking the steering-wheel. This because of the antiphase of the motion of the road-wheel and the steering-wheel in the supercritical case.

3. Application of the theory for piece-wise linear system

As has been stated before, due to the occurrence of dry friction in the real system, the linear treatment, described in Sec.1, cannot give a realistic view of the behaviour of the system near the centre position. Also with the method of the harmonic balance, we were not able to judge the stability of the centre position, i.e. of the stationary motion. It is because of these that we proceed to treat the system as a piece-wise linear system, which fortunately is possible here, and which enables us to give a rigorous description of the motion near the position of rest. The method can also be used for approximately finding the small unstable limit-cycle of which the amplitude and the stability have already been determined in Sec.2.3 with the aid of the method of equivalent linearization. As will be seen, a good agreement with the latter findings has been obtained.

For motions with only small deflections with respect to the undisturbed rectilinear motion, the tyre characteristic may be considered as a linear function of the slip angle. In that case the dry friction is the only remaining non-linear element and the motion can be considered as linear in successive time intervals. Owing to the complexity of the treatment of more elaborate systems we will restrict ourselves to the investigation of the third-order system with damping due to dry friction only; clearance will not be considered.

With the use of the relations (61), (62) and III.(85b, 97b, 98b), for $\kappa = e = 0$ the equations (60) can be reduced to:

$$\left. \begin{aligned} \ddot{\gamma} + K \operatorname{sgn} \dot{\gamma} &= -e' \alpha, \\ \sigma \dot{\alpha} + V \alpha &= -\dot{\gamma} + V \gamma, \end{aligned} \right\} \quad (99)$$

For this special case new variables and parameters are introduced:

$$\underline{\gamma} = \frac{\gamma e'}{K}, \quad \underline{\alpha} = \frac{\alpha e'}{K}, \quad \underline{\zeta} = \frac{V^2}{e'}. \quad (100)$$

The underlinings will be omitted henceforth. The equations (99) read now, when, in addition, the independent variable is replaced by the travelled distance $s = Vt$:

$$\zeta \frac{d^2 \gamma}{ds^2} + \operatorname{sgn} \frac{d\gamma}{ds} = -\alpha, \quad (101)$$

$$\sigma \frac{d\alpha}{ds} + \alpha = -\frac{d\gamma}{ds} + \gamma. \quad (102)$$

For the description of the motion in the phase space $(\gamma, \frac{d\gamma}{ds}, \alpha)$ the introduction of the new variable

$$v = \frac{d\gamma}{ds} \quad (103)$$

is convenient. The equations (101,102) reduce to two first order equations:

$$\zeta v \frac{dv}{d\gamma} + \operatorname{sgn} v = -\alpha, \quad \left. \vphantom{\frac{dv}{d\gamma}} \right\} \quad (104)$$

$$\sigma v \frac{d\alpha}{d\gamma} + \alpha = -v + \gamma. \quad \left. \vphantom{\frac{d\alpha}{d\gamma}} \right\} \quad (105)$$

3.1. Stability of the stationary motion

In the investigation of the stability of the position of rest the motion of the system should be examined after a small arbitrary disturbance of the determining components γ , v and α . When the deviation from the original situation remains within certain limits, the stationary motion will be stable.

The system is in equilibrium (i.e. performs a stationary motion) when all derivatives with respect to s (except the forward velocity V) equal zero. When taking into account the property of dry friction, viz. that in state of rest the frictional couple can be smaller than its maximum value, we obtain from (101) and (102):

$$\left. \begin{aligned} |\alpha| &\leq 1, \\ \alpha &= \gamma. \end{aligned} \right\} \quad (106)$$

Equilibrium occurs on the line piece $(\gamma=\alpha, v=0, |\alpha|\leq 1)$ indicated in figure 23. The stability of the extreme positions

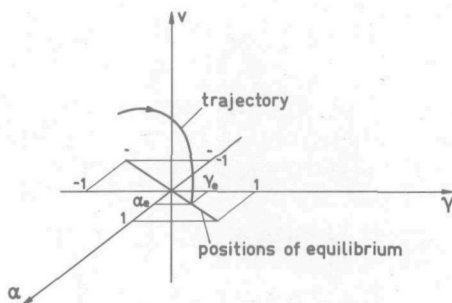


Fig. 23. The phase-space with positions of equilibrium.

of equilibrium $\gamma_e = \pm 1$ will not be examined owing to the greater complexity involved.

We consider the position of equilibrium ($\gamma = \gamma_e$, $\alpha = \alpha_e = \gamma_e$, $v = v_e = 0$), where $|\gamma_e| < 1$. Small motions in the neighbourhood of this position of equilibrium will be indicated by $\bar{\gamma}$, \bar{v} and $\bar{\alpha}$. The following relations hold:

$$\left. \begin{aligned} \gamma &= \gamma_e + \bar{\gamma}, \\ v &= v_e + \bar{v} = \bar{v}, \\ \alpha &= \alpha_e + \bar{\alpha} = \gamma_e + \bar{\alpha}. \end{aligned} \right\} \quad (107)$$

These expressions inserted in equations (104) and (105) yield:

$$\zeta \bar{v} \frac{d\bar{v}}{d\bar{\gamma}} + \text{sgn } \bar{v} = -(\alpha_e + \bar{\alpha}), \quad (108)$$

$$\sigma \bar{v} \frac{d\bar{\alpha}}{d\bar{\gamma}} + \bar{\alpha} = -\bar{v} + \bar{\gamma}. \quad (109)$$

The values of the variables after a disturbance at $s = 0$ are given by the quantities:

$$\left. \begin{aligned} \bar{\gamma} &= \bar{\gamma}_1, \\ \bar{v} &= \bar{v}_1, \\ \bar{\alpha} &= \bar{\alpha}_1, \end{aligned} \right\} \quad (110)$$

These quantities are assumed to be much smaller than the value $\text{sgn } \bar{v} + \alpha_e$. In that case we can neglect $\bar{\alpha}$ in equation (108). This equation becomes then:

$$\zeta \bar{v} \frac{d\bar{v}}{d\bar{\gamma}} + \text{sgn } \bar{v} + \alpha_e = 0. \quad (111)$$

In the half space where \bar{v} keeps its initial sign, we can integrate this equation:

$$\zeta \bar{v}^2 = -2(\text{sgn } \bar{v} + \alpha_e) \bar{\gamma} + A, \quad (112)$$

where according to (110)

$$A = \zeta \bar{v}_1^2 + 2(\text{sgn } \bar{v}_1 + \alpha_e) \bar{\gamma}_1. \quad (113)$$

This inserted in (112) yields:

$$\zeta (\bar{v}^2 - \bar{v}_1^2) = -2(\text{sgn } \bar{v} + \alpha_e)(\bar{\gamma} - \bar{\gamma}_1). \quad (114)$$

This solution represents two collections of half parabolas with the γ -axis as axis of symmetry. Figure 24 shows the

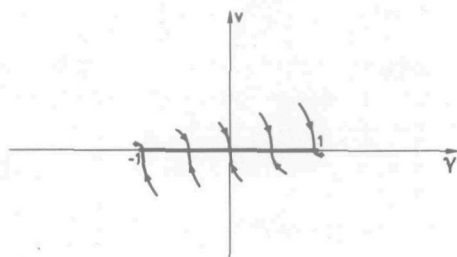


Fig. 24. Projection of trajectories leading towards positions of equilibrium.

projections of the trajectories on the (γ, v) plane in the neighbourhood of the line piece where equilibrium can exist. The radius of curvature of trajectories projected on the (γ, v) plane, near the γ -axis, amounts:

$$\rho = -\left(\frac{d^2\bar{\gamma}}{d\bar{v}^2}\right)^{-1} = (\text{sgn } \bar{v} + \alpha_e)/\zeta. \quad (115)$$

With the use of this expression we obtain for $\bar{\gamma}$ with (114):

$$\bar{\gamma} = \bar{\gamma}_1 + \frac{1}{2}(\bar{v}_1^2 - \bar{v}^2)/\rho. \quad (116)$$

The slope of the projected trajectories reads:

$$\frac{d\bar{\gamma}}{d\bar{v}} = -\frac{\bar{v}}{\rho} (<0) \quad (117)$$

Due to the fact that in the half space $v > 0$, the points will move to the right in figure 24 and in the other half space $v < 0$ to the left, it is obvious that the points move towards the (γ, α) plane. This plane cannot be crossed because of the opposite direction of motion which occurs on the other side of the (γ, α) plane. Once the (γ, α) plane is attained, the point remains on that plane. The final values for \bar{v} and $\bar{\gamma}$ read consequently:

$$\left. \begin{aligned} \bar{v}_f &= 0, \\ \bar{\gamma}_f &= \bar{\gamma}_1 + \frac{1}{2} \bar{v}_1^2 / \rho, \end{aligned} \right\} \quad (118)$$

It can be stated that the trajectory of the disturbed motion

remains in the limited space:

$$\left. \begin{aligned} |\bar{v}| &\leq |\bar{v}_1|, \\ |\bar{\gamma}| &\leq |\bar{\gamma}_1| + \frac{1}{2} |\bar{v}_1^2/\rho|. \end{aligned} \right\} \quad (119)$$

By making use of the solution for $\bar{\gamma}$ (116) we obtain for $\bar{\alpha}$ the following solution of (109):

$$\bar{\alpha} = \left\{ \bar{\alpha}_1 + (1+\sigma)(\sigma\rho + \bar{v}_1) - \bar{\gamma}_1 \right\} \left(e^{\frac{\bar{v}-\bar{v}_1}{\sigma\rho}} - 1 \right) + \bar{\alpha}_1 + (1+\sigma)(\bar{v}_1 - \bar{v}) + \frac{1}{2}(\bar{v}_1^2 - \bar{v}^2)/\rho, \quad (120)$$

which holds for $\bar{v} \neq 0$. At the instant $s = s_f$ when the point reaches the (γ, α) plane, $\bar{\alpha}$ obtains the value:

$$\bar{\alpha} = \bar{\alpha}'_f = \left\{ \bar{\alpha}_1 + (1+\sigma)(\sigma\rho + \bar{v}_1) - \bar{\gamma}_1 \right\} \left(e^{-\bar{v}_1/\sigma\rho} - 1 \right) + \bar{\alpha}_1 + (1+\sigma)\bar{v}_1 + \frac{1}{2}\bar{v}_1^2/\rho. \quad (121)$$

For $s < s_f$ thus for $\bar{v} \neq 0$ the variable $\bar{\alpha}$ remains in between limits expressed by:

$$\left| \bar{\alpha} \right| < \left| \bar{\alpha}_1 + (1+\sigma)(\sigma\rho + \bar{v}_1) - \bar{\gamma}_1 \right| \left| e^{-\bar{v}_1/\sigma\rho} - 1 \right| + \left| \bar{\alpha}_1 \right| + (1+\sigma) \left| \bar{v}_1 \right| + \frac{1}{2} \left| \bar{v}_1^2/\rho \right|. \quad (122)$$

For $s \geq s_f$ we have: $\bar{\gamma} = \bar{\gamma}_f$ and $\bar{v} = 0$. By making use of these expressions and the relations (103) and (107) we find for the solution of the differential equation (102) for $s \geq s_f$:

$$\bar{\alpha} = (\bar{\alpha}'_f - \bar{\gamma}_f) e^{-\frac{s-s_f}{\sigma}} + \bar{\gamma}_f. \quad (123)$$

The final value of $\bar{\alpha}$ becomes for $s \rightarrow \infty$:

$$\bar{\alpha}_f = \bar{\gamma}_f = \bar{\gamma}_1 + \frac{1}{2} \bar{v}_1^2/\rho. \quad (124)$$

It appears from (123) that for $s \geq s_f$ the variable $\bar{\alpha}$ remains in the range:

$$\left| \bar{\alpha} \right| < \left| \bar{\alpha}'_f \right| + \left| \bar{\gamma}_f \right|. \quad (125)$$

From the expressions (118) and (124) it is noted that the disturbed motion $(\bar{\alpha}, \bar{\gamma}, \bar{v})$ does not tend to zero for $s \rightarrow \infty$.

New positions of equilibrium $(\bar{\alpha}_f, \bar{\gamma}_f, \bar{v}_f)$ are attained after the disturbance $(\bar{\alpha}_1, \bar{\gamma}_1, \bar{v}_1)$. The fact that the disturbed motion remains in between limits, the magnitudes of which being determined by the disturbance in such a way (119, 122, 125) that for any given value ϵ a value $\delta(\epsilon)$ can be indicated so that for any $|\bar{\alpha}_1| < \delta$, $|\bar{\gamma}_1| < \delta$ and $|\bar{v}_1| < \delta$ the solution will be such that $|\bar{\alpha}| < \epsilon$, $|\bar{\gamma}| < \epsilon$ and $|\bar{v}| < \epsilon$ after the disturbance, gives rise to the conclusion that the positions of equilibrium ($v = 0$, $\alpha = \gamma$, $|\alpha| < 1$) are stable. However, they are not asymptotically stable as not each of the variables $\bar{\alpha}$, $\bar{\gamma}$ and \bar{v} tend to zero for $s \rightarrow \infty$.

3.2. The small limit-cycle

We shall now proceed to determine the small limit-cycle. The result will be an approximation owing to the fact that in reality the tyre characteristic is non-linear.

Due to the symmetry of the system, the limit-cycle is expected to be situated symmetrically with respect to the origin in the (γ, v, α) space. We will derive expressions for the trajectories in the half space $v > 0$. The trajectory which has crossings with the (γ, α) plane, located symmetrically with respect to the origin, represents the limit-cycle. The equations of motion which hold for $v > 0$, read according to (101) and (102):

$$\left. \begin{aligned} \zeta \frac{d^2 \gamma}{ds^2} + 1 &= -\alpha, \\ \sigma \frac{d\alpha}{ds} + \alpha &= -\frac{d\gamma}{ds} + \gamma. \end{aligned} \right\} \quad (126)$$

It is convenient to introduce the new variables:

$$\alpha' = \alpha + 1, \quad \gamma' = \gamma + 1, \quad v' = v. \quad (127)$$

This means that the origin is shifted to the extreme position of equilibrium ($\gamma = -1$, $\alpha = -1$). The equations (126) become now:

$$\left. \begin{aligned} \zeta \frac{d^2 \gamma'}{ds^2} + \alpha' &= 0, \\ \sigma \frac{d\alpha'}{ds} + \alpha' + \frac{d\gamma'}{ds} - \gamma' &= 0. \end{aligned} \right\} \quad (128)$$

The characteristic equation of this set of equations reads:

$$\sigma \zeta p_s^3 + \zeta p_s^2 - p_s + 1 = 0. \quad (129)$$

The solution of this equation reads in general:

$$\left. \begin{aligned} p_{s,1,2} &= x \pm iy, \\ p_{s,3} &= z. \end{aligned} \right\} \quad (130)$$

With the use of (127) and the first equation of (128) we obtain for γ , v and α the following expressions:

$$\left. \begin{aligned} \gamma &= -1 + A e^{-zs} + (B \sin ys + C \cos ys) e^{xs}, \\ v &= -z A e^{-zs} + (B \sin ys + C \cos ys) x e^{xs} + \\ &\quad + (B \cos ys - C \sin ys) y e^{xs}, \\ \alpha &= -1 - z^2 \zeta A e^{-zs} - 2 \zeta (B \cos ys - C \sin ys) y x e^{xs} + \\ &\quad + \zeta (B \sin ys + C \cos ys) (y^2 - x^2) e^{xs}. \end{aligned} \right\} \quad (131)$$

The constants of integration A, B and C are to be determined from the initial conditions at $s = 0$:

$$\gamma = \gamma_0, \quad v = 0, \quad \alpha = \alpha_0. \quad (132)$$

Half a wavelength later ($s = \frac{1}{2} \lambda$), when the (γ, α) plane is crossed again, the following relations are valid in case we are on a limit-cycle:

$$\gamma = -\gamma_0, \quad v = 0, \quad \alpha = -\alpha_0. \quad (133)$$

These values inserted in (131) result in the three equations for the unknowns γ_0 , α_0 and λ . After elimination of γ_0 and α_0 one equation may be obtained in λ alone. This complicated equation will not be reproduced here.

We will examine the case already studied before (cf. Fig. 13):

$$\sigma = 3, \quad e' = 0.57, \quad \zeta = V^2/e' = 6.66^2/0.57 = 78. \quad (134)$$

For the solution (130) we obtain in that case:

$$x = 0.0208, \quad y = 0.105, \quad z = 0.375. \quad (135)$$

Numerically the following solution for γ_0 , α_0 and λ has been found with the underlinings introduced again:

$$\underline{\gamma}_0 = \frac{\gamma_0 e'}{K} = -3.37, \quad \underline{\alpha}_0 = \frac{\alpha_0 e'}{K} = -2.88, \quad \lambda = \frac{2\pi V}{\omega} = 60.032. \quad (136)$$

The maximum value of γ equals $|\gamma_0|$; the maximum value of α , however, will be somewhat greater than $|\alpha_0|$. For various values of the dry-frictional couple K the table below shows the results according to the piece-wise linear method, compared with those obtained with the aid of the approximate equivalent linear theory (cf. Fig.13) where, in contrast to the theory above, a non-linear tyre characteristic is considered.

Table 2. Comparison of amplitudes and frequencies according to two methods.

K	piece-wise		equivalent	
	$ \gamma_0 $	ω	$ \gamma_0 $	ω
0.002	0.0118	0.697	0.0118	0.705
0.0045	0.0266	0.697	0.0278	0.695
0.007	0.0414	0.697	0.0504	0.657

We note that a good agreement exists in the low amplitude range. For higher amplitudes the non-linearity of the tyre characteristic causes the values of $|\gamma_0|$, obtained with the equivalent linear theory, to deviate from a linear variation with K .

3.3. Stability of the small limit-cycle

We are interested in the stability of the limit-cycle, i.e. of the orbit in the phase space. We will consequently, not use the stability criterium of Ljapunov but that of the orbital stability (cf. Stoker [56, p.253]), often called the Poincaré criterium of stability.

A disturbed motion will be considered, which is governed by the equation (99) and of which the trajectory intersects the (γ, α) plane at a certain instant in a point $(\gamma_0 + \Delta\gamma_i, \alpha_0 + \Delta\alpha_i)$ situated near the limit-cycle (see Fig.25). For given deviations $(\Delta\gamma_i, \Delta\alpha_i)$ the deviations at the subsequent crossing $(\Delta\gamma_{i+1}, \Delta\alpha_{i+1})$ can be calculated. Comparison of both pairs of deviations may lead to a decision about the stability of the limit-cycle. Expressions (131) form the solution of the motion. The constants A , B and C as well as λ will be changed somewhat with respect to their values on the limit-

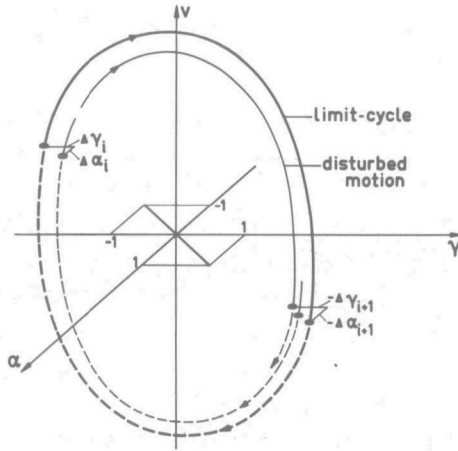


Fig. 25. Trajectories in the phase-space.

cycle. Their increments will be denoted by ΔA , ΔB , ΔC and $\Delta \lambda$ respectively. At the crossing we choose $s = 0$. The following equations obtained from (131) hold for the deviations at the i -th crossing:

$$\left. \begin{aligned} \Delta \gamma_i &= \Delta A + \Delta C, \\ 0 &= -z \Delta A + y \Delta B + x \Delta C, \\ \Delta \alpha_i &= -\zeta \left\{ z^2 \Delta A + 2xy \Delta B - (y^2 - x^2) \Delta C \right\}. \end{aligned} \right\} \quad (137)$$

The increments ΔA , ΔB and ΔC can be calculated from the equations above. The deviations at the $(i+1)$ -th crossing where $s = \frac{1}{2}(\lambda + \Delta \lambda)$ follow from linearized equations which are obtained from (131):

$$\left. \begin{aligned} \Delta \gamma_{i+1} &= a_1 \Delta A + b_1 \Delta B + c_1 \Delta C + d_1 \Delta \lambda, \\ 0 &= a_2 \Delta A + b_2 \Delta B + c_2 \Delta C + d_2 \Delta \lambda, \\ \Delta \alpha_{i+1} &= a_3 \Delta A + b_3 \Delta B + c_3 \Delta C + d_3 \Delta \lambda. \end{aligned} \right\} \quad (138)$$

The increments $\Delta \lambda$ can be eliminated from these equations, after which two equations arise which are of the following form:

$$\left. \begin{aligned} \Delta \gamma_{i+1} &= a_{11} \Delta \gamma_i + a_{12} \Delta \alpha_i, \\ \Delta \alpha_{i+1} &= a_{21} \Delta \gamma_i + a_{22} \Delta \alpha_i. \end{aligned} \right\} \quad (139)$$

The very complicated expressions for the coefficients a_{kl} will

not be reproduced here. For the special case considered ($\sigma=3$, $\xi=78$) we obtain:

$$\left. \begin{aligned} a_{11} &= -1.756, \quad a_{12} = -0.087, \\ a_{21} &= -1.865, \quad a_{22} = -0.100. \end{aligned} \right\} \quad (140)$$

Because of the coupling between the equations (139) we cannot draw a conclusion yet about the stability from these equations. We shall therefore introduce new variables ΔX and ΔY which are related to $\Delta \gamma$ and $\Delta \alpha$ in such a way that we can write for (139):

$$\left. \begin{aligned} \Delta X_{i+1} &= \beta_1 \Delta X_i, \\ \Delta Y_{i+1} &= \beta_2 \Delta Y_i. \end{aligned} \right\} \quad (141)$$

It can be shown that β_1 and β_2 are the two different roots of the equation:

$$\begin{vmatrix} a_{11} - \beta & a_{12} \\ a_{21} & a_{22} - \beta \end{vmatrix} = 0. \quad (142)$$

We find for the case considered:

$$\left. \begin{aligned} \beta_1 &= 0.007, \\ \beta_2 &= -1.863. \end{aligned} \right\} \quad (143)$$

Owing to the fact that the absolute value of at least one of the roots is greater than one, the deviation will increase after each crossing of the (γ, α) plane. The limit-cycle will consequently be orbitally unstable.

CHAPTER V

INVESTIGATIONS WITH THE AID OF AN ELECTRICAL COMPUTER

For a more detailed study of the autonomous third-order system and for the investigation of the non-autonomous third-order system provided with unbalances, and the elaborate tenth and twelfth-order systems we have proceeded to use an electrical analogue computer.

New aspects of the behaviour of the system such as the influence of the application of the more exact tyre theory of Von Schlippe, the appearance of domains in the phase space from where the motion must start in order to attain the limit-cycle, and synchronous response and combination oscillations in case of the application of unbalances will be discussed in this chapter.

1. *The third-order system*

1.1. Circuit diagrams

For the formulation of the machine equations it is necessary to introduce a time scale factor α_t . The machine time τ is then related to s in the following way:

$$\tau = s / \alpha_t. \quad (1)$$

The third-order system is governed by the equations III. (80, 82b) until III. (98b) when the variables y , φ , y^* , φ^* and γ_{st} are made equal to zero. The equations given below are derived in a similar way as displayed in Secs. IV. 1.2 and IV. 2.3. In contrast to the presentation in chapter IV, we will regard now both tyre approximations I and II and an impressed couple due to unbalance. Concerning the damping couple $g(\dot{\gamma}, \gamma)$ again the three possibilities III. (85a, b, c) will be applied. As before, the rotational stiffness c is not taken into account.

The equations III. (80, 82b, 91, 92, 93, 94a, 95a) become, when dots refer to derivations with respect to the machine time τ :

$$\left. \begin{aligned} \frac{V^2}{\alpha_t^2} \ddot{\gamma} + \frac{1}{\alpha_t} \kappa \dot{\gamma} + g \left(\frac{V}{\alpha_t} \dot{\gamma}, \gamma \right) &= M' - e F + \mu_{un} V^2 \cos \alpha_t \tau / R, \quad (a) \\ \frac{1}{\alpha_t} \dot{v}_1 + \frac{1}{\sigma} v_1 &= \gamma - \frac{1-e}{\alpha_t} \dot{\gamma}, \quad (b) \end{aligned} \right\} (2)$$

APPROXIMATION I APPROXIMATION II

$$\begin{aligned} y_{c1} &= (1-e) \gamma + v_1, \quad (c) \\ y_{c2}(\tau) &= y_{c1}(\tau - 2/\alpha_t) \quad (d) \\ v_2 &= \frac{\sigma + 2}{\sigma} v_1, \quad (f) \\ v_2 &= y_{c2} + (1+e) \gamma, \quad (e) \\ F &= F_1(v_1) + F_2(v_2), \quad (g) \\ M' &= F_1(v_1) - F_2(v_2). \quad (h) \end{aligned}$$

Through equation (2f) we have realised, in fact, the straight tangent concept of approximation II. The original equations III.(96, 97a, 98a) are replaced by (2f,g,h) which leads to the same result, but which has the advantage that the same pair of function generators can be used for either approximation, so that a more accurate and easier way of comparison is obtained.

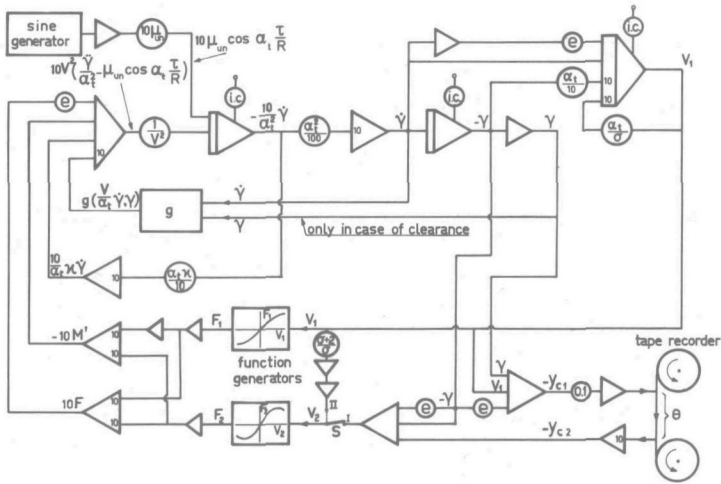


Fig. 1. Analogue computer circuit for the third-order system with possibility of introducing retardation term (tyre approximation I: switch S in horizontal position).

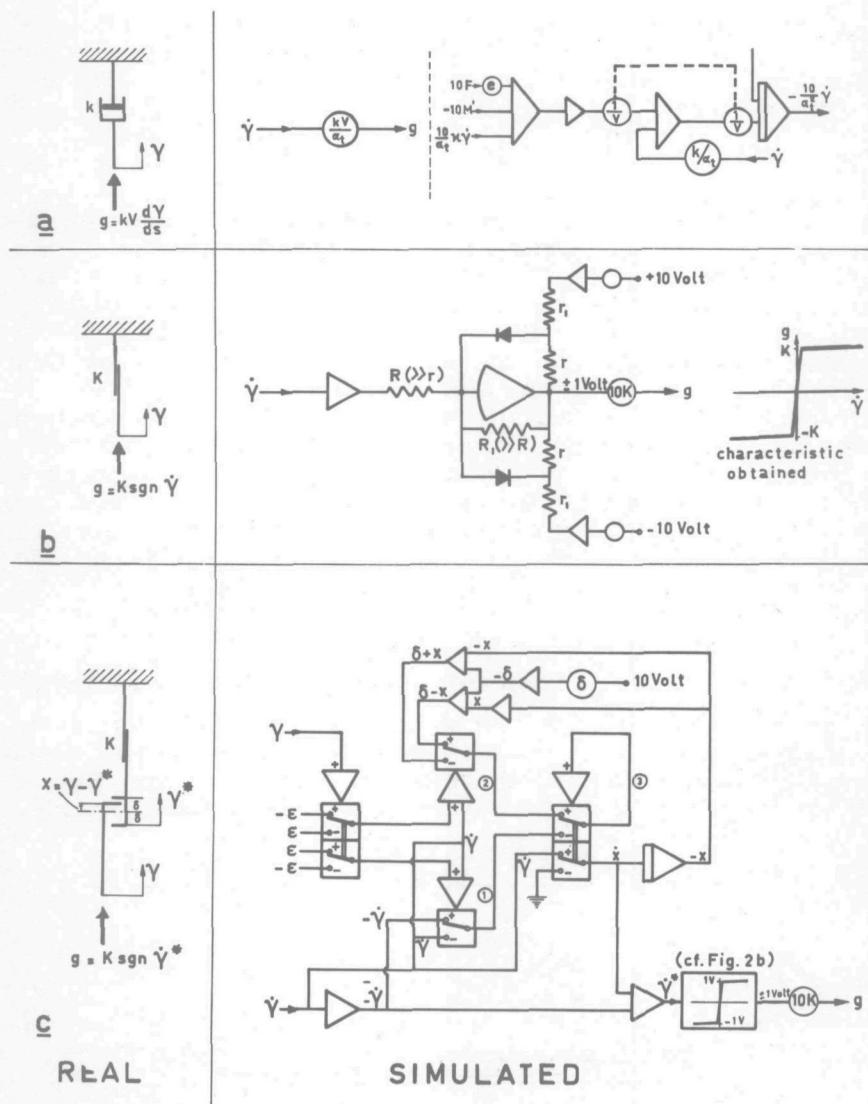


Fig. 2. Circuit diagrams for generation of damping term $g(\dot{\gamma}, \gamma)$,

- a: Linear damping,
- b: Dry friction,
- c: Dry friction with clearance.

For generating the retardation term $y_{c1} (\tau - 2/\alpha_t)$ we made use of a tape recorder by means of which a constant time delay can be achieved. The time delay must have the following value:

$$\theta = 2/\alpha_t. \tag{3}$$

It is the difference in time between recording and reproducing. The scale factor α_t is determined by the fixed time difference θ through (3). In our case we have chosen for the value of the scale factor: $\alpha_t = 5.6$. It appeared furthermore to be convenient for obtaining a proper voltage level to multiply equation (2a) by the factor 10 and equation (2b) by the factor α_t . The machine unit is 10 Volt.

Figure 1 shows the circuit for the case that approximation I is employed. The function generators generate the functions F_1 and F_2 , which are obtained in a way as shown in figure II.18. Through switch S we may disconnect the tape recorder and thereby obtain approximation II. The block denoted by g is a general indication of the element generating the damping term in equation (2a); input γ is used only in the case with clearance. In figure 2 three possibilities for the damping term g are shown. Figure 2a shows the linear representation $g = \frac{V}{\alpha_t} k \dot{\gamma}$. For easier manipulation another construction shown at the right-hand side, which fits in the circuit of figure 1, is used. The speed can be varied continuously with the aid of the coupled potentiometers. Figure 2b shows block g in the case of a dry-frictional couple.

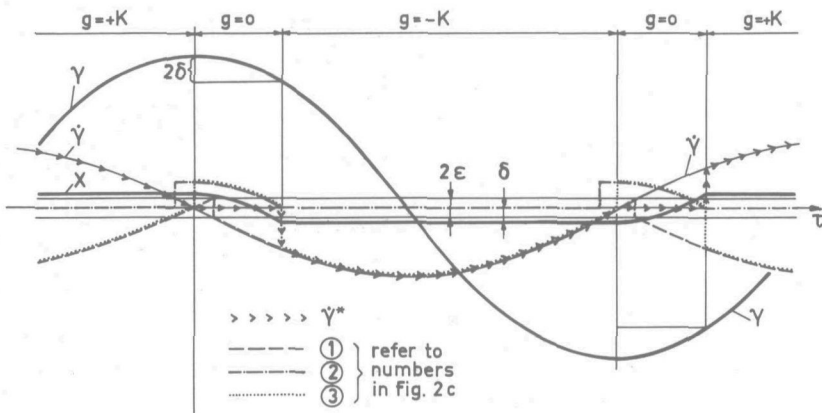


Fig.3. Variation of voltages occurring in circuit of figure 2c.

The actual characteristic obtained appears to differ slightly from the ideal characteristic due to the finite values of the resistances R_1 and R . Figure 2c gives the elaborate scheme necessary for the simulation of clearance and dry friction in series. In figure 3 the variations of several signals occurring in this scheme are shown. The small voltages e are used for controlling two relays shown in the centre of the diagram of figure 2c.

For the simulation of the linear third-order system both function generators for the tyre characteristics should be replaced by linear elements; in addition, the linear representation of the damping term should be used. When investigating the autonomous system, where the unbalance couple vanishes, the sine generator should be disconnected.

1.2. Stability of the linear system

The boundaries of the speed region where instability occurs for a certain configuration of the system, may be found by varying the position of the coupled potentiometers for $1/V$. Those positions should be chosen where the self-excited motion remains stationary in amplitude.

In figure 4 a diagram is shown indicating areas of instability in the (V, e) plane. As before we have chosen the values $\sigma = 3$, $e' = 0.5$. In order to obtain a clearer picture of the influence of the retardation term (approximation I of tyre behaviour), the damping coefficient κ is not taken into account in this section. The caster length e may again be obtained by varying the position of the king-pin either by shifting or by inclining, where we must bear in mind that the theory holds only for small values of the caster angle ϵ .

In the graph of figure 4, the results for both approximations of tyre theory are shown. The curves for approximation II (i.e. switch S of Fig.1 in position II) correspond to those of figure IV.2. Also the curves for constant reduced frequency applicable for approximation II are drawn. As expected, it appears that at high values of ω_s approximation II does not longer follow the more exact approximation I. Above $\omega_s \approx 0.2$ the decrease in self-excitation due to the retardational effect becomes appreciable (cf. Fig.II.13a). The stability boundaries which are open at the left-hand side for each value of the damping coefficient k when approximation II is employed, may become closed for higher values of k in the Von Schlippe representation (approximation I). It is noted that the simple approximation II fortunately leads to conclusions which are on the safe side.

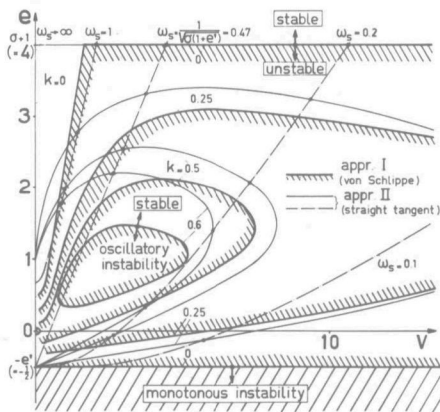


Fig. 4. Unstable areas of the third-order system showing influence of retardation term (approximation I) with respect to simplified system (approximation II) ($e'=0.5, \sigma=3$).

1.3. The phase space for the non-linear system

The motion of a system with parameters characterized through a point in the unstable area of figure 4 would always increase in amplitude when the system is considered to be linear. For the case that non-linear elements are introduced, it appears, as has been found already analytically, that one or more limit-cycles may appear. The trajectories from or towards such limit-cycles can only be presented in complete form in a three-dimensional space with coordinates γ , γ and α .

A detail study has been carried out for a given system travelling with a certain speed, in which the limit-cycles and the conditions necessary for approaching a stable situation are determined.

For the sake of comparison with results obtained analytically, we have chosen the same parameter values as used in figure IV.13 and IV.14:

$$\sigma = 3, e = 0, \kappa = 0, V = 6.66.$$

The tyre characteristic to be used again is shown in figure IV.12 (original curve). In the point considered in the graph of figure 4 it makes practically no difference whether approximation I or II is used, because of the low value of ω_s occurring in that point. This frequency will become even lower at increasing amplitude due to the decrease in equivalent cornering stiffnesses. It is very well permissible to

use approximation II for this detail study. The tape-recorder is disconnected in that case which makes the manipulation a lot simpler.

Figure IV.15 giving an overall picture of analytically obtained results appears to apply for the analogue computer results as well. The variation of the limit-amplitude with viscous and dry damping for certain values of clearance as found with the aid of the analogue computer, is shown in figure 5. The agreement with the analytical results shown

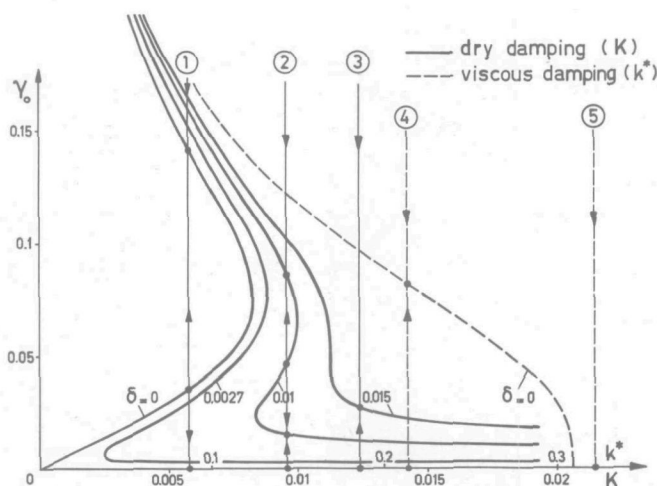


Fig. 5. Limit-amplitudes as a function of damping for a number of values of clearance δ ($V=6.66$, $\sigma=3$, $e=0$, $\kappa=0$).

in figure IV.13 and IV.14 is very good. Due to the considerable deviation from an elliptical shape of the limit-cycle at large amplitudes, the difference in amplitude becomes relatively larger in that region of amplitudes.

We notice that in the case of viscous damping the limit-cycle is the only possible stable situation when the centre position is unstable, i.e. when a point in an unstable region of figure 4 is regarded. From each point in the phase space $(\gamma, \dot{\gamma}, \alpha)$ this limit-cycle will be reached in that case. In the case of dry friction, however, it is not at all sure to which stable situation, centre position or limit-cycle, the trajectory will go when the motion starts with some arbitrary set of initial values of γ , $\dot{\gamma}$ and α .

For the dry-frictional couple $K = 0.0035$ and two cases of clearance $\delta = 0$ and $\delta = 0.0027$ this problem is examined more closely. In the case without clearance two limit-cycles

occur of which the smaller is unstable; the centre position is stable. In the case with clearance three limit-cycles are found of which the second one is unstable; the centre position is unstable.

By trying out a large number of combinations of initial values of γ , $\dot{\gamma}$ and α , it is found that in the case without clearance ($\delta=0$) a "limit-surface" in the shape of a curved tube exists in the phase space, situated symmetrically with respect to the origin (see Fig. 6). It appears, that from its

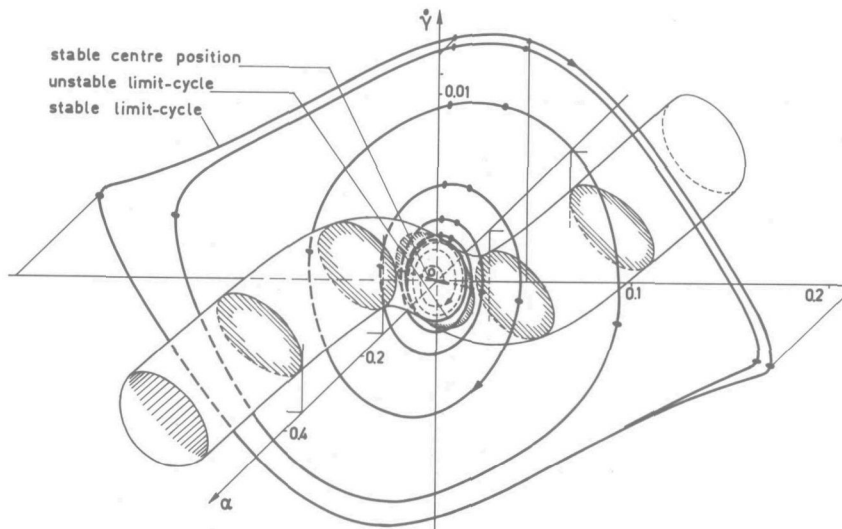


Fig. 6. The limit-surface of initial values and the limit-cycles with trajectories starting from the unstable limit-cycle in the case of dry friction and absence of clearance ($V=6.66, \sigma=3, e=0, \kappa=0, K=0.0035, \delta=0$).

interior always the stable centre position on the line piece ($\gamma=\alpha, \dot{\gamma}=0, |\gamma| \leq K/e'$) is reached (cf. Sec. IV.3). When starting outside the tube, the stable limit-cycle is attained. When starting from a spot on the tube, the point travels over the limit-surface towards the unstable limit-cycle which is a closed curve situated on the limit-surface. When starting not exactly on this limit-surface the point will tend towards either the centre position or the stable limit-cycle after having circulated a few times in the neighbourhood of the unstable limit-cycle. It may be noted that the amplitude γ_0 of the unstable limit-cycle can be indicated approximately by the point of intersection of the tube wall and the γ -axis; this value of γ has to be exceeded in order to reach the

stable limit-cycle when the other initial values ($\dot{\gamma}, \alpha$) are taken equal to zero. It appears that this approximation applies fairly well in general.

When regarding the case with clearance, it is obvious that for a complete representation of the solution a fourth dimension is needed owing to the additional variable γ^* (see Fig.III.4). We will confine ourselves to the initial value $\gamma_i^* = 0$. The limit-surface and the projection of the three limit-cycles upon the three-dimensional space ($\gamma, \dot{\gamma}, \alpha$) are shown in figure 7. The limit-surface is symmetric with

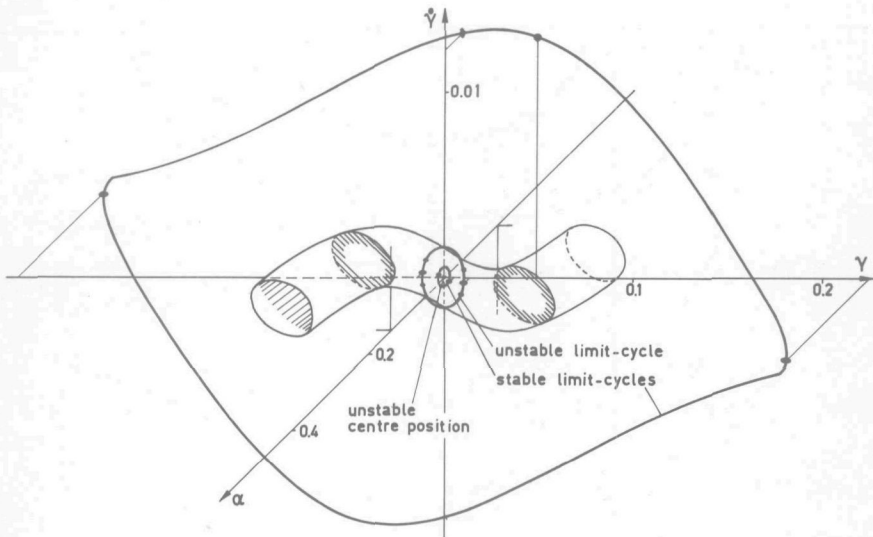


Fig.7. The limit-surface of initial values and the limit-cycles in the case of dry friction and clearance ($V=6,66$, $\sigma=3$, $e=0$, $\kappa=0$, $K=0,0035$, $\delta=0,0027$).

respect to the origin in the case considered ($\gamma_i^*=0$). From its interior, the stable small limit-cycle is always reached. When starting outside the limit-surface, the trajectories will tend to the stable large limit-cycle. It may be noted that in general the unstable limit-cycle does not lie on the three-dimensional surface but intersects it in a few points. This limit-cycle does lie completely on the four-dimensional limit-surface.

As an illustration, figure 8 shows the projection of the limit-cycles and some trajectories leading to them for the case $\delta = 0,01$ and $K = 0,009$ (cf. Fig.5).

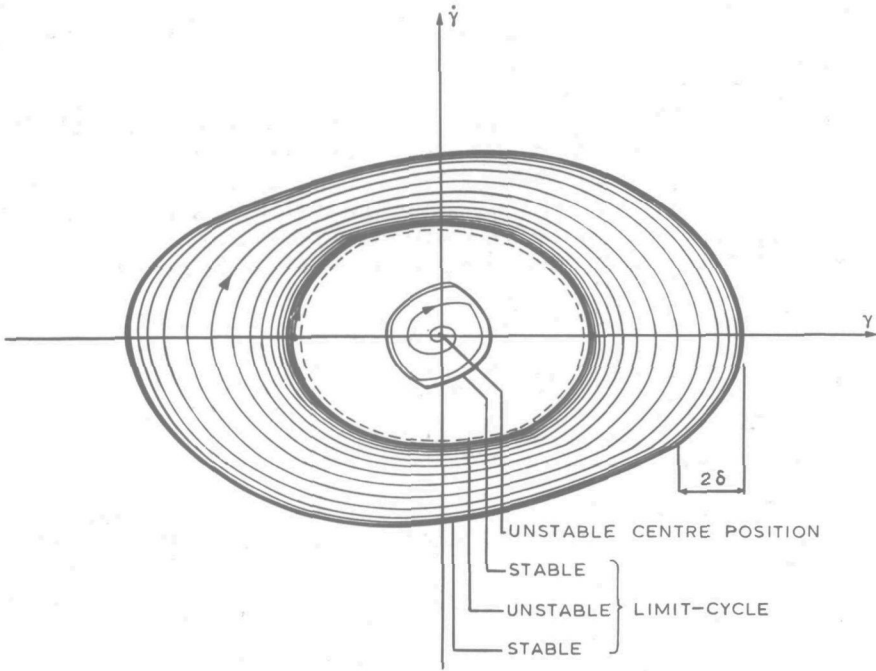


Fig.8. Limit-cycles and some trajectories in the case of dry friction and clearance (Fig.5, case 2).

1.4. The self-excitation area

With the use of the simple approximation II of the tyre theory, which has been employed throughout the analytical investigations, we have found, also with higher-order systems, self-excitation areas very similar to those obtained analytically. As mentioned in Sec. 1.3 the limit-amplitudes appear to be somewhat larger than would be predicted analytically. As a consequence, also the boundaries (especially the upper one) of the self-excitation area will rise a little, which results in an increase in area.

For $e = 0$, $\sigma = 3$ and the original tyre characteristics as shown in figure IV.18, curves are obtained as presented in figure 9, together with curves for constant reduced frequency. They may be compared with the analytical results shown in figure IV.20.

We now consider the case of switch S (Fig.1) in position I so that the tape-recorder is connected and thereby the more exact approximation I comes into play. Figure 10

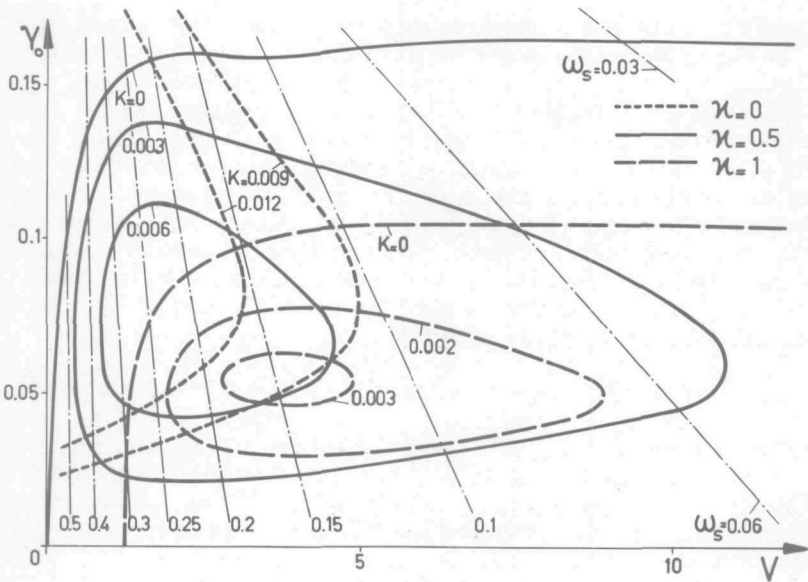


Fig. 9. Self-excitation areas according to approximation II ($\sigma=3, e=0$).

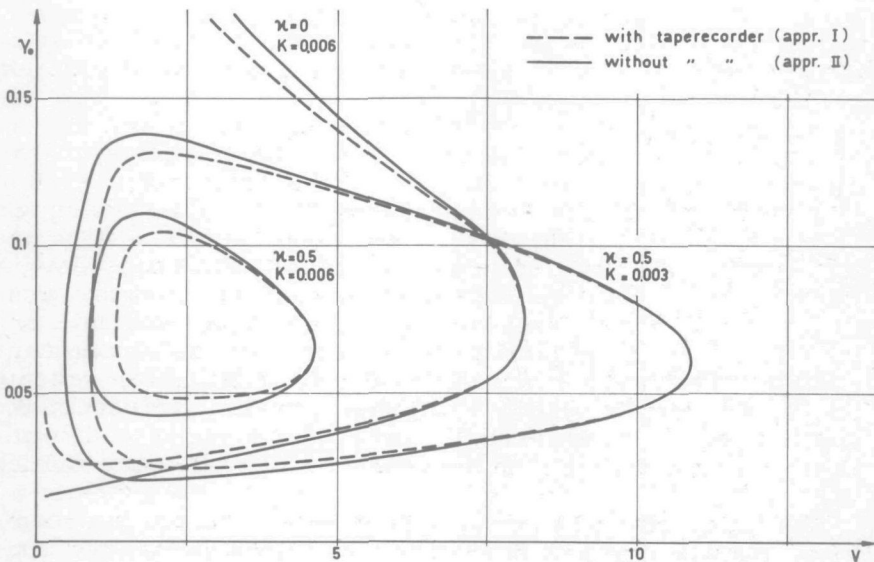


Fig. 10. Comparison of self-excitation areas calculated with approximation I and II ($\sigma=3, e=0$).

shows the curves obtained together with the boundaries according to approximation II for some combinations of damping. We find, as expected, less self-excitation at low velocities V or in other terms at high values of ω_s . The left-hand boundaries of the areas are shifted a little towards higher values of speed, which means that according to approximation I the shimmy will die out, while slowing down, at a somewhat higher speed than would be predicted with the simpler tyre theory according to approximation II. This effect owing to the retardation term in the equations does not influence the nature of shimmy and will therefore be disregarded in the sequel.

1.5. The response to unbalance torque

When connecting the sine generator in the analogue computer circuit of figure 1, the non-autonomous system is simulated. For several values of unbalance moment coefficient μ_{un} and the reduced excitation frequency $\omega_{un} = 1/R$, stationary response characteristics are produced. Figure 11 shows the curves for different values of μ_{un} and ω_{un} for a given combination of damping. The area of self-excitation of the autonomous system is indicated by a dashed curve. Figure 12 illustrates the effect of varying the damping.

The full thick lines (curves 1 and 3 in Fig. 11c) designate the amplitude response in the case that a synchronous motion occurs, which implies that the motion is periodic with the same frequency as the frequency of excitation by unbalance. Synchronous response will occur when the frequency of excitation is close to the frequency of the autonomous system (Fig. 9) at the amplitude level occurring in the non-autonomous case. When the difference in these frequencies becomes too great, the synchronous oscillation may pass into a motion with a beat character. Combined oscillations occur then, one with the frequency of the unbalance moment and the other with a frequency close to that of the autonomous system. The shaded areas (4 and 5 in Fig. 11c) indicate the speed ranges where combined oscillations occur; the boundaries of these areas represent the upper and lower limit in between which the amplitude of the stationary motion varies.

A similar phenomenon of synchronous motions and combined oscillations has been treated in an approximate analytical way by Stoker [57, p.166] for the second-order system of Van der Pol provided with a forcing member. He shows that when the system is excited with a frequency near the frequency of the free oscillations, synchronous

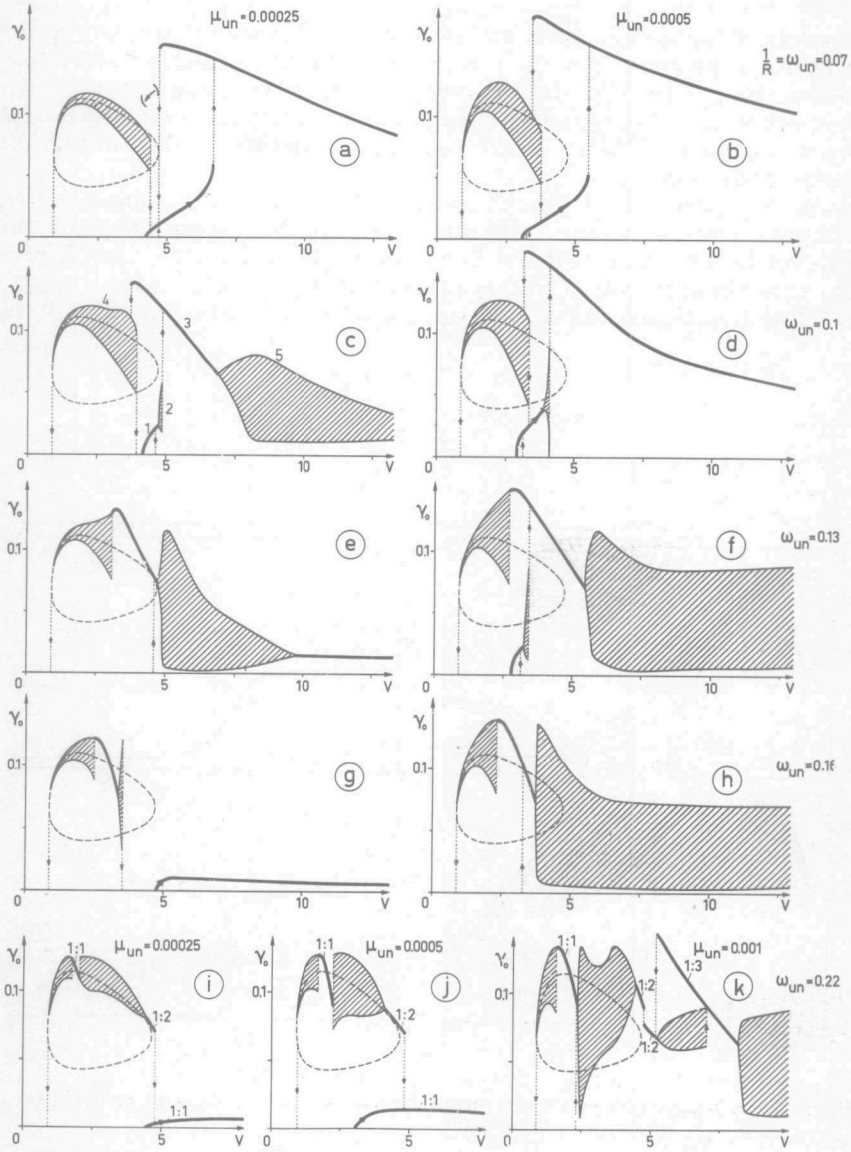


Fig.11. The response to unbalance torque for various values of unbalance μ_{un} and wheel radius R ($\sigma=3, e=0, \alpha=0.5, K=0.006$).

response occurs. Beyond a certain degree of detuning the synchronous motion appears to become unstable; a transition takes place to combined oscillations. It appears that the response of our third-order system and, as we shall see later, also of more elaborate systems basically show the same features.

At low values of wheel radius or damping, subharmonic response may occur. In such a case the frequency of the motion is a fraction of the frequency of excitation. In figure 11 this occurs at a reduced frequency of excitation $\omega_{un} = 0.22$ and in figure 12 at the combination of damping $\kappa = 0.5$,

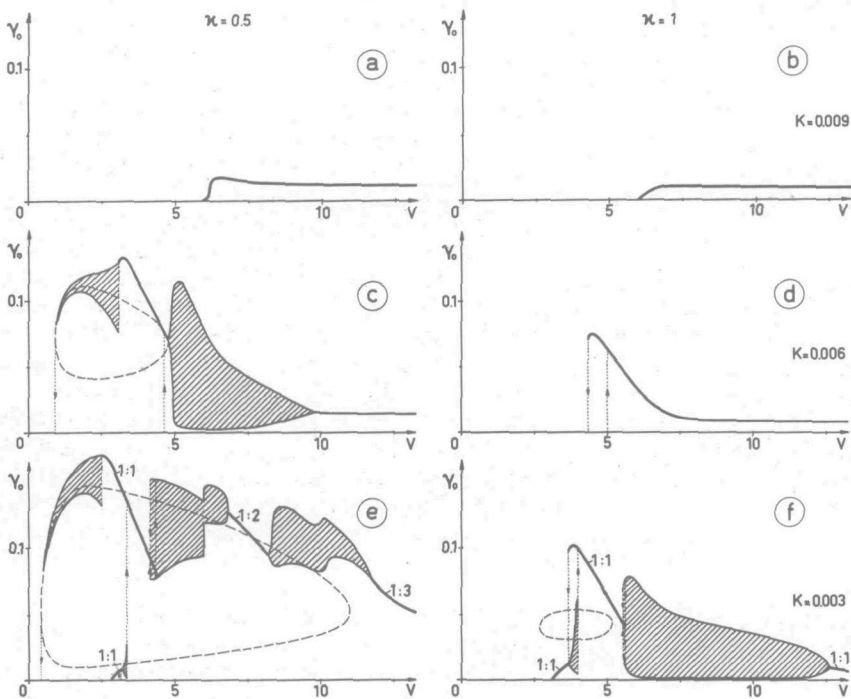


Fig. 12. The response to unbalance torque for various combinations of damping ($\sigma=3$, $e=0$, $\mu_{un}=0.00025$, $\omega_{un}=0.13$).

$K = 0.003$. For the periodic motions, represented by the full thick lines, the fractions are indicated.

These general considerations will be followed now by a more detailed discussion of the course of things in the figures 11 and 12. The way in which the motion changes is indicated by means of arrows. The system will get into motion as

soon as the velocity and consequently the unbalance moment has exceeded a certain critical value depending on the dry-frictional couple K . It may happen (Fig. 11a, b, c, d, f) that in the first instant a synchronous curve is followed on low amplitude level (curve 1 in Fig. 11c), after which the motion jumps over to a high amplitude level (curve 3) sometimes via a combined oscillation (area 2); on this high level the motion is synchronous in most cases. At decreasing values of ω_{un} (larger R) the synchronous region shifts more to the right where the influence of self-excitation decreases and the moment due to unbalance increases so that due to both reasons a more extended synchronous region arises.

When a sufficient amount of self-excitation is present, the synchronous character may pass into a combined oscillatory type when the speed is changed sufficiently. It is shown that the correspondence of the combined oscillations, represented by the left-hand shaded area (4 in Fig. 11c), with the autonomous motion (dashed curve) becomes closer at decreasing values of the velocity of travel. At low values of ω_{un} and μ_{un} it may occur that this area of combined oscillations is isolated and cannot be attained through the unbalance alone. The arrow in between brackets (Fig. 11a) indicates a possible jump towards such an isolated area when the forward speed is lowered in short time. Of course a single external impulse may also cause entrance in this area. At somewhat higher values of ω_{un} and μ_{un} (Fig. 11b, c, d) the area may become isolated only in the direction towards the synchronous region. The area can then be reached in the normal manner but cannot be left in the same way. When varying the velocity from the point where the beat area is reached, the combined oscillation will continue until it dies out or is passed into a synchronous oscillation of low amplitude level.

When subsequently the velocity is increased sufficiently, the synchronous response with high amplitude level (3 in Fig. 11c) will be reached again. A further increase in speed may lead to a second non-synchronous response as indicated by the right-hand shaded areas (5 in Fig. 11c). The difference between maximum and minimum amplitude increases rapidly with speed until in some cases (Fig. 11g) the minimum amplitude becomes zero which results in vanishing of the motion. The latter behaviour can occur alone, when at that value of speed the unbalance is not large enough to excite the motion from the situation of rest. The high amplitude shimmy is isolated completely in that case. Due to unbalance alone the system will vibrate only at high velocities and then mostly with very low amplitudes.

In most cases this motion will be synchronous. In the other case (Fig.11e) where the high amplitude shimmy is not isolated, the combined oscillatory motion will not die out at increasing speed but may pass into a synchronous motion of low amplitude level when μ_{un} is not too large.

A complicated response picture, showing the occurrence of subharmonic responses, arises at the high value of excitation frequency $\omega_{un} = 0.22$ (Fig.11i,j,k). For $\mu_{un} = 0.001$ the subharmonic response shows a fraction of even 1:3. In figure 12e a more regular response occurs at the low damping combination $\kappa = 0.5$, $K = 0.003$. Figures 12a,b,d show the influence of high damping where no area of self-excitation exists and where a forced vibration can occur alone. A peculiar situation arises at the combination $\kappa = 1$ and $K = 0.003$ (Fig.12f). In spite of the existence of a small self-excitation area the non-autonomous response does not behave as in cases with larger areas where the left-hand part of the boundary is followed closely.

2. The tenth- and twelfth-order system

2.1. Mathematical description

In the elaborate system shown in figure III.1, to be studied now, approximation II will be applied for the tyre simulation (cf. Sec. II. 6) and a dry-frictional couple for the representation of the damping couple -D. The system will be simplified by making h^* and h equal to zero. After the elimination of some variable quantities and the introduction of the time scale α_t , the non-dimensional equations III. (76) to III. (99) transferred into machine equations read:

$$\mu \frac{V^2}{\alpha_t^2} (\ddot{y} + h_m \ddot{\phi}) - c_y^* y^* - \underline{N' \phi} = 0, \quad (a)$$

$$\mu h_m \frac{V^2}{\alpha_t^2} \ddot{y} + \beta \frac{V^2}{\phi \alpha_t^2} \ddot{\phi} + (c_\phi + c_\phi^*) \phi + \underline{N' y^*} - c_\phi^* \phi^* = 0, \quad (b)$$

$$\mu^* \frac{V^2}{\alpha_t^2} (\ddot{y} + \ddot{y}^*) + \underline{N' \phi} - N (\phi^* + \epsilon \gamma) + c_y^* y^* = F(\alpha), \quad (c)$$

$$\beta_{\varphi}^* \frac{V^2}{\alpha_t^2} \ddot{\varphi}^* + \epsilon \frac{V^2}{\alpha_t^2} \ddot{\gamma} + \beta \frac{V^2}{\alpha_t} \dot{\gamma} - \underline{c_{\varphi}^* (\varphi - \varphi^*)} = -RF(\alpha) + \underline{\mu_{un} V^2 \sin(\alpha_t \tau / R - \epsilon)}, \quad (d) \quad (4)$$

$$\frac{V^2}{\alpha_t^2} \ddot{\gamma} + \epsilon \frac{V^2}{\alpha_t^2} \ddot{\varphi}^* - \beta \frac{V^2}{\alpha_t} \dot{\varphi}^* + K \operatorname{sgn} \dot{\gamma} + \frac{1}{\alpha_t} \kappa \dot{\gamma} + c (\gamma - \gamma_{st}) = -eF(\alpha) + M'(\alpha) + \mu_{un} V^2 \cos \alpha_t \tau / R, \quad (e)$$

$$\beta_{st} \frac{V^2}{\alpha_t^2} \ddot{\gamma}_{st} + c (\gamma_{st} - \gamma) = 0, \quad (f)$$

$$\sigma \dot{\alpha} + \alpha_t \alpha = \alpha_t \dot{\gamma} - \dot{\gamma} - \dot{\gamma}^* + R\dot{\varphi}^* - (1-e) \dot{\gamma}. \quad (g)$$

The terms underlined, which are small with respect to neighbouring terms in the case considered (calculations revealed that amplitude ratios are of the order of 1%), are omitted in the ensuing calculations. Some of these terms, containing N and N' , which were easy to introduce in the circuit have afterwards been checked with the computer; they indeed appeared to have no visible effect on the motion. The second terms in equations (4d,e) accomplish a coupling of the order of magnitude ϵ^2 between φ^* and γ , which will be very small indeed for the case to be considered ($\epsilon \approx 0.01$). In equation (4d), furthermore, the impressed couple (last term) is negligible with respect to $RF(\alpha)$.

2.2. Simulation of test vehicle

The system described in the preceding section will be examined now for parameter values close to those applicable to the test vehicle. The experiments on the road, carried out with the test truck, are discussed in chapter VI. The results from this experimental investigation may be compared with the results obtained here through simulation.

The parameter values based on measurements on the vehicle are listed in table 1 (for definition of non-dimensional quantities cf. Table III.1, p. 79). For distinction, the symbols indicating non-dimensional quantities are underlined again.

Table 1. Parameters values of test vehicle

WITH DIMENSION	NON-DIMENSIONAL
TYRE (cf. Sec. II.6) (9.00-16 in; $p_1=1.75$ bar = 25 lb/in ² \approx half of normal pressure)	
$F(\alpha)$ and $M'(\alpha)$: cf. Fig.13 $C = 70000$ N/rad $e' = 0.086$ m $a = 0.138$ m $\sigma = \sigma^* = 0.21$ m $R = 0.5$ m $x = 810$ Nm ² $N = 10000$ N	$e' = 0.62$ $\frac{a}{R} = 1.5$ $\frac{R}{N} = 3.6$ $\frac{x}{N} = 0.6$ $\frac{N}{N} = 0.143$
WHEEL/STEERING SYSTEM	
$\epsilon = 0.0094$ $e = 0.0047$ m $K = 44$ Nm $\delta = 0$ $c = \begin{cases} 6700 \text{ Nm/rad (locked st.syst.)} \\ 3750 \text{ Nm/rad (released st.syst.)} \end{cases}$ $I = 5.4$ kgm ² $I_a = 5.3$ kgm ² $n^2 I_{st} = 3.8$ kgm ² $m_{un} = 0.11$ kg $\lambda_{un} = 3.15$ m	$\epsilon = 0.0094$ $\frac{e}{K} = 0.034$ $\frac{K}{\delta} = 0.0045$ $\frac{c}{I} = \begin{cases} 0.69 \\ 0.39 \end{cases}$ $\beta = 0.27$ $\beta_{st} = 0.7$ $\mu_{un} = 0.00038$ $\lambda_{un} = 2\pi R = 23$ $\omega_{un} = 1/R = 0.274$
UNSPRUNG MASS/SUSPENSION	
$c_y^* = 2 \times 10^6$ N/m $c_\phi^* = 2.7 \times 10^5$ Nm/rad $m^* = 170$ kg $I_\phi^* = 10$ kgm ²	$\frac{c_y^*}{m^*} = 3.95$ $\frac{c_\phi^*}{I_\phi^*} = 28$ $\mu^* = 0.6$ $\beta_\phi^* = 1.85$
SPRUNG MASS	
$c_\phi = 8 \times 10^5$ Nm/rad $m = 850$ kg $I_\phi = 350$ kgm ² $h_m = 0.4$ m	$\frac{c_\phi}{m} = 80$ $\mu = 30$ $\beta_\phi = 65$ $\frac{h_m}{m} = 2.9$

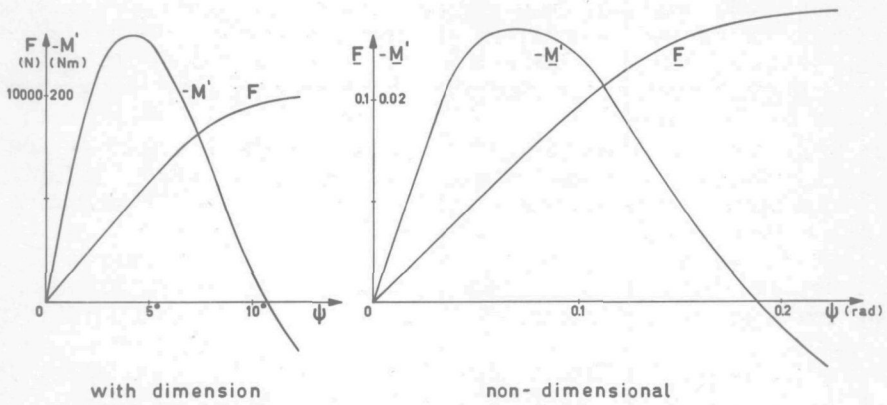


Fig.13. Cornering characteristics of tyre of test vehicle.

Furthermore the following relations hold (cf. Table III.1):

$$\left. \begin{aligned}
 V &= 5.87 \frac{V}{R} \quad (\text{m/s}) = 21 \frac{V}{R} \quad (\text{km/h}) \\
 \omega &= 42.4 \frac{\omega}{R} \quad (\text{rad/s}) = 6.75 \frac{\omega}{R} \quad (\text{c/s}) \\
 \omega_s &= 7.25 \frac{\omega_s}{R} \quad (\text{rad/m}) \\
 \omega_{un} &= 7.25 \frac{\omega_{un}}{R} = 7.25/R \quad (\text{rad/m}) \\
 \lambda &= 0.138 \frac{\lambda}{R} \quad (\text{m}) \\
 \lambda_{un} &= 0.138 \frac{\lambda_{un}}{R} = 0.87 \frac{R}{\lambda_{un}} \quad (\text{m})
 \end{aligned} \right\} \quad (5)$$

The results of the analogue computations will be given in dimensional form. Since most features are similar to those found in the lower order systems, discussed before, we may restrict ourselves to a short treatment of the results.

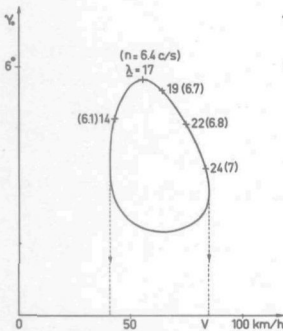


Fig.14. The area of self-excitation.

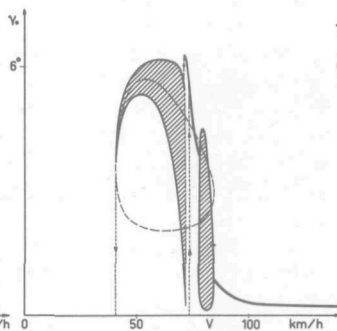


Fig.15. The response to unbalance torque.

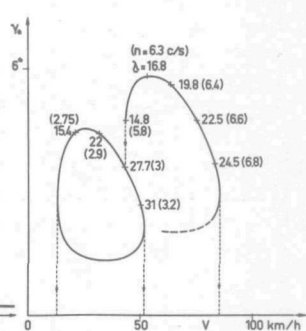


Fig.16. The influence of releasing the steering system.

Figure 14, qualitatively corresponding to figure 9, shows the area of self-excitation of the 10th-order system with the steering system clamped at the node ($\gamma_{st} = 0$, $\underline{c} = 0.69$). The instantaneous frequencies are indicated along the stable part of the curve.

Figure 15, qualitatively corresponding to for instance figure 11e, shows the non-autonomous response of the same system. The dotted curve indicates again the area of self-excitation of the autonomous system. The predominant frequency varies approximately according to values indicated in figure 14. A remarkable agreement with results obtained experimentally appears to exist (cf. Fig. VI.4). The speed at which shimmy starts, the synchronous response, the beating area, the amplitude level, the order of magnitude of the frequency and the speed at which shimmy dies out appear all to be in agreement with the actual behaviour. It may be noted that in contrast to the third-order system (Fig. 11c) the amplitude decreases here rather sharply at higher speeds which is a result of the gyroscopic action.

Figure 16 illustrates for the autonomous system the effect of releasing the steering system ($\gamma_{st} \neq 0$, $\underline{c} = 0.39$). The additional area of self-excitation, predicted in the analytical study (see Fig. IV.22), indeed appears. The area for supercritical shimmy is nearly unchanged with respect to that of figure 14. The motion jumps over from this area to the left-hand area where subcritical shimmy occurs. A way back does not appear to be possible. When varying the velocity V the motion will follow the upper boundary of the subcritical area until it dies out as indicated in the figure. It appears that a stable stationary oscillation of both modes combined is not possible. Only a transient combination of the two oscillations has been observed at the transition from one vibration to the other. Due to the fact that at lower frequencies and velocities the gyroscopic couple due to tyre deformations decreases, the amplitudes are expected to become somewhat larger in reality in the subcritical range than as predicted with the aid of the approximate tyre simulation employed (cf. Sec. II.6). The qualitative correspondence with the behaviour of the mechanical model was very good (cf. Sec. VI.3). By loosely holding the steering-wheel, the driver may very easily suppress the subcritical oscillations.

2.3. Influence of changing parameter values

The influence of changing tyre quantities, damping and caster will not be discussed again. An influence similar

to that of the third-order system as discussed in Secs. IV.1.2 and IV.2.3D has been found.

How the non-autonomous response is influenced by a reduction in self-excitation, in this case due to an increase in κ , is shown in figure 17, the first part of which being identical to figure 15. The self-excitation area vanishes and the amplitudes become smaller and occur only at high speeds.

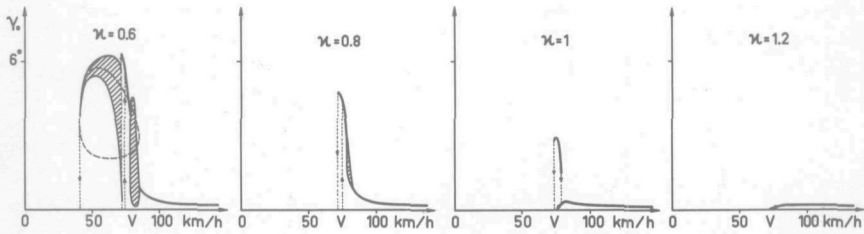


Fig.17. The influence of more damping (κ) upon the response to unbalance torque.

A small change in wheel radius has almost no influence on the area of self-excitation. It, however, does influence the unbalance frequency directly. The latter effect is shown in figure 18. A change in wavelength of the unbalance tor-

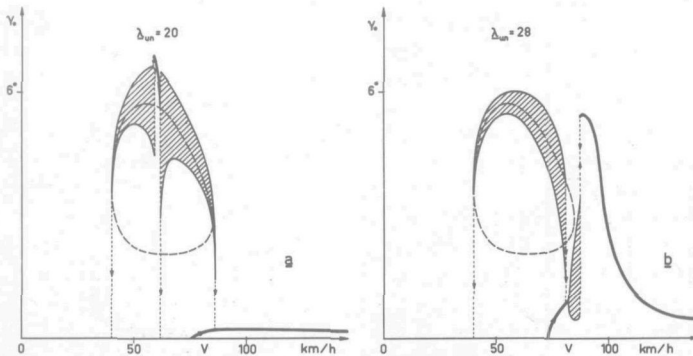


Fig.18. The influence of changing the wavelength of unbalance torque λ_{un} upon the response.

que (i.e. the wheel circumference) from $\lambda_{un} = 23$ (original value, Fig.15) to $\lambda_{un} = 20$ ($\omega_{un} = 0.274$ to 0.315) which corresponds to a decrease in wheel radius to the same ratio, results in an isolation of the self-excitation area and in an amplitude course of the forced vibrations on a very low level. For the unbalance mass considered the high amplitude shimmy may only be reached through an ex-

ternal disturbance. An increase in unbalance wavelength to $\lambda_{un} = 28$ ($\omega_{un} = 0.225$) also causes isolation of the self-excitation area, which illustrates that the required wheel radius for attaining self-excited shimmy is rather critical

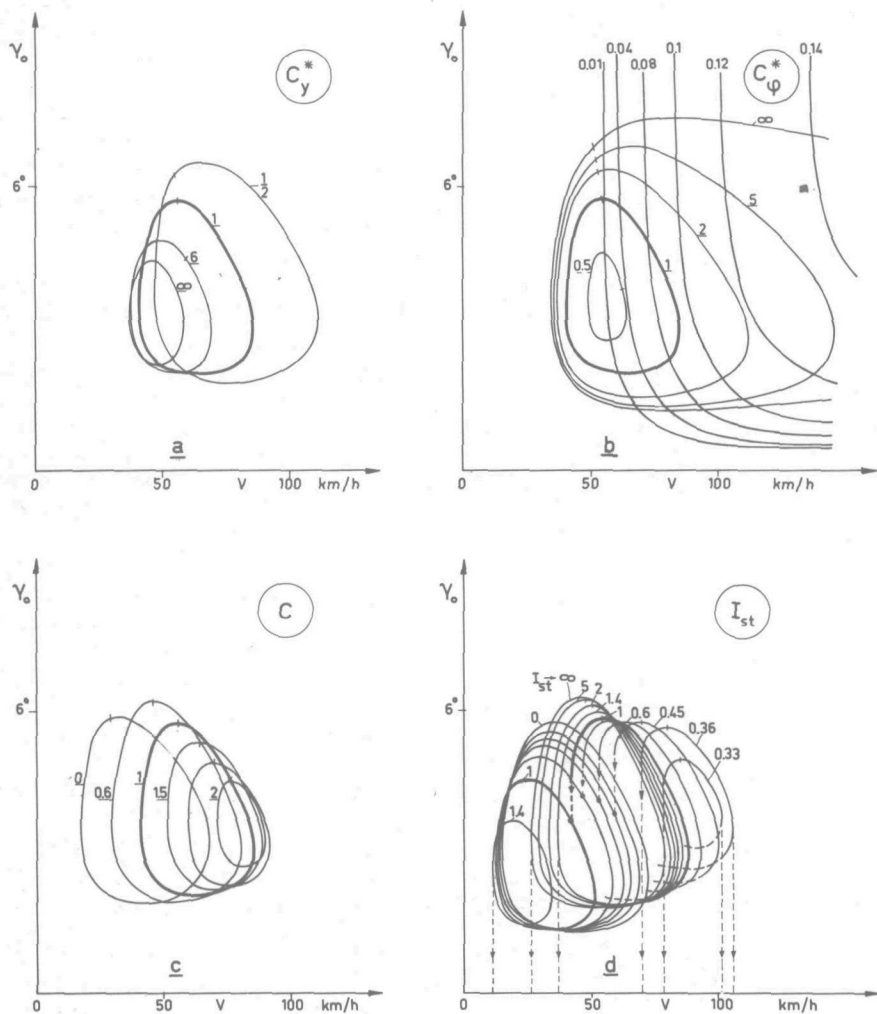


Fig. 19. The influence of some parameters upon the area of self-excitation,
 a: Lateral suspension stiffness C_y^*
 b: Torsional suspension stiffness C_ϕ^*
 c: Torsional stiffness of steering system c .
 d: Moment of inertia of steering-wheel I_{st} (steering system released).

in this case. It appears that in the case of $\lambda_{un} = 28$ the amplitude can reach high values but only in a narrow band at higher speeds, where resonance occurs.

How the area of self-excitation is influenced by the parameters c_y^* , c_ϕ^* , c and I_{st} is shown in figure 19. On the curves, points are indicated (dashes), where the wavelength of the motion equals 17 times half the contact length. The parameter values are given as a ratio to the original values.

An increase in c_y^* , i. e. a lateral stiffening of the suspension, causes a decrease in area of self-excitation. Finding that an increase in torsional stiffness c_ϕ^* stimulates shimmy results from the reduction in stabilizing effect due to gyroscopic coupling. When $c_\phi^* \rightarrow \infty$ we find nearly the same curve as that obtained in the case that both terms, denoting the gyroscopic coupling (β), are omitted in the equations (4). A sharp decrease in torsional stiffness may cause gyroscopic shimmy, a phenomenon which has been discussed before. The amplitude of the gyroscopic shimmy does not appear to be limited with the model simulated since no stops restricting the torsional motion are employed.

The torsional stiffness c_ϕ of the chassis appears to have an influence similar to that of the suspension c_ϕ^* . A decrease in sprung mass m , furthermore, causes the area to reduce in size. At about one tenth of its original value the area vanishes.

Again referring to figure 19 we note that with a clamped steering system an increase in stiffness c of the steering system causes the area to shift to the right and finally to vanish due to gyroscopic action. The points representing a certain wavelength shift at practically the same amount, which means that the variation in shimmy frequency occurs almost proportionally to the shift in area. By changing the stiffness it is obviously not possible to get the frequency of excitation out of the area of self-excitation. The phenomenon takes place only in another velocity range.

How a change in moment of inertia of the steering-wheel I_{st} influences the system can only be found with the aid of the 12th-order system, thus with the released steering system. As figure 19d shows, it appears that at a sufficiently low or high moment of inertia the two areas separate from each other. Finally one of the areas will vanish. The two extreme cases, viz. blocked steering-wheel or $I_{st} \rightarrow \infty$, and no steering-wheel or $I_{st} = 0$, are indicated.

A picture similar to figure 19d arises for the released steering system when c is varied. Concerning the supercritical motion, the area varies similarly to the variations shown in figure 19c. In general it is found that an increase

in the moment of inertia I_{st} has an effect opposite to the influence of an increase in the stiffness c which indicates that in fact the natural frequency of the steering system is of basic importance.

CHAPTER VI

EXPERIMENTAL INVESTIGATIONS

In order to substantiate the preceding theories developed, we carried out a series of full scale tests with an automobile on the road, full scale tyre experiments on the drum test stand and experiments with a small mechanical model capable of showing shimmy. In the subsequent sections, these investigations will be described.

1. *Full-scale experiments with test vehicle on the road*

With a one-ton weapon carrier tests have been carried out on a two mile long landing strip. The truck, equipped with independent front and rear wheel suspensions (trailing arms) was driven through its rear wheels. The tyres were provided with NATO terrain profile (blocked pattern with



Fig.1. Test vehicle equipped with measuring apparatus.

centre rib). The parameter values of the vehicle have been enlisted in section V.2.2. Figure 1 shows the vehicle with apparatus for measurements and a special device for pulling off the unbalance from the front wheel during running. In figure 2 a diagrammatic view of the vehicle is shown;

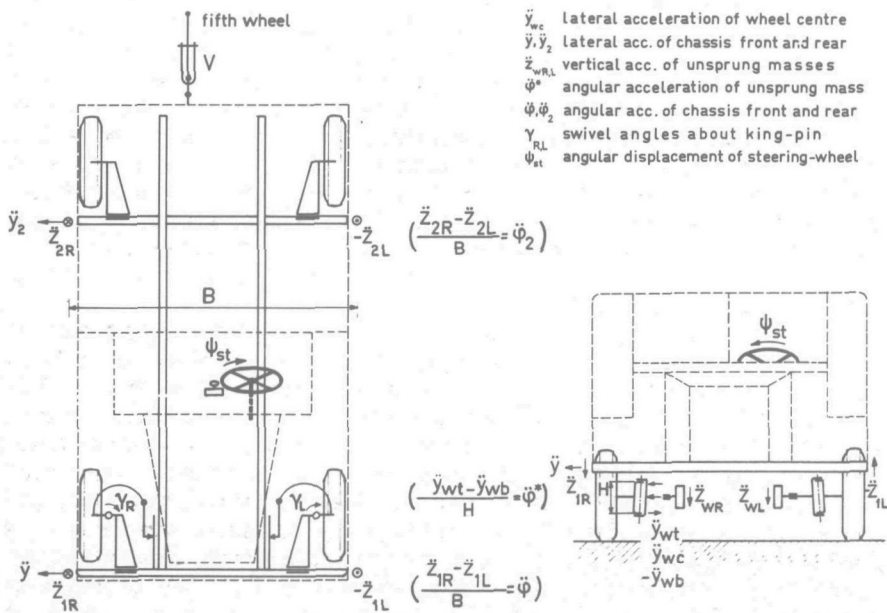


Fig.2. Diagrammatic view of test vehicle showing signals registered.

arrows indicate signals measured by means of accelerometers and potentiometers. In addition to the signals shown in the figure, also the period of revolution of the right front wheel, measured by means of an inductive pick-up situated opposite to the unbalance mass, and the moment of removing the unbalance were registered on a magnetic tape.

A series of tests were carried out in order to find the amount of unbalance mass on both front wheels capable of initiating shimmy. As a result of these tests, unbalance masses of 600 gram on each of the front wheels, which corresponds to the value $\mu_{un} = 0.38 \times 10^{-3}$, were chosen for the subsequent experiments with which the influence of varying several parameters such as suspension stiffnesses, unsprung- and sprung mass, damping, tread pattern and inflation pressure, was investigated. The normal tyre inflation pressure of 55 lb/in² was reduced to 40 lb/in² and

finally to 25 lb/in², the latter normally being used under off-road conditions. The pressure of 25lb/in² effected a violent self-excited shimmy motion and is taken as the basic value for the investigation of the influence of the remaining parameters and for the analogue computations.

The time history of the shimmy motion for three cases of inflation pressure, $p_i = 55, 40$ and 25 lb/in², where the degree of self-excitation increases with decreasing p_i , is shown in figure 3a,b,c. In the graphs are shown: the curve for the amplitude γ_o of the right front wheel, the variation in forward speed V as well as the periods of the swivel motion T_γ and of the revolutions of the right front wheel T_χ ; all values are shown as functions of time. The situation of the unbalances left and right with respect to each other, are also indicated in the figures. The phase lead $\phi_{\gamma\chi}$ of the shimmy motion with respect to the wheel revolutions, i.e. to the unbalance moment, of the right front wheel are shown in separate diagrams.

In the figures 3a,b a slowly increasing and dying out of the wheel motion in periods of about 15 seconds is noted. This feature of slow beats is the result of a small difference in effective rolling radius left and right, which causes the unbalances to vary their relative position continuously and thereby causes the resulting unbalance moment to vary periodically in amplitude. This amplitude will attain its maximum when the unbalance masses are situated opposite in phase and the amplitude will be reduced to zero when the unbalance masses are in phase (cf. indications in the figures). These beats are closely connected to systems showing no or little self-excitation. In the case shown in figure 3c this sort of beats does not occur, which points to the existence of sufficient self-excitation.

When driving carefully, with a speed at which the system is most sensitive for the initiation of shimmy, it appears that also in the former two cases, a and b, rather large amplitudes may be reached. Even a tendency to exert a self-sustained motion, thus not depending on unbalances, is shown to exist in these cases (cf. differences in courses of T_γ and T_χ curves). In the case of figure 3a, with $p_i = 55$ lb/in², the component of the shimmy motion which tries to sustain itself, is suppressed immediately as soon as the unbalance moment differs too much in phase with respect to the motion. One period of the motion T_γ suddenly became large in duration (note peak), thereby causing the motion to get in its original phase again. The shimmy motion does not appear to be able to sustain itself under the action of the unbalance moment. Various tests where

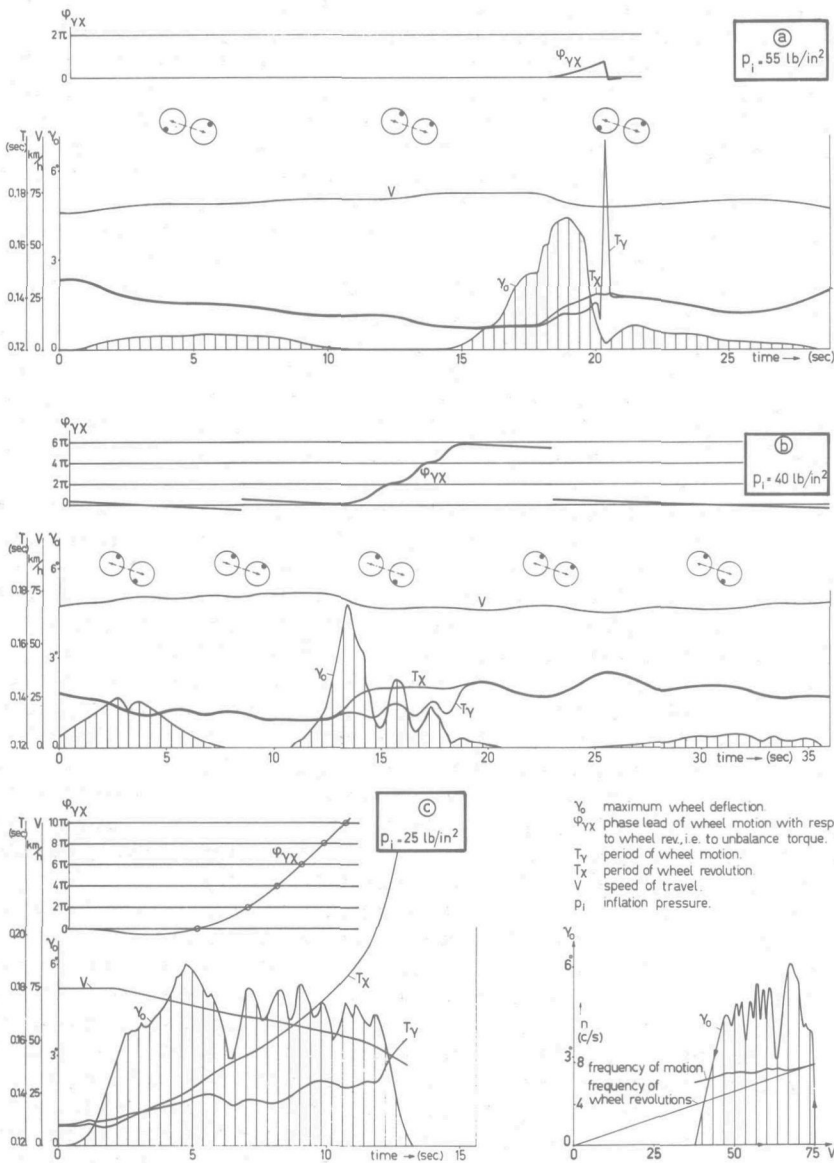


Fig. 3. Time histories for three cases of inflation pressure: $p_i=55$ (a), 40 (b), 25 lb/in² (c).

γ_0 maximum wheel deflection
 Φ_{YX} phase lead of wheel motion with respect to wheel rev, i.e. to unbalance torque.
 T_Y period of wheel motion.
 T_X period of wheel revolution.
 V speed of travel.
 p_i inflation pressure.

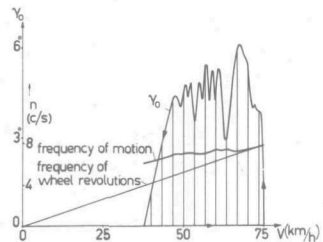


Fig. 4. Wheel deflection and frequencies as functions of speed ($p_i=25 \text{ lb/in}^2$).

the unbalance mass is pulled off during the violent oscillations, reveal furthermore that the motion under the circumstances of figure 3a always dies out directly or within short time after that the unbalance mass has been removed. In the case of figure 3b with $p_i = 40 \text{ lb/in}^2$, obviously a greater degree of self-excitation occurs. During the second beat the speed has the most sensitive value and the shimmy motion is able to get ahead in phase a few times 2π radians with respect to the wheel revolutions; this in contrast to the former case where the motion returns to its original phase. The drop in speed during the violent oscillations might have been the reason that the motion did not sustain itself. Pulling off the unbalance at the right instant probably might have resulted in a self-sustained oscillation.

In the case of figure 3c the inflation pressure is reduced to 25 lb/in^2 which results in a real self-sustained shimmy motion. Figure 3c is transformed to the amplitude - velocity graph of figure 4, which may be compared with the graph of figure V.15 obtained with the aid of the analogue computer. We notice a very good correspondence between the two. It appears that shimmy occurs in a velocity range between 75 and 40 km/h. It is always required, however, to raise the speed of travel first, until the unbalance moment becomes large enough to start the vibration. When the frequency of the forced oscillation approaches the natural frequency of the system, larger amplitudes arise and the motion may sustain itself from that instant on, owing to the fact that then the lower amplitude range, where the dry friction has predominant influence, has been exceeded. When the speed is lowered again, it is seen that after some time the periods of the wheel revolution and of the shimmy motion obtain courses completely different and independent of each other, which strengthens the opinion that here the motion sustains itself. From the phase diagram (Fig. 3c) it is seen that a peak of the amplitude occurs each time when the phase difference amounts to an integer times 2π .

For the same case ($p_i = 25 \text{ lb/in}^2$) another test has been carried out with an unbalance mass attached to the right front wheel alone. After the violent shimmy oscillations had started, the unbalance mass was removed from the wheel. From then on the wheels were completely in balance. The shimmy appeared to continue without showing much difference in amplitude course with respect to the case with unbalance as shown in figure 3c. This experiment formed the final proof that the shimmy observed was a self-sustained oscillation. The phase and amplitude relationships measured at an instant shortly after the unbalance was removed,

are plotted in vectorial form in the complex plane as shown in figure 5. The vectors rotate counter-clockwise with an

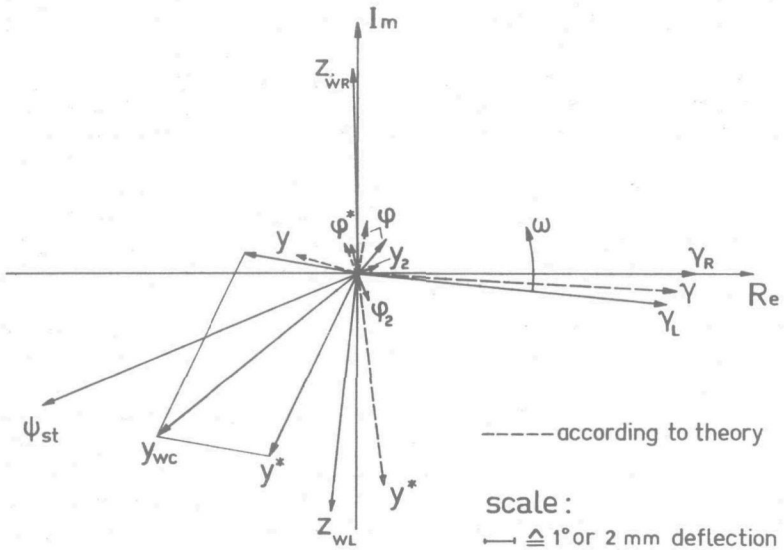


Fig. 5. Phase diagram of signals according to Fig. 2.

angular velocity ω . The dashed vectors originate from analogue computer results for the case shown in figure V.14. A fair correspondence has been found considering the fact that the measurements of the phase relationships for both analogue computer and full scale test results are rather inaccurate.

A change in unsprung and sprung mass of 10 - 20 % obtained by attaching weights to the respective parts did not show an essential difference in behaviour. The same results arose with a nearly locked steering-wheel and in the case of locking the vertical springing action of the suspension arms relatively to the chassis. A lateral stiffening of the suspension by a ratio of about six through the introduction of cross arms resulted in an improvement in behaviour. Only a forced oscillation with an angular wheel deflection of about two degrees occurred within the speed range of 70 - 80 km/h. This result has been predicted indeed theoretically; the maximum resonance amplitude found with the analogue computer, however, was of the order of 4° . A hydraulic steering-damper which acts on the steering-rod connecting the two wheels, influenced the behaviour in a

similar way, as has been expected. The employment of tyres with a special tread pattern consisting of three longitudinal ribs and with a somewhat shorter contact length resulted in a complete disappearance of any tendency to shimmy. The effect may be explained by the fact that through the stiff longitudinal ribs and the shorter contact length (the latter resulting in a smaller cornering stiffness C_M) the ratio $\kappa/C_M a$ is increased with respect to the corresponding value for the original tyre (cf. Sec.2), so that a relatively higher damping by longitudinal tread deformations is obtained. These results correspond to those obtained by Marstrand [42] who carried out experiments with aircraft fitted with two-rib tyres.

2. Tyre frequency response tests on rotating drum

The tyre response to sinusoidal inputs could not be measured on the road since no adequate equipment was available for that purpose. In order to obtain an idea of the qualitative aspects of the response we have carried out tests on a rotating drum (2.5 m diameter) which replaces the road surface. Similar experiments with a small model tyre have been carried out by Saito [31].

Owing to the curvature of the drum surface and the difference in tangential contact properties we may expect a quantitative difference between the response on the drum and on the road. As an illustration, the stationary characteristics of the original tyre with blocked tread pattern and with an inflation pressure of 25 lb/in², as measured on the drum shown in figure 7, may be compared with the characteristics shown in figure V.13 which resulted from road measurements.

The frequency response experiments have been carried out with the aid of an excitation test stand shown in figure 6. The wheel is swivelled, as it rolls over the drum, together with the whole structure in which the wheel axle is mounted. The structure is excited against four coil-springs in the resonance frequency, so that only a small force of excitation is needed. A special measuring device mounted in the wheel (cf. Van Eldik Thieme [44]) gives the electrical signals from which the resulting forces and moments acting in the contact area can be derived. Because of the fact that the mass of the wheel distorts the signal, a correction needs to be applied to account for this.

A number of experiments have been carried out in which the swivel amplitude and frequency are kept constant, but

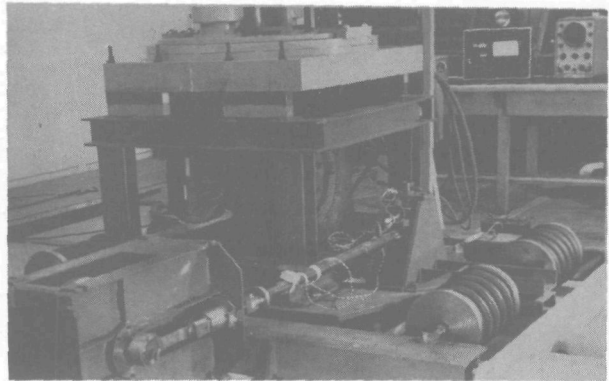
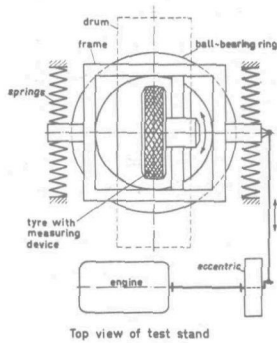


Fig. 6. Shimmy excitation test stand for measuring tyre frequency response.

where the drum speed is varied and consequently the wavelength is changed proportionally with the speed. The block patterned tyre is compared with the ribbed tyre and the in-

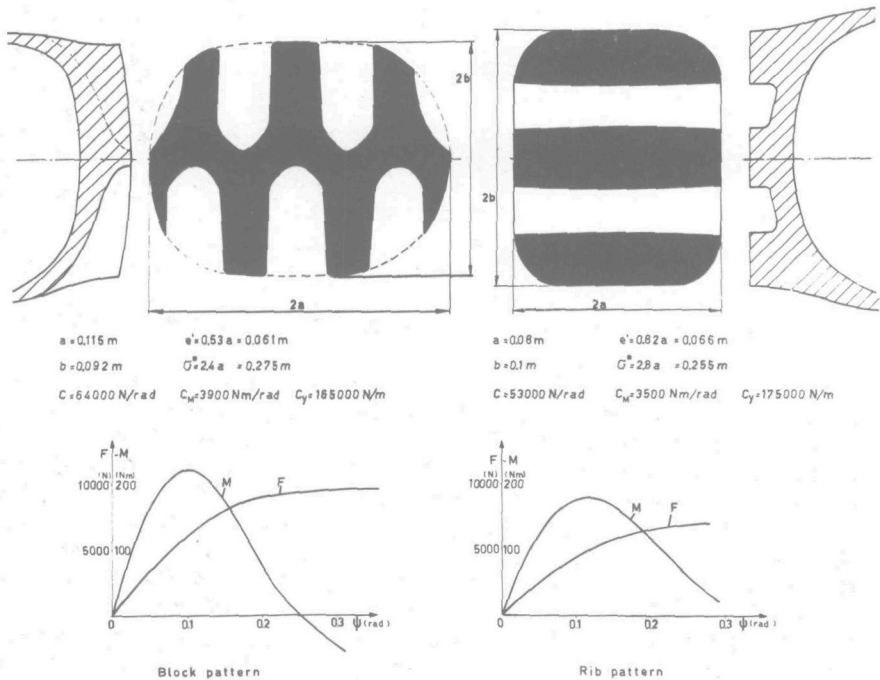


Fig. 7. Tyre data according to measurements on drum test stand (9.00-16 in; $p_1=25 \text{ lb/in}^2$).

fluence of amplitude and frequency is studied for the original block patterned tyre. The prints of the contact patches and the cross-sections of the tyres together with the stationary tyre characteristics and tyre constants at zero slip angle are shown in figure 7. The relaxation length σ^* is computed again by means of the formula II. (144).

The frequency response curves measured for both tyres are shown in figure 8. The moment and force are divided

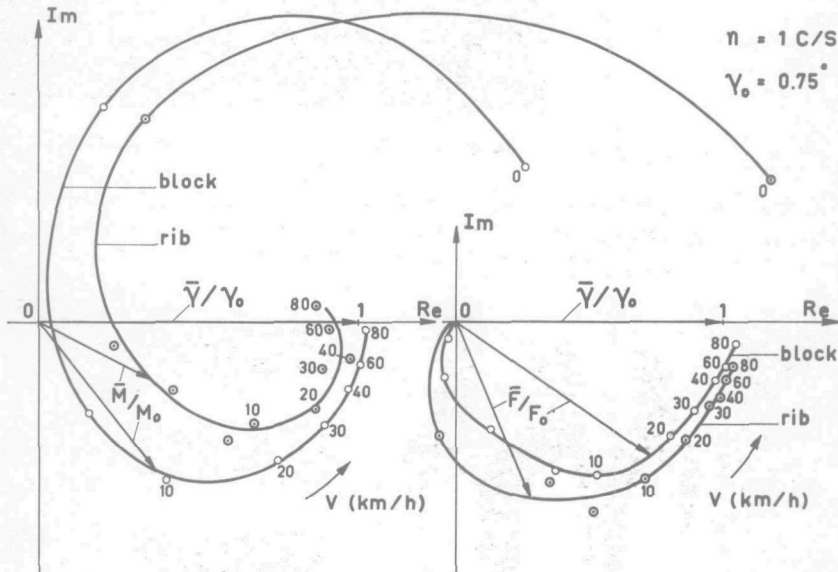


Fig.8. Experimentally obtained tyre response curves to sinusoidal inputs.

by their respective stationary values M_0 and F_0 ($\omega_s \rightarrow 0$). The experiments are carried out with an amplitude $\gamma_0 = 0.75^\circ$ and a frequency $n = 1 \text{ c/s}$. In figure 9 theoretically obtained curves are shown for $\sigma^* = 2.4a$ and $\epsilon = 1/7.5$; the gyroscopic effect of the tyre is neglected here (cf. figure II.14 where $\sigma^* = 3a$). We note the similar shape of the theoretical and experimental curves. The speed values, indicated along both sets of curves, agree very well with each other. Comparison between the theoretical curves and the experimental curve for the block patterned tyre leads to the estimation $\kappa = 0.25C_M a = 112 \text{ Nm}^2$. The relation between velocity and frequency for a given wavelength is governed by the equation:

$$V = \omega/\omega_s = 2\pi n/\omega_s = n\lambda$$

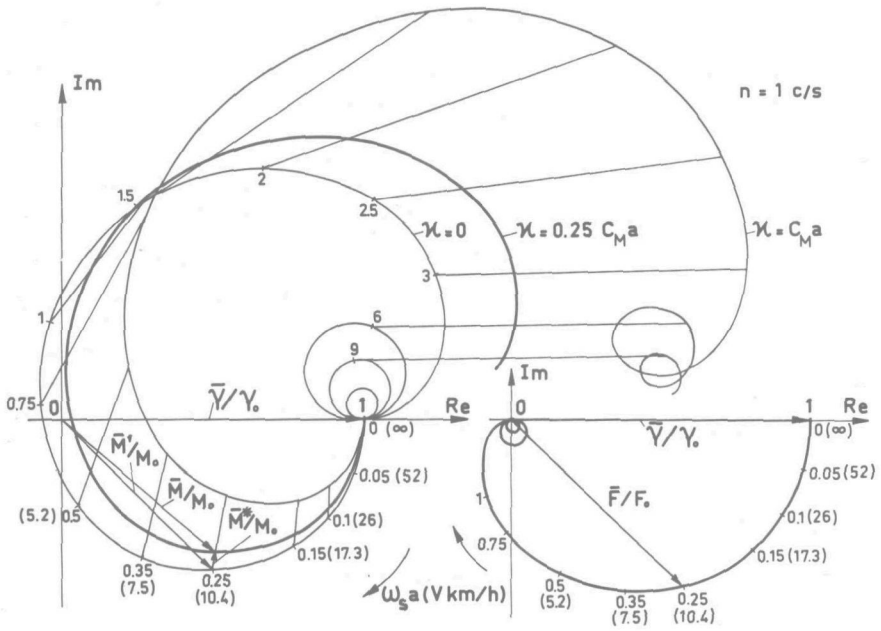


Fig.9. Theoretically obtained tyre response curves to sinusoidal inputs.

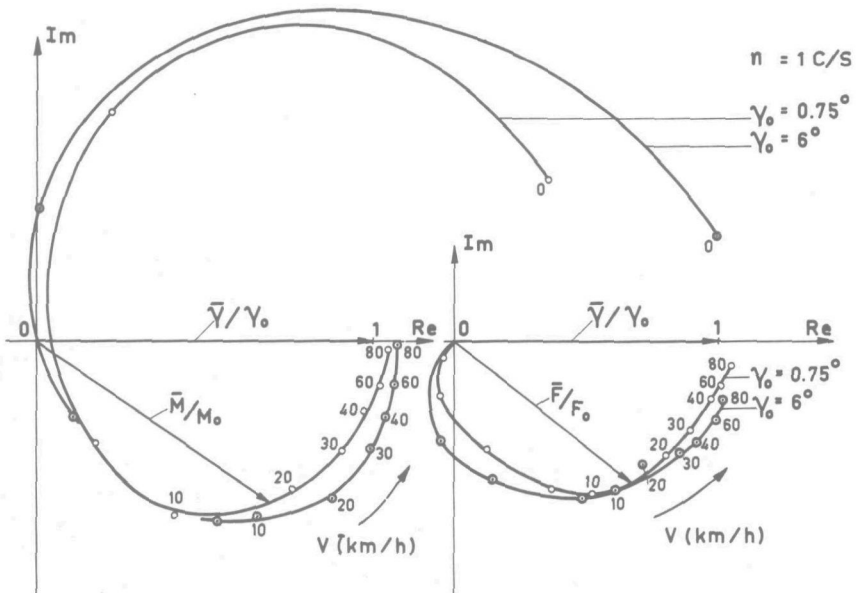


Fig.10. The influence of the amplitude of the motion upon the response (experimental).

already being introduced in Sec.II.4A.

In figure 10 the influence of an increase in amplitude is shown. The moments and forces are again divided by their stationary values. We notice that the velocity values, indicated along the curve for the moment at $\gamma_0 = 6^\circ$, are shifted slightly counter-clockwise with respect to those for $\gamma_0 = 0.75^\circ$. This may point to the existence of a lower average value of the relaxation length, already predicted theoretically (cf. Sec.II.3B, p.29). We have estimated that the effective relaxation length is reduced from $\sigma^* = 2.4$ for vanishing amplitudes to $\sigma^* = 2$ when the amplitude is increased to $\gamma_0 = 6^\circ$. The fact that the final point of the moment for $V=0$ is located further to the right at higher amplitudes, is due to the property that the cornering characteristic has a more degressive shape than the torsion characteristic of the non-rolling tyre.

Figures 11 and 12 show the influences of the frequency

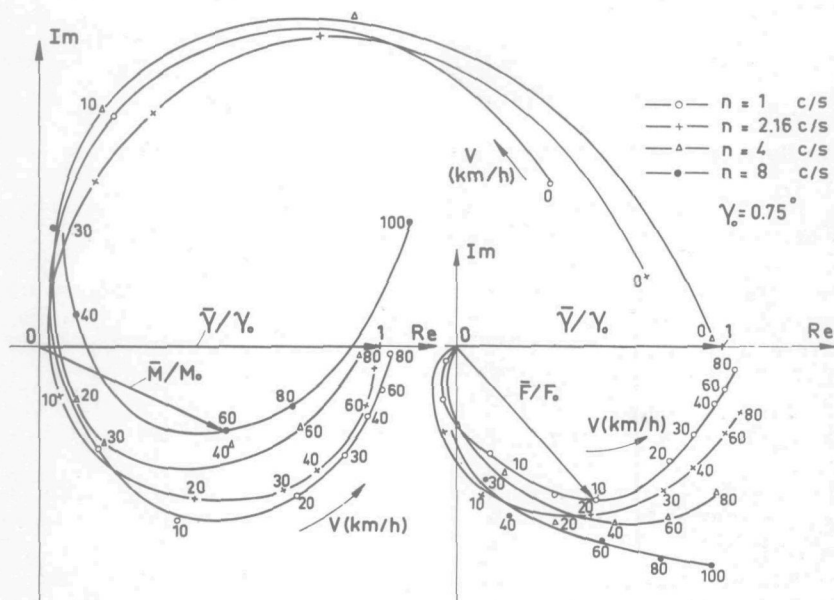


Fig. 11. The influence of the frequency of the motion upon the response (experimental).

of the swivel motion. The curves obtained experimentally (Fig.11) show clearly that a time influence exists. With increasing frequency the curves rise in the lower right quadrant. This phenomenon is explained theoretically by introducing

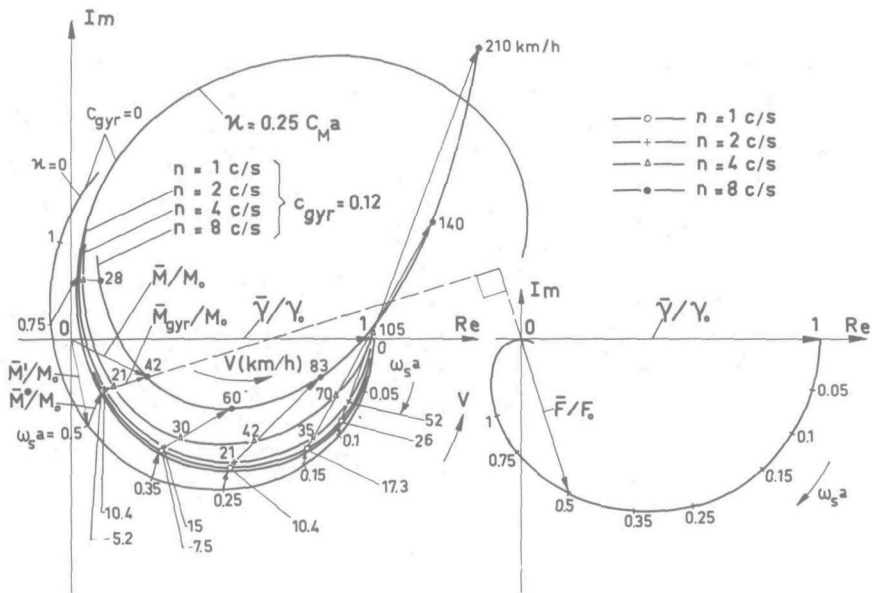


Fig. 12. The influence of the frequency of the motion upon the response (theoretical).

the gyroscopic effect in the tyre theory (cf. Sec. II. 6). Theoretically obtained curves are shown in figure 12. We have made use of the value $\kappa = 0.25 C_M a$ and of the tyre data listed in figure 7 for the block patterned tyre; the value $C_{gyr} = 2.5 \times 10^{-5} \text{ sec}^2$, furthermore, appeared to fit best. With a tyre mass $m_t = 35 \text{ kg}$ and a lateral stiffness $C_y = 165000 \text{ N/m}$ we obtain for the non-dimensional quantity c_{gyr} the value $c_{gyr} = 0.12$; from this value it can be derived that about $1/5$ of the tyre polar moment of inertia takes part in producing the gyroscopic couple.

The end points where $V=0$, shown in figure 11, appear to get situated farther to the right and somewhat lower at increasing frequencies. This may be explained by means of the visco-elastic property of tyre rubber, which shows larger stiffness and less damping at higher frequencies (cf. Van Eldik Thieme [44]). The amplitude of the force appears to increase with increasing frequency, while the phase lag remains about constant for a given wavelength. This property has not yet been explained theoretically. The influence of a larger force amplitude has been tried out in the simulation of the test vehicle; it appeared to be negligible.

3. Experiments with mechanical model

Figure 13 shows a model capable of showing shimmy.

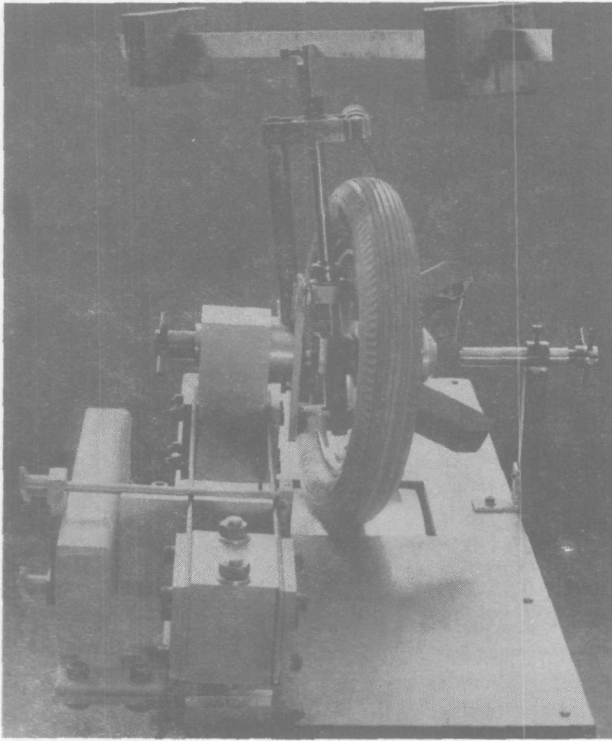


Fig. 13. Model capable of showing shimmy.

The miniature wheel with a $12\frac{1}{2}$ - $2\frac{1}{4}$ in tyre rolls over a drum driven by an electric motor. The caster can be varied by changing the angle of inclination of the king-pin. The lateral stiffness of the king-pin suspension can be adjusted by varying the effective length of the two leaf-springs which are clamped at the ends. The king-pin bearings, which are practically frictionless, can be provided with adjustable damping with the aid of a dry-friction element. The steering system is simulated by a thin leaf-spring mounted on top of the king-pin, carrying two masses at its ends. An unbalance mass can be attached to the wheel. Provision has been made for removal of the unbalance mass during running.

The test results were found to be in good agreement with the theory. In figure 14 an example of the response to unbalance torque is shown. The synchronous response to-

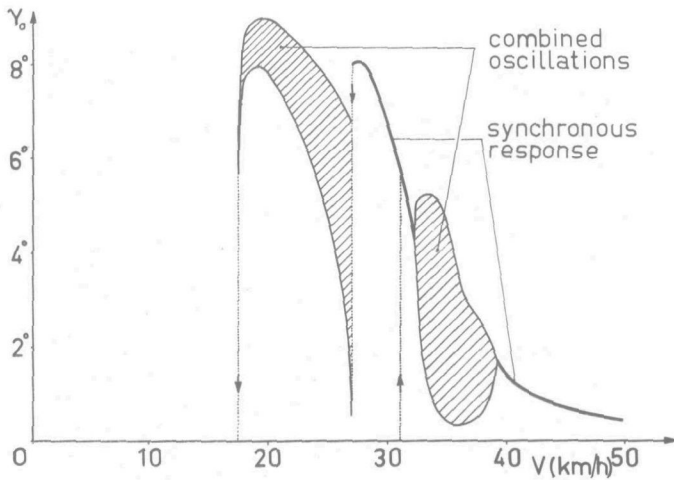


Fig. 14. Test results of mechanical model with clamped steering system. The response to unbalance torque.

gether with the adjoining regions of combination oscillations, found in chapter V (Figs. V. 11, 15), were also observed with this model. Other characteristics of the motion, such as the dying out of the shimmy below a certain speed and the decrease of the amplitude at higher speeds, also occurred. When the steering-wheel was released, indeed an additional range of low frequency shimmy at lower speeds arose. As anticipated, the limited change in lateral stiffness of the suspension showed a relatively small effect on the shimmy motion. The variation of the wheel caster, however, influenced the behaviour considerably. Pulling off the unbalance mass during running did not affect the shimmy deflection appreciably; the beat phenomenon, however, did disappear as anticipated. Apart from the excitation with unbalance masses the shimmy could also be initiated by an imparting jerk.

CHAPTER VII

CONCLUDING REMARKS

The theory presented gives an adequate description of the observed shimmy phenomenon in both qualitative and quantitative respect. The close agreement obtained especially owes its success to the introduction of non-linear elements.

Concerning the theoretical analysis we may state the following. The method of equivalent linear equations is a useful tool in solving the non-linear differential equations. When used in connection with the digital computer, it gives reasonably accurate results in a relatively short time. The analogue computer, however, allows for an investigation of the system in much greater detail; transient motions and the influence of an exciting couple can be examined.

Concerning the results of this investigation we may conclude that shimmy is caused either by a relatively low lateral stiffness of the tyre, sometimes in combination with the suspension, or by the gyroscopic coupling when the wheel system has a very low natural frequency about a longitudinal axis (live axle, especially when the wheels bounce off the road). Shimmy gets initiated only when sufficient external excitation such as a moment due to wheel unbalance is present.

The principle factors which influence shimmy, are listed below (items 2 and 4 have not been investigated in detail). Numbers in between brackets refer to sections in which the influence is investigated.

1. Increase of the following quantities stimulates tyre shimmy:
 - a) Pneumatic trail e' , which is a function of tyre construction, contact patch length $2a$, inflation pressure p_i , wear, etc. (IV.1, IV.2.3D).
 - b) Caster length, i.e. the mechanical trail e (IV.1.2).
 - c) Tyre relaxation length σ^* , effected by the same factors as mentioned in 1a (IV.1.2).
 - d) The reciprocal value of the lateral stiffness of the suspension $1/c_y^*$ (IV.1.3, IV.2.4).
 - e) The stiffness of the wheel system about a longitudinal axis c_ϕ^* (IV.1.3, IV.2.4).

- f) Wheel bearing play δ (IV.2.3B).
2. Increase of the following quantities stimulates gyroscopic shimmy:
 - a) The reciprocal value of camber torsional stiffness $1/c_{\phi}^*$ (IV.1.3, IV.2.4).
 - b) Certain range of gyroscopic coupling I_a/I (IV.1.3, IV.2.4).
 - c) The height of longitudinal axis of rotation above road level $R + h^*$ (IV.1.3, IV.2.4).
 3. Increase of the following quantities reduces tyre shimmy:
 - a) King-pin viscous damping coefficient k (IV.1.2).
 - b) King-pin dry-frictional couple K (IV.2.3A).
 - c) Coefficient of damping due to longitudinal tread deformation κ (IV.2.3D).
 - d) Tyre mass m_t (II.6).
 - e) Natural frequency of steering system $\sqrt{c/n^2 I_{st}}$ (V.2.3).
 4. Increase of the following quantities reduces gyroscopic shimmy:
 - a) Damping about longitudinal axis by shock absorbers (most likely).
 - b) Quantities 3 a, b and c (IV.2.4).
 5. Quantities causing shift of shimmy speed range:
 - a) The moment of inertia of the wheel assembly about the king-pin I . Increasing I brings down speed range and shimmy frequency (IV.2.3D).
 - b) Natural frequency of steering system $\sqrt{c/n^2 I_{st}}$. Increasing natural frequency raises speed range and shimmy frequency (V.2.3).
 6. Quantities which control the initiation of shimmy:
 - a) Wheel unbalance. For eliminating shimmy this should be less than a certain critical value, depending on the maximum speed and the king-pin dry-frictional couple (V.1.5, V.2.3).
 - b) Wheel rolling circumference. This wavelength of shimmy excitation is significant in relation to the wavelength of shimmy motion (V.1.5, V.2.3).
 - c) Road irregularities, wheel and tyre non-uniformities and sudden steering inputs (VI.3).

As a final remark we may state that the theory presented does not lay claim to be a complete answer to the problems which arise in connection with the shimmy phenomenon. A few points to which attention may be paid in future work are the following:

- a) Non-stationary tyre response at finite values of slip, taking into account the possibility of both partial sliding in longitudinal and in lateral directions (II.5).
- b) Exact influence of tyre inertia and hysteresis on non-stationary tyre response (II.6).
- c) More general analogue simulation of tyre considering the effect of longitudinal deformation and of gyroscopic coupling at vanishing values of slip (II.4, II.6).
- d) Behaviour of total vehicle with more realistic layout of wheel assembly, which may be analyzed by means of the mathematical description given in [47] (III).
- e) Solving the non-linear differential equations of motion by means of numerical integration.
- f) Analytical treatment of combination oscillations occurring with the non-autonomous system and with the system with released steering system (V.1.5, V.2.2).
- g) Influence of second-order terms on limit-cycles and their stability; the latter particularly in relation to the influence of the rate of change of frequency with amplitude (IV.2.2).
- h) Influence of limiting stops and shock absorbers on the gyroscopic shimmy (IV.1.3, IV.2.4).
- i) Influence of road irregularities causing amongst other things variations in dry friction in king-pin bearings.

NOTATIONS

(For non-dimensional quantities cf. Tables II.1 (p. 23), III.1 (p. 79) and IV.1 (p. 92)).

A	amplitude of reference variable
A_0	amplitude of reference variable on the limit-cycle
\bar{A}	transformation matrix
a	half of contact length
$a_{1,2}$	ξ co-ordinates indicating boundaries of adhesion region
a_i	coefficient of characteristic equation
a_{ij}^*	equivalent linear coefficient (stiffness)
b_{ij}^*	equivalent linear coefficient (damping)
b	half of contact width
C	origin of co-ordinate system (C, ξ, η, ζ), contact centre
C	$= \partial F / \partial \psi$, cornering stiffness, Eqs. II. (78-81); equivalent cornering stiffness (non-dim.), Eq. IV. (71)
C_M	$= -\partial M' / \partial \psi$, cornering stiffness, Eqs. II. (78-81); equivalent cornering stiffness (non-dim.), IV. (71)
C_y	static lateral stiffness of non-rolling tyre
C_0	$= \partial F / \partial \alpha$ at zero slip angle ($\alpha=0$)
C_{M0}	$= -\partial M' / \partial \alpha$ at zero slip angle ($\alpha=0$)
C^*	$\approx C_M + eC$, equivalent total cornering stiffness about kingpin (non-dim.)
C_c	$= dF_c / d\phi_w \approx N$, camber stiffness of tyre
C_{gyt}	tyre constant for gyroscopic action, Sec. II. 6
c	half of torsional stiffness of steering system; equivalent stiffness (non-dim.)
c	$\approx 1 / (1/c_p + 1/c_s)$, overall lateral stiffness of tyre per unit length
c_ϕ	half of torsional chassis stiffness
c_y^*	lateral suspension stiffness
c_ϕ^*	torsional suspension stiffness
c_p	lateral stiffness of profile element per unit length
c_s	lateral stiffness of carcass (string + elastic support) per unit length
c^*	longitudinal stiffness of profile elements per unit area

c_{gyr}	non-dimensional tyre constant for gyroscopic action, Sec. II. 6.
D	frictional couple about king-pin acting on wheel, Eqs. III. (62a, b, c, 85a, b, c)
e	= $R\epsilon$, caster length
e'	= C_M/C , pneumatic trail
F	lateral force acting from road on tyre in point C in η -direction
F_c	camber force acting from road on tyre in η -direction
F_{tot}	= $F+F_c$, total lateral tyre force
F_o	stationary cornering force
$F_{1,2}$	lateral forces acting on leading and trailing edge, Figs. II. 16, 18
$f^*(\alpha)$	= $-M^1 + eF$ (non-dimensional)
g	acceleration due to gravity
$g(\dot{\gamma}, \gamma)$	= - D, frictional couple, function of $\dot{\gamma}$ and γ , Eqs. III. (62a, b, c, 85a, b, c)
$g^*(\dot{\gamma}, \gamma)$	= $g(\dot{\gamma}, \gamma) + \kappa\dot{\gamma}/V$
H_j	Hurwitz determinant, Eq. IV. (4)
(H_{n-1})	cf. Sec. IV. 1. 1
h, h_o, h_m, h^*	cf. Fig. III. 1
I	moment of inertia of swivelling part about king-pin axis
I_a	moment of inertia of wheel about wheel axis
I_{st}	half of moment of inertia of steering-wheel about its axis
I_x	half of moment of inertia of front part of sprung mass about longitudinal axis through its mass centre
I_x^*	moment of inertia of non-swivelling part of unsprung mass about longitudinal axis through its mass centre
I_φ	= $I_x + mh_m^2 + m^*h^2$, half of moment of inertia of front part of sprung mass about axis of rotation (φ)
I_φ^*	= $I + I_x^* + m^*h^{*2}$, moment of inertia of unsprung mass about longitudinal axis of rotation (φ^*)
K	dry-frictional couple about king-pin axis
k	constant of viscous damping about king-pin axis, equivalent coefficient of damping (non-dim.)
k^*	= $k + \kappa/V$, equivalent total coefficient of damping (non-dim.)
M	= $M^1 + M^*$, total moment acting from road on tyre about vertical axis
M^1	moment acting from road on tyre due to lateral tyre deformations

M_0	stationary aligning torque M
M^*	moment acting from road on tyre due to longitudinal tyre deformations
M_{un}	moment acting on wheel due to unbalance, Fig.III.1
M_{gyr}	gyroscopic couple due to lateral tyre deformations, Sec.II.6
m	half the mass of front part of sprung mass, Fig.III.1
m^*	mass of unsprung part, Fig.III.1
m_t	tyre mass, Sec.II.6
$m_{un 1,2}$	unbalance masses on wheel (right and left of wheel plane), Fig.III.1
m_{un}^*	$= m_{un 1} + m_{un 2}$, total unbalance mass
N	vertical tyre load (static)
n	reduction factor of steering systems; frequency (c/s)
O	origin of co-ordinate system $(0, x, y, z)$ fixed to the road
p	unknown of characteristic equation
p_s	operator; unknown of characteristic equation
p_ξ, η, ζ	components of pressure acting from tyre on road
p_i	inflation pressure
\bar{p}	vector indicating position of point with respect to the system $(0, x, y, z)$, Fig.III.2
Q_i	generalized force
q_i	general co-ordinate
R	wheel radius
r	real part of complex root
\bar{r}	vector indicating position of point with respect to moving system $(0, \underline{x}, \underline{y}, \underline{z})$, Fig.III.2
S	$= S_1 + S_2$, tyre constant; stability value
s	travelled distance
T	kinetic energy
t	time
U	potential energy
u	displacement of contact point in ξ -direction due to tyre deformations
V	forward velocity
v	displacement of contact point in η -direction due to tyre deformations; $d\gamma/ds$
v_s	deflection of point on string in η -direction
v_p	deflection of profile element in η -direction

$v_{1,2}$	lateral tyre deflection at leading and trailing edge respectively
W	virtual work; sliding velocity
$W_{\xi, \eta}$	sliding velocities in ξ - and η -direction respectively
x	longitudinal co-ordinate with respect to system fixed to road; reference variable
x_c	x co-ordinate of contact point
y	lateral co-ordinate with respect to system fixed to road
y	lateral displacement of chassis, Fig. III.1
y_c	y co-ordinate of contact point
y_w	y co-ordinate of point C
y^*	lateral deflection of suspension, Fig. III.1
z	vertical co-ordinate with respect to system fixed to road
α	$= v_1/\sigma$, slope of peripheral line at leading edge
α_t	time scale factor
α_o	amplitude of α on the limit-cycle
β	angle between velocity vector of C and x -axis, Fig. II.1; cf. Tables III.1 and IV.1
γ	$= \beta + \psi$, angle between ξ - and x -axis; swivel angle about king-pin
γ_o	amplitude of γ on the limit-cycle
γ^*	additional variable in case of clearance, Fig. III.4
γ_{st}	$= \psi_{st} / n$
Δ	symbol denoting increment
δ	variation symbol; half clearance angle
ϵ	caster angle; $\epsilon = \sigma_c/\sigma$, tyre constant
ξ	vertical co-ordinate with respect to system moving with wheel plane; $\xi = V^2/e^1$, Eq. IV.(100)
η	lateral co-ordinate with respect to system moving with wheel plane; cf. Table IV.1
θ	$= \omega t$, non-dimensional time; $\theta = 2/\alpha_t$, time delay
κ	constant of damping due to longitudinal tyre deformations
λ	wavelength of motion; $\lambda = (\omega/\omega_{sto})^2$
λ_{un}	$= 2\pi R$, wavelength of exciting couple due to unbalance
μ	coefficient of friction between road and tyre; cf. Tables III.1 and IV.1
ξ	longitudinal co-ordinate with respect to system moving with wheel plane
ρ	change in tyre radius

σ	tyre constant, Eq. II. (23); relaxation length of tyre without profile elements
σ_c	tyre constant, Eq. II. (23)
σ^*	relaxation length of tyre
τ	$= \omega t - \varphi$, non-dimensional time; machine time; cf. Table II. 1
φ	$= d\gamma/ds$, spin; phase angle; torsion angle of chassis, Fig. III. 1
φ_w	angle between wheel plane and vertical (camber angle), Fig. III. 3
φ^*	angular displacement of unsprung mass about longitudinal axis, Fig. III. 1
χ	$= \Omega t - \pi - \epsilon$, angle between vector of M_{un} (fixed to wheel) and vertical plane through wheel-axis, Fig. III. 1
ψ	angle between ξ -axis and velocity vector of C, Fig. II. 1
ψ_{st}	angle of rotation of steering-wheel
ψ_w	angle between x-axis and line of intersection of wheel plane and road surface, Fig. III. 3
Ω	$= V/R$, rolling velocity of wheel about its axle
ω	frequency; angular velocity
ω_s	$= \omega/V = 2\pi/\lambda$, reduced frequency
ω_o	natural frequency; frequency on limit-cycle
ω_{sto}	natural frequency of steering system, Eq. IV. (31)
$\omega_{\eta o}$	natural frequency of torsional motion of unsprung mass
ω_{un}	reduced frequency of exciting couple M_{un} due to unbalance

Subscripts

o	stationary; natural; amplitude; on limit-cycle
1	leading edge; right-hand side
2	trailing edge; left-hand side
un	unbalance
st	steering system

REFERENCES

- 1 Becker, G., Fromm, H. and Maruhn, H., Schwingungen in Automobillenkungen ("Shimmy"), Berlin, 1931, 150 p.
- 2 Hartog, J. P. den, Mechanical Vibrations, New York, 1940, p.372.
- 3 Rocard, Y., Dynamique générale des vibrations, Paris, 1949, p.259.
- 4 Olley, M., Road manners of the modern car, J.Inst.Auto.Engrs. 15 (1947), Nos. 4-9, p.147.
- 5 Carter, F.W., The electrical locomotive, Min.Proc.Inst.Civ. Engng. 201 I (1915-16), p.221.
-----, On the stability of running of locomotives, Proc.Roy.Soc. A121 (1928), p.585.
- 6 Pater, A.D.de, Exposé de la théorie de l'interaction entre la voile et le véhicule de chemin de fer. ORE, Utrecht, 1963, 111 p.
- 7 Pater, A.D.de, The approximative determination of the hunting movement of a railway vehicle by aid of the method of Krylov and Bogoljubov, Appl.Sci.Res.10 (1961), p.205.
- 8 Bommel, P.van, Application de la théorie des vibrations non-lineaires sur le problème de mouvement de lacet d'un véhicule de chemin de fer, Utrecht, 1964, 303 p.
- 9 Pacejka, H.B., Analysis of the shimmy phenomenon, Proc. Auto.Div.Inst.Mech.Engrs. 180 (1965-66), part 2A.
- 10 Pacejka, H.B., Theoretisch en experimenteel shimmy onderzoek, De Ingenieur 50 (1965), p. W 127.
- 11 Carter, F.W., On the action of a locomotive driving wheel, Proc.Roy.Soc. A 112 (1926), p.151.
- 12 Fromm, H., Berechnung des Schlupfes beim Rollen deformierbarer Scheiben, ZAMM. 7 (1927), p.27.
- 13 Johnson, K.L., The effect of spin upon the rolling motion of an elastic sphere on a plane, J.Appl.Mech. 80 (1958), p.332.
- 14 Pater, A.D.de, On the reciprocal pressure between two elastic bodies, Proc. Symp. Rolling Contact Phenomena. Amsterdam, 1962, p.29.
- 15 Kalker, J.J., The transmission of force and couple between two elastically similar rolling spheres, Proc.Kon.Ned.Akad.Wet. Amsterdam B 67 (1964), p.135.
- 16 Kalker, J.J., On the rolling contact of elastic bodies in the presence of dry friction, Doctoral Thesis, Delft (to be published).
- 17 Kalker, J.J., private communication.
- 18 Brouhiet, M.G., Direction de la voiture automobile, Soc.des Ing. civ. (1925), p.540.

- 19 From, H., Seitenschlupf und Führungswert des rollenden Rades, Bericht der Lilienthalgesellschaft für Luftfahrtforschung 140 (1941), p.56; NACA TN 1365, p.191.
- 20 Fiala, E., Seitenkräfte am rollenden Luftreifen, VDI-Z 96 (1964), p.973.
- 21 Freudenstein, G., Luftreifen bei Schräg- und Kurvenlauf, Dtsch. Kraftfahrtforsch. 152 (1961), 56 p.
- 22 Frank, F., Grundlagen zur Berechnung der Seitenführungskennlinien von Reifen, Kautschuk und Gummi 18 (1965) Heft 8, p.515.
- 23 Pacejka, H.B., Study of the lateral behaviour of an automobile moving upon a flat level road, Cornell Aer. Lab. YC-857-F-23 (1958), 60 p.
- 24 Pacejka, H.B., Theoretisch onderzoek naar de invloed van longitudinale krachten op de bandkarakteristieken, Rapport P 061, Veh. Res. Lab. Techn. Univ. Delft, 1966.
- 25 Bergman, W., Theoretical prediction of the effect of traction on cornering force, SAE Transactions, 1961, p.614.
- 26 Nordeen, D.L. and Cortese, A.D., Force and moment characteristics of rolling tyres, SAE Transactions, 1964, p.325.
- 27 Savkoor, A., The development of lateral force by a pneumatic tyre rolling at a slip angle on dry road surfaces, Doctoral thesis, Delft (to be published).
- 28 Kantrowitz, A., Stability of castering wheels for aircraft landing gears, NACA Rep. 686 (1937), 16p.
- 29 Wylie, J., Dynamic problems of the tricycle alighting gear, Journ. Aero.Sci. 7 (1939) 2, p.56.
- 30 Greidanus, J.H., Besturing en stabiliteit van het neuswielonderstel (Control and stability of the nose wheel landing gear), NLL, Rep. V 1038, Amsterdam, 1942, 42 p.
- 31 Saito, Y., A study of the dynamic steering properties of tyres, Ninth Int. Aut. Techn. Congress (FISITA) (1962), p.101, 246, 282.
- 32 Fromm, H., Kurzer Bericht über die Geschichte der Theorie des Radflatterns, Bericht 140 der Lilienthal-Gesellschaft (1941), p.53; NACA TM 1365 (1954), p.181.
- 33 Bourcier de Carbon, C., Etude theorique du shimmy des roues d'avion, Off. Nat. d'Etude et de Rech. Aér. 7 (1948); NACA TM 1337 (1952), 126 p.
- 34 Schlippe, B. von, und Dietrich, R., Das Flattern eines bepneuten Rades, Bericht der Lilienthal-Gesellschaft 140 (1941), p.35; NACA TM 1365 (1954), p.125.
- 35 Schlippe, B. von, und Dietrich, R., Zur Mechanik der Luftreifens, Zentrale für wissenschaftliches Berichtswesen, Berlin-Adlershof, 1942, 20 p.
- 36 Schlippe, B. von, und Dietrich, R., Das Flattern eines mit Luftreifen versehenen Rades, Jahrbuch der deutsche Luftfahrtforschung, 1943, 16 p.

- 37 Hadekel, R., The mechanical characteristics of pneumatic tyres, Technical information bureau for chief scientist, Ministry of Supply, London, 1952, 80p.
- 38 Segel, L., Force and moment response of pneumatic tires to lateral motions inputs, Transactions ASME, Journ. of Engineering for Industry, 88 B (1966) 1, 8 p.
- 39 Moreland, W. J., Landing gear vibrations, Wright Air Dev. Center, AF Techn. Rep. 6590 (1951), 70 p.
-----, The story of shimmy, Journ. of the Aer. Sc., 21 (1954) 12, p. 793.
- 40 Smiley, R. F., Correlation, evaluation and extension of linearized theories for tire motion and wheel shimmy, NACA Techn. Note 3632 (1956), 139 p.
- 41 Fonda, A. G., and Radt, H., Summary of C.A.L. tire test data, C.A.L. report YD-1059-F-2, Buffalo, 1958, 49 p.
- 42 Marstrand, O. J., Prevention of caster shimmy by the twin-contact tyre, A.R.C. Techn. Rep. R&M 2508, London, 1951, 15 p.
- 43 Schrode, H., Reduction of the shimmy tendency of tail and nose-wheel landing gears, NASA TM 1391 (1955), 13 p.
- 44 Eldik Thieme, H. C. A. van, Experimental and theoretical research on mass-spring systems by the Veh. Res. Lab. of the Technological Univ. of Delft, Proc. 8th FISITA Congress (1960), p. 375.
- 45 Martin, H., Druckverteilung in der Berührungsfläche zwischen Reifen und Fahrbahn, ATZ 38 (1936), p. 230.
- 46 Effertz, F. H. and Kolberg, F., Einführung in die Dynamik selbsttätiger Regelungssysteme, Düsseldorf, 1963, 401 p.
- 47 Pacejka, H. B., Equations of motion of an automobile with particular reference to the shimmy motion. Report A 105, Veh. Res. Lab. Tech. Univ. Delft, 1966, 40 p.
- 48 Pacejka, H. B., Theoretische beschouwingen over de shimmy bewegingen van wegvoertuigen, Report P 021, Veh. Res. Lab., Techn. Univ. Delft, 1962, 88 p.
- 49 Pacejka, H. B., Theoretische studie van het niet-lineaire shimmy-probleem. Report A 094, Veh. Res. Lab., Techn. Univ. Delft, 1964, 121 p.
- 50 Hurwitz, A., Über die Bedingungen unter welchem eine Gleichung nur Wurzeln mit negativen reellen Teilen besitzt, Math. Ann. Bd. 46 (1895), p. 273.
- 51 Cremer, L., Die Verringerung der Zahl der Stabilitätskriterien bei Voraussetzung positiver Koeffizienten der charakteristischen Gleichung, Z. angew. Math. Mech. 33 (1953), p. 221.
- 52 Klotter, K., Technische Schwingungslehre II, Berlin, 1960, 483 p.
- 53 Orlando, L., Sul problema di Hurwitz relativo alle parti reali delle radici di un' equazione algebrica, Math. Ann. 71 (1911), p. 233.

- 54 Magnus, K., Über die Verfahren zur Untersuchung nicht-linearer Schwingungs- und Regelungs-Systeme, VDI-Forschungsheft 451 Ausg. B 21 (1955), 27 p.
- 55 Cremer, L., Ein neues Verfahren zur Beurteilung der Stabilität linearer Regelungs-Systeme. Z. angew. Math. Mech. 25/27 (1947) p. 161.
- 56 Krylov, N., and Bogoljubov, N., Introduction to non-linear mechanics, Princeton, 1947, 106 p.
- 57 Stoker, J. J., Non-linear vibrations, New York, 1950, 273 p.
- 58 Kauderer, H., Nicht-lineare Mechanik, Berlin, 1958, 684 p.
- 59 Pacejka, H. B., Limit-cycles and their stability, Report A 108, Veh. Res. Lab., Techn. Univ. Delft, 1966, 26 p.

SUMMARY

The phenomenon of the violent self-excited vibrations exerted by the steerable wheels of a road vehicle about the almost vertically situated swivel axes, popularly known as wheel shimmy, occurs both with automobiles and aircraft on the runway. In grave cases shimmy can attain amplitudes of about six degrees at a frequency of for instance seven cycles per second.

Various factors can give rise to instability of the stationary motion of the vehicle. These factors are: (1) a small lateral stiffness of the tyre and (2) of the wheel suspension, or (3) the gyroscopic coupling between rotations of the wheel about its swivel axis and about a longitudinal axis. For aircraft, the combination of the first two factors is presumed to be responsible for the occurrence of shimmy. For automobiles provided with a live axle at the front, the gyroscopic coupling is most likely the cause of the violent self-sustained oscillations. Automobiles with independent suspensions appear, however, to exhibit shimmy as well. It is a shimmy which corresponds to the phenomenon occurring with aircraft, and is to be attributed to the first factor or to a combination of the first two factors. It is the latter sort of shimmy in particular to which attention has been paid in this thesis.

As far as the author is aware of, theoretical investigations so far described in the literature on the subject are based exclusively on linear models. Several non-linear elements such as tyre characteristics, dry friction in the king-pin bearings and clearance in the wheel bearings, appear to have a considerable influence on the behaviour. This influence is studied analytically with the aid of an approximative method based on the principle of the harmonic balance. This method of the equivalent linear equations for the determination of the amplitudes of the limit-cycles and of the stability of these periodic motions, is enunciated at length and in a general sense. For checking and for extending the results obtained along analytical lines, investigations are carried out with the use of an analogue computer. More realistic and complicated systems as well as non-autonomous systems excited by unbalances could be examined by means of the analogue computer.

Before the actual shimmy analysis is started, a mathematical description of the moving vehicle is given. Much attention has been paid to tyre behaviour, which plays the most important role in the shimmy phenomenon considered. Partial sliding in the contact area between tyre and road has been taken into account. In principle, the tyre is considered massless; a correction has been introduced, however, to account for the gyroscopic couple due to the rate of change of lateral tyre deflections with time. The theoretical tyre response to swivel oscillations shows good correspondence with experimentally obtained results.

The mathematical model of the vehicle in its most extended form is of the twelfth order and has seven degrees of freedom, viz.: the

lateral tyre deformation, the rotation of the wheel about the king-pin, the lateral deformation and the torsion about a longitudinal axis of the wheel suspension, the lateral deformation and the torsion of the front part of the chassis and finally the rotation of the steering-wheel.

The investigation shows that for certain combinations of values of parameters such as caster, lateral tyre stiffness, damping and speed of travel, self-excited oscillations may occur. In the case of viscous damping about the swivel axis, the stationary motion may become unstable and a stable limit-cycle will be attained due to the degressive shape of the tyre cornering characteristics. In the case of dry friction in the king-pin bearings the stationary motion is always stable. Two limit-cycles may, however, still arise in that case. The smaller limit-cycle will be unstable and the larger one will be stable. Through an external disturbance or by means of unbalances the stable limit-cycle may be attained. By introducing clearance in the wheel bearings the stationary motion becomes unstable and the large shimmy amplitude may be reached without an external disturbance. The influence of varying certain parameter values has been examined.

The results obtained theoretically have been substantiated by experiments carried out with a test vehicle equipped with independent front wheel suspensions and in addition with a simple mechanical model.

SAMENVATTING

Het verschijnsel van de heftige, zich zelf in stand houdende slingeren uitgevoerd door de bestuurbare wielen van een wegvoertuig om de nagenoeg verticale zwenkassen, kortweg aangeduid met "shimmy", komt zowel bij automobielen als bij vliegtuigen op de landingsbaan voor. In ernstige gevallen kan een amplitude van omstreeks 6° bij een frequentie van bijvoorbeeld 7 Hz bereikt worden.

Verscheidene factoren blijken aanleiding te kunnen geven tot het ontstaan van instabiliteit van de "hoofdbeweging" van het voertuig. Deze zijn: (1) een kleine zijdelingse stijfheid van de band en (2) van de wielophanging, of (3) de gyroscopische koppeling tussen de rotaties van het wiel om zijn zwenkas en om een langas. Bij vliegtuigen wordt de combinatie van de eerste twee factoren verantwoordelijk geacht voor het optreden van shimmy. Bij niet van onafhankelijke voorwielophanging voorziene auto's (stijve as) is de gyroscopische koppeling waarschijnlijk de oorzaak van het ontstaan van heftige zichzelf in stand houdende slingeren. Automobielen voorzien van onafhankelijke voorwielophangingen bleken echter eveneens een shimmy, overeenkomend met het bij vliegtuigen voorkomende verschijnsel, te kunnen vertonen, hetgeen toe te schrijven is aan de eerste factor of een combinatie van de eerste twee factoren. Deze laatste soort shimmy krijgt in het bijzonder de aandacht in dit proefschrift.

Voor zover bekend vond het in de literatuur beschreven theoretisch onderzoek tot nu toe uitsluitend plaats aan gelineariseerde modellen. Verscheidene niet-lineaire elementen, zoals bandkarakteristieken, droge wrijving in de lagering van de zwenkas en speling in het systeem, blijken het gedrag in hoge mate te beïnvloeden. In dit proefschrift is de invloed van de genoemde niet-lineariteiten langs analytische weg volgens een benaderingsmethode, gebaseerd op het principe van de harmonische balans, onderzocht. De gevolgde methode der equivalente lineaire vergelijkingen, ter bepaling van de amplitude der grenskringlopen en van de stabiliteit van deze periodische bewegingen, wordt uitvoerig en in algemene zin uiteengezet. Ter controle en ter uitbreiding van de met behulp van analytische methoden verkregen resultaten zijn onderzoeken verricht met gebruikmaking van een analoge rekenmachine. Uitgebreidere, meer met de werkelijkheid overeenkomende systemen, alsmede niet-autonome, van onbalansen voorziene systemen konden hiermede onderzocht worden.

Aan het eigenlijke shimmyonderzoek gaat een beschrijving van het mathematische model van het bewegende voertuig vooraf. Hierbij wordt aan het gedrag van de band, die de voornaamste rol bij het beschouwde shimmyverschijnsel speelt, veel aandacht besteed. Zowel stationaire als niet-stationaire wielbewegingen worden in de beschouwing betrokken. Partiële slip in het contactvlak tussen band en wegdek wordt in rekening gebracht. In beginsel wordt de band massaloos verondersteld; een correctie in de vorm van het gyroscopisch koppel tengevolge van zijdelings uitbuigen van de band wordt echter wel ingevoerd. De theoretische bandresponsie op zwenkoscil-

laties komt goed overeen met de gemeten responsie.

Het wiskundig model van het voertuig is in zijn meest uitgebreide vorm van de twaalfde orde en heeft zeven graden van vrijheid, te weten: de zijdelingse bandvervorming, de rotatie van het wiel om zijn zwenkas, de zijdelingse vervorming en de torsie om een langsas van de wielophanging, de zijdelingse verplaatsing en de torsie van het voorste deel van het chassis en tenslotte de rotatie van het stuurwiel.

Het onderzoek laat zien dat bij bepaalde combinaties van waarden van zekere parameters zoals wielnaaloo, zijdelingse bandstijfheid, demping en rijsnelheid, zichzelf in stand houdende bewegingen kunnen bestaan. In het geval van visceuze demping om de zwenkas kan de hoofdbeweging labiel worden in welk geval een stabiele grenskringloop bereikt zal worden tengevolge van het degressieve verloop van de bandkarakteristieken. In het geval van droge demping in de zwenkaslagering is de hoofdbeweging weliswaar stabiel, maar kunnen er twee grenskringlopen bestaan, waarvan de kleinste labiel en de grootste stabiel is. Door een storing van buitenaf of tengevolge van onbalansen dient, ruwweg gezegd, de beweging buiten de labiele grenskringloop gebracht te worden om de stabiele shimmyamplitude te kunnen bereiken. Door toepassing van speling in de wielagers wordt de hoofdbeweging labiel en kan de grote shimmyamplitude in bepaalde gevallen zonder storing van buitenaf bereikt worden. De invloed van het veranderen van een aantal belangrijke parameters is onderzocht. De theoretisch verkregen resultaten worden gestaafd door experimenten, uitgevoerd met een van onafhankelijke voorwielophangingen voorzien proefvoertuig en bovendien met een eenvoudig mechanisch model.

STELLINGEN

I

Het is mogelijk om een exacte theorie te geven voor het gedrag van het door Saito ontworpen balkmodel van een band. Saito heeft zich met een benaderingsoplossing tevreden moeten stellen, omdat hij bij de afleiding van de randvoorwaarden onjuiste aannamen over de vorm van de elastische lijn heeft gedaan.

Y. Saito, Dynamic steering properties of tyres, Proc. FISITA 1962, p. 101, 246, 282.

II

De opvatting van Bourcier de Carbon dat de gyroscopische koppeling tussen de rotaties van het bestuurbare wiel om zijn zwenkas en om een langsas in geen geval de oorzaak van het ontstaan van zich zelf in stand houdende trillingen om de zwenkas kan zijn, is onjuist.

Chr. Bourcier de Carbon, Etude théorique du shimmy des roues d'avion, Off. Nat. d'Etudes et des Recherches Aer. 1948, p. 94.

III

De gemiddelde driftstijfheid van een band waarvan de wielas verticale trillingen uitvoert, wordt in belangrijke mate beïnvloed door de (met de bandindrukking variërende) relaxatie-eigenschap van de band, en is daardoor behalve van de amplitude ook van de frequenties van deze trillingen afhankelijk.

De term driftstijfheid ("cornering stiffness") is in het proefschrift gedefinieerd door formule II. (78, eerste gedeelte) en wordt daar met het symbool C aangeduid.

IV

Het door Bergman gebezigde bandmodel mist enige essentiële kenmerken die nodig zijn om een volledig inzicht te krijgen in de invloed van rem- en aanzetkrachten op de driftkracht en het driftmoment. De door hem voor dit bandmodel ontwikkelde theorie is bovendien aanvechtbaar.

W. Bergman, Die Seitenkraft am rollenden Luftreifen während des Antriebes, ATZ 64 (1962) 10, p. 296.

9

V

Automobielen kunnen bij het stationair doorlopen van een bocht zonder verkanting in het algemeen een geringere centripetale kracht ontwikkelen dan de totaal beschikbare adhesiekracht. Dit vindt zijn oorzaak niet alleen in het feit dat de horizontale bandkrachten niet evenwijdig aan elkaar gericht zijn, maar ook in het feit, dat tengevolge van gewichtsoverdracht van binnen naar buiten het binnenste aangedreven wiel boven een zeker aandrijfkoppel zal doorslaan voordat het andere aangedreven wiel hieraan toe zou zijn.

H.S.Radt and H.B.Pacejka, Analysis of the steady-state turning behaviour of an automobile, Proc.Symp. Control of Vehicles, London, 1963, p.66.

VI

De door Mitterlehner uitgevoerde berekeningen van de stabiliteit der rechthoekige beweging van een wegvoertuig voorzien van vrij zwenkbare voorwielen zijn foutief.

G.Mitterlehner, Die Lenkstabilität des Luftbereiften Kraftwagens, Ing. Archiv XXVII, 1959, p.88.

VII

De door de Russische onderzoeker Pevsner uitgevoerde originele en betrekkelijk eenvoudige behandeling van het probleem van het gedrag van wegvoertuigen in bochten verdient bredere belangstelling.

Ja. M.Pevsner, Teoriya ustojcivosti avtomobilja. (Theorie van de stabiliteit van automobielbewegingen), Leningrad, 1947, p.26-55.

VIII

De in het als Nederlandse Norm N 1055 gepubliceerde bouwvoorschrift gegeven methode voor het berekenen van centrisch op druk belaste samengestelde staven met een of meer materiaalvrije assen is in principe onaanvaardbaar. Volgens deze methode zouden deze samengestelde staven, uitgevoerd in staal Fe 37, een toelaatbare belasting hebben die bij grote slankheden een waarde kan bereiken gelijk aan anderhalf maal de toelaatbare belasting van dezelfde constructie uitgevoerd in staal Fe 52. De voorkeur verdienen in dit verband de methoden gegeven in de normen NEN 1008 en DIN 4114, die onderling tot praktisch gelijke resultaten leiden.

T.G.B. 1949/1955 (N 1055), p.23/24.

V.O.S.B. 1963, (NEN 1008), p.54.

Stahl im Hochbau, 12e Aufl. p.141.

IX

De axiale en de zijdelingse stijfheid alsmede de stabiliteit van een luchtveer zijn in belangrijke mate afhankelijk van de aanlighoeken van de balg op de afwikkeloppervlakken.

H.B.Pacejka, Theoretische beschouwingen over het gedrag van luchtveren, De Ingenieur 72 (1960) 10, p. W 61.

X

Bij de invoering van lastafhankelijke veersystemen bij wegvoertuigen, verdient het met het oog op het comfort en de variaties in de verticale bandkracht sterke aanbeveling alle aandacht te schenken aan de verwezenlijking van een lastafhankelijke bandstijfheid.

XI

De in de elasticiteitsleer gebruikelijke term buigpunt van een elastische lijn geeft de verkeerde indruk dat bij bedoelde punten buiging zal optreden. Het verdient overweging een betere benaming in te voeren.

XII

Ter aanduiding van het in de Angelsaksische literatuur onder de naam "shimmy" bekend staande verschijnsel, verdienen in het Nederlandse taalgebruik de termen "wapperen" of "fladderen" de voorkeur boven de door de Centrale Taalcommissie voor de Techniek aanbevolen woorden "schuddewielen" of "zwabberen".

Technische woorden behandeld door de Centrale Taalcommissie voor de Techniek, Den Haag, 1958, p.231.